UNIVERSIDAD COMPLUTENSE DE MADRID

Facultad de Ciencias Físicas
Departamento de Óptica

TESIS DOCTORAL

INTERACTION BETWEEN RANDOMLY FLUCTUATING LIGTH AND SMALL PARTICLES:
Optical forces, effects of partial coherence and phenomena due to magneto-dielectric exictations.

INTERACCIÓN ENTRE LUZ ALEATORIA FLUCTUANTE Y PARTÍCULAS PEQUEÑAS:
Fuerzas ópticas, efectos de coherencia parcial y fenómenos debidos a excitaciones magneto-dieléctricas

MEMORIA PARA OPTAR AL GRADO DE DOCTOR

PRESENTADA POR

Juan Miguel Auñón García

Director

Manuel Nieto Vesperinas

Madrid, 2014

UNIVERSIDAD COMPLUTENSE DE MADRID
FACULTAD DE CIENCIAS FÍSICAS
Departamento de Óptica

TESIS DOCTORAL

INTERACTION BETWEEN RANDOMLY FLUCTUATING LIGHT AND SMALL PARTICLES:

Optical forces, effects of partial coherence and phenomena
due to magneto-dielectric excitations

INTERACCIÓN ENTRE LUZ ALEATORIA FLUCTUANTE Y PARTÍCULAS PEQUEÑAS:

Fuerzas ópticas, efectos de coherencia parcial y fenómenos debidos
a excitaciones magneto-dieléctricas

MEMORIA PARA OPTAR AL GRADO DE DOCTOR PRESENTADA POR

JUAN MIGUEL AUÑÓN GARCÍA

DIRECTOR

MANUEL NIETO VESPERINAS

Madrid, 2014

UNIVERSIDAD COMPLUTENSE DE MADRID

FACULTAD DE CIENCIAS FÍSICAS

Departamento de Óptica

TESIS DOCTORAL

INTERACTION BETWEEN RANDOMLY FLUCTUATING LIGHT AND SMALL PARTICLES:

Optical forces, effects of partial coherence and phenomena
due to magneto-dielectric excitations

INTERACCIÓN ENTRE LUZ ALEATORIA FLUCTUANTE Y PARTÍCULAS PEQUEÑAS:

Fuerzas ópticas, efectos de coherencia parcial y fenómenos debidos
a excitaciones magneto-dieléctricas

MEMORIA PARA OPTAR AL GRADO DE DOCTOR PRESENTADA POR

JUAN MIGUEL AUÑÓN GARCÍA

DIRECTOR

MANUEL NIETO VESPERINAS

Instituto de Ciencia de Materiales de Madrid
Consejo Superior de Investigaciones Científicas
Madrid, 2014

DEDICADA A MIS PADRES, ALFONSO E HILARIA,

A MI HERMANO JOSÉ,

Y A TI TAMARA.

The style of this thesis is based on the classicthesis package

ABSTRACT

T he work of this thesis is focused on the analysis of fluctuating electromagnetic fields (area denoted optical coherence) applied to optical forces (conservation of momentum of light). The theory of optical forces for deterministic fields is a thoroughly studied area. The main consequences are commonly applied to the area of biology, where the trapping of particles is of vital importance. However, the effect of the fluctuations of the fields generated by an optical source is often neglected. Hitherto, we did not know almost anything about the effects of the fluctuation fields in the mechanical action of particles, i.e, if they could be beneficial or harmful when put into practice. This thesis will try to propose simple models which will help to understand this new feature of light. Although this thesis is purely theoretical, we have attempted to provide experimental proposals as well as we have tried to estimate the physical quantities which could be measured in a laboratory.

The origin of optical coherence became important around the 50s with the early work in theory of coherence and polarization of light with E. Wolf as the main precursor. A seemingly unrelated domain of study arose with the works of such renowned names as Casimir, Liftshitz and Liftshitz among others, on forces generated by the vacuum energy fluctuations. These studies showed the attraction between objects due to the vacuum energy ($E = \hbar\omega/2$, the quantum harmonic oscillator).

My role in this thesis has been to develop, analyze and demonstrate the effect of the randomness of light in different types of particles of current interest. To this end, the thesis is divided into 5 parts:

The first part (Part I), which includes Chapter 1, is dedicated to the introduction of the main topic: the theory of random processes. Emphasis will be put on some definitions such as average, ensemble average, correlations of processes, etc., in connection with the problems at hand. Section 1.3 is more focused on stochastic processes in optics, it develops the difference between spatial and temporal coherence of light, being this the concept that will play a more important role in this work. The van Cittert - Zernike theorem will be discussed (Section 1.4) as well as an illustrative example of some random processes in nature (Subsection 1.4.1). On the other hand, we will put the basis of the theory of the angular spectrum representation of electromagnetic fields (Section 1.5). This tool will be used several times throughout this thesis.

The second part (Part II) is composed of chapters 2 and 3. In these Chapters we will develop the coherence (Chapter 2) and polarization (Chapter 3) phenomena produced by statistically homogeneous sources respectively. In particular, Chapter 2 studies the spatial evolution of the cross spectral density function, which will give us an idea about the correlation of the fields at

distances shorter than the wavelength. We will show the role of the evanescent waves and the surface plasmon polariton excitation. Appendix A supports the results presented here and it has not been published in any scientific journal. In Chapter 3 we shall study the polarization of light, considering surface wave excitation. The first Section contains the classical two-dimensional degree of polarization (Section 3.3), and the different ways to characterize it, this helps to study its three-dimensional analogue (Section 3.4). Later we focus on the controversy to find a suitable definition for the degree of polarization for three-dimensional electromagnetic fields.

The interaction between a stochastic field and small particle will be studied in Part III. Prior to this, we introduce the concept of optical force for a deterministic wavefield, and the contribution of the different momenta of light (linear, orbital and spin). Next, it will be shown how the usual equations for the optical forces from deterministic fields may be extended to random fields due to their ergodicity. In order to see the influence of the degree of coherence of light in optical forces, we will study the classical double slit experiment to see if the coherence affects, and in which way, to the dynamics of the particle. It is demonstrated that, like with visibility of fringes, the coherence affects the optical forces.

Part IV, which includes Chapters 5 and 6, will study in detail the forces produced by statistically homogeneous sources. In Chapter 5, we will use a simple model to show how the evanescent modes (relevant in near field optics) and the propagating ones affect the conservative and non-conservative forces respectively. A test particle will be used in order to illustrate the main results. Chapter 6 will make emphasis on particles with a magnetodielectric response, taking into account the force resulting from the electric and magnetic dipoles and the interference between them. We will make an optical analog to the effect studied by Liftshitz for purely thermal sources. We will show how using a quasi-monochromatic optical source, the results are very similar to those obtained previously using the fluctuation-dissipation theorem. Also, we will show how certain asymptotic laws are not correct in the limit at which the particles can not be characterized by the static polarizability.

Finally Part V comprises the last two chapters of this thesis. Up to this point, we were using sources whose spectrum is spatially homogeneous along the plane source ($S(\rho, \omega) = S(\omega)$). Later on, we develop a theory of optical forces for *Schell* model sources. In Chapter 7 we show the use of an optical tweezer setup to observe the trapping of dielectric particles by fluctuating sources. We will demonstrate how a suitable choice of the source parameters can benefit the optical trap with a power density at the plane of the source smaller with respect to what a fully coherent source (such as a laser) would need to trap it. In Chapter 8, we will implement a numerical model to calculate optical forces (or other phenomena associated with the randomness of the light) for *Schell* sources. The study of the propagation of light through nontrivial geometries is a very difficult task to solve analytically. Although throughout the thesis analytical calculations have prevailed over numerical study, the task of characterizing structures is almost impossible with the conventional techniques. Therefore, we will implement the coherent mode representation of a Gaussian Schell model source with a commercial difference finite element code. This method will allow us to study complex configurations. In this chapter we focus mainly on the creation

of photonic states on a pair of dielectric particles forming bonding and antibonding associated with resonances of the isolated particles.

RESUMEN

l trabajo de esta tesis está enfocado al análisis de campos electromagnéticos fluctuantes (área denominada coherencia óptica) aplicado a fuerzas ópticas (conservación del momento de la luz). La teoría de fuerzas ópticas por campos deterministas es un área estudiada en profundidad. Sus principales consecuencias son comúnmente aplicadas al área de la biología, donde el atrapamiento y manejo de partículas es de vital importancia. No obstante, el efecto que tienen las fluctuaciones de los campos generados por una fuente de luz, suelen ser pasados por alto. Hasta ahora, no se sabia prácticamente nada sobre cual era el efecto de las fluctuaciones de la luz en la acción mecánica de las partículas, es decir, si podían ser favorables o perjudiciales a la hora de llevarlos a la practica. En esta tesis se ha intentado proponer sencillos modelos que ayuden al entendimiento de esta nueva característica de la luz. Aunque esta tesis es puramente teórica, siempre se han intentando dar propuestas experimentales, así como se ha intentado estimar las magnitudes físicas que se podrían medir en un laboratorio.

El origen de la coherencia óptica toma importancia en torno a la década de los 50 con los primeros trabajos en teoría de coherencia y polarización de la luz con E. Wolf como principal precursor. Por otro lado, en esa misma época surgieron también los primeros trabajos de fuerzas generadas por fluctuaciones energéticas del vacío, con nombres tan reconocidos como Casimir, London o Liftshitz entre otros. En estos trabajos se demostraba la atracción entre objetos debido a la energía del vacío ($E = \hbar\omega/2$, el oscilador armónico cuántico).

Mi papel aquí es el de desarrollar, analizar y demostrar el efecto que tiene la aleatoriedad de la luz en distintos tipos de partículas de actual interés. Para tal fin, la tesis se ha dividido en 5 partes:

La primera parte de la tesis (Parte I), que engloba el Capítulo 1, está dedicado exclusivamente a la introducción del tema principal: la teoría de procesos aleatorios. Se hará hincapié en algunas definiciones como promedio, conjunto promedio, correlaciones de procesos, etc., válidas para cualquier proceso no determinista. Más centrados en los procesos estocásticos que se dan en óptica, la Sección 1.3 desarrollará la diferencia entre la coherencia espacial y temporal de la luz, siendo la primera característica la que jugará un papel más importante en este trabajo. Se demostrará el teorema de van Cittert-Zernike (Sección 1.4), así como un ejemplo ilustrativo de lo que ocurre en algunos procesos aleatorios en la naturaleza (Subsección 1.4.1). Por otro lado, se pondrán las bases sobre la representación angular en ondas planas de campos electromagnéticos (Sección 1.5). Esta herramienta será usada varias veces a lo largo de esta tesis.

La segunda parte de la tesis (Parte II) esta constituida por los Capítulos 2 y 3. En estos capítulos se desarrollarán los fenómenos de coherencia (Capítulo 2) y polarización (Capítulo 3)

producidos por fuentes homogéneas. Concretamente, en el Capítulo 2 se estudiará la evolución espacial de la densidad espectral cruzada, que nos dará una idea de la correlación de los campos a distancias menores que la longitud de onda. Se demostrará el papel de las ondas evanescentes y de la excitación de plasmones superficiales. El Apéndice A corrobora los resultados aquí presentados y no ha sido publicado en ninguna revista científica. En el Capítulo 3 se estudiará la polarización de la luz, teniendo en cuenta la excitación de ondas superficiales. En la primera sección de este capitulo se estudiará el usual grado de polarización bidimensional (Sección 3.3), así como las distintas formas de caracterizarlo, para más adelante estudiar su análogo tridimensional (Sección 3.4). Aquí profundizaremos en la controversia a la hora de encontrar una definición adecuada para el grado de polarización para campos electromagnéticos tridimensionales.

Una vez terminado el desarrollo y estudio de los fenómenos propiamente derivados de la coherencia de la luz, en la Parte III se estudiará la interacción entre los campos estocásticos y partículas pequeñas. Antes de esto, introduciremos el concepto de fuerza óptica para un campo determinista, y la contribución de los diferentes momentos de la luz (lineal, orbital y de espín). A continuación se demostrará como las ecuaciones usuales para fuerzas ópticas a partir de campos deterministas se pueden extrapolar a campos aleatorios gracias a la ergodicidad de los mismos. Para ver la influencia del grado de coherencia de la luz en las fuerzas ópticas, se estudiará un experimento clásico como el de la doble rendija para ver si la coherencia afecta, y en que manera, a la dinámica de la partícula. Del mismo modo que se demostró que la coherencia influía en la visibilidad de las franjas, está también influirá en las fuerzas ópticas.

La Parte IV, que engloba los Capítulos 5 y 6 estudiará en detalle las fuerzas producidas por fuentes estadísticamente homogéneas. En el Capítulo 5, se usará un sencillo modelo de fuente para demostrar como los modos evanescentes (relevantes en óptica de campo cercano) y propagantes afectan a las fuerzas conservativas y no conservativas respectivamente. Se usará una partícula tipo test para visualizar los resultados. Por otro lado, en el Capítulo 6 se hará un fuerte hincapié en la respuesta magnetodieléctrica de la partícula, teniendo en cuenta la fuerza resultante del dipolo eléctrico, el magnético y la interferencia entre ambos. Se hará un análogo óptico al efecto estudiado por Liftshitz para fuentes puramente térmicas. Se demostrará como con una fuente óptica cuasi-monocromática, los resultados obtenidos son muy similares a los ya obtenidos previamente usando el teorema de fluctuación-disipación. También se demostrará como algunas leyes asintóticas son erróneas en el límite en el cual las partículas no pueden ser caracterizadas por una polarizabilidad estática.

En la última parte (Parte V) se desarrollan los dos últimos capítulos de la tesis. Hasta este punto, se han utilizado fuentes cuyo espectro es homogéneo respecto a la posición a lo largo de la fuente ($S(\rho, \omega) = S(\omega)$). A partir de ahora desarrollaremos una teoría de fuerzas para fuente denominadas de *Schell*. En el Capítulo 7 usaremos una configuración de pinza óptica para ver el atrapamiento de partículas puramente dieléctricas por este tipo de fuentes fluctuantes. Demostraremos como una elección adecuada de los parámetros que la definen, puede beneficiarnos a la hora de atrapar partículas con una intensidad en el plano de la fuente menor que la que una fuente totalmente coherente (como por ejemplo la de un láser) necesitaría para atraparla. En el Capítulo 8 se implementará un modelo numérico para calcular fuerzas ópticas (o cualquier

otro fenómenos asociado a la aleatoriedad de la luz) para fuentes de *Schell*. El estudio de la propagación de la luz a través de espacios no triviales es un tema muy complicado de resolver analíticamente. Aunque a lo largo de toda la tesis ha prevalecido el cálculo analítico por encima del numérico, la idea de estudiar otras estructuras se hace casi imposible con las técnicas clásicas. Por ello, implementaremos la representación en modo coherentes para una fuente Gaussiana de Schell en un programa comercial de diferencias de elementos finitos. Este método nos dará la posibilidad de estudiar estructuras complejas. En este capítulo nos centraremos sobretodo en la creación de estados fotónicos sobre un par de partículas dieléctricas que a su vez formarán estados de enlace y antienlace que estarán asociados a las resonancias de las partículas aisladas.

PUBLICATIONS

Here is the list of publications containing my original contributions in this thesis. They will be cited in Roman numerals.

[I] J. M. Auñón and M. Nieto-Vesperinas, "Near-field spatial correlations from partially coherent homogeneous planar sources: effects on surface wave excitation," Opt. Lett. **36**, 3410–3412 (2011).
doi: 10.1364/OL.36.003410.

[II] J. M. Auñón and M. Nieto-Vesperinas, "On two definitions of the three-dimensional degree of polarization in the near field of statistically homogeneous partially coherent sources," Opt. Lett. **38**, 58–60 (2013).
doi: 10.1364/OL.38.000058.

[III] J. M. Auñón and M. Nieto-Vesperinas, "Optical forces on small particles from partially coherent light," J. Opt. Soc. Am. A **29**, 1389–1398 (2012).
doi: 10.1364/JOSAA.29.001389.

[IV] J. M. Auñón and M. Nieto-Vesperinas, "Photonic forces in the near field of statistically homogeneous fluctuating sources," Phys. Rev. A **85**, 053828 (2012).
doi: 10.1103/PhysRevA.85.053828.

[V] J. M. Auñón, C. W. Qiu, and M. Nieto-Vesperinas, "Tailoring photonic forces on a magnetodielectric nanoparticle with a fluctuating optical source," Phys. Rev. A **88**, 043817 (2013).
doi: 10.1103/PhysRevA.88.043817.

[VI] J. M. Auñón and M. Nieto-Vesperinas, "Partially coherent fluctuating sources that produce the same optical force as a laser beam," Opt. Lett. **38**, 2869–2872 (2013).
doi: 10.1364/OL.38.002869.

[VII] J. M. Auñón, F. J. Valdivia-Valero and M. Nieto-Vesperinas, "Optical binding of cylinder photonic molecules in the near-field of partially coherent fluctuating Gaussian Schell model sources. A coherent mode representation," J. Opt. Soc. Am. A **31**, 206–216 (2014).
doi: 10.1364/JOSAA.31.000206.

ACKNOWLEDGMENTS

Tengo que dar las gracias a mucha gente, ya que si he llegado hasta aquí, es por la suma de varias personas que de un modo u otro, han aportado algo en mi vida.

Mi primer mil y un gracias es a mi supervisor, el Prof. Manuel Nieto Vesperinas. Para mi ha sido un gran apoyo en todo momento, ya que me ha enseñado a trabajar duro, pero también me ha enseñado a parar y mirar a mi alrededor. Gracias por todos los consejos que me has dado, por enseñarme a intentar dar más de mi, por gastar tu tiempo en innumerables charlas, y no solo de física, sino también de la vida. He aprendido mucho de ti.

Mi segundo gracias es a mis amigos y compañeros de profesión Álvaro Gómez y Nacho Minaya, con ellos empecé la licenciatura, y después de tantos años, seguimos siendo los mismos. También agradecer en este apartado a mis amigos de la carrera: David, Irene, Jorge, Juan, Miguel, Sara, Silvia, Toni y Yizeh, que también aportaron su granito de arena.

Gracias a las personas con las que he colaborado en algún momento u otro. Resaltar al anterior estudiante de Manuel, el ahora Doctor Francisco Javier Valdivia, con el que compartí muchos congresos, ratos y una publicación. También gracias a Rémi Carminati y a todo su grupo, por acogerme como un miembro más durante mis meses en París.

Gracias a las autoridades competentes que han financiado mi investigación, en concreto a los proyectos: FIS2009-13430-C02-01, Consolider NanoLight CSD2007-00046 y FIS2012-36113-C03-03. Espero que sigan impulsando la investigación entre los jovenes, y que los que vengan detrás de mi, tengan como poco las mismas oportunidades que yo.

Gracias en especial a mis amigos del instituto: Sergio, Borja e Irene. Ellos son los que más de cerca han seguido mi evolución como persona. Gracias por tantas cenas y ratos juntos, de todos estos momentos guardo mis mejores recuerdos y anécdotas. Resaltar la aportación de Sergio, que se preocupó en echarme una mano y se ha convertido en un apoyo fundamental.

Ahora gracias a todas las personas con las que he compartido algún momento de estos 4 años: En especial a mi compañero de despacho Hugo Aramberri, que me ayudó con las correcciones, empezamos el doctorado a la vez y la verdad es que ha sido un placer compartir estos años con él. También gracias a mis dos últimas compañeras de despacho: Marzia Marciello y Yurena Luengo, porque en el último año de tesis no he parado de reírme, el buen ambiente en el trabajo influye (y mucho) en el rendimiento. Gracias a los anteriores compañeros: Hernan, Armando...y alguno que otro que seguro me dejo por el camino. También gracias por compartir su tiempo conmigo al grupo de las comidas: Mónica, Fernando, Robert, Sigmund, Mathias...

Mi más profundo y sincero agradecimiento a mis padres, gracias por enseñarme a valorar las cosas. Respecto a mi madre, gracias por forjar en mi tu actitud ante la vida. A mi padre, por enseñarme (y demostrarme cada día) a hacer lo que es correcto. A mi hermano, porque sin decirlo sabemos que estamos ahí.

La última frase para Tamara. Gracias por intentar hacer de mi un gran chico. Gracias porque todo este camino lo he recorrido contigo a mi lado. En fin, gracias.

"It's not about how to achieve your dreams, it's about how to lead your life, ... If you lead your life the right way, the karma will take care of itself, the dreams will come to you.

Randy Pausch, *The Last Lecture*

CONTENTS

LIST OF FIGURES

Part I

INTRODUCTION TO THE THEORY OF COHERENCE AND ANGULAR SPECTRUM REPRESENTATION OF WAVEFIELDS

1

SOME PRELIMINARY CONCEPTS

The main goal of this chapter is to introduce many of the concepts that will be used in one way or another throughout this thesis. Firstly, I will talk about the characterization of a stochastic process, and for this purpose we will need to familiarize with most of the definitions which will be presented. Secondly, I will pay attention to the meaning of temporal and spatial coherence of a wavefield, trying to explain these two concepts. Thirdly, I will develop one of the main theorems in the theory of partially coherent waves: the van Cittert-Zernike theorem. Finally, and due to its importance on this thesis, I will also explain the basis of the angular plane wave representation of a wavefield.

Although most of the definitions here presented are based on a scalar formulation, a large amount of problems found in optics can be described without using a complete electromagnetic theory. We will not explain the details about the transition to a scalar theory, however a generalization of the correlation functions and its laws, discussed next, to vector fields can be found in [1] (Subsection 8.4) and in [2] (Subsection 3.2).

1.1 SOME BASIC CONCEPTS ABOUT STOCHASTIC PROCESSES

Throughout this thesis, we will work with random or stochastic processes and some key concepts as *ensemble average*, *correlations, stationary* or *ergodicity* will appear. Therefore, it is worth introduce and explain them. The following concepts are completely general for any type of classical wave such as mechanical or electromagnetic perturbations.

All the concepts introduced here can be found in some textbooks like [3–5].

1.1.1 *The ensemble average*

Firstly, we shall assume a random function $x(t)$ to be real, at least in some domain of t, with a probability density $p(x,t)$. All the different realizations of $x(t)$ constitute the totality of the random process. Hence the expectation value of $x(t)$ is

$$\langle x(t) \rangle = \int_{-\infty}^{\infty} x p(x,t) \mathrm{d}x, \tag{1.1}$$

where $\int_{-\infty}^{\infty} p(x,t)\mathrm{d}x = 1$.

In a different way, we can also consider the countable collection of the possible realizations of $x(t)$, i.e., $^{(1)}x(t)$, $^{(2)}x(t)$, $^{(3)}x(t)$... If we have access to every realization of the process, we can alternatively define

$$\langle x(t) \rangle = \lim_{N \to \infty} \frac{1}{N} \sum_{r=1}^{\infty} {}^{(r)}x(t). \tag{1.2}$$
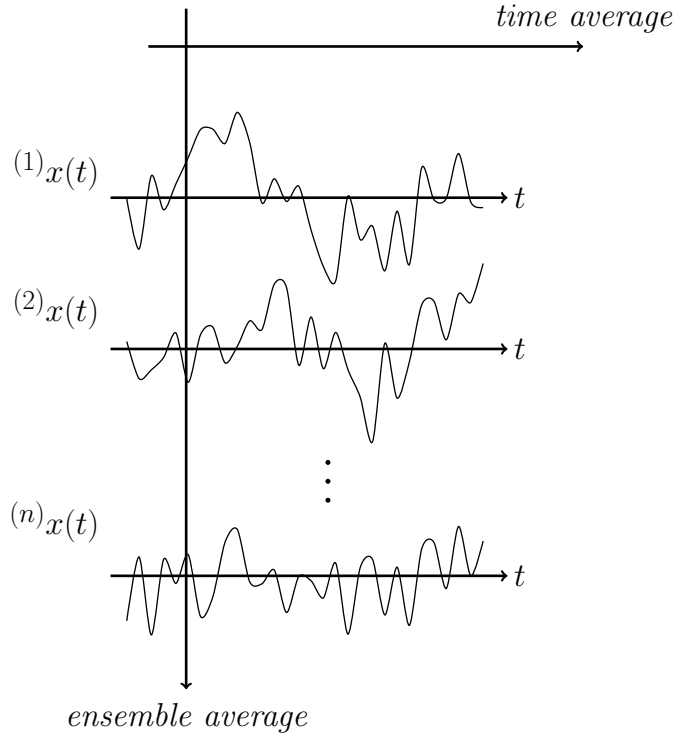
Figure 1.1: Ensemble realization $^{(r)}x(t)$ ($r = 1, 2, ..$) of a random process $x(t)$

Equations (1.1) and (1.2) are equivalent definitions of the *ensemble average*. Analogously we can define the mean-square and the variance as

$$\langle x(t)^2 \rangle = \int_{-\infty}^{\infty} x^2 p(x,t) \mathrm{d}x = \lim_{N \to \infty} \frac{1}{N} \sum_{r=1}^{\infty} {}^{(r)}x(t)^2, \tag{1.3}$$

and

$$\sigma^2 = \langle x(t)^2 \rangle - \langle x(t) \rangle^2, \tag{1.4}$$

respectively. Notice that, in general, this average is different from the usual time-average, an averaged quantity of a single system over a time interval

$$\overline{x(t)} = \underset{T\to\infty}{\text{Lim}} \frac{1}{2T} \int_{-T}^{T} x(t)\mathrm{d}x. \tag{1.5}$$

1.1.2 *Correlations*

The probability density $p(x,t)$ does not describe the random process completely. Imagine that we want information about what is happening in two different instants of time, $x(t_1)$, $x(t_2)$ and the correlation between them. Such information is provided by the joint probability density of the variates t_1, t_2

$$p_2\left(x_2,\, t_2;\, x_1,\, t_1\right). \tag{1.6}$$

The function $p_2\left(x_2,\, t_2;\, x_1,\, t_1\right)$ contains more information about the general process than its counterpart $p_1\left(x_1,\, t_1\right)$, i.e., p_2 carries information about the correlation in two different times and $p(x,t)$ (c.f. Eq. (1.1))

$$\int_{-\infty}^{\infty} p_2\left(x_2,\, t_2;\, x_1,\, t_1\right)\mathrm{d}x_2 = p_1(x_1, t_1) = p(x,t). \tag{1.7}$$

Thus, $p_2\left(x_2,\, t_2;\, x_1,\, t_1\right)$ allows us to calculate the mean value $\langle x(t)\rangle$ and the two-time correlation function $\Gamma\left(t_1, t_2\right)$

$$\Gamma\left(t_1, t_2\right) = \langle x(t_1)x(t_2)\rangle = \int_{-\infty}^{\infty} x(t_1)x(t_2)p_2\left(x_2,\, t_2;\, x_1,\, t_1\right)\mathrm{d}x_1\mathrm{d}x_2. \tag{1.8}$$

As we have commented, the function p_2 contains more information than p_1, however, if we want to calculate the correlation at three different instant of times, we will need, analogously to p_2, a more general function $p_3\left(x_3,\, t_3; x_2,\, t_2;\, x_1,\, t_1\right)$. Obviously, this can be extended to an infinite probability density p_n

$$p_n\left(x_n,\, t_n; x_{n-1},\, t_{n-1}; \ldots;\, x_1,\, t_1\right). \tag{1.9}$$

Although in this section we have considered $x(t)$ as a real random function, the phenomena here discussed can be extrapolated to complex stochastic functions $z(t) = x(t) + iy(t)$, being $x(t)$ and $y(t)$, in general, two real non-deterministic functions. In this case, the correlation function $\Gamma\left(t_1, t_2\right)$ is defined as

$$\Gamma\left(t_1, t_2\right) = \langle z^*(t_1)z(t_2)\rangle = \int_{-\infty}^{\infty} z^*(t_1)z(t_2)p_2\left(z_2,\, t_2;\, z_1,\, t_1\right)\mathrm{d}x_1\mathrm{d}x_2\mathrm{d}y_1\mathrm{d}y_2. \tag{1.10}$$

1.1.3 *Stationary*

Many random functions of time have the property that its behavior does not change with time. In a more rigorous way, we say that a random process is stationary if its probability density $p(x, t)$ is invariant under a translation of the origin of time, i.e.,

$$p(x, t) = p(x, t + T). \tag{1.11}$$

Under this condition, the expectation value is also invariant under the same translation

$$\langle x(t) \rangle = \int_{-\infty}^{\infty} x p(x, t) \mathrm{d}x = \int_{-\infty}^{\infty} x p(x, t + T) \mathrm{d}x. \tag{1.12}$$

The correlation function $\Gamma(t_1, t_2)$ leads to

$$\begin{aligned}
\Gamma(t_1, t_2) &= \langle x(t_1) x(t_2) \rangle \\
&= \int_{-\infty}^{\infty} x(t_1) x(t_2) p_2(x_2, t_2; x_1, t_1) \, \mathrm{d}x_1 \mathrm{d}x_2 \\
&= \int_{-\infty}^{\infty} x(t) x(t + t_2 - t_1) p_2(x_2, t + t_2 - t_1; x_1, t) \, \mathrm{d}x_1 \mathrm{d}x_2 \\
&= \langle x(t) x(t + t_2 - t_1) \rangle,
\end{aligned} \tag{1.13}$$

where we can see that $\Gamma(t_1, t_2)$ only depends on t_1 and t_2 through its difference. Therefore, $\Gamma(t_1, t_2)$ is usually written as $\Gamma(t_2 - t_1)$. From Eq. (1.13) is easy to demonstrate that $\Gamma(t_1, t_2)$ is symmetric

$$\Gamma(t_2 - t_1) = \Gamma(t_1 - t_2). \tag{1.14}$$

For a complex random function, if the process is stationary, the correlation function $\Gamma(t_1, t_2)$ obeys the Hermiticity condition

$$\Gamma(t_2 - t_1) = \Gamma^*(t_1 - t_2). \tag{1.15}$$

1.1.4 *Ergodicity*

As introduced in Section 1.1.1, calculating the expectation value $\langle x(t) \rangle$ can be a difficult task because we need to have access to every realization of the ensemble $\{x(t)\}$. Nevertheless, it is common that every realization carries the same information about the stationary random process as the rest of them. In this case the time-average of every realization is given by

$$\overline{^{(r)}x(t)} = \operatorname*{Lim}_{T \to \infty} \frac{1}{2T} \int_{-T}^{T} {}^{(r)}x(t) \mathrm{d}x. \tag{1.16}$$

If the time-averages $\overline{^{(r)}x(t)}$ are then all equal and coincide with the ensemble average $\langle x(t) \rangle$,

$$\overline{^{(r)}x(t)} = \langle x(t) \rangle, \tag{1.17}$$

the random process is then said to be an *ergodic process*. Although at first glance it may seem surprising that these two quantities can coincide because it looks like it will depend on every

realization, and although we can not generalize, this feature is very common in optics. However, we invite the reader to delve into this topic by reading references [3–5]

From now on, we will assume that we are dealing with statistically stationary and ergodic processes, hence, there will be no difference between time-average (Eq. (1.5)) and ensemble average (Eq. (1.1)).

1.2 SPECTRAL PROPERTIES

The Fourier spectrum is a useful tool employed in many technical disciplines as physics or engineering because it provides information about the components of a signal in the frequency-domain. In the case that concerns us, the task of defining a Fourier transform of a random process is not as trivial, nevertheless, we will ignore some mathematical details assuming that it is possible.[I.1]

1.2.1 *The Wiener-Khintchine theorem*

Let us consider a complex random process $z(t)$ and we will assume that one of the realizations can be expressed as a Fourier integral

$$^{(r)}z\left(t\right) = \int_{-\infty}^{\infty} {}^{(r)}\tilde{z}\left(\omega\right)e^{-i\omega t}\mathrm{d}\omega, \tag{1.18}$$

$$^{(r)}\tilde{z}\left(\omega\right) = \frac{1}{2\pi}\int_{-\infty}^{\infty} {}^{(r)}z\left(t\right)e^{i\omega t}\mathrm{d}t. \tag{1.19}$$

The spectral product of two different components of the process $z(t)$ is

$$^{(r)}\tilde{z}^*\left(\omega\right){}^{(r)}\tilde{z}\left(\omega'\right) = \frac{1}{\left(2\pi\right)^2}\iint_{-\infty}^{\infty} {}^{(r)}z^*\left(t\right)e^{-i\omega t (r)}z\left(t'\right)e^{i\omega' t'}\mathrm{d}t\mathrm{d}t'. \tag{1.20}$$

Taking the ensemble average $\langle\cdots\rangle$ of the previous equation and assuming that the process is stationary (see Subsection 1.1.3), Eq. (1.20) leads to

$$\left\langle\tilde{z}^*\left(\omega\right)\tilde{z}\left(\omega'\right)\right\rangle = \frac{1}{\left(2\pi\right)^2}\iint_{-\infty}^{\infty}\Gamma\left(\tau\right)e^{i(\omega-\omega')t}e^{i\omega'\tau}\mathrm{d}t\mathrm{d}\tau, \tag{1.21}$$

where $\tau = t' - t$ and $\Gamma\left(\tau\right) = \langle z^*(t)z\left(t+\tau\right)\rangle$. Performing one of the integrations in Eq. (1.21), and taking the definition of the Dirac delta distribution[I.2] into account, we obtain

$$\left\langle\tilde{z}^*\left(\omega\right)\tilde{z}\left(\omega'\right)\right\rangle = S\left(\omega\right)\delta\left(\omega-\omega'\right), \tag{1.22}$$

where

$$S\left(\omega\right) = \frac{1}{2\pi}\int_{-\infty}^{\infty}\Gamma\left(\tau\right)e^{i\omega\tau}\mathrm{d}\tau, \tag{1.23}$$

I.1 some details can be found in [3] and references therein.

I.2 $\frac{1}{2\pi}\int e^{i\left(\omega-\omega'\right)t}\mathrm{d}t = \delta\left(\omega-\omega'\right)$

$$\Gamma(\tau) = \int_{-\infty}^{\infty} S(\omega) e^{-i\omega\tau} d\omega. \tag{1.24}$$

Equation (1.22) manifests the importance of the formalism in Fourier space. For a random process the spectral components at different frequencies ω, ω' are uncorrelated (delta-correlated). Eqs. (1.23,1.24) are generally known as the *Wiener-Khintchine theorem* and Eq. (1.23) is usually denoted as the *spectral density* or the *power spectrum*.

1.2.2 *Cross-spectral density (generalized Wiener-Khintchine theorem)*

Let us consider two different complex random processes $z_1(t_1)$ and $z_2(t_2)$. We define the cross-correlation function as

$$\Gamma_{12}(t, t+\tau) = \langle z_1^*(t_1) z_2(t+\tau) \rangle. \tag{1.25}$$

As in Eqs. (1.14,1.15), if the two process $z_i(t_i)$, $i = 1, 2$, are stationary

$$\Gamma_{12}(\tau) = \Gamma_{12}^*(-\tau). \tag{1.26}$$

By analogy to Eq. (1.22) of the spectral density $S(\omega)$, we may define the cross-spectral density of two (or n different) process as

$$\langle \tilde{z}_i^*(\omega) \tilde{z}_j(\omega') \rangle = W_{ij}(\omega) \delta(\omega - \omega'), \quad (i, j = 1, 2, 3 \ldots) \tag{1.27}$$

where $\tilde{z}_i^*(\omega)$ has been defined in Eq. (1.19). In the case of $i = j$, we recover the definition of the spectral density (c.f. Eq. (1.23))

$$W_{ii}(\omega) = S_i(\omega). \tag{1.28}$$

In a similar way to the previous section:

$$W_{ij}(\omega) = \frac{1}{2\pi} \int_{-\infty}^{\infty} \Gamma_{ij}(\tau) e^{i\omega\tau} d\tau, \tag{1.29}$$

$$\Gamma_{ij}(\tau) = \int_{-\infty}^{\infty} W_{ij}(\omega) e^{-i\omega\tau} d\omega, \tag{1.30}$$

where W_{ij} and Γ_{ij} give us information about the processes denoted as i, j. Eqs. (1.29) and (1.30) are usually known as the *generalized Wiener-Khintchine* theorem.

Instead of $W_{ij}(\omega)$, we may also define a normalized cross-spectral density function $\mu_{ij}(\omega)$:

$$\begin{aligned} \mu_{ij}(\omega) &= \frac{W_{ij}(\omega)}{[W_{ii}(\omega)]^{1/2} [W_{jj}(\omega)]^{1/2}} \\ &= \frac{W_{ij}(\omega)}{[S_i(\omega)]^{1/2} [S_j(\omega)]^{1/2}}, \end{aligned} \tag{1.31}$$

where

$$0 \leq \left| \mu_{ij}(\omega) \right| \leq 1, \tag{1.32}$$

being the lower limit the case when the processes are totally uncorrelated and the upper one when they are totally correlated. Notice that $\mu_{ii}(\omega) = 1$. This normalized cross-spectral function will be referenced as *the spectral degree of coherence*.

1.3 TEMPORAL COHERENCE VERSUS SPATIAL COHERENCE

In Sections 1.1 and 1.2 we have been dealing with general stochastic situations, however, we are concerned about random processes which appear in optics.

Precisely because the optical sources have a finite size and the wavefield emerged is not completely monochromatic, it is said that the light is not completely coherent. Now we will introduce some important aspects in optical coherence from a conceptual point of view (the most important formal aspects have already been explained in the previous section).

1.3.1 *Temporal coherence*

The temporal coherence gives us information about the bandwidth of a source and describes the possibility of a wave to interfere with a time-shifted version of itself. Hence, let us consider a partially coherent quasi-monochromatic source with a bandwidth $\Delta\nu$ smaller than the mean frequency $\tilde{\nu}$, i.e., $\Delta\nu/\tilde{\nu} \ll 1$. The beam from the source is divided in two through a beam splitter (see Fig. 1.2) and it is recombined and projected on a screen after a path difference $\Delta l = c\Delta t$. It is well-known that the interference pattern will be observed if

$$\Delta t \Delta \nu < 1. \tag{1.33}$$

Hence, we can define the *coherence time* as

$$t_c \sim \frac{1}{\Delta\nu}, \tag{1.34}$$

and the *longitudinal coherence length* as

$$l_c \sim \frac{c}{\Delta\nu} = \frac{\tilde{\lambda}^2}{\Delta\lambda}, \tag{1.35}$$

where $\tilde{\lambda}$ is the mean wavelength. We shall assume that the path difference between the mirrors in Fig. 1.2 is $\Delta l = 2(d_2 - d_1)$. An interference pattern will be observed only if the coherence length l_c is larger than the path difference Δl. If we consider an ideal source emitting a monochromatic wavefield ($\Delta\nu \to 0$), from Eq. (1.35) we can estimate that the coherence length will tend to infinity ($l_c \to \infty$).

In order to provide an estimation of the coherence length, let us consider a white source with bandwidth $\Delta\lambda = (800 - 400)$nm centered at $\tilde{\lambda} = 600$nm. Substituting these parameters in Eq. (1.35) we obtain $l_c = 900$nm, hence, in order to obtain an interference pattern we should have a path difference $\Delta l \simeq 0$, in fact, the use of broadband sources is a way to calibrate the optical setup. Nowadays, optical sources such as He-Ne can achieve values around $l_c = 300$m. Due to this large l_c, lasers are usually denoted as coherent sources.

Now we will define the auto-correlation function at different instants of time $\Gamma(\mathbf{r}, \mathbf{r}, \tau)$ and the complex degree of temporal coherence $g(\mathbf{r}, \mathbf{r}, \tau)$ as

$$\Gamma(\mathbf{r}, \mathbf{r}, \tau) = \langle U^*(\mathbf{r}, t)U(\mathbf{r}, t + \tau)\rangle, \tag{1.36}$$
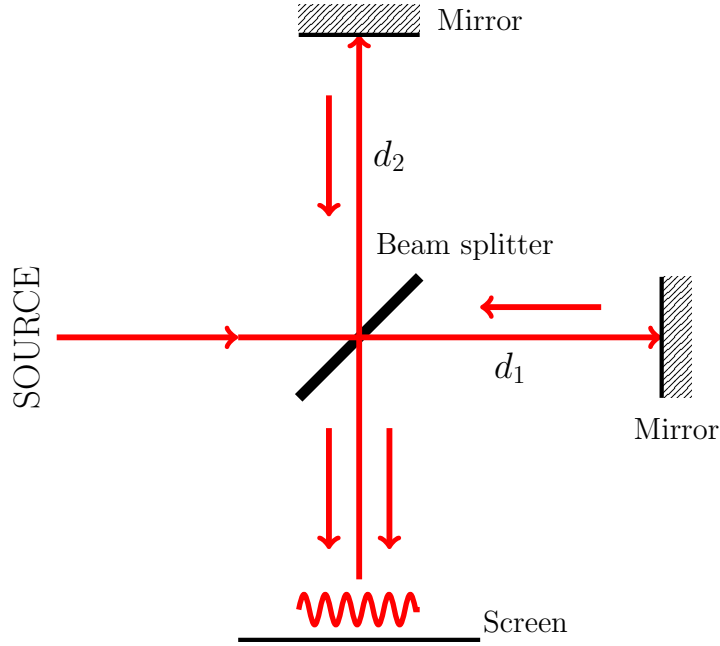
Figure 1.2: Michelson interferometer.

and

$$g\left(\mathbf{r},\mathbf{r},\tau\right) = \frac{\langle U^*(\mathbf{r},t)U(\mathbf{r},t+\tau)\rangle}{\langle U^*(\mathbf{r},t)U(\mathbf{r},t)\rangle}, \tag{1.37}$$

respectively. A way to measure the coherence time is to calculate the value at which the function $|g\left(\mathbf{r},\mathbf{r},\tau\right|$ drops to $1/e$.

1.3.2 *Spatial coherence*

Now we will discuss spatial coherence. Temporal coherence and spatial coherence are two phenomena independent of each other, i.e., an optical source with a high degree of temporal coherence can have a low degree of spatial coherence and vice versa. For instance, in the experiment of reference [6], the light is assumed quasi-monochromatic, however the source is partially coherent (in terms of spatial coherence).

The physical meaning is also different, the time coherence provides information about how monochromatic a wavefield is, whereas the spatial coherence gives information about the size of the source. Let us imagine a point source (Fig. 1.3(a)) whose light is not necessarily monochromatic. At the points denoted as P_1 and P_2 the field is identical because they belong to the same wavefront, or in other words, the points P_1 and P_2 are totally correlated. Let us now imagine a secondary point source near of the original (Fig. 1.3(b)). Due to the fact that each wavefield comes from a different point source which fluctuates independently, it is said that P_1 and P_2 are *uncorrelated* or *partially correlated*. In 1.3.1 we have described the Michelson interferometer experience in order to provide an idea about the concept of temporal coherence. Let us now consider another interference problem, the double slit experiment (Fig. 1.4). The observed in-

(a) Point source   (b) Extended source
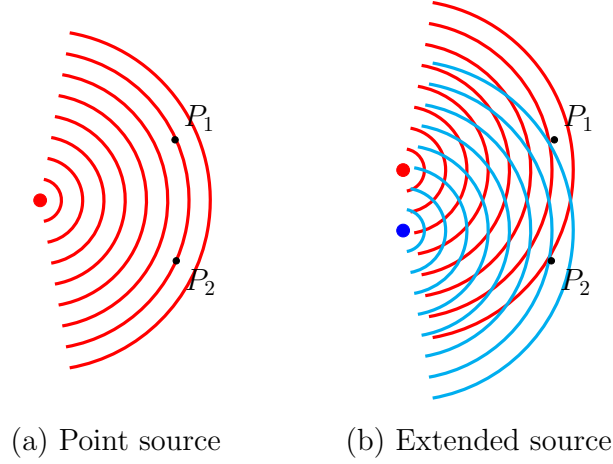
Figure 1.3: Schemes about point (a) and extended sources (b).

terference fringes in $\mathcal{B}$ are an estimation of the correlation between points P_1 and P_2. In this experiment the interference pattern will be observed if the two pinholes are contained in a region in the plane $\mathcal{A}$ whose area is of the order of the *coherence area*

$$A_c = \frac{R^2 \lambda^2}{S^2}, \tag{1.38}$$

where S refers to the linear dimension of the source and R is the distance from the source to the source plane. The square-root of this quantity is denoted as the *transverse coherence length*[I.3]. Analogously, if we denote by d the maximum distance between the pinholes for which we can observe the interference fringes, the coherence area is defined as

$$A_c = \pi d^2. \tag{1.39}$$

Precisely, this maximum distance would be the transverse coherence length. Let us pay attention to Eq. (1.38). We can see that as we reduce the dimensions of the source (point source $S \to 0$), the coherence area tends to infinity ($A_c \to \infty$). Another important consequence of this simple formula is that by increasing the distance between the source and the plane $\mathcal{A}$, the coherence area also increases. This phenomenon will be explained in Section 1.4.

Next we will give some numerical examples regarding the coherence area [3]. For sunlight, which can be considered as a collection of independently radiating atoms, the coherence area is $A_c \simeq 10^{-3} \text{mm}^2$, however for stars this value is increased up to $A_c \simeq 1 \text{m}^2$. This is another manifestation of how sources which are placed far away from the observation plane have a large coherence area and manifests the build-up of coherence on propagation, as shown by the van Cittert-Zernike theorem to be discussed. Light from common laser sources are spatially coherent.

Now we will define the equal-time correlation function at different positions $\Gamma(\mathbf{r}_1, \mathbf{r}_2, 0)$, and the complex degree of spatial coherence $g(\mathbf{r}_1, \mathbf{r}_2, 0)$ as

$$\Gamma(\mathbf{r}_1, \mathbf{r}_2, 0) = \langle U^*(\mathbf{r}_1, t) U(\mathbf{r}_2, t) \rangle, \tag{1.40}$$

[I.3] In this thesis, we will more concern with the effects of spatial coherence in different problems, thus, this transverse coherence length will be simply denoted in the following as *coherence length* or *correlation length*
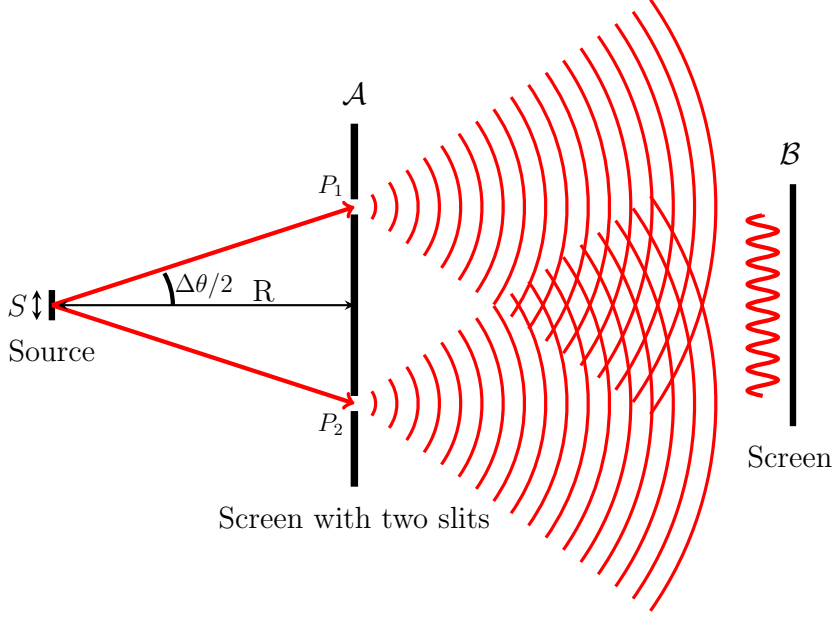
Figure 1.4: Schemes about point (a) and extended sources (b).

and

$$g\left(\mathbf{r}, \mathbf{r}, 0\right) = \frac{\langle U^*(\mathbf{r}_1, t) U(\mathbf{r}_2, t)\rangle}{\langle U^*(\mathbf{r}, t) U(\mathbf{r}, t)\rangle}. \tag{1.41}$$

respectively. In the same way as we have defined the coherence time, the transverse coherence length is usually calculated as the value at which the function $|g\left(\mathbf{r}_1, \mathbf{r}_2, 0\right|$ drops to $1/e$.

1.4 THE VAN CITTERT-ZERNIKE THEOREM IN FREQUENCY DOMAIN

Having reached this point, we can study one of the main features of the classical theory of optical coherence, the van Cittert-Zernike theorem, which, as its name suggests, was developed by P.H. van Cittert in 1934 [7] and F. Zernike in 1938 [8].

For simplicity, we shall assume an ensemble of scalar random fields $\{U\left(\mathbf{r}, \omega\right)\}$. The correlation properties of the field are characterized by the cross-spectral density function (cf. Eq. 1.27)

$$W\left(\mathbf{r}_1, \mathbf{r}_2, \omega\right) = \langle U^*\left(\mathbf{r}_1, \omega\right) U\left(\mathbf{r}_2, \omega\right)\rangle, \tag{1.42}$$

and for $\mathbf{r}_1 = \mathbf{r}_2 = \mathbf{r}$, $W\left(\mathbf{r}_1, \mathbf{r}_2, \omega\right)$ becomes the spectral density

$$S\left(\mathbf{r}, \omega\right) = W\left(\mathbf{r}, \mathbf{r}, \omega\right) = \langle U^*\left(\mathbf{r}, \omega\right) U\left(\mathbf{r}, \omega\right)\rangle. \tag{1.43}$$

According to the Huygens-Fresnel principle, if the extent of the source plane is small compared to the distance between the source plane and the observation one, the field $U\left(\mathbf{r}, \omega\right)$ diffracted by the planar screen can be expressed as [2]

$$U\left(\mathbf{r}, \omega\right) = \frac{e^{ikz}}{i\lambda z} \iint_{-\infty}^{\infty} U\left(\xi, \eta\right) e^{i\frac{k}{2z}\left[(x-\xi)^2 + (y-\eta)^2\right]} \mathrm{d}\xi \mathrm{d}\eta \tag{1.44}$$
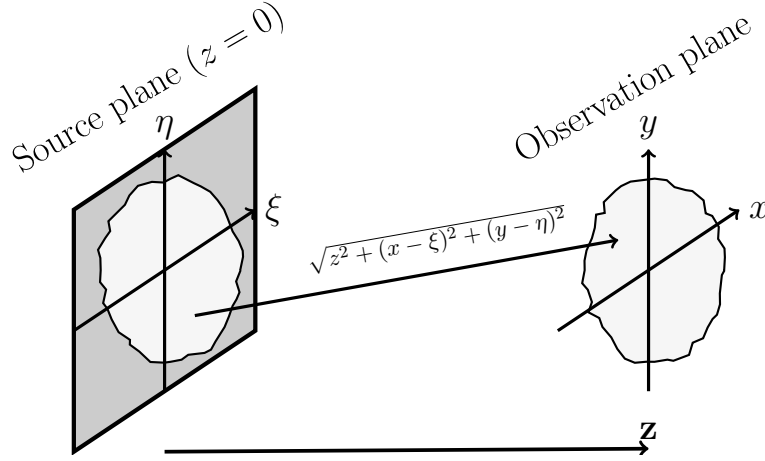
Figure 1.5: Optical system considered.

where $k = 2\pi/\lambda$, being λ the wavelength of light. The coordinates (ξ, η) refer to the coordinates of the aperture (see Fig. 1.5). Now, substituting Eq. (1.44) into Eq. (1.42) we can calculate the cross-spectral density function at the plane $z_1 = z_2 = z = \text{constant}$

$$
\begin{aligned}
&W\left(x_1, y_1, x_2, y_2, z, \omega\right) \\
&= \left(\frac{1}{\lambda z}\right)^2 \iint_{-\infty}^{\infty} W^{(0)}\left(\xi_1, \eta_1, \xi_2, \eta_2\right) \\
&\quad \times e^{-i\frac{k}{2z}\left[(x_1-\xi_1)^2+(y_1-\eta_1)^2\right]} e^{i\frac{k}{2z}\left[(x_2-\xi_2)^2+(y_2-\eta_2)^2\right]} \mathrm{d}\xi_1 \mathrm{d}\eta_2 \mathrm{d}\xi_1 \mathrm{d}\eta_2,
\end{aligned} \tag{1.45}
$$

where $W^{(0)}\left(\xi_1, \eta_1, \xi_2, \eta_2\right) = \left\langle U^*\left(\xi_1, \eta_1\right) U\left(\xi_2, \eta_2\right)\right\rangle$ is the cross-spectral density at the plane $z = 0$. Eq. (1.45) represents the change on propagation of the correlation function $W\left(\mathbf{r}_1, \mathbf{r}_2, \omega\right)$.

We shall assume that all the points at our source plane $z = 0$ are completely uncorrelated. This is expressed mathematically as

$$
\begin{aligned}
&W^{(0)}\left(\xi_1, \eta_1, \xi_2, \eta_2, \omega\right) \\
&= A\sqrt{S^{(0)}\left(\xi_1, \eta_1, \omega\right)}\sqrt{S^{(0)}\left(\xi_2, \eta_2, \omega\right)}\delta\left(\xi_1-\xi_2\right)\delta\left(\eta_1-\eta_2\right),
\end{aligned} \tag{1.46}
$$

being A a positive constant. Using Eq. (1.46) into Eq. (1.45) and the properties of the delta function we can calculate the cross-spectral density

$$
\begin{aligned}
&W\left(x_1, y_1, x_2, y_2, z, \omega\right) \\
&= \frac{A}{(\lambda z)^2} e^{-i\frac{k}{2z}\left[x_1^2-x_2^2+y_1^2-y_2^2\right]} \int_{-\infty}^{\infty} S^{(0)}\left(\xi, \eta\right) e^{-i\frac{k}{z}\left[(x_2-x_1)\xi+(y_2-y_1)\eta\right]} \mathrm{d}\xi \mathrm{d}\eta.
\end{aligned} \tag{1.47}
$$

Instead of using $W\left(\mathbf{r}_1, \mathbf{r}_2, \omega\right)$, it is more appropriate to calculate the spectral degree of coherence (c.f. Eq. (1.31))

$$
\mu\left(\mathbf{r}_1, \mathbf{r}_2, \omega\right) = \frac{W\left(\mathbf{r}_1, \mathbf{r}_2, \omega\right)}{\sqrt{S\left(\mathbf{r}_1, \omega\right)}\sqrt{S\left(\mathbf{r}_2, \omega\right)}}. \tag{1.48}
$$

Hence, using Eqs. (1.47) and (1.48), the degree of coherence leads to

$$
\mu\left(x_1, y_1, x_2, y_2, z, \omega\right) = \frac{\int_{-\infty}^{\infty} S^{(0)}\left(\xi, \eta, \omega\right) e^{-i\left[\frac{k\Delta x}{z}\xi+\frac{k\Delta y}{z}\eta\right]} \mathrm{d}\xi \mathrm{d}\eta}{\int_{-\infty}^{\infty} S^{(0)}\left(\xi, \eta, \omega\right) \mathrm{d}\xi \mathrm{d}\eta}, \tag{1.49}
$$

13

where $\Delta x = x_2 - x_1$ and analogously for Δy. The numerator of Eq. (1.49) is the Fourier transform of the spectral density of the source $S^{(0)}(\xi, \eta, \omega)$ with the spatial frequency $\frac{k\Delta x}{z}$ $\left(\frac{k\Delta y}{z}\right)$. Eq. (1.49) leads to the following conclusions:

- In the far zone, the spectral degree of coherence $\mu(x_1, y_1, x_2, y_2, z, \omega)$ is proportional to the two-dimensional Fourier transform of the power spectrum $S^{(0)}(\xi, \eta)$ across the spatially incoherent source. Eq. (1.49) is usually denoted as the *van Cittert-Zernike theorem in space frequency domain.*

- The spectral degree of coherence increases on propagation. A light wave from an uncorrelated source becomes spatially coherent as it propagates. This phenomenon was briefly commented in 1.3.2

1.4.1 *An illustrative example: Spatial coherence from ducks*

In the previous section we have introduced an important concept in classical optical coherence theory: the change of the cross-spectral density function with the propagation due to an uncorrelated source.

At first, it seems a difficult concept to interpret. It is not trivial to understand that the most uncorrelated source can generate a collection of waves whose interference, in propagation, will be coherent. One of the tasks of a researcher is to try to extrapolate what we do to real life situations, and this is what Wayne H. Knox, Miguel Alonso and Emil Wolf did in Reference [9].

The experiment is the study of the theorem developed in Section 1.4 in a very visual way. In this unusual experiment the random wave generation is performed by thirteen Rouen ducks, i.e., the role of the source $W^{(0)}(\xi_1, \eta_1, \xi_2, \eta_2)$ in Eq. (1.45) is played by the ducks, in other words, the ducks behave like *atoms*, *light bulb* or any optical source.

The ducks randomly enter the water (obviously independently of one another), generating a collection of independent waves. As we can see in Fig. 1.6(a)-(b), the waves are uncorrelated, they are propagating without interfering with the rest of them, at least in a perfect (totally coherent) way, showing the lack of correlation. Nevertheless, as they are propagated, the correlation between the waves increase (see Fig. 1.6(d)), behaving as a single wave formed by a single duck.

It is worth remarking the latter conclusion. Let us imagine that the only thing we can see is the far-field. There is no way to distinguish whether the observed wave comes from a point source (a single duck or a single emitter) or a set of them (a group of ducks or emitters). Mathematically this is expressed by Eq. (1.49).
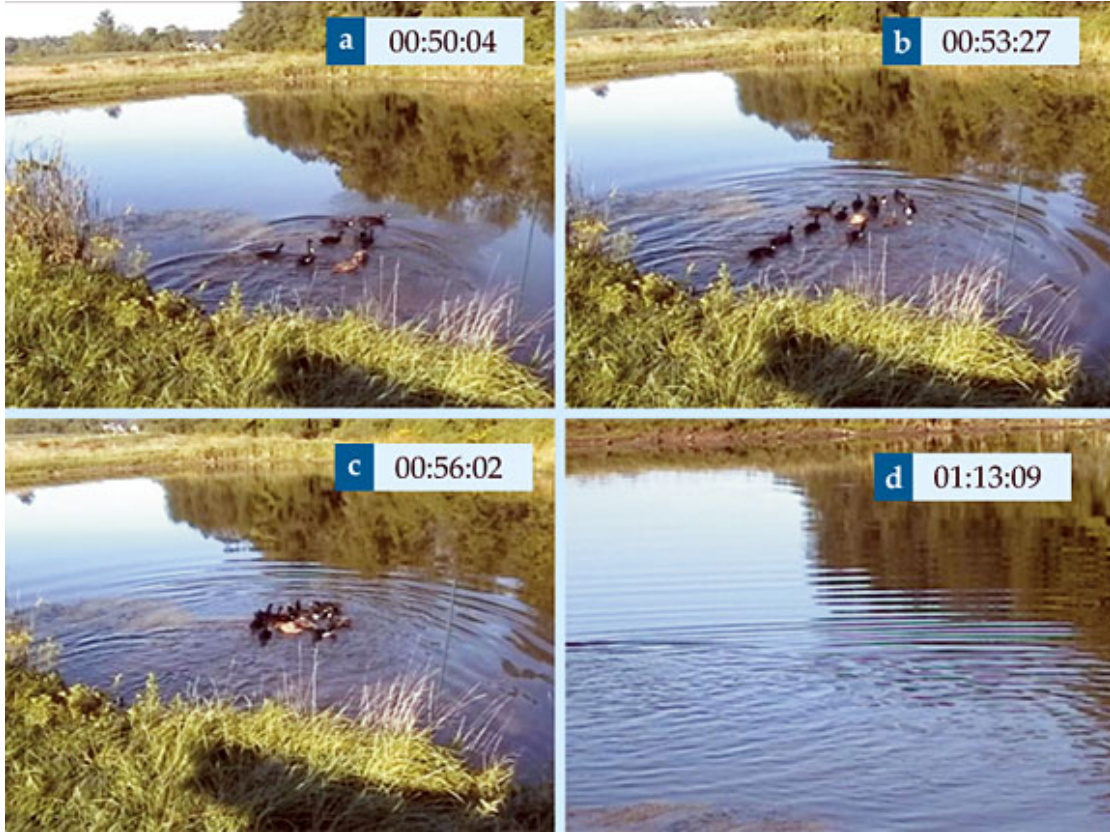
Figure 1.6: Frames of the experiment from ducks. The whole video can be found at this link http://www.youtube.com/watch?v=4o48J4streE

1.5 ANGULAR SPECTRUM REPRESENTATION OF WAVEFIELDS

Throughout this thesis, we could say that one of the most powerful tools that we have used in order to calculate the propagation of electromagnetic fields is the angular plane wave spectrum of a wavefield. This technique gives us the possibility to take into account all the contributions to the electromagnetic field, i.e., the propagating (homogeneous) and evanescent (inhomogeneous) waves and allows us to decompose complex fields to simpler ones such as plane waves.

In this representation, any wavefield is represented as a superposition of propagating and evanescent plane waves as a solution of source-free Maxwell's equations

$$\nabla \times \mathbf{H} = \frac{1}{c}\frac{\partial \mathbf{D}}{\partial t}, \tag{1.50a}$$

$$\nabla \times \mathbf{E} = -\frac{1}{c}\frac{\partial \mathbf{B}}{\partial t}, \tag{1.50b}$$

$$\nabla \cdot \mathbf{D} = 0, \tag{1.50c}$$

$$\nabla \cdot \mathbf{B} = 0. \tag{1.50d}$$

Let us consider the geometry of Fig. 1.7. We shall assume that our physical electromagnetic field depends on time in the following way

$$\mathbf{E}\left(\mathbf{r},t\right) = \mathrm{Re}\left\{\mathbf{E}\left(\mathbf{r}\right)e^{-i\omega t}\right\}, \tag{1.51}$$
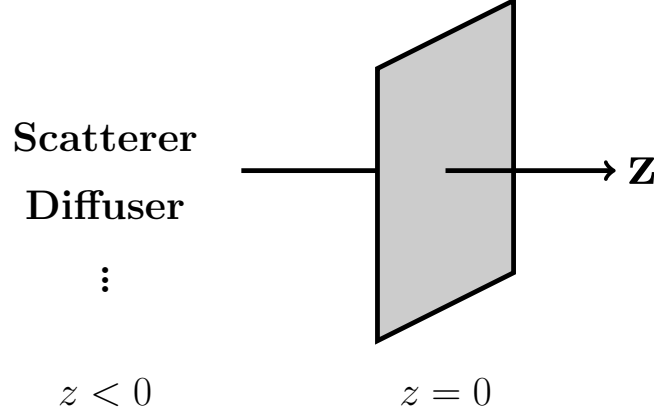
Figure 1.7: Notation of the angular spectrum representation.

and is placed in a region of space $z \geq 0$. This field may be coming from a scattering process, a diffuser, etc. These secondary sources will be considered located at $z < 0$, remaining the half-space $z \geq 0$ a source-free region. The space-dependent part of the wave will satisfy the Helmholtz equation

$$\left(\nabla^2 + k^2\right) \mathbf{E}\left(\mathbf{r}\right) = 0, \tag{1.52}$$

where $k = k_0 n = n\omega/c$, being c the speed of light in vacuum and n the refractive index of the medium. Now, let us assume that we know the value of the electric field at a given plane $z = constant = 0$ and we can write it as a Fourier integral, namely [3, 10]

$$\mathbf{E}\left(x, y, 0\right) = \iint_{-\infty}^{\infty} \mathbf{e}\left(s_x, s_y\right) e^{ik(s_x x + s_y y)} \mathrm{d}s_x \mathrm{d}s_y, \tag{1.53}$$

where the angular amplitude $\mathbf{e}\left(s_x, s_y\right)$ can be written in connection to the boundary value of the electric field at the constant plane $z = 0$

$$\mathbf{e}\left(s_x, s_y\right) = \left(\frac{k}{2\pi}\right)^2 \iint_{-\infty}^{\infty} \mathbf{E}\left(x, y, 0\right) e^{-ik(s_x x + s_y y)} \mathrm{d}x \mathrm{d}y. \tag{1.54}$$

Now, introducing Eq. (1.53) into Eq. (1.52), we can write the propagation of the angular spectrum either in terms of the value of the electric field $\mathbf{E}\left(x, y, 0\right)$, i.e., [3, 10]

$$\begin{aligned} \mathbf{E}\left(x, y, z\right) &= \left(\frac{k}{2\pi}\right)^2 \iint_{-\infty}^{\infty} \iint_{-\infty}^{\infty} \mathbf{E}\left(x', y', 0\right) \\ &\times e^{ik(s_x(x-x') + s_y(y-y'))} e^{\pm iks_z z} \mathrm{d}s_x \mathrm{d}s_y \mathrm{d}x' \mathrm{d}y', \end{aligned} \tag{1.55}$$

or in terms of the angular spectrum $\mathbf{e}\left(s_x, s_y\right)$

$$\mathbf{E}\left(x, y, z\right) = \iint_{-\infty}^{\infty} \mathbf{e}\left(s_x, s_y\right) e^{ik(s_x x + s_y y)} e^{\pm iks_z z} \mathrm{d}s_x \mathrm{d}s_y, \tag{1.56}$$

where the symbol $\pm$ refers to the plane of propagation (+ if it is propagated towards planes $z > 0$ and vice versa). In Eq. (1.55) the third component of the propagation unit vector $\mathbf{s} = \left(s_x, s_y, s_z\right) = \left(\mathbf{s}_\perp, s_z\right)$ is defined as

$$s_z = \sqrt{1 - (s_x^2 + s_y^2)}. \tag{1.57}$$

Depending on the value of $s_x^2 + s_y^2$, the third component of the propagation vector (s_z) can be real or purely imaginary. Assuming that the wave is propagated towards $z \geq 0$, we shall discuss two cases:

1) Evanescent (inhomogeneous) waves: $s_x^2 + s_y^2 > 1$. In this case,

$$s_z = i\sqrt{s_x^2 + s_y^2 - 1}, \qquad (1.58)$$

and substituting into the integrand of Eq. (1.56) we have

$$e^{ik(s_x x + s_y y)}e^{-k\sqrt{s_x^2 + s_y^2 - 1}z}. \qquad (1.59)$$

The propagated field decays exponentially as $e^{-k|s_z||z|}$ along the z-axis, hence the modes are attenuated with the distance to the source and they propagate along a plane parallel to the plane $z = 0$. As an example, we shall assume a value of $|s_z| = 2$. Expressing $k = 2\pi/\lambda$, being λ the wavelength of the spectrum, we have $e^{-\frac{4\pi}{\lambda}|z|}$. For a distance of $z = \lambda$, the exponential gives us $e^{-4\pi} \simeq 3.5 \times 10^{-6}$!. The integrand of Eq. (1.56) is almost zero. Hence, these waves will be negligible at distances $z \geq \lambda$ and if we want to work with them, our laboratory has to be placed at subwavelength distances from $z = 0$. For optical waves, this conveys nanoscale dimensions.

2) Propagating (homogeneous) waves: $s_x^2 + s_y^2 < 1$. In this second point,

$$s_z = \sqrt{1 - s_x^2 + s_y^2}, \qquad (1.60)$$

and

$$e^{ik(s_x x + s_y y)}e^{ik\sqrt{1 - s_x^2 + s_y^2}z} = e^{ik(s_x x + s_y y + \sqrt{1 - s_x^2 + s_y^2}z)}, \qquad (1.61)$$

being the contribution to the angular wave spectrum due to oscillating plane waves. The plane wave components propagate into $z \geq 0$ with a propagation vector $\mathbf{s} = (\mathbf{s}_\perp, s_z) = (s_x, s_y, s_z)$.

As it follows from Maxwell's equations, the electric field is connected with the magnetic vector, which in a similar way leads to

$$\mathbf{H}(x, y, z) = \iint \mathbf{h}(s_x, s_y)\, e^{ik(s_x x + s_y y)}e^{\pm iks_z z}\mathrm{d}s_x\mathrm{d}s_y, \qquad (1.62)$$

where $\mathbf{h}(s_x, s_y)$ is the angular spectrum of the magnetic field $\mathbf{H}(x, y, z)$. Hence, applying Maxwell's equations to Eqs. (1.56) and (1.62), we have that for each plane wave component [10]

$$\mathbf{s} \cdot \mathbf{e}(s_x, s_y) = \mathbf{s} \cdot \mathbf{h}(s_x, s_y) = 0, \qquad (1.63)$$

$$\mathbf{h}(s_x, s_y) = \mathbf{s} \times \mathbf{e}(s_x, s_y). \qquad (1.64)$$

In summary, Eqs. (1.56) and (1.62) give us the relationship between the electromagnetic field $\mathbf{E}(\mathbf{r})$, $\mathbf{H}(\mathbf{r})$ at any point of the half-space $z > 0$ and its boundary value $\mathbf{E}(x, y, 0)$, $\mathbf{H}(x, y, 0)$.

1.5.1 *The Rayleigh formulation of diffraction*

Although it will not be demonstrated in detail, we will show the connection between the angular wave spectrum and the classical formulas of diffraction. In Eq. (1.55) the integral

$$G\left(x - x', y - y', z\right) = \left(\frac{k}{2\pi}\right)^2 \iint_{-\infty}^{\infty} e^{ik\left(s_x(x-x')+s_y(y-y')\right)} e^{\pm iks_z z} \mathrm{d}s_x \mathrm{d}s_y \qquad (1.65)$$

is usually denoted as *propagator*. On the other hand, one can demonstrate that the angular wave representation of a spherical divergent wave is

$$\frac{e^{ikr}}{r} = \frac{ik}{2\pi} \iint_{-\infty}^{\infty} \frac{1}{s_z} e^{ik(s_x x + s_y y + s_z |z|)} \mathrm{d}s_x \mathrm{d}s_y, \qquad (1.66)$$

also known as the Weyl's representation of the spherical wave. Looking into detail the Eqs. (1.65) and (1.66), one can observe that they are related by the following relationship

$$G\left(x - x', y - y', z\right) = -\frac{1}{2\pi} \frac{\partial}{\partial z}\left(\frac{e^{ikR}}{R}\right), \qquad (1.67)$$

where $R = |\mathbf{r} - \mathbf{r}'|$. From Eqs. (1.67) and (1.55), we can write $\mathbf{E}\left(x, y, z\right)$ as

$$\mathbf{E}\left(x, y, z\right) = \frac{-1}{2\pi} \iint_{-\infty}^{\infty} \mathbf{E}\left(x', y', 0\right) \frac{\partial}{\partial z}\left(\frac{e^{ikR}}{R}\right) \mathrm{d}x \mathrm{d}y, \qquad (1.68)$$

which is usually called the *Rayleigh diffraction formula of first kind* [2, 3, 10] and it is the solution of the Dirichlet boundary value problem of the Helmholtz equation for a half-space. The solution of the Neumann problem may be obtained in a similar manner.

Part II

SPATIAL CORRELATIONS AND THREE-DIMENSIONAL DEGREE OF POLARIZATION IN THE NEAR-FIELD OF STATISTICALLY HOMOGENEOUS SOURCES: EFFECTS ON SURFACE WAVES

2

SUBWAVELENGTH SPATIAL CORRELATIONS FROM PARTIALLY COHERENT SOURCES: SURFACE WAVE EXCITATION

2.1 MOTIVATION

We saw in Section 1.4 that the behavior of the cross spectral density in the far-field is governed by the van-Cittert-Zernike-theorem, however, at these distances the evanescent modes are completely negligible (see Section 1.5). From the beginning of near-field optics, there have been very few publications (most of them will be listed in this chapter) which have studied in detail the interaction between the different electromagnetic field fluctuations in this regime.

In this chapter I will show in detail, from a simple scalar formulation, the effects on the cross-spectral density of the evanescent modes, and the consequence of exciting surface plasmon polaritons (SPP) on the surface where is contained the source. To this end, using the angular spectrum representation I will separate the contributions of evanescent and propagating modes, showing that evanescent waves are relevant for incoherent sources but irrelevant for spatially coherent systems.

2.2 INTRODUCTION

The resolution limit is a well-known issue in classical optics. The Rayleigh criterion of resolution establishes that the minimum resolvable separation between two image points is

$$R = \frac{0.61\lambda}{NA},$$ (2.1)

where $NA = n \sin \theta$ is the numerical aperture for a lens and n, θ are the refractive index of the surrounded medium and the half-angle of the cone of light which can enter in the lens, respectively. This definition comes from the first minimum of the Airy pattern produced by the diffraction of a circular pinhole [2]. One way to interpret this resolution limit lies on the loss

of evanescent waves in the angular spectrum. As we commented in Section 1.5, if we want to take these evanescent modes into account, our observation has to be made at subwavelength distances, in this way, near-field techniques can obtain substantially higher resolution.

On the other hand, this resolution limit is also connected with the transversal coherence length σ. Let us take, for instance, the Lambertian source [3] (this is an example of homogeneous source, a concept which will be defined in the next section). A Lambertian source has a far-field radiant intensity $(J(\mathbf{r}, \omega) = r^2 W(\mathbf{r}, \mathbf{r}, \omega)$ for the scalar case) proportional to $\cos\theta$ and a degree of spectral coherence equals to

$$\mu^{(0)}(\boldsymbol{\rho}_1, \boldsymbol{\rho}_2, \omega) = \frac{\sin(k\rho)}{k\rho}, \tag{2.2}$$

being $\rho = |\boldsymbol{\rho}_1 - \boldsymbol{\rho}_2|$. Fig. 2.1 (right) shows the degree of coherence given by Eq. (2.2) as a function of the normalized distance ρ/λ, thus, if we recover the definition of coherence length (see Section 1.3.2), we see that $\sigma \sim \lambda/2$, i.e., the classical resolution limit.

To overcome this limit, the incorporation of evanescent modes is crucial, being this feature demonstrated theoretically [11–13] and experimentally [14]. Namely, reference [11] demonstrates the subwavelength spatial correlations of radiated fields for uncorrelated (δ-correlated) thermal sources and the role of surface plasmon polaritons (SPP) on the source surface (the concept of SPP will be also introduced). A delta-correlated source is that whose coherence length σ tends to zero, however, a partially coherent source adopts any possible σ. If we have no SPPs, the role of the spatial coherence of the source has been analyzed on both, the spectrum and the spatial coherence of the near field, for free-space propagation at subwavelength distances [13, 14].

Then, this chapter studies the effects on the cross spectral density $W(\mathbf{r}_1, \mathbf{r}_2, \omega)$ due to the interplay between SPP excitation and the spatial coherence of the source. Radiative and non-radiative parts of the angular correlation tensor are analyzed in order to see the contributions (or not) of the evanescent modes.
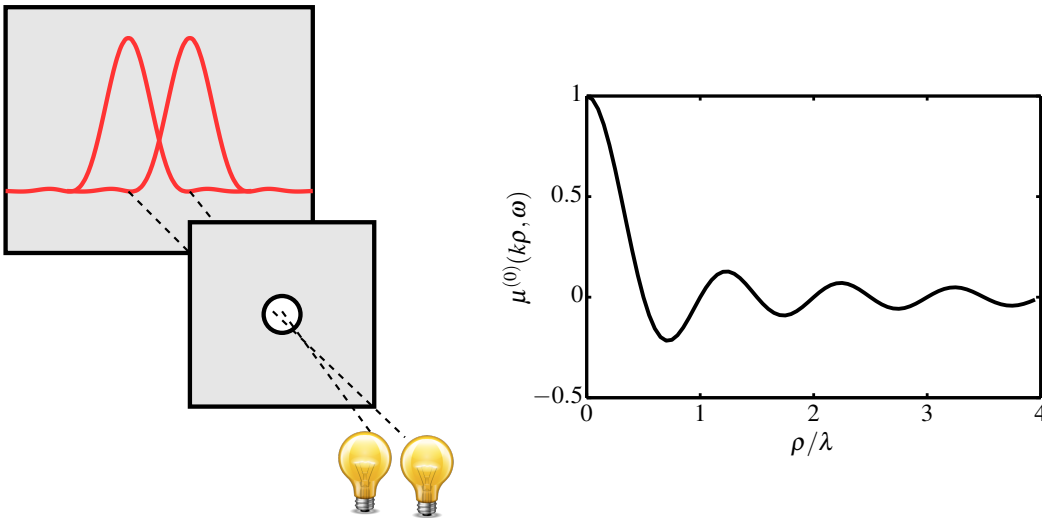
Figure 2.1: Left: Illustration about the resolution limit. Right: Degree of coherence for a Lambertian source
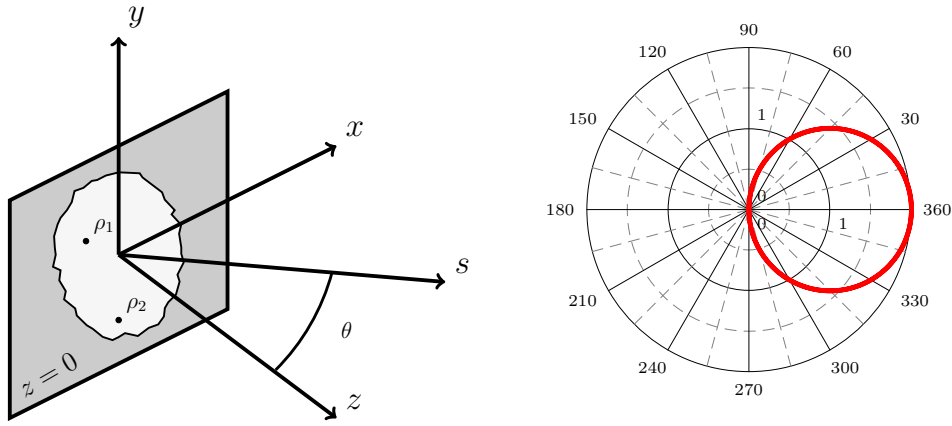
Figure 2.2: Left: Illustrating the notation. Right: Radiation pattern of a Lambertian source.

Prior to analyze these effects, we will introduce the concept of homogeneous source and surface wave.

2.3 ON THE CONCEPT OF STATISTICALLY FLUCTUATING HOMOGENEOUS SOURCES

Throughout this and some others chapters, we will study the effects of fluctuating electric fields which emerge from a statistically homogeneous source. Then, it is worth introducing this concept. For this task, it seems most appropriate to borrow a footnote from an article by Emil Wolf [15]:

"By statistically homogeneous source one means a source for which all the probability densities that characterize the behavior of the field at an arbitrary number of source points are invariant with respect to translation of all the points on the source plane. This requirement implies, in particular, that the second-order cross-spectral density function is also invariant with respect to such a translation, this being the fact expressed by eq. (5)[II.1]. It is clear that strict statistical homogeneity demands that the source occupies the whole z-plane. Throughout this paper we will use the term "statistical homogeneity" also for a finite source in the approximate sense that eq. (5) hold whenever the points $\mathbf{r}_1$ and $\mathbf{r}_2$ both lie within the source area."

In other words, the spectrum is *homogeneous* (with respect to the position) across the plane of the source. Many common sources such as the recently cited Lambertian or thermal obey this law [16]

II.1 This equation is the same that Eq. (2.18) of this thesis
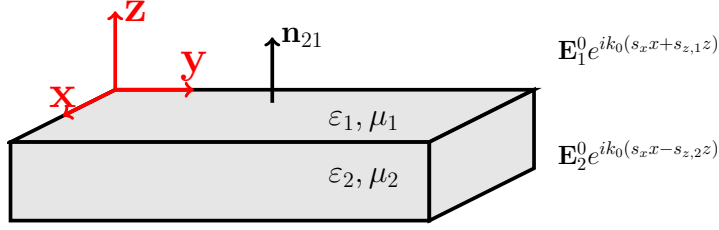
Figure 2.3: Geometry considered

2.4 INTRODUCTION TO SURFACES WAVES

In this chapter (and in Chapters 3 and 5), the surface waves will be added to the properties of the source. A surface wave is a type of electromagnetic wave which is propagated along the surface between two different media and is evanescent in the direction perpendicular to the surface $(\exp\left(-k_0\left|s_z\right|z\right))$. In particular, a surface plasmon polariton (SPP) can be understood as the coupling between a coherent electron oscillation and an electromagnetic wave [17, 18].

Let us analyze under which conditions SPPs can be excited. Thus, we shall consider the geometry of Fig. 2.3. This geometry consist of two different media characterized by their electric permittivity, and magnetic permeability values $\varepsilon_i\left(\omega\right)$, $\mu_i\left(\omega\right)$ $(i = 1, 2)$ respectively. The fields in these two media can be written as

$$
\begin{aligned}
\mathbf{E}_1\left(\mathbf{r}, \omega\right) &= \mathbf{E}_1^0 e^{ik_0\left(\mathbf{s}_\perp\boldsymbol{\rho}+s_{z,1}z\right)} & z > 0, & \qquad (2.3)\\
\mathbf{E}_2\left(\mathbf{r}, \omega\right) &= \mathbf{E}_2^0 e^{ik_0\left(\mathbf{s}_\perp\boldsymbol{\rho}-s_{z,2}z\right)} & z < 0, & \qquad (2.4)
\end{aligned}
$$

being $k_0 = \omega/c$ the wavenumber in free-space, c the speed of light in vacuum, $\boldsymbol{\rho}$ a two-dimensional position vector and $k_0 s_z$ the third component of the propagation vector $(k_0\mathbf{s} = k_0\left(\mathbf{s}_\perp, s_z\right) = (\mathbf{K}, k_z))$ which fulfills the relation

$$
s_{z,i}^2 = \varepsilon_i\mu_i - s_\perp^2, \qquad \mathrm{Im}\, s_{z,i} \geq 0. \qquad (2.5)
$$

On the other hand, across an interface, the electromagnetic field satisfies some continuity conditions. If we denote as $\mathbf{n}_{21}$ the unit normal vector to the interface directed from region 2 to region 1 (see Fig. 2.3), these conditions are:

$$
\begin{aligned}
\mathbf{n}_{21} \times \left(\mathbf{E}_2 - \mathbf{E}_1\right) &= 0, & \qquad (2.6a)\\
\mathbf{n}_{21} \times \left(\mathbf{H}_2 - \mathbf{H}_1\right) &= \frac{4\pi}{c}\mathbf{J}, & \qquad (2.6b)\\
\mathbf{n}_{21} \cdot \left(\mathbf{D}_2 - \mathbf{D}_1\right) &= 4\pi\sigma, & \qquad (2.6c)\\
\mathbf{n}_{21} \cdot \left(\mathbf{B}_2 - \mathbf{B}_1\right) &= 0. & \qquad (2.6d)
\end{aligned}
$$

In these equations $\mathbf{J}$ and σ are the electric current and the charge density at the interface respectively.

In order to discuss the behavior of surface waves, we will consider two different states of polarization: s- and p-polarization.

2.4.1 *s-polarization*

In *s*-polarization, the electric field is perpendicular to the plane (y, z), thus $\mathbf{E}_i \parallel \mathbf{u}_x$ $(i, = 1, 2)$. From Maxwell's equations (see Eqs. 1.50) and Eqs. (2.6a) and (2.6b) we obtain

$$E_{x,1}^0 - E_{x,2}^0 = 0, \tag{2.7}$$

$$\frac{s_{z,1}}{\mu_1} E_{x,1}^0 + \frac{s_{z,2}}{\mu_2} E_{x,2}^0 = 0, \tag{2.8}$$

respectively. For these equations the non-trivial solution is obtained if and only if $s_{z,1}\mu_2 + s_{z,2}\mu_1 = 0$. Using Eq. (2.5) the surface-wave dispersion relation is

$$k_0^2 s_\perp^2 \;=\; \left(\frac{\omega}{c}\right)^2 \frac{\mu_1 \mu_2 \left[\varepsilon_1 \mu_2 - \varepsilon_2 \mu_1\right]}{\mu_2^2 - \mu_1^2}, \tag{2.9}$$

where we have omitted the frequency dependence in ε_i, μ_i for brevity. Namely, for $\varepsilon_1 = \varepsilon_2 = \varepsilon$, Eq (2.9) leads to

$$K \;=\; \frac{\omega}{c} \sqrt{\frac{\mu_1 \mu_2}{\mu_2 + \mu_1}} \varepsilon. \tag{2.10}$$

Eq. (2.10) represents the dispersion relation for *s*-polarization. For non-magnetic media $\mu_2 + \mu_1 > 0$, then, there are no poles in Eq. (2.10), i.e. no surface waves are excited for *s*-polarization.

2.4.2 *p-polarization*

In *p*-polarization the electric field lies in the plane (y, z), thus $E_{x,i} = 0$. In a similar way to the previous section, from the continuity conditions, we obtain that at the interface

$$E_{y,1}^0 - E_{y,2}^0 = 0, \tag{2.11}$$

$$\varepsilon_1 E_{z,1}^0 - \varepsilon_2 E_{z,2}^0 = 0. \tag{2.12}$$

On the other hand, we apply the Maxwell equation $\nabla \cdot \mathbf{E} = 0$ to the two media

$$s_y E_{y,1}^0 + s_{z,1} E_{z,1}^0 \;=\; 0, \tag{2.13}$$

$$s_y E_{y,2}^0 + s_{z,2} E_{z,2}^0 \;=\; 0. \tag{2.14}$$

Using the two previous equations in order to write $E_{z,i}^0$ in terms of $E_{y,i}^0$, we can solve the system equations. Again, the non-trivial solution is obtained if and only if $s_{z,1}\varepsilon_2 + s_{z,2}\varepsilon_1 = 0$. The dispersion relation for *p*-polarization is

$$k_0^2 s_\perp^2 = \left(\frac{\omega}{c}\right)^2 \frac{\varepsilon_1 \varepsilon_2 \left[\mu_1 \varepsilon_2 - \mu_2 \varepsilon_1\right]}{\varepsilon_2^2 - \varepsilon_1^2}, \tag{2.15}$$

which is identical to Eq. (2.9) making the change $\varepsilon_i \leftrightarrow \mu_i$. If we consider $\mu_1 = \mu_2 = \mu$, Eq. (2.15) leads to

$$K = \frac{\omega}{c} \sqrt{\frac{\varepsilon_1 \varepsilon_2}{\varepsilon_2 + \varepsilon_1}} \mu \tag{2.16}$$

and for material-vacuum interfaces ($\varepsilon_1 = \mu_1 = 1$)

$$K = \frac{\omega}{c}\sqrt{\frac{\varepsilon_2}{\varepsilon_2 + 1}}. \tag{2.17}$$

Eq. (2.17) expresses the dispersion relation for a material-vacuum interface and shows that a SPP cannot be excited with a plane wave whose lateral component of the wavevector is such that $k_0 s_\perp \leq k_0$. Coupling of photons into SPPs can be achieved, for instance, using total internal reflection (TIR) with a prism. Under this condition $s_\perp$ can fulfill the condition $s_\perp > 1$, i.e., Eq. (2.5) is purely imaginary showing the evanescent character of the field along the z-direction.

2.5 CORRELATION EFFECTS AT SUBWAVELENGTH DISTANCES: EFFECT OF SURFACE PLASMON POLARITONS

Let us now address the interplay between SPPs and spatial coherence. To this end, let a planar source be statistically stationary and homogeneous. Its emission surface is the plane $z = 0$, where p-polarized fields excite plasmon polaritons (SPPs). Then the source cross-spectral density at frequency ω is [3]

$$W^{(0)}(\boldsymbol{\rho}_1, \boldsymbol{\rho}_2, \omega) = F(\boldsymbol{\rho}_1 - \boldsymbol{\rho}_2, \omega), \tag{2.18}$$

where $\boldsymbol{\rho}_1$ and $\boldsymbol{\rho}_2$ stand for two position vectors in the plane $z = 0$.

The spectrum of the light at a point $\boldsymbol{\rho}$ of the source plane is: $S^{(0)}(\boldsymbol{\rho}, \omega) = W^{(0)}(\boldsymbol{\rho}, \boldsymbol{\rho}, \omega) = F(0, \omega) = S^{(0)}(\omega)$, and the spectral degree of coherence is written down as

$$\mu^{(0)}(\boldsymbol{\rho}_1, \boldsymbol{\rho}_2, \omega) = F(\boldsymbol{\rho}_1 - \boldsymbol{\rho}_2, \omega)/S^{(0)}(\omega). \tag{2.19}$$

We shall assume that the source is also statistically isotropic. Let us choose it Gaussian correlated, so that

$$\begin{aligned} \mu^{(0)}(\boldsymbol{\rho}_1, \boldsymbol{\rho}_2, \omega) &= \mu^{(0)}(\boldsymbol{\rho}, \omega) \\ &= \exp[-\rho^2/2\sigma^2], \end{aligned} \tag{2.20}$$

where σ is the source coherence length and $\rho = |\boldsymbol{\rho}_1 - \boldsymbol{\rho}_2|$

The cross-spectral density of the field emitted by this source into the half space $z > 0$ is [19]

$$W(\mathbf{r}_1, \mathbf{r}_2, \omega) = k^2 \int G(k\mathbf{s}_\perp, \omega)e^{ik(\mathbf{s}\cdot\mathbf{r}_1 - \mathbf{s}^*\cdot\mathbf{r}_2)}\mathrm{d}^2 s_\perp, \tag{2.21}$$

where the angular spectrum G, corresponding to the Fourier transform of the limiting value of $W(\mathbf{r}_1, \mathbf{r}_2, \omega)$ at $z = 0$, is

$$G(k\mathbf{s}_\perp, \omega) = S^{(0)}(\omega)\tilde{\mu}^{(0)}(k\mathbf{s}_\perp, \omega)|A(k\mathbf{s}_\perp, \omega)|^2, \tag{2.22}$$

In Eq. (2.22) $\tilde{\mu}^{(0)}(k\mathbf{s}_\perp, \omega)$ must be substituted by the two-dimensional Fourier transform of $\mu^{(0)}(\boldsymbol{\rho}, \omega)$:

$$\tilde{\mu}^{(0)}(k\mathbf{s}_\perp, \omega) = (\sigma^2/2\pi)\exp[-(k\sigma s_\perp)^2/2], \tag{2.23}$$

where $s_\perp = \sqrt{s_x^2 + s_y^2}$. The unit vector $\mathbf{s} = (\mathbf{s}_\perp, s_z)$, $(\mathbf{s}_\perp = (s_x, s_y))$, has explicitly (see Eq. (2.5))

$$s_z = \sqrt{1 - s_\perp^2}, \qquad s_\perp^2 \leq 1, \tag{2.24}$$

$$s_z = i\sqrt{s_\perp^2 - 1}, \qquad s_\perp^2 > 1, \tag{2.25}$$

for propagating waves and for inhomogeneous (evanescent) components respectively. $A(k\mathbf{s}_\perp, \omega)$ stands for the p-polarization Fresnel coefficient, (either on reflection or on transmission) at $z = 0$. Notice that on writing the angular spectrum $e(\mathbf{s}_\perp, \omega)$ of the field propagated from the source into the half space $z > 0$ as: $e(\mathbf{s}_\perp, \omega) = e^{(0)}(\mathbf{s}_\perp, \omega)A(k\mathbf{s}_\perp, \omega)$, ($e^{(0)}(\mathbf{s}_\perp, \omega)$ represents the angular spectrum of the field emitted by the random source without reflection or transmission effects at any interface that it might content, and hence without plasmon polariton excitation), then on making use of Eq. (3.15) of [19] for $\left\langle e^{(0)}\left(\mathbf{s}_{1,\perp}\right) e^{(0)*}\left(\mathbf{s}_{2,\perp}\right)\right\rangle$ in the expression $G(k\mathbf{s}_\perp, \omega) = \langle e(\mathbf{s}_{1\perp}, \omega)e^*(\mathbf{s}_{2\perp}, \omega)\rangle$ of the angular spectrum of $W(\mathbf{r}_1, \mathbf{r}_2, \omega)$ (cf. Eqs. (3.6) and (3.7) of [19]), one readily obtains Eq. (2.22).

On considering Eqs. (2.19) and the Gaussian form of $\mu^{(0)}$, we shall write

$$S^{(0)}(\omega) = \mathcal{S}(\omega)/(2\pi\sigma^2), \tag{2.26}$$

to formally express that the source is δ-correlated when $\sigma \to 0$, so that $F(\boldsymbol{\rho}) \to \mathcal{S}(\omega)\delta^{(2)}(\boldsymbol{\rho})$ (This way of expressing correlation functions is customary in several studies of statistical fields, see e.g. Eqs. (2.13) and (3.4) of Refs. [20] (Section 6.3.2) and [21], respectively.); where $\delta^{(2)}$ represents the two-dimensional δ-function.

Also, $\tilde{F}(k\mathbf{s}_\perp, \omega) = S^{(0)}(\omega)\tilde{\mu}^{(0)}(k\mathbf{s}_\perp) \to \mathcal{S}(\omega)/(2\pi)^2$ when $\sigma \to 0$. $\mathcal{S}(\omega)$ is a positive quantity such that $\mathcal{S}(\omega) = \int F(\rho, \omega)\mathrm{d}^2\boldsymbol{\rho}$ for any σ.

We shall evaluate $W(\mathbf{r}_1, \mathbf{r}_2, \omega)$ at planes: $z = constant > 0$. It will now be useful to decompose Eq. (2.21) into the sum of the homogeneous and of the evanescent wave contributions: $W_h(\mathbf{r}_1, \mathbf{r}_2, \omega)$ and $W_e(\mathbf{r}_1, \mathbf{r}_2, \omega)$, respectively. Namely: $W(\mathbf{r}_1, \mathbf{r}_2, \omega) = W_h(\mathbf{r}_1, \mathbf{r}_2, \omega) + W_e(\mathbf{r}_1, \mathbf{r}_2, \omega)$. Then, using Eqs. (2.19)-(2.26) one has for the homogeneous part of $W(\mathbf{r}_1, \mathbf{r}_2, \omega)$:

$$\begin{aligned} W_h(\mathbf{r}_1, \mathbf{r}_2, \omega) &= W_h(\rho, z, \omega) \\ &= (k/2\pi)^2 \mathcal{S}(\omega) \int_{s_\perp^2 \leq 1} e^{-\frac{1}{2}(k\sigma s_\perp)^2}|A(k\mathbf{s}_\perp, \omega)|^2 e^{ik\mathbf{s}_\perp \cdot \boldsymbol{\rho}}\mathrm{d}^2 s_\perp. \end{aligned} \tag{2.27}$$

In a similar way, the evanescent wave contribution $W_e(\mathbf{r}_1, \mathbf{r}_2, \omega)$ is:

$$\begin{aligned} W_e(\rho, z, \omega) &= (k/2\pi)^2 \mathcal{S}(\omega) \int_{s_\perp^2 > 1} e^{-\frac{1}{2}(k\sigma s_\perp)^2}|A(k\mathbf{s}_\perp, \omega)|^2 \\ &\times e^{(ik\mathbf{s}_\perp \cdot \boldsymbol{\rho})}e^{-2k\sqrt{s_x^2 + s_y^2 - 1}z}\mathrm{d}^2 s_\perp. \end{aligned} \tag{2.28}$$

Let the random source surface be Gold. Choosing for instance the wavelength $\lambda = 2\pi/k = 495.9nm$, the permittivity is $\epsilon = -2.546 + i3.37$. The wavevector $k\mathbf{s}_\perp^{SPP} = \pm k[\epsilon/(\epsilon + 1)]^{1/2}$ corresponds to a pole of $A(k\mathbf{s}_\perp, \omega)$ [10, 17] that characterizes the SPP excited at $z = 0$.

Figs. 2.4(a) and 2.4(b) show $(2\pi/k)^2 \mathcal{S}(\omega)^{-1}W(\rho, z, \omega)$ versus ρ/λ at the two planes: $z = \lambda/20$ and 2λ, respectively, and for different values of σ. Notice that $(2\pi/k)^2 \times \mathcal{S}(\omega)^{-1}W_h(\rho, z, \omega)$ and
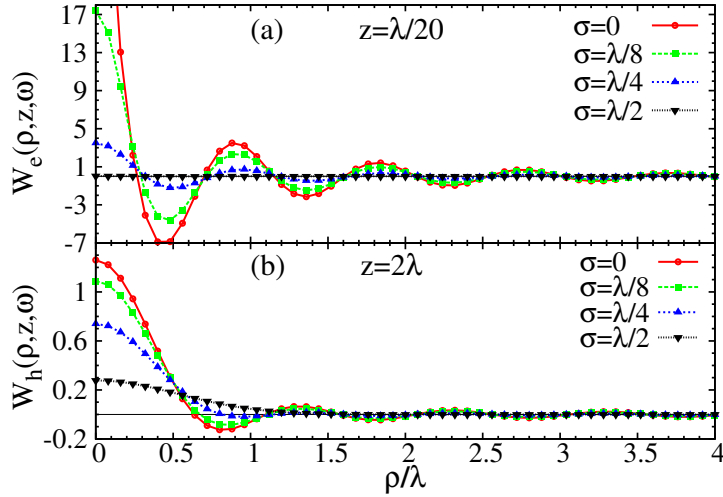
Figure 2.4: $(2\pi/k)^2 \mathcal{S}(\omega)^{-1} W(\rho, z, \omega)$, in arbitrary units (a.u.), versus ρ/λ at $\lambda = 495.9\,nm$, for different values of the source coherence length σ. (a) Evanescent part at the plane $z = \lambda/20$. The maximum normalized $W_e(0, \lambda/20, \omega)$ for $\sigma = 0$ is 52.1 a.u.. The normalized homogeneous part $W_h(0, \lambda/20, \omega)$ (not shown) is smaller than 1.2. (b) Homogeneous part at the plane $z = 2\lambda$. The normalized evanescent part $W_e(0, 2\lambda, \omega)$ (not shown) is smaller than 0.1.

$(2\pi/k)^2 \mathcal{S}(\omega)^{-1} W_e(\rho, z, \omega)$ are negligible in Fig. 2.4(a) and 2.4(b), respectively; and thus they are not represented. The reflection Fresnel coefficient is employed in all calculations, although similar results would be obtained by using the transmission coefficient. In Fig. 2.4(a), ($z = \lambda/20$), one sees a pure near-field effect on $W(\mathbf{r}_1, \mathbf{r}_2, \omega)$. An increase of σ diminishes the short range correlation of this normalized $W(\mathbf{r}_1, \mathbf{r}_2, \omega)$, (namely, the values of the central lobe at $\rho < \lambda/2$, which has subwavelength width up to $\sigma \simeq \lambda/4$). The increase of σ also diminishes the oscillating long range normalized correlation at $\rho > \lambda/2$. This is due to a decrease of the amplitude of the oscillations of $(2\pi/k)^2 \mathcal{S}(\omega)^{-1} W(\rho, z, \omega)$, contributed by the evanescent wave part of the angular spectrum, which in this case is concentrated in the vicinity of the angular frequencies: $\pm k \mathbf{s}_\perp^{SPP}$ of SPP excitation.

We anticipate that the large value of $(2\pi/k)^2 \mathcal{S}(\omega)^{-1} W(0, z, \omega)$ at $z \ll \lambda$ and as $\sigma \to 0$, is a manifestation of the contribution of the surface wave resonances to near field intensity enhancements. This was known for deterministic surfaces [17], but now [cf. Eq. (2.28)] we show it in the normalized spectral density close to the surface of a statistical source. All this is next shown.

We thus emphasize that, as seen in Fig. 2.4(a), *the amplitude of the oscillations of $W(\mathbf{r}_1, \mathbf{r}_2, \omega)$ have a subwavelength period for $z \ll \lambda$ and are maximum for δ-correlated sources.* On the other hand, these oscillations disappear when σ grows up to values about $\sigma = \lambda/2$ and larger; [as we shall next see, this is due to the then narrower low pass filter $(2\pi/k)^2 \mathcal{S}(\omega)^{-1} \tilde{F}(k\mathbf{s}_\perp, \omega) = \exp[-\frac{1}{2}(k\sigma s_\perp)^2]$ in the integrand of Eqs. (2.27) and (2.28)].

At larger z, (cf. Fig. 2.4(b) for $z = 2\lambda$) the main lobe of W becomes broader, as expected, and its width tends to a value which is not smaller than the well known value [3, 20]: $\lambda/2$, correspond-
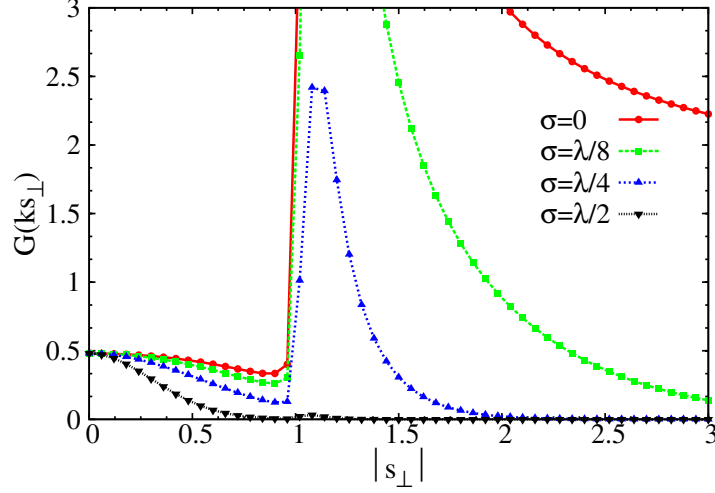
Figure 2.5: $(2\pi/k)^2 \mathcal{S}(\omega)^{-1} G(k\mathbf{s}_\perp, \omega)$, (a.u.), for a Gaussian correlated source with an Au surface. The effect of the SPP excitation is characterized by the peaks of the Fresnel reflection coefficient magnitude $|A(k\mathbf{s}_\perp)|^2$ in Eq. (2.22). The wavelength $\lambda = 495.9\,nm$ and the coherence lengths σ are the same as in Figs. 2.4(a) and 2.4(b). For $\sigma = 0$ and $\lambda/8$ the SPP peaks of G are 11.97 at $s_\perp^{SPP} = \pm 1.13$ and 8.10 at $s_\perp^{SPP} = \pm 1.12$, respectively. Notice that for $\sigma = 0$ this normalized angular spectrum coincides with $|A(k\mathbf{s}_\perp, \omega)|^2$

ing to the spatial resolution limit imposed by the evanescent wave filter $\exp(-2k\sqrt{s_x^2 + s_y^2 - 1}z)$ in Eq. (2.28); and which was established as the effective width of an incoherent (e.g. thermal) source from observations that, at the time, were not yet made in the near field region [3, 20]. Nevertheless, as remarked above, *the contribution of W_e to the subwavelength features of W, to its value $W(0, z, \omega)$, as well as to those values of W at large ρ/λ, not only decreases with the observation distance z, but also with an increase of the source coherence length σ.*

Fig. 2.5 illustrates the fundamentals of all these effects. There the normalized angular spectrum $(2\pi/k)^2 \mathcal{S}(\omega)^{-1} G(k\mathbf{s}_\perp, \omega) = \exp[-(k\sigma s_\perp)^2/2]\,|A(k\mathbf{s}_\perp, \omega)|^2$ is shown as a function of $s_\perp$. Notice that since the planar source has statistical isotropy, there is no preferential direction for $\mathbf{s}_\perp$ to excite the SPP, and hence this vector can be represented by its magnitude $s_\perp$ in the argument of $G(k\mathbf{s}_\perp, \omega)$. As seen in Fig. 2.5, the excitation of the SPPs is characterized by two high peaks of the factor $|A(k\mathbf{s}_\perp, \omega)|^2$ of Eq. (2.22) at $s_\perp = \pm s_\perp^{SPP}$ in the non radiative zone, whose height and width are larger and smaller, respectively, as the metal losses decrease. These two spikes, symmetrically situated with respect to $s_\perp = 0$, are responsible for the oscillations of $W(\rho, z, \omega)$ whose period in this ρ-variable of Fourier transformation, [cf. Eq. (2.28)], is inversely proportional to the peak separation: $2ks_\perp^{SPP} > 2k$, and hence is subwavelength as mentioned above; even though it is broadened by non-zero values of σ.

As σ increases, the width of the random wavefield normalized power spectrum $(2\pi/k)^2 \times \mathcal{S}(\omega)^{-1} \tilde{F}(k\mathbf{s}_\perp, \omega) = \exp[-(k\sigma s_\perp)^2)/2]$ diminishes until it obliterates the Fresnel coefficient contribution $|A|^2$, first in the evanescent region with a fast disappearance of the SPP peak contributions, and hence of the oscillations of $W(\mathbf{r}_1, \mathbf{r}_2, \omega)$; and then in the radiative region as σ increases further. In any case, *this increase of σ lowers the area enclosed by $(2\pi/k)^2 \mathcal{S}(\omega)^{-1} G(k\mathbf{s}_\perp, \omega)$*
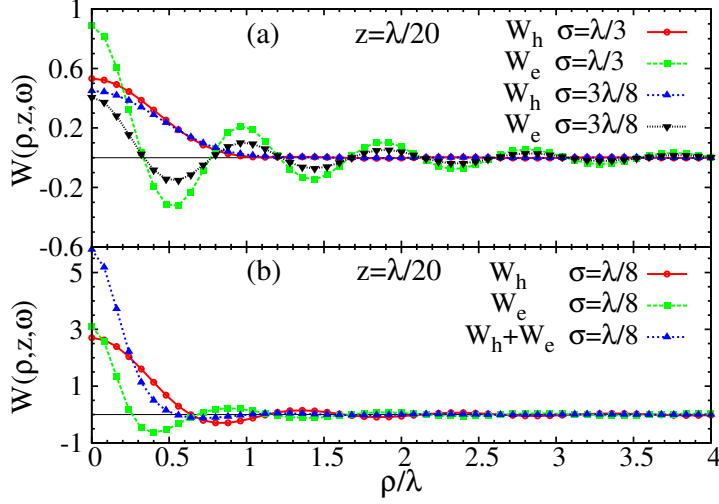
Figure 2.6: Homogeneous and evanescent parts of the normalized cross-spectral density $(2\pi/k)^2\mathcal{S}(\omega)^{-1}W(\rho,z,\omega)$ at $z = \lambda/20$, $\lambda = 495.9\,nm$. (a) $\sigma = \lambda/3$ and $3\lambda/8$. (b) $\sigma = \lambda/8$ but with no SPP excitation. Notice the subwavelength width of the main lobe of $W_e(\mathbf{r}_1,\mathbf{r}_2,\omega)$ when it dominates upon $W_h(\mathbf{r}_1,\mathbf{r}_2,\omega)$.

with the $s_\perp$-axis, as shown in Fig. 2.5, and hence *diminishes the normalized correlation value* $(2\pi/k)^2\mathcal{S}(\omega)^{-1}W(0,z,\omega)$, *while it broadens the main central lobe of* $(2\pi/k)^2\mathcal{S}(\omega)^{-1}W(\rho,z,\omega)$, [cf. Figs. 2.4(a) and 2.4(b)]. As mentioned before, this means a decrease of the enhancement of the normalized spectrum of the emitted near field, and even its eventual disappearance.

It should be remarked in this connection that for $z \ll \lambda$, W_e is dominant for very small σ, while it approximately equals the contribution of W_h for $\lambda/4 < \sigma < \lambda/3$. From $\sigma \simeq \lambda/2$ onwards, W_h is dominant even for $z \ll \lambda$. Fig. 2.6(a) illustrates this for instance at $z = \lambda/20$. There one sees that $W_e(\mathbf{r}_1,\mathbf{r}_2,\omega) = W_h(\mathbf{r}_1,\mathbf{r}_2,\omega)$ near $\sigma = 3\lambda/8$. If there were no plasmon polariton excitation, and hence no peaks in the angular spectrum G, one can guess from Fig. 2.5 that the much lower value $\sigma \simeq \lambda/8$ would not be far from that at which the contribution of $W_h(\mathbf{r}_1,\mathbf{r}_2,\omega)$ and $W_e(\mathbf{r}_1,\mathbf{r}_2,\omega)$ would be comparable. This is shown in Fig. 2.6(b) at $z = \lambda/20$.

2.6 CONCLUSIONS

In this chapter I have analyzed the effects of SPPs excitation on the surface of a statistically homogeneous source. To this end, we have introduced the concept of surface waves. Then, we have focused on the role of the coherence length σ in the correlation properties of the emitted field. We have addressed the long range correlation at near-field distances due to the non-radiative part of the angular spectrum. We have also shown and analyzed that an increase of σ in the statistically properties of the source leads to a decrease on the correlation, losing the subwalength character of these oscillations.

3

DEGREE OF POLARIZATION: FROM ITS DEFINITION IN TWO DIMENSIONS TO THAT CONTROVERSIAL IN THREE DIMENSIONS

3.1 MOTIVATION

nce we have seen the change on propagation of the cross-spectral density $W(\mathbf{r}_1, \mathbf{r}_2, \omega)$ in the near-field, I will turn to study the effects of the spatial coherence on the degree of polarization (DOP) in this regime. However, the degree of polarization in the near-field is a not resolved problem because there is not only one definition.

Thus, after a general outline, in Section 3.3, I will introduce the usual concept of degree of polarization for two-dimensional fields and the equivalent ways of defining it. In Chapter 2 we did not need a vector theory of electromagnetic coherence, however, to discuss the degree of polarization we must take into account the different components of the fluctuating electromagnetic field.

Secondly in Section 3.4, I will examine in detail the controversy between two definitions on the DOP for three-dimensional fields found in the literature. Nevertheless, I am obliged to mention that the definitions we have used here are not unique, there are others that should be mentioned [22, 23]. In that section I will try to discuss the definitions that are used more frequently in optics. I will extend the statistically homogeneous model used for sources in Chapter 2 for electromagnetic fields rather than for a scalar wavefield.

3.2 INTRODUCTION

The *degree of polarization* gives us information about the portion of light which is polarized [3]. This quantity is well-defined in 2-D fields like beams, then the field can be considered planar, hence, the DOP can be written in terms of a 2×2 coherence matrix $W_{ij}(\mathbf{r}_1, \mathbf{r}_2, \omega) = \langle E_i^*(\mathbf{r}_1, \omega) E_j(\mathbf{r}_2, \omega) \rangle$ with $i, j = 1, 2 = x, y$ [3, 24]. Section 3.3 deals with this definition.

Nevertheless, in the near field a two-dimensional formalism is not enough, we need to introduce a third index in order to take the z-fluctuations of the field into account. Then, we have to define a new degree of polarization in terms of a 3×3 coherence matrix

To this end, a three-dimensional formalism was introduced by references [25, 26]. However a unique definition of a 3-D DOP is not at all trivial. This difficulty comes from the fact that the 3×3 coherence matrix cannot be written as a sum of a completely polarized and an unpolarized field matrix [25], arising two main controversial definitions [25–29]

What follows is an overview about the two-dimensional degree of polarization which will help us to understand this concept.

3.3 TWO-DIMENSIONAL DEGREE OF POLARIZATION FOR PLANAR FIELDS.

Throughout this section the DOP will be understood as a consequence of a 2-D electromagnetic field $\mathbf{E} = (E_x, E_y)$. Hence, as we have commented in the Introduction 3.2, for planar fields $(i, j = x, y)$, there is a consensus on the definition of the degree of polarization. For two-dimensional random fields, the coherence matrix $W_{ij}(\mathbf{r}_1, \mathbf{r}_2, \omega)$ at the same point, $\mathbf{r}_1 = \mathbf{r}_2 = \mathbf{r}$, can be expressed as a sum of two matrices: one of which represents a state of total polarization $(P = 1)$ and the other being the opposite case of totally unpolarized wavefield $(P = 0)$ [3]

$$W_{ij}(\mathbf{r}, \mathbf{r}, \omega) = W_{ij}^{unpol}(\mathbf{r}, \mathbf{r}, \omega) + W_{ij}^{pol}(\mathbf{r}, \mathbf{r}, \omega), \quad (i, j = x, y), \tag{3.1}$$

where

$$W_{ij}^{unpol}(\mathbf{r}, \mathbf{r}, \omega) = A \begin{pmatrix} 1 & 0 \\ 0 & 1 \end{pmatrix}, \quad W_{ij}^{pol}(\mathbf{r}, \mathbf{r}, \omega) = \begin{pmatrix} B & D \\ D^* & C \end{pmatrix}, \tag{3.2}$$

being $A, B, C \geq 0$ and $BC - DD^* = 0$ [3]. From Eqs. (3.1) and (3.2) is easy to see that

$$W_{xx}(\mathbf{r}, \mathbf{r}, \omega) = A + B, \tag{3.3a}$$

$$W_{yy}(\mathbf{r}, \mathbf{r}, \omega) = A + C, \tag{3.3b}$$

$$W_{xy}(\mathbf{r}, \mathbf{r}, \omega) = D, \tag{3.3c}$$

$$W_{yx}(\mathbf{r}, \mathbf{r}, \omega) = D^*. \tag{3.3d}$$

Taking into account these equations one can readily express the values of the coefficients A, B, C in terms of the elements of the cross-spectral density matrix, i.e., [3]

$$A = \frac{1}{2} \left[\text{Tr} W_{ij} \pm \left[(\text{Tr} W_{ij})^2 - 4 \det W_{ij} \right]^{1/2} \right], \tag{3.4a}$$

$$B = \frac{1}{2}(W_{xx} - W_{yy}) + \frac{1}{2} \left[(\text{Tr} W_{ij})^2 - 4 \det W_{ij} \right]^{1/2}, \tag{3.4b}$$

$$C = \frac{1}{2}(W_{yy} - W_{xx}) + \frac{1}{2} \left[(\text{Tr} W_{ij})^2 - 4 \det W_{ij} \right]^{1/2}, \tag{3.4c}$$

where we have omitted the dependence on the position and on the frequency for brevity. It follows from Eqs. (3.4) and Eq. (3.2) that the trace of polarized portion of the light W_{ij}^{pol} is given by

$$\text{Tr} W_{ij}^{pol}(\mathbf{r}, \mathbf{r}, \omega) = \left[(\text{Tr} W_{ij}(\mathbf{r}, \mathbf{r}, \omega))^2 - 4 \det W_{ij}(\mathbf{r}, \mathbf{r}, \omega) \right]^{1/2}. \tag{3.5}$$

The degree of polarization can be expressed as the ratio of the intensity of the polarized part (trace of W_{ij}^{pol}) to the total intensity of the electromagnetic field (trace of W_{ij}), giving the classical definition of DOP for planar fields

$$P\left(\mathbf{r},\omega\right) = \frac{\mathrm{Tr}W_{ij}^{pol}\left(\mathbf{r},\mathbf{r},\omega\right)}{\mathrm{Tr}W\left(\mathbf{r},\mathbf{r},\omega\right)} = \left[1 - \frac{4\det W_{ij}\left(\mathbf{r},\mathbf{r},\omega\right)}{\left(\mathrm{Tr}W_{ij}\left(\mathbf{r},\mathbf{r},\omega\right)\right)^2}\right]^{1/2}, \tag{3.6}$$

where this quantity is bounded between 0 and 1, corresponding to the cases of an unpolarized and polarized fields, respectively. Notice that this definition is invariant under a unitary transformation.

3.3.1 *Two-dimensional degree of polarization in terms of the eigenvalues*

There is a second way to express the value of P. Due to the hermiticity of the cross-spectral density W_{ij}, one can find a basis of vectors where the coherence matrix is diagonal. Hence, from the definition of DOP (c.f. Eq. (3.6)), it is straightforward to demonstrate that $P\left(\mathbf{r},\omega\right)$ can be written as

$$P\left(\mathbf{r},\omega\right) = \left|\frac{\lambda_1 - \lambda_2}{\lambda_1 + \lambda_2}\right|, \tag{3.7}$$

being λ_1, λ_2 the real and non-negative eigenvalues of the coherence matrix. The representation of $P\left(\mathbf{r},\omega\right)$ in terms of the eigenvalues will be used in the rest of the sections of this chapter for the case of arbitrary 3D electromagnetic fields.

3.3.2 *Two-dimensional degree of polarization in terms of the Stokes parameters: the Poincaré sphere*

A more visual way to express the different states of the polarization is writing the DOP as a linear combination of the 2×2 unit matrix and the three Pauli matrices σ_j $(j = 1, \ldots, 3)$, being the coefficients the four Stokes parameters S_j, $(j = 0, \ldots, 3)$

$$\overset{\leftrightarrow}{W}\left(\mathbf{r},\mathbf{r},\omega\right) = \sum_{j=0}^{3} S_j\left(\mathbf{r},\mathbf{r},\omega\right)\sigma_j, \tag{3.8}$$

where we have written $\overset{\leftrightarrow}{W}\left(\mathbf{r},\mathbf{r},\omega\right)$ representing the coherence matrix $W_{ij}\left(\mathbf{r},\mathbf{r},\omega\right)$ in order to avoid confusion in the notation of Pauli matrices. In Eq. (3.8) the Stokes parameters are expressed in terms of the elements of $W_{ij}\left(\mathbf{r},\mathbf{r},\omega\right)$ as

$$\begin{align}
S_0 &= W_{xx}\left(\mathbf{r},\mathbf{r},\omega\right) + W_{yy}\left(\mathbf{r},\mathbf{r},\omega\right), \tag{3.9a} \\
S_1 &= W_{xx}\left(\mathbf{r},\mathbf{r},\omega\right) - W_{yy}\left(\mathbf{r},\mathbf{r},\omega\right), \tag{3.9b} \\
S_2 &= W_{xy}\left(\mathbf{r},\mathbf{r},\omega\right) + W_{yx}\left(\mathbf{r},\mathbf{r},\omega\right), \tag{3.9c} \\
S_3 &= i\left(W_{yx}\left(\mathbf{r},\mathbf{r},\omega\right) + W_{xy}\left(\mathbf{r},\mathbf{r},\omega\right)\right), \tag{3.9d}
\end{align}$$
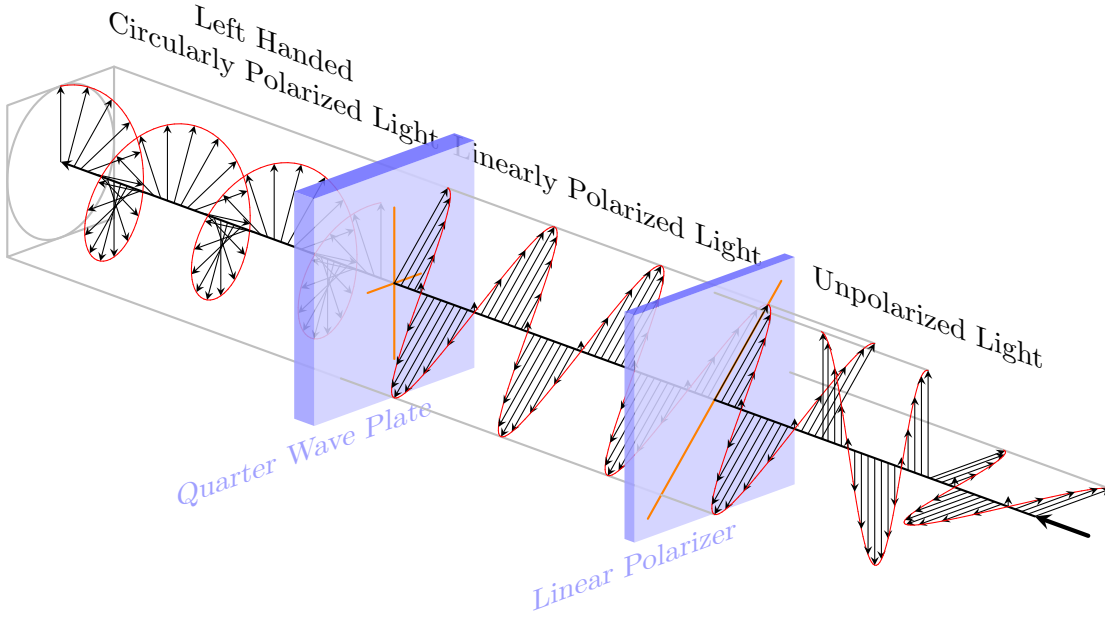
Figure 3.1: Three-dimensional view of polarization states. This figure is based on (see this link: http://tex.stackexchange.com/questions/113900/draw-polarized-light)

and vice-versa as

$$W_{xx}(\mathbf{r},\mathbf{r},\omega) = \frac{1}{2}(S_0 + S_1), \tag{3.10a}$$

$$W_{yy}(\mathbf{r},\mathbf{r},\omega) = \frac{1}{2}(S_0 - S_1), \tag{3.10b}$$

$$W_{xy}(\mathbf{r},\mathbf{r},\omega) = \frac{1}{2}(S_2 + iS_3), \tag{3.10c}$$

$$W_{yx}(\mathbf{r},\mathbf{r},\omega) = \frac{1}{2}(S_2 - iS_3), \tag{3.10d}$$

where the first Stokes parameter S_0 represents the total intensity ($S_0 = \mathrm{Tr}W_{ij}(\mathbf{r},\mathbf{r},\omega)$). On substituting from these formulas into Eq. (3.6), we obtain the expression for the DOP in term of the Stokes parameters

$$P(\mathbf{r},\omega) = \frac{\left(S_1^2 + S_2^2 + S_3^2\right)^{1/2}}{S_0}. \tag{3.11}$$

If the field is completely polarized, i.e, $P(\mathbf{r},\omega) = 1$ we have

$$S_0^2 = S_1^2 + S_2^2 + S_3^2, \tag{3.12}$$

however, if the optical field is partially polarized, $S_1^2 + S_2^2 + S_3^2$ represents the part of $P(\mathbf{r},\omega)$ that is completely polarized, i.e., $S_1^2 + S_2^2 + S_3^2 < 1$ and $S_0^2 \neq S_1^2 + S_2^2 + S_3^2$. In this case, the Stokes parameters are generally normalized to the total intensity S_0

$$s_1 = \frac{S_1}{S_0}, \quad s_2 = \frac{S_2}{S_0}, \quad s_1 = \frac{S_3}{S_0}. \tag{3.13}$$

According to Eq. (3.11), the DOP is

$$P(\mathbf{r},\omega) = \left(s_1^2 + s_2^2 + s_3^2\right)^{1/2}. \tag{3.14}$$
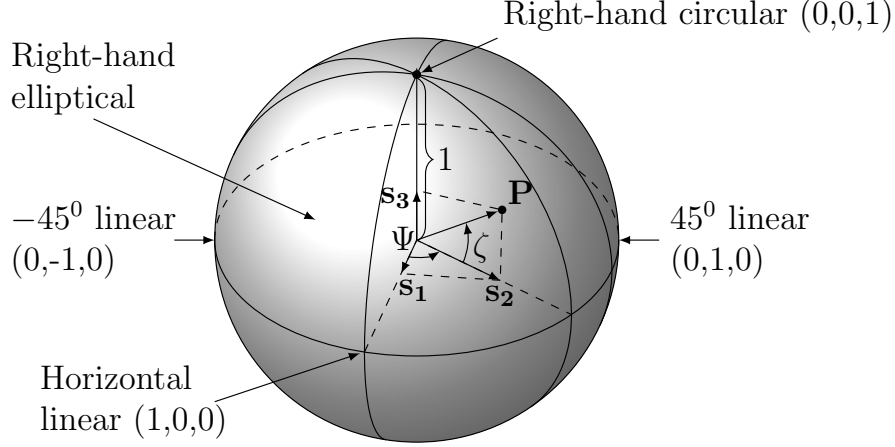
Figure 3.2: Representation of a normalized Stokes vector and different states of polarization.

It is intuitive to see that equation (3.14) represents a sphere of radius equal to the degree of polarization, therefore any polarization state can be drawn using the unit vector $\mathbf{s} = (s_1, s_2, s_2)$. If the field is fully polarized, the normalized Stokes vector endpoint is on a sphere with unit radius. This sphere is usually denoted as *Poincaré sphere*. On the other hand, if the field is not fully polarized, the Stokes vector endpoint will be inside the sphere and the length of the vector will be P.

In order to represent the vector $\mathbf{s}$ in spherical polar coordinates we introduce the azimuthal angle Ψ $(0 < \Psi < 2\pi)$ and the polar angle ζ $(-\pi/2 < \zeta < \pi/2)$ (see Fig. 3.2). With these variables the vector $\mathbf{s}$ can be expressed as

$$s_1 = |s| \cos \zeta \cos \Psi, \tag{3.15a}$$

$$s_2 = |s| \cos \zeta \sin \Psi, \tag{3.15b}$$

$$s_3 = |s| \sin \zeta. \tag{3.15c}$$

With this representation, each state of polarization is represented by a specific point on the Poincaré sphere. Some of them are represented in Fig. 3.2. For example, for a value of $\zeta = 90^o$, $s_1 = s_2 = 0$ and $s_3 = |s|$, the Poincaré vector represent a circular polarization state, therefore, the North and the South Poles of the sphere represent right and left circular polarization, respectively. When the Poincaré vector lies in the equator of the sphere $(s_3 = 0)$, linear states of polarization are represented.

3.4 THREE-DIMENSIONAL DEGREE OF POLARIZATION

In this section I will address the problem of the DOP for three-dimensional electromagnetic fields $\mathbf{E} = (E_x, E_y, E_z)$, hence, $P(\mathbf{r}, \omega)$ has to be redefined in order to consider E_z.

Under this consideration, I will focus on two definitions adopted by Setälä et al. [25] and by Ellis et al.[26], that will be denoted by P_S and P_E, respectively. Both have led to a scientific

debate on their merits [28, 29] not yet settled. Whereas the justification of P_S is based on the generalized Stokes parameters in 3-D [25], P_E is defined as the rate of a total polarized and of a totally unpolarized field [26] as the usual way (see. Eq. (3.6)). When the 3-D electromagnetic field components oscillates equally in the three directions, both definitions converge to zero (like the 2-D field, being $\lambda_1 = \lambda_2$ in Eq. (3.7)), however, if the field is 2-D and it oscillates in the xy plane, the formalism of Setälä et al. establishes that the field cannot be completely unpolarized, since then $1/2 \leq P_S \leq 1$; however the definition by Ellis et al. recovers the usual one for planar fields with $0 \leq P_E \leq 1$[3].

The aim of this section is demonstrating that, for the wide variety of statistically homogeneous sources (cf. Section 2.3), those two definitions are identical when either the source coherence length tends to zero or when the field is considered at subwavelength distance from the source in such a way that it tends to zero as this coherence length increases. We will also address excitation of surface plasmon polaritons on the source [11, I], showing that they enlarge those ranges of equality of both DOP definitions.

Let us consider a planar source at $z = 0$, emitting a quasi-monochromatic random electric field at frequency ω into the space $z \geq 0$. We shall express it as an angular wave spectrum of plane waves [3, 10]

$$\mathbf{E}\left(\mathbf{r}, \omega\right) = \int_{-\infty}^{\infty} \mathbf{e}\left(k\mathbf{s}_\perp, \omega\right) e^{ik\mathbf{s}\cdot\mathbf{r}} \mathrm{d}^2 \mathbf{s}_\perp, \tag{3.16}$$

where the propagation vector $\mathbf{k} = k\mathbf{s} = k\left(\mathbf{s}_\perp, s_z\right)$ is defined in Eq. (2.25) of the previous chapter. The angular amplitude $\mathbf{e}\left(k\mathbf{s}_\perp, \omega\right)$ is the Fourier inverse of the limiting value of the electric vector at $z = 0$ (see Section 1.5).

We assume that the source is statistically homogeneous, i.e. the cross-spectral density tensor at $z = 0$ only depends on the position $\boldsymbol{\rho}_i$ $(i = 1, 2)$ trough the difference $\boldsymbol{\rho}_1 - \boldsymbol{\rho}_2$. Hence, the angular correlation tensor is expressed as [16]

$$
\begin{aligned}
\mathcal{A}_{ij}\left(k\mathbf{s}_\perp, k\mathbf{s}'_\perp, \omega\right) &= \left\langle e_i^*\left(k\mathbf{s}_\perp, \omega\right) e_j\left(k\mathbf{s}'_\perp, \omega\right)\right\rangle \\
&= k^2 \tilde{\mathcal{E}}_{ij}\left(k\mathbf{s}_\perp, k\mathbf{s}'_\perp, \omega\right) \\
&= k^4 \delta^{(2)}\left[k\left(\mathbf{s}_\perp - \mathbf{s}'_\perp\right)\right] \mathcal{E}_{ij}^{(0)}\left[\frac{k}{2}\left(\mathbf{s}_\perp + \mathbf{s}'_\perp\right)\right],
\end{aligned}
\tag{3.17}
$$

where $\delta^{(2)}$ is the two-dimensional Dirac delta function and $\tilde{\mathcal{E}}_{ij}\left(k\mathbf{s}_\perp, k\mathbf{s}'_\perp, \omega\right)$ is the four dimensional Fourier transform of $\mathcal{E}_{ij}^{(0)}\left(\boldsymbol{\rho}_1, \boldsymbol{\rho}_2, \omega\right)$. Thus, the cross-spectral density tensor at $\mathbf{r}_1 = \mathbf{r}_2 = \mathbf{r}$ is

$$W_{ij}\left(\mathbf{r}, \mathbf{r}, \omega\right) = k^2 \int_{-\infty}^{\infty} \tilde{\mathcal{E}}_{ij}\left(k\mathbf{s}_\perp, \omega\right) e^{ik(s_z - s_z^*)z} \mathrm{d}^2 \mathbf{s}_\perp. \tag{3.18}$$

Notice, that Eq. (3.18) is the same as Eq. (2.21) if we write $\mathbf{r}_1 = \mathbf{r}_2 = \mathbf{r}$, however, the difference is given by the electromagnetic formulation used in this chapter. We shall decompose the angular amplitude $\mathbf{e}\left(k\mathbf{s}_\perp, \omega\right)$ into s and p polarized modes [31]:

$$\mathbf{e}\left(k\mathbf{s}_\perp, \omega\right) = e_s\left(k\mathbf{s}_\perp, \omega\right) \hat{\mathbf{s}} + e_p\left(k\mathbf{s}_\perp, \omega\right) \hat{\mathbf{p}}, \tag{3.19}$$

where the caret denotes a unit vector and $\hat{\mathbf{s}} = \hat{\mathbf{s}}_\perp \times \hat{z}$ and $\hat{\mathbf{p}} = |\mathbf{s}_\perp| \hat{z} + s_z \hat{\mathbf{s}}_\perp$. Remark that $\mathbf{e}(k\mathbf{s}_\perp) \cdot \mathbf{s} = \hat{\mathbf{s}} \cdot \hat{\mathbf{p}} = 0$. Hence, in terms of these modes the angular correlation tensor is written as

$$
\begin{aligned}
\tilde{\mathcal{E}}_{ij}(k\mathbf{s}_\perp, \omega) &= \mathcal{A}_{ss}(k\mathbf{s}_\perp, \omega)\, \hat{s}_i \hat{s}_j + \mathcal{A}_{pp}(k\mathbf{s}_\perp, \omega)\, \hat{p}_i^* \hat{p}_j \\
&+ \mathcal{A}_{sp}(k\mathbf{s}_\perp, \omega)\, \hat{s}_i \hat{p}_j + \mathcal{A}_{ps}(k\mathbf{s}_\perp, \omega)\, \hat{p}_i^* \hat{s}_j,
\end{aligned}
\tag{3.20}
$$

being $\mathcal{A}_{mn} = \langle e_m^*(k\mathbf{s}_\perp, \omega) e_n(k\mathbf{s}_\perp, \omega) \rangle$, $(m, n = s, p)$. For a statistically homogeneous, and also isotropic, source $(W_{ij}^{(0)}(\mathbf{r}_1, \mathbf{r}_2, \omega) = \mathcal{E}_{ij}^{(0)}(|\boldsymbol{\rho}_1 - \boldsymbol{\rho}_2|, \omega))$, the symmetry of this tensor implies that $\mathcal{A}_{ij} = 0$ if $i \neq j$ and $\mathcal{A}_{ss} = \mathcal{A}_{pp} = \mathcal{A}$ [32], thus

$$
\tilde{\mathcal{E}}_{ij}(k\mathbf{s}_\perp, \omega) = \mathcal{A}(k\mathbf{s}_\perp, \omega)\,(\hat{s}_i \hat{s}_j + \hat{p}_i^* \hat{p}_j).
\tag{3.21}
$$

Now we can calculate the 3×3 coherence matrix at $\mathbf{r}_1 = \mathbf{r}_2 = \mathbf{r}$. Substituting Eq. (3.21) into Eq. (3.18) and employing cylindrical coordinates: $s_x = s_\perp \cos\phi$, $s_y = s_\perp \sin\phi$ to perform the integral, one sees after integration in the azimuthal variable ϕ that the non-diagonal elements are zero, i.e. $W_{ij}(\mathbf{r}, \mathbf{r}, \omega) = 0$ if $i \neq j$ and $W_{xx} = W_{yy} \neq W_{zz}$. Hence the cross-spectral density at $\mathbf{r}_1 = \mathbf{r}_2 = \mathbf{r}$ is diagonal, viz.

$$
W_{ij}(\mathbf{r}, \mathbf{r}, \omega) = \begin{pmatrix} W_{xx} & 0 & 0 \\ 0 & W_{xx} & 0 \\ 0 & 0 & W_{zz} \end{pmatrix}.
\tag{3.22}
$$

We next address the two definitions of the DOP of the emitted field, namely:

$$
P_S(\mathbf{r}, \omega) = \frac{\sqrt{(\lambda_1 - \lambda_2)^2 + (\lambda_1 - \lambda_3)^2 + (\lambda_2 - \lambda_3)^2}}{\sqrt{2}(\lambda_1 + \lambda_2 + \lambda_3)},
\tag{3.23}
$$

and

$$
P_E(\mathbf{r}, \omega) = \frac{\lambda_1' - \lambda_2'}{\lambda_1' + \lambda_2' + \lambda_3'}.
\tag{3.24}
$$

In 3-D both quantities are bounded by 0 and 1. λ_1, λ_2 and λ_3 are the eigenvalues of the diagonal coherence matrix (3.22) which directly are W_{xx}, W_{yy} and W_{zz}, respectively. Moreover, Eq. (3.22) conveys that $\lambda_1 = \lambda_2$. On the other hand, λ_1', λ_2' and λ_3' are also the eigenvalues of the coherence matrix but ordered such that $\lambda_1' \geq \lambda_2' \geq \lambda_3'$. We distinguish two cases: (i) When $\lambda_1 > \lambda_3$ then $\lambda_1' = \lambda_1 = \lambda_2' = \lambda_2$ and $\lambda_3' = \lambda_3$, then one sees from (3.23) and (3.24) that $P_S = \frac{\lambda_1 - \lambda_3}{2\lambda_1 + \lambda_3}$ and $P_E = 0$. (ii) When $\lambda_3 > \lambda_1$ then $\lambda_1' = \lambda_3$ and $\lambda_3' = \lambda_1 = \lambda_2' = \lambda_2$; in this case the 3-D P_S and P_E are identical and equal to $\frac{\lambda_3 - \lambda_1}{2\lambda_1 + \lambda_3}$. Notice that when $\lambda_1 = \lambda_3$, (which of course also means that $\lambda_2 = \lambda_3$), both definitions coincide being zero and hence describing completely unpolarized fields.

In Chapter 2 we have demonstrated the sub-diffraction-limited coherence lengths in near-field. In particular, for thermal (δ-correlated) sources, the coupling of SPPs implies a high polarization of the emitted field [33], however, the spatial coherence of the source will play an important role as we have demonstrated for the correlation function[I].

Hence, in order to see the effects of the coherence length of the source, of permittivity $\varepsilon = \varepsilon' + i\varepsilon''$, in the three-dimensional DOP, we consider the field transmission through its boundary
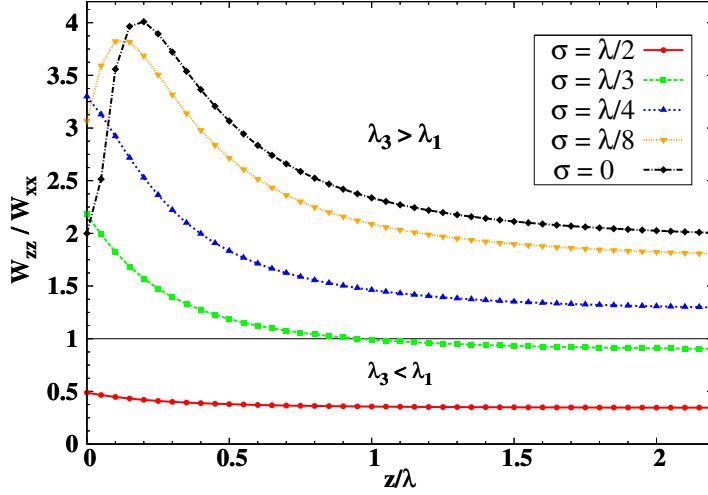
Figure 3.3: $W_{zz}\left(\mathbf{r},\mathbf{r},\omega\right)/W_{xx}\left(\mathbf{r},\mathbf{r},\omega\right)$ versus distance from the source, (in units of wavelength λ), for different values of the coherence length σ. The calculations are done at $\lambda = 500\,\mathrm{nm}$, $(\varepsilon = 4.2 + i18.1)$.

surface $z = 0$ by addressing the Fresnel coefficients for s and p modes. From Eqs. (3.18) and (3.21) the expression of the cross-spectral density $W_{ij}\left(\mathbf{r},\mathbf{r},\omega\right)$ is

$$W_{ij}(\mathbf{r},\mathbf{r},\omega) = k^2 \int_{-\infty}^{\infty} \mathcal{A}(k\mathbf{s}_\perp,\omega)(s_i s_j |t_s|^2 + p_i^* p_j |t_p|^2) e^{ik(s_z - s_z^*)z} d^2 \mathbf{s}_\perp, \qquad (3.25)$$

where $t_s\left(\mathbf{s}_\perp\right)$ and $t_p\left(\mathbf{s}_\perp\right)$ are the Fresnel transmission coefficients for s and p polarizations respectively, (cf. also [I]). The dielectric-vacuum interface supports SPPs when $\varepsilon' < 1$; they propagate along the surface with a wave vector $k\mathbf{s}_\perp^{spp}$. Only for p-polarization have the Fresnel coefficients a pole at $k\mathbf{s}_\perp^{spp} = \pm k\sqrt{\varepsilon/(\varepsilon + 1)}$ (see dispersion relation given by Eq. (2.17))

We shall consider a source with $\mathcal{E}^{(0)}\left(\rho,\omega\right) = \exp\left(-\rho^2/2\sigma^2\right)/2\pi\sigma^2$, where $\rho = |\boldsymbol{\rho}_1 - \boldsymbol{\rho}_2|$ and σ is the *source coherence length*, then the 2-D Fourier transform of $\mathcal{E}^{(0)}\left(\rho,\omega\right)$ is given by $\mathcal{A}\left(k\mathbf{s}_\perp\right) = \exp\left(-(k\sigma s_\perp)^2/2\right)$ (cf. Eq. (2.20)). Figure 3.3 shows $W_{zz}\left(\mathbf{r},\mathbf{r},\omega\right)/W_{xx}\left(\mathbf{r},\mathbf{r},\omega\right) = \lambda_3/\lambda_1$, [which by Eq. (3.22) is the same as $W_{zz}\left(\mathbf{r},\mathbf{r},\omega\right)/W_{yy}\left(\mathbf{r},\mathbf{r},\omega\right) = \lambda_3/\lambda_2$], for different values of σ. The horizontal line at the unity value of the ordinate divides the plot into two regimes according to whether $W_{zz}\left(\mathbf{r},\mathbf{r},\omega\right)/W_{xx}\left(\mathbf{r},\mathbf{r},\omega\right)$ is smaller or larger than 1. Evidently these two regions correspond to the two above discussed cases: (i) and (ii), respectively. One observes that when σ approaches zero $W_{zz}\left(\mathbf{r},\mathbf{r},\omega\right)/W_{xx}\left(\mathbf{r},\mathbf{r},\omega\right) \geq 1$, which corresponds to case (ii) and hence both definitions P_S and P_E tend to be equivalent. However, as one moves beyond one wavelength away from the source, and thus the contribution of evanescent waves disappears, one approaches case (i), the two definitions P_S and P_E tend to differ from each other, more markedly the larger σ is, and to be constantly equal to their far zone values for any σ, except for those sources with σ very small or zero for which the ratio λ_3/λ_1 tends to 1, or close to it, then both P_S and P_E are close to 0 so that the emitted field becomes completely unpolarized. On the other hand, as σ grows to $\lambda/2$ and above, the contribution of evanescent waves tend to appear at progressively extremely shorter distances from the source plane and the ratio λ_3/λ_1 approaches zero, which means that P_S tends to $1/2$ while $P_E = 0$. In this respect, we see the crucial role played by the
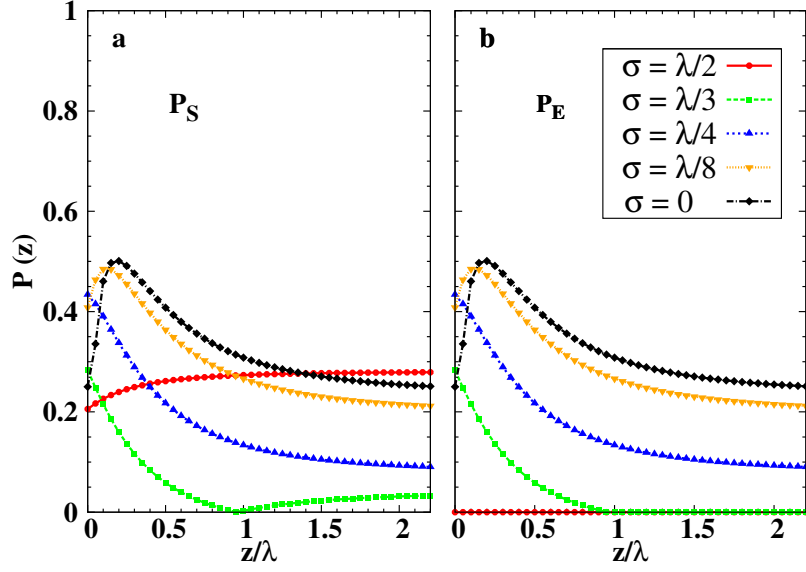
Figure 3.4: Degree of polarization versus distance to the source for the two definitions: a) Setälä et al. definition P_S, b) Ellis et al. definition P_E, for different values of the coherence length σ of the source. Calculations of W are done at $\lambda = 500$ nm ($\varepsilon = 4.2 + i18.1$).

coherence length of the source, analogously to that observed in correlation effects of the near field (cf. Chapter 2).
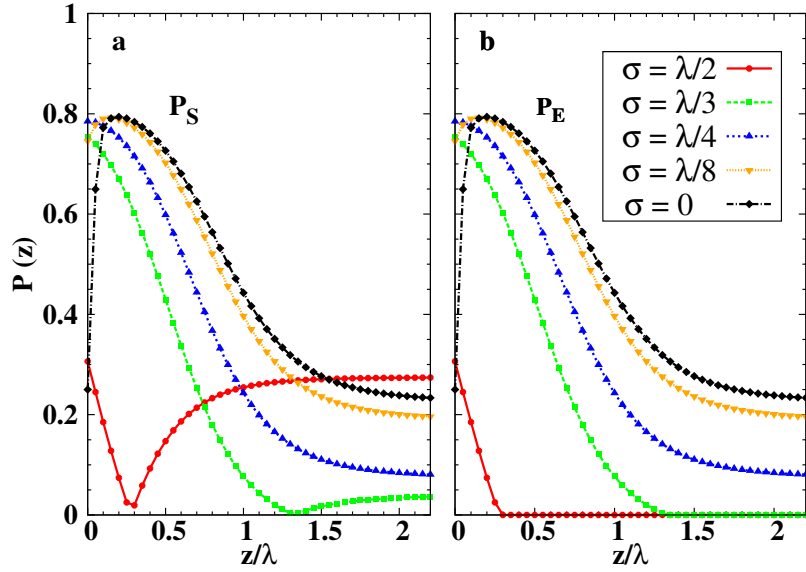
Figure 3.5: P_S and P_E versus distance to the source when SPPs are excited on its surface. The surface metal is Au at 620 nm ($\varepsilon = -9.1 + i1.2$).

To better illustrate the above, Fig. 3.4 shows the 3-D P_S and P_E. As said before, while when $\sigma \to 0$ both definitions tends to coincide, for larger σ we see an "anomalous" behavior in P_S; namely while P_E monotonically decays to 0 as σ or z/λ grow, P_S decreases to 0 ($\lambda_1 = \lambda_2$) at a certain value of z/λ which is smaller the larger σ is, and then grows again with z/λ up to a constant value. When σ approaches $\lambda/2$ the abscisa z/λ of this zero-minimum tends to 0 and

P_S grows right from $z = 0$ with values that are bounded by $1/2$. By contrast, the maximum $P_E = P_S \simeq 0.5$ occurs from a δ-correlated source while P_E is zero for $\sigma \geq \lambda/2$.

We now address excitation of SPPs on the source surface. Figure 3.5 shows the corresponding P_S and P_E; both are now enhanced. This agrees with the results obtained in [33] for P_S from δ-correlated sources. Their maxima coincide: $P_S = P_E \simeq 0.8$ when $\sigma = 0$. It was mentioned above (cf. Fig. 3.4) that both DOP tend to coincide when $\sigma < \lambda/2$; now we see that the contribution of SPPs, a pure near-field effect, helps to fulfil this coincidence (and hence the condition $\lambda_1 = \lambda_3$) for larger values of z. Although not discussed here, analogous effects are found when we address homogeneous sources like those thermal, whose source function correlations are given by the *fluctuation-dissipation theorem* [11]. As we have commented previously, in this case, these source functions are δ-correlated and the two definitions of *DOP are equivalent*. However, again once we assume non-zero correlation lenghts, we obtain different values for P_S and P_E.

3.5 CONCLUSIONS

This chapter analyzes the DOP under different situations. Firstly, we have described the classical two-dimensional DOP for planar fields. Then, we have focused on the three-dimensional DOP trying to find a way to clarify it. We have shown how two different definitions established for the 3-D degree of polarization may be equivalent both in the near and far field. This occurs depending on the correlation properties of the source, i.e., when $\sigma \to 0$, both definitions have an identical behavior, nevertheless, for $\sigma > \lambda/4$, they show a different behavior on propagation: for $z > \lambda$ both definitions tend to zero, however, Ellis et al. definition remains constant, and Setälä et al. definition increases. In particular, when SPPs are addressed, the distance up to which both definitions coincide is larger than when they are not excited

Part III

THEORY OF OPTICAL FORCES FROM PARTIALLY COHERENT LIGHT

4

MECHANICAL ACTION ON SMALL PARTICLES OF RANDOM LIGHT

4.1 MOTIVATION

T he earlier chapters deal with the main concepts and ideas on the theory of coherence and polarization. Nevertheless, this is not the main aim of this thesis, indeed, the previous chapters emerged as answers to questions that we asked ourselves when we decided to study this topic. From this point I will go beyond: what are the effects of the spatial coherence in optical forces?. As far as I know, this question has not been addressed before, at least in a detailed and systematic way.

I could say that before this work, the studies in this field were almost inexistent. However, I am obliged to mention that some authors (they will be referenced below) put the bases for studying this subject because they demonstrated that both energy and momentum are conserved in a partially coherent wave. Therefore, in the next chapter I will introduce the concept of optical force due to a fluctuating stochastic field.

Before entering in detail with the coherence of light, I will describe the interaction between deterministic fields and small particles. In most of the chapters of this thesis, the force will be expressed by two components: one conservative (also denoted gradient force) proportional to the gradient of the intensity, and one non-conservative (without any special name) proportional to $\mathrm{Im}E_j^*\partial_i E_j$. The latter is usually associated to the radiation pressure of light, nevertheless, this is not completely truth. In recent years there have been several studies in which the dynamics of the particle is written through the different contributions to the total density momentum of light [34–40].

Once I have defined the most important equations for deterministic fields, I will recover the stochastic character of light. To this end, and since the spatial coherence can be defined as the ability of light to interfere at different points, the most famous experiment to check this property is the double slit experiment. However, this experiment also gives us information about the coherence of light. Hence, it seems logical to think that the first step in order to see the
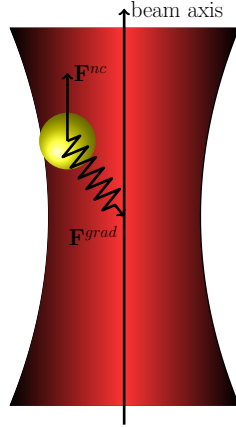
Figure 4.1: Optical forces on a dipolar spherical particle. The particle will be pushed toward the beam waist.

effects of the spatial coherence on optical forces is to reproduce theoretically this experiment for a test particle.

4.2 INTRODUCTION

It is well-known that an optical wavefield in free-space propagation will push a particle in the propagation direction, however, a highly focused beam can trap a particle in areas where the electromagnetic energy is maximum (see Fig. 4.1). This experimental demonstration of optical trapping was carried out by Ashkin [41, 42]. Since then, the manipulation of particles has been a tool of great interest in disciplines such as chemistry or biology.

The optical forces arise as consequence of the momentum conservation law [43]. Most of the studies about this law deal with coherent wavefields [44–47], however, some of them introduce the spatial coherence of light, demonstrating that these conservations laws are also valid for partially coherent illumination [48, 49].

Photonic trapping manipulation is usually developed under coherent wavefields [34, 50–54], however, classical textbooks demonstrate how coherence properties of the source affect the spectral distribution of energy [3–5, 20].

Prior to this thesis (and in particular to reference [III]), three works [56–58] studied the mechanical action of light on Rayleigh particles in some particular focusing and beam configurations. Nevertheless, this chapter will deal with a general formulation of optical forces from partially coherent light without assuming any particular configuration. Because the spatial coherence increases in free-space propagation (cf. Section 1.4), this feature of light should become increasingly important as one enters in the nanoscale (or subwavelength region) [50].

In this chapter I focus primarily on the contribution to the total optical force of the electric and magnetic orbital and spin momentum density from a fully coherent illumination. Secondly, I

analyze in detail the case of the force exerted on a small magnetodielectric particle by a random stationary and ergodic partially coherent external field [3]. I emphasize the influence of the degree of coherence on these forces. To this end, I address a system that, since early studies, has been paradigmatic to observe the nature of light and matter waves, as well as to characterize the degree of coherence of wavefields [3]. This is the Young interference pattern from two small apertures of an opaque screen. Concerning our study, I shall consider this configuration as discussed in the classical work by Thompson and Wolf [6] that relates the observed visibility of the interference fringes with the estimated degree of coherence of the light at those two apertures.

I should remark that this chapter establishes a new theory for the mean optical force on a dipolar particle, (understood as that whose electric and/or magnetic polarizability is due to the corresponding first electric and/or magnetic Mie coefficient [59–61]). This includes the limiting case of Rayleigh particles, although this fact will be discussed in detail in Chapter 6.

In summary, I will study the dependence of the gradient (density energy), scattering (radiation pressure) and curl components (spin momentum density) of the force on the cross-spectral density of the fluctuating stationary wavefield.

4.3 averaged optical force from a coherent wavefield: linear, orbital and spin momentum of light

In this section I will address the mechanical action on a magnetodielectric particle from a deterministic wavefield. In the rest of the chapter I will demonstrate the analogy between this formulation and that for a fluctuating random field. From Maxwell's theory we know that radiation carries energy and momentum. When a photon interacts with matter, there is an exchange of momentum. In general, this momentum can be seen as the sum of two contributions: one orbital and one from the spin of light. Whereas the orbital momentum [62, 63] is associated with the spatial distribution of the wavefronts, the spin [64] is associated with the polarization of the field (cf. Chapter 3).

The main goal of this section is to make a complete overview of this new point and demonstrate the relation with the usual expressions that we will manage in this thesis.

4.3.1 *Relations between linear, orbital and spin momentum densities.*

Let us begin defining the linear momentum density $\mathbf{p}$. Considering a monochromatic electromagnetic field $[\exp(-i\omega t)]$, the time-averaged[III.1] Poynting vector and the linear momentum density $\mathbf{p}$ are related by the expression [1, 43]:

$$\mathbf{p}(\mathbf{r}) = \frac{\langle \mathbf{S}(\mathbf{r}) \rangle}{c^2} = \frac{1}{8\pi\mu c} \text{Re}\{\mathbf{E}(\mathbf{r}) \times \mathbf{B}^*(\mathbf{r})\}. \tag{4.1}$$

III.1 Notice that only in this section the average $\langle \cdot \rangle$ is understood as the time-average

From now on, the spatial dependence of the electric and magnetic fields will be assumed for brevity. This definition is associated to the commonly addressed *radiation pressure* (see Section 4.3.3), which appears in many textbooks as the main consequence of the conservation of momentum.

For the harmonic electromagnetic field, we can express the electric field in terms of the curl of the magnetic vector and vice-versa [35]

$$\nabla \times \mathbf{B} = -ink\mathbf{E}, \tag{4.2}$$

$$\nabla \times \mathbf{E} = (ik/n)\,\mathbf{B}, \tag{4.3}$$

where we have defined the radiation wavenumber $k = n\omega/c$, being $n = \sqrt{\varepsilon\mu}$ the refractive index of the arbitrary medium. As I have commented in the introduction of this chapter, the (total linear) momentum density (cf. Eq. (4.1)) can be written in terms of the orbital momentum density $\mathbf{p}_i^\circ$ and the spin momentum density $\mathbf{p}_i^s$ ($i = e, m$ for the electric (e) and magnetic (m) densities) [35, 36]. Using the vectorial relation

$$\mathbf{A} \cdot (\nabla)\,\mathbf{B} = \mathbf{A} \times (\nabla \times \mathbf{B}) + (\mathbf{A} \cdot \nabla)\,\mathbf{B}, \tag{4.4}$$

where $\mathbf{A} \cdot (\nabla)\,\mathbf{B}$ is understood as the scalar product of a vector $\mathbf{A}$ with the gradient of a vector $\mathbf{B}$ (or in a tensorial way $A_j\partial_i B_j$, with $i, j = 1, 2, 3 = x, y, z$), and Eqs. (4.2)-(4.3), we can express it involving only electric field terms, namely

$$
\begin{aligned}
\mathbf{p} &= \frac{1}{8\pi c\mu}\mathrm{Re}\left\{\mathbf{E} \times \mathbf{B}^*\right\} \\
&= \frac{n}{8\pi c\mu k}\mathrm{Im}\left\{\mathbf{E}^* \times (\nabla \times \mathbf{E})\right\} \\
&= \frac{n}{8\pi c\mu k}\left[\mathrm{Im}\left\{\mathbf{E}^* \cdot (\nabla)\,\mathbf{E}\right\} + \frac{1}{2}\nabla \times \mathrm{Im}\left\{\mathbf{E}^* \times \mathbf{E}\right\}\right] \\
&= \mathbf{p}_e^\circ + \mathbf{p}_e^s.
\end{aligned}
\tag{4.5}
$$

Thus, the electric orbital and spin momentum densities are explicitly:

$$\mathbf{p}_e^\circ = \frac{1}{8\pi\omega\mu}\mathrm{Im}\left\{\mathbf{E}^* \cdot (\nabla)\,\mathbf{E}\right\} \tag{4.6}$$

$$\mathbf{p}_e^s = \frac{1}{16\pi\omega\mu}\nabla \times \mathrm{Im}\left\{\mathbf{E}^* \times \mathbf{E}\right\} \tag{4.7}$$

This interpretation of the linear momentum is not unique, there is an analogous way to express this momentum $\mathbf{p}$ using only the magnetic fields:

$$
\begin{aligned}
\mathbf{p} &= \frac{1}{8\pi c\mu}\mathrm{Re}\left\{\mathbf{E} \times \mathbf{B}^*\right\} \\
&= \frac{1}{8\pi c\mu nk}\mathrm{Im}\left\{\mathbf{B}^* \times (\nabla \times \mathbf{B})\right\} \\
&= \frac{1}{8\pi c\mu nk}\left[\mathrm{Im}\left\{\mathbf{B}^* \cdot (\nabla)\,\mathbf{B}\right\} + \frac{1}{2}\nabla \times \mathrm{Im}\left\{\mathbf{B}^* \times \mathbf{B}\right\}\right] \\
&= \mathbf{p}_m^\circ + \mathbf{p}_m^s.
\end{aligned}
\tag{4.8}
$$

Thus, the magnetic orbital and spin momentum densities are explicitly

$$\mathbf{p}_m^\circ = \frac{1}{8\pi\omega\mu^2\varepsilon}\mathrm{Im}\left\{\mathbf{B}^* \cdot (\nabla)\,\mathbf{B}\right\} \tag{4.9}$$

$$\mathbf{p}_m^s = \frac{1}{16\pi\omega\mu^2\varepsilon}\nabla \times \mathrm{Im}\left\{\mathbf{B}^* \times \mathbf{B}\right\} \tag{4.10}$$

(a) Orbital momentum density of light.

(b) Spin momentum density of light.
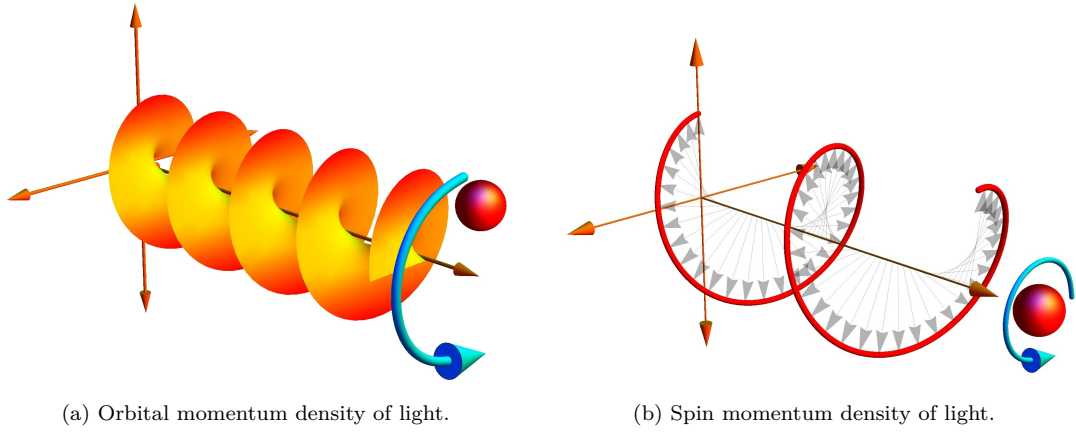
Figure 4.2: Three-dimensional view of momentum densities

As follow from Eqs. (4.7)-(4.10), if the electric (magnetic) field is linearly polarized, the contribution to the total momentum of the spin momentum density is zero, in other words, its existence is associated with the rotation of the electric (magnetic) field along the axis of propagation. This situation occurs for circular polarization, having two states of polarization: (left-)right-handed/(counter-)clockwise circularly polarized light. [III.2]

4.3.2 *Contribution of the momentum densities to the optical force*

Now, we will make emphasis on the contribution of the different momentum densities to the force. For a magnetodielecric particle, the force can be written in terms of the electric and magnetic dipoles, arising a third term as consequence of the interference between them [44, 59, 65]:

$$\langle \mathbf{F}_e \rangle = \frac{1}{2} \mathrm{Re} \left\{ \mathbf{d} \cdot (\nabla) \mathbf{E}^* \right\}, \tag{4.11}$$

$$\langle \mathbf{F}_m \rangle = \frac{1}{2} \mathrm{Re} \left\{ \mathbf{m} \cdot (\nabla) \mathbf{B}^* \right\}, \tag{4.12}$$

$$\langle \mathbf{F}_{em} \rangle = -\frac{k^4}{3} \sqrt{\frac{\mu}{\varepsilon}} \mathrm{Re} \left\{ \mathbf{d} \times \mathbf{m}^* \right\}. \tag{4.13}$$

If we express the induced dipoles moments $\mathbf{d}, \mathbf{m}$ in terms of the incident fields $\mathbf{E}, \mathbf{B}$, i.e. $\mathbf{d} = \alpha_e \mathbf{E}$ and $\mathbf{m} = \alpha_m \mathbf{B}$, being α_e, α_m the electric and magnetic polarizabilities[III.3], we can split the total (electric or magnetic) force $\langle \mathbf{F}_{e,m} \rangle$ in two: one conservative ($\nabla \times \mathbf{F}_{e,m}^{cons} = 0$) and one non-conservative ($\nabla \times \mathbf{F}_{e,m}^{nc} \neq 0$) [59, 66]:

$$
\begin{aligned}
\langle \mathbf{F}_e \rangle &= \frac{1}{2} \mathrm{Re} \left\{ \alpha_e \mathbf{E} \cdot (\nabla) \mathbf{E}^* \right\} \\
&= \frac{1}{4} \mathrm{Re} \alpha_e \nabla |\mathbf{E}|^2 + \frac{1}{2} \mathrm{Im} \alpha_e \mathrm{Im} \left\{ \mathbf{E}^* \cdot (\nabla) \mathbf{E} \right\} \\
&= \langle \mathbf{F}_e^{cons} \rangle + \langle \mathbf{F}_e^{nc} \rangle.
\end{aligned}
\tag{4.14}
$$

III.2 Notice also that these definitions coincide with the expressions of references [38, 40], however, there is a difference in a factor 1/2 due to they split the total momentum as $\mathbf{p} = \mathbf{p}_e^\circ + \mathbf{p}_e^s + \mathbf{p}_m^\circ + \mathbf{p}_m^s$,

III.3 In order to avoid any confusion with the momentum densities, in this section we will denote the induced electric dipole as $\mathbf{d}$ instead of the usual notation $\mathbf{p}$.

$$
\begin{aligned}
\langle \mathbf{F}_m \rangle &= \frac{1}{2}\mathrm{Re}\left\{\alpha_m \mathbf{B} \cdot (\nabla)\,\mathbf{B}^*\right\} \\
&= \frac{1}{4}\mathrm{Re}\alpha_m \nabla \left|\mathbf{B}\right|^2 + \frac{1}{2}\mathrm{Im}\alpha_m \mathrm{Im}\left\{\mathbf{B}^* \cdot (\nabla)\,\mathbf{B}\right\} \\
&= \langle \mathbf{F}_m^{cons} \rangle + \langle \mathbf{F}_m^{nc} \rangle.
\end{aligned} \tag{4.15}
$$

$$
\begin{aligned}
\langle \mathbf{F}_{em} \rangle &= -\frac{k^4}{3}\sqrt{\frac{\mu}{\varepsilon}}\mathrm{Re}\left\{\alpha_e \alpha_m^* \mathbf{E} \times \mathbf{B}^*\right\} \\
&= -\frac{k^4}{3}\sqrt{\frac{\mu}{\varepsilon}}\left(\mathrm{Re}\left\{\alpha_e \alpha_m^*\right\}\mathrm{Re}\left\{\mathbf{E} \times \mathbf{B}^*\right\} - \mathrm{Im}\left\{\alpha_e \alpha_m^*\right\}\mathrm{Im}\left\{\mathbf{E} \times \mathbf{B}^*\right\}\right).
\end{aligned} \tag{4.16}
$$

From Eqs. (4.14) and (4.15) and Eqs. (4.6) and (4.9), we see that the non-conservative force *is proportional to the orbital momentum density* (see [67])

$$
\begin{aligned}
\langle \mathbf{F}_e^{nc} \rangle &= \frac{1}{2}\mathrm{Im}\alpha_e \mathrm{Im}\left\{\mathbf{E}^* \cdot (\nabla)\,\mathbf{E}\right\} \\
&= 4\pi\omega\mu\,\mathrm{Im}\left\{\alpha_e\right\}\mathbf{p}_e^{\circ},
\end{aligned} \tag{4.17}
$$

$$
\begin{aligned}
\langle \mathbf{F}_m^{nc} \rangle &= \frac{1}{2}\mathrm{Im}\alpha_m \mathrm{Im}\left\{\mathbf{B}^* \cdot (\nabla)\,\mathbf{B}\right\} \\
&= 4\pi\omega\mu^2\varepsilon\,\mathrm{Im}\left\{\alpha_m\right\}\mathbf{p}_m^{\circ}.
\end{aligned} \tag{4.18}
$$

If we write the orbital momentum density as the difference of the linear and spin, i.e., $\mathbf{p}_e^{\circ} = \mathbf{p} - \mathbf{p}_e^s$ (analogously for the magnetic field) and we use the definitions of the previous subsection, we obtain [34, 59]:

$$
\langle \mathbf{F}^e \rangle = \frac{1}{4}\mathrm{Re}\alpha_e \nabla \left|\mathbf{E}\right|^2 + \frac{k}{2n}\mathrm{Im}\alpha_e \mathrm{Re}\left\{\mathbf{E} \times \mathbf{B}^*\right\} - \frac{1}{2}\mathrm{Im}\alpha_e \frac{1}{2}\nabla \times \mathrm{Im}\left(\mathbf{E}^* \times \mathbf{E}\right) \tag{4.19}
$$

$$
\langle \mathbf{F}^m \rangle = \frac{1}{4}\mathrm{Re}\alpha_m \nabla \left|\mathbf{B}\right|^2 + \frac{kn}{2}\mathrm{Im}\alpha_m \mathrm{Re}\left\{\mathbf{E} \times \mathbf{B}^*\right\} - \frac{1}{2}\mathrm{Im}\alpha_m \frac{1}{2}\nabla \times \mathrm{Im}\left(\mathbf{B}^* \times \mathbf{B}\right) \tag{4.20}
$$

Notice that these equations are exactly the same as the Eqs. (42), (45) and (43), (50) respectively of reference [59]. Now we see three contributions: the first term in Eqs. (4.19) and (4.20), which is proportional to the gradient of the density of electromagnetic energy [1, 10], will push the particle towards zones of maximum intensity and it is the main responsible in nanomanipulation techniques (see Fig. 4.1). The second one is the traditional radiation pressure term, and will push the particle in the Poynting vector direction. The third shows the force due to the spatial distribution of spin density.

On the other hand, Eq. (4.16) reveals the fundamentals of the relevant topic of tractor forces [68–71]. As we can see, this force is directed towards the $-\mathrm{Re}\left\{\mathbf{E} \times \mathbf{B}^*\right\}$ direction, thus, if we are capable of making this term much larger than their electric and magnetic counterparts, the particle will be pushed to the source.

4.3.3 *Dimensional analysis: radiation pressure and momentum density*

Now we will make a small digression to justify the use of the previous expressions for the momentum densities. This is based on dimensional analysis. Let us begin expressing the dimensions of the Poynting vector (see Eq. (4.1)):

$$
\begin{aligned}
\langle \mathbf{S} \rangle &= \text{velocity} \times \text{electric field} \times \text{magnetic field} \\
&= \text{velocity} \times \text{electric field}^2 \\
&= \frac{\text{length}}{\text{time}} \times \frac{\text{energy}}{\text{length}} \\
&= \frac{\text{power}}{\text{area}}.
\end{aligned}
\tag{4.21}
$$

This quantity represents the density of flow of energy, i.e., the rate of energy transfer per unit area. Now, for photons we know from the energy-momentum relation that $E = pc$, thus, if we consider instead of this expression the ratio $\langle \mathbf{S} \rangle / c$, this leads to

$$
\begin{aligned}
\frac{\langle \mathbf{S} \rangle}{c} &= \frac{\text{time} \times \text{power}}{\text{length} \times \text{area}} \\
&= \frac{\text{force}}{\text{area}} \equiv \text{pressure}.
\end{aligned}
\tag{4.22}
$$

This is the well-known radiation pressure term. If we divide this expression by c, as in Eq. (4.1) we obtain

$$
\begin{aligned}
\frac{\langle \mathbf{S} \rangle}{c^2} &= \frac{\text{time} \times \text{Force}}{\text{length} \times \text{area}} \\
&= \frac{\text{momentum}}{\text{volume}} \equiv \text{momentum density},
\end{aligned}
\tag{4.23}
$$

which is the quantity on which we have been working in the previous subsection.

4.4 AVERAGED OPTICAL FORCE FROM A PARTIALLY COHERENT WAVEFIELD

Now I turn to the main topic. The goal is to demonstrate how the previous expressions for the force are also valid for a partially coherent illumination. To this end, we shall consider fluctuating time stationary and ergodic fields [1, 3]. For a single realization whose real electric and magnetic vectors are $\mathbf{E}^{(r)}(\mathbf{r}, t)$ and $\mathbf{B}^{(r)}(\mathbf{r}, t)$, respectively, at a space point $\mathbf{r}$ and time t, the frequency decomposition is [3]

$$
\mathbf{E}^{(r)}(\mathbf{r}, t) = \int_{-\infty}^{\infty} \tilde{\mathbf{E}}^{(r)}(\mathbf{r}, \omega) e^{-i\omega t} d\omega,
\tag{4.24}
$$

$$
\mathbf{B}^{(r)}(\mathbf{r}, t) = \int_{-\infty}^{\infty} \tilde{\mathbf{B}}^{(r)}(\mathbf{r}, \omega) e^{-i\omega t} d\omega.
\tag{4.25}
$$

The corresponding complex analytic signals are [1, 3]:

$$
\mathbf{E}(\mathbf{r}, t) = \int_{-\infty}^{\infty} \tilde{\mathbf{E}}(\mathbf{r}, \omega) e^{-i\omega t} d\omega,
\tag{4.26}
$$

$$
\mathbf{B}(\mathbf{r}, t) = \int_{-\infty}^{\infty} \tilde{\mathbf{B}}(\mathbf{r}, \omega) e^{-i\omega t} d\omega,
\tag{4.27}
$$

where those Fourier integrals should be considered in the sense of distribution theory. In addition, we have

$$
\begin{aligned}
\tilde{\mathbf{E}}\left(\mathbf{r}, \omega\right) &= \tilde{\mathbf{E}}^{(r)}\left(\mathbf{r}, \omega\right) \quad , \omega \geq 0 \\
&= \quad 0 \qquad\quad , \omega < 0
\end{aligned}
, \tag{4.28}
$$

$$
\begin{aligned}
\tilde{\mathbf{B}}\left(\mathbf{r}, \omega\right) &= \tilde{\mathbf{B}}^{(r)}\left(\mathbf{r}, \omega\right) \quad , \omega \geq 0 \\
&= \quad 0 \qquad\quad , \omega < 0
\end{aligned}
. \tag{4.29}
$$

The analytical signal is related to the real and imaginary parts trough

$$
\mathbf{E}\left(\mathbf{r}, t\right) = \frac{1}{2}\left[\mathbf{E}^{(r)}\left(\mathbf{r}, t\right) + i\mathbf{E}^{(i)}\left(\mathbf{r}, t\right)\right], \tag{4.30}
$$

$$
\mathbf{B}\left(\mathbf{r}, t\right) = \frac{1}{2}\left[\mathbf{B}^{(r)}\left(\mathbf{r}, t\right) + i\mathbf{B}^{(i)}\left(\mathbf{r}, t\right)\right], \tag{4.31}
$$

where superscripts (r) and (i) denote the real and imaginary parts, respectively. For each Cartesian component of these electric and magnetic vectors, they form a Hilbert transform pair in the t variable [1, 3]. We shall now calculate the *ensemble average* (cf. Section 1.1.1) of the force exerted by the random field on a dipolar particle, (understood in the sense mentioned in Section 4.4), over its different realizations:

$$
\langle \mathbf{F}(\mathbf{r}, t) \rangle = \left\langle \left(\mathbf{p}^{(r)}(\mathbf{r}, t) \cdot \nabla\right) \mathbf{E}^{(r)}(\mathbf{r}, t) + \frac{1}{c}\frac{\partial \mathbf{p}^{(r)}(\mathbf{r}, t)}{\partial t} \times \mathbf{B}^{(r)}(\mathbf{r}, t) \right\rangle, \tag{4.32}
$$

$\mathbf{p}^{(r)}$ is the real part of the dipole moment induced by the fluctuating incident wave on the particle. If α_e denotes the particle electric polarizability, one has that

$$
\mathbf{p}(\mathbf{r}, t) = \alpha_e \mathbf{E}(\mathbf{r}, t). \tag{4.33}
$$

Denoting: $\partial p/\partial t = \dot{p}$, and due to a well-known property of the derivative of Hilbert transforms [3], the real and imaginary parts of each Cartesian component of $\dot{\mathbf{p}}$ are Hilbert transforms of each other in t.

Let us evaluate the fist term of Eq. (4.32). Taking Eqs. (4.26), (4.27), (4.30), (4.31) and (4.33) into account, omitting the explicit $\mathbf{r}, t$ dependence in the forthcoming notation; this is (cf. [1, 3, 4]):

$$
\begin{aligned}
&\left\langle p_j^{(r)} \partial_j E_i^{(r)} \right\rangle \\
=\ & \left\langle \left(p_j + p_j^*\right) \partial_j \left(E_i + E_i^*\right) \right\rangle \\
=\ & \underset{\mathrm{T}\to\infty}{\mathrm{Lim}} \frac{1}{2T} \int_{-T}^{T} \mathrm{d}t \left[\int_{-\infty}^{\infty} e^{-i(\omega_1 + \omega_2)t} \left\langle \tilde{p}_j(\mathbf{r}, \omega_1) \partial_j \tilde{E}_i(\mathbf{r}, \omega_2) \right\rangle \mathrm{d}\omega_1 \mathrm{d}\omega_2 \right. \\
& + \int_{-\infty}^{\infty} e^{-i(\omega_1 - \omega_2)t} \left\langle \tilde{p}_j(\mathbf{r}, \omega_1) \partial_j \tilde{E}_i^*(\mathbf{r}, \omega_2) \right\rangle \mathrm{d}\omega_1 \mathrm{d}\omega_2 \\
& + \int_{-\infty}^{\infty} e^{-i(-\omega_1 + \omega_2)t} \left\langle \tilde{p}_j^*(\mathbf{r}, \omega_1) \partial_j \tilde{E}_i(\mathbf{r}, \omega_2) \right\rangle \mathrm{d}\omega_1 \mathrm{d}\omega_2 \\
& \left. + \int_{-\infty}^{\infty} e^{+i(\omega_1 + \omega_2)t} \left\langle \tilde{p}_j^*(\mathbf{r}, \omega_1) \partial_j \tilde{E}_i^*(\mathbf{r}, \omega_2) \right\rangle \mathrm{d}\omega_1 \mathrm{d}\omega_2 \right],
\end{aligned} \tag{4.34}
$$

Where $i, j = 1, 2, 3$ and Einstein's convention of omitting the sum symbol $\sum_{j=1}^{3}$ on the repeated index j has been used. Using the properties of Dirac delta distribution: $2\pi\delta(\omega) = \int_{-\infty}^{\infty} e^{-i\omega t} \mathrm{d}t$ and $\delta(\omega) = \delta(-\omega)$, the previous equation reduces to

$$
\begin{aligned}
\left\langle p_j^{(r)} \partial_j E_i^{(r)} \right\rangle \;=\;& 2\pi \Bigg[\int_{-\infty}^{\infty} g_i^{(p,E)}(\mathbf{r}, \omega_1, \omega_2)\, \delta(\omega_1 + \omega_2)\, \mathrm{d}\omega_1 \mathrm{d}\omega_2 \\
& + \int_{-\infty}^{\infty} g_i^{(p,E^*)}(\mathbf{r}, \omega_1, \omega_2)\, \delta(\omega_1 - \omega_2)\, \mathrm{d}\omega_1 \mathrm{d}\omega_2 \\
& + \int_{-\infty}^{\infty} g_i^{(p^*,E)}(\mathbf{r}, \omega_1, \omega_2)\, \delta(\omega_1 - \omega_2)\, \mathrm{d}\omega_1 \mathrm{d}\omega_2 \\
& + \int_{-\infty}^{\infty} g_i^{(p^*,E^*)}(\mathbf{r}, \omega_1, \omega_2)\, \delta(\omega_1 + \omega_2)\, \mathrm{d}\omega_1 \mathrm{d}\omega_2 \Bigg],
\end{aligned}
\tag{4.35}
$$

where the cross-spectral function $g_i^{(U,V)}(\mathbf{r}, \omega_1, \omega_2)$ is

$$
g_i^{(U,V)}(\mathbf{r}, \omega_1, \omega_2) = \operatorname*{Lim}_{\mathrm{T}\to\infty} \frac{1}{2T} \left\langle \tilde{U}_j(\mathbf{r}, \omega_1) \partial_j \tilde{V}_i(\mathbf{r}, \omega_2) \right\rangle,
\tag{4.36}
$$

$\tilde{U}_j(\mathbf{r}, \omega)$ and $\tilde{V}_i(\mathbf{r}, \omega)$ $(i, j = 1, 2, 3)$ being the spectra of two analytic signal Cartesian components.

On performing the ω_2 integration in Eq. (4.35) and taking into account that due to Eqs. (4.26) - (4.29), and to Eq. (4.36), one has that

$$
g_i^{(U,V)}(\mathbf{r}, \omega_1, -\omega_1) = 0,
\tag{4.37}
$$

only the second and third terms of Eq. (4.35) are different from zero. Thus finally

$$
\begin{aligned}
\left\langle p_j^{(r)} \partial_j E_i^{(r)} \right\rangle \;=\;& 4\pi \operatorname{Re} \int_{-\infty}^{\infty} \operatorname*{Lim}_{\mathrm{T}\to\infty} \frac{1}{2T} \left\langle \tilde{p}_j(\mathbf{r}, \omega_1) \partial_j \tilde{E}_i^{*}(\mathbf{r}, \omega_1) \right\rangle \mathrm{d}\omega_1 \\
=\;& 4\pi \operatorname{Re} \int_{-\infty}^{\infty} g_i^{(p^*,E)}(\mathbf{r}, \omega_1, \omega_1)\, \mathrm{d}\omega_1,
\end{aligned}
\tag{4.38}
$$

where Re denotes the real part.

On the other hand, writing as ϵ_{ijk} the antisymmetric Levi – Civita tensor, $(i, j, k = 1, 2, 3)$; the second term of Eq. (4.32) is:

$$
\frac{1}{c} \epsilon_{ijk} \left\langle \dot{p}_j^{(r)} B_k^{(r)} \right\rangle = \frac{1}{c} \epsilon_{ijk} \left\langle (\dot{p}_j + \dot{p}_j^*)(B_k + B_k^*) \right\rangle.
\tag{4.39}
$$

$$
\begin{aligned}
& \frac{1}{c} \epsilon_{ijk} \left\langle (\dot{p}_j + \dot{p}_j^*)(B_k + B_k^*) \right\rangle \\
=\;& \frac{\epsilon_{ijk}}{c} \operatorname*{Lim}_{\mathrm{T}\to\infty} \frac{1}{2T} \int_{-T}^{T} \mathrm{d}t \Bigg[\int_{-\infty}^{\infty} (-i\omega_1) e^{-i(\omega_1+\omega_2)t} \left\langle \tilde{p}_j(\mathbf{r}, \omega_1) \tilde{B}_k(\mathbf{r}, \omega_2) \right\rangle \mathrm{d}\omega_1 \mathrm{d}\omega_2 \\
& + \int_{-\infty}^{\infty} (-i\omega_1) e^{-i(\omega_1-\omega_2)t} \left\langle \tilde{p}_j(\mathbf{r}, \omega_1) \tilde{B}_k^{*}(\mathbf{r}, \omega_2) \right\rangle \mathrm{d}\omega_1 \mathrm{d}\omega_2 \\
& + \int_{-\infty}^{\infty} i\omega_1 e^{-i(-\omega_1+\omega_2)t} \left\langle \tilde{p}_j^{*}(\mathbf{r}, \omega_1) \tilde{B}_k(\mathbf{r}, \omega_2) \right\rangle \mathrm{d}\omega_1 \mathrm{d}\omega_2 \\
& + \int_{-\infty}^{\infty} i\omega_1 e^{+i(\omega_1+\omega_2)t} \left\langle \tilde{p}_j^{*}(\mathbf{r}, \omega_1) \tilde{B}_k^{*}(\mathbf{r}, \omega_2) \right\rangle \mathrm{d}\omega_1 \mathrm{d}\omega_2 \Bigg].
\end{aligned}
\tag{4.40}
$$

Or in a more compact form

$$\frac{1}{c}\epsilon_{ijk}\left\langle(\dot{p}_j+\dot{p}_j^*)(B_k+B_k^*)\right\rangle$$

$$= \frac{2\pi}{c}\epsilon_{ijk}\left[\int_{-\infty}^{\infty}(-i\omega_1)W_{jk}^{(p,B)}(\mathbf{r},\omega_1,\omega_2)\delta(\omega_1+\omega_2)\mathrm{d}\omega_1\mathrm{d}\omega_2\right.$$

$$+\int_{-\infty}^{\infty}(-i\omega_1)W_{jk}^{(p,B^*)}(\mathbf{r},\omega_1,\omega_2)\delta(\omega_1-\omega_2)\mathrm{d}\omega_1\mathrm{d}\omega_2$$

$$+\int_{-\infty}^{\infty}i\omega_1 W_{jk}^{(p^*,B)}(\mathbf{r},\omega_1,\omega_2)\delta(\omega_1-\omega_2)\mathrm{d}\omega_1\mathrm{d}\omega_2$$

$$\left.+\int_{-\infty}^{\infty}i\omega_1 W_{jk}^{(p^*,B^*)}(\mathbf{r},\omega_1,\omega_2)\delta(\omega_1+\omega_2)\mathrm{d}\omega_1 d\omega_2\right], \tag{4.41}$$

where the cross-frequency density tensor $W_{jk}^{(U,V)}(\mathbf{r},\omega_1,\omega_2)$ is

$$W_{jk}^{(U,V)}(\mathbf{r},\omega_1,\omega_2) = \mathop{\mathrm{Lim}}_{\mathrm{T}\to\infty}\frac{1}{2T}\left\langle\tilde{U}_j(\mathbf{r},\omega_1)\tilde{V}_k(\mathbf{r},\omega_2)\right\rangle, \tag{4.42}$$

On performing the ω_2 integration in Eq. (4.41) and taking into account that due to Eqs. (4.27) - (4.29), one has that

$$W_{jk}^{(U,V)}(\mathbf{r},\omega_1,-\omega_1) = 0. \tag{4.43}$$

only the second and third terms of Eq. (4.41) remain different from zero.

Now, since $\mathbf{B} = c/i\omega\nabla\times\mathbf{E}$, i.e. $-i\omega B_k^* = c\epsilon_{klm}\partial_l E_m^*$, and taking into account that $\epsilon_{ijk}\epsilon_{klm} = \delta_{il}\delta_{jm}-\delta_{im}\delta_{jl}$, δ_{il} being the Kronecker delta unit tensor, Eq. (4.41) becomes

$$\frac{1}{c}\epsilon_{ijk}\left\langle\dot{p}_j^{(r)}B_k^{(r)}\right\rangle = 4\pi\mathrm{Re}\int_{-\infty}^{\infty}\mathop{\mathrm{Lim}}_{\mathrm{T}\to\infty}\frac{1}{2T}\left[\left\langle\tilde{p}_j(\mathbf{r},\omega_1)\partial_i\tilde{E}_j^{\,*}(\mathbf{r},\omega_1)\right\rangle\right.$$
$$\left.-\left\langle\tilde{p}_j(\mathbf{r},\omega_1)\partial_j\tilde{E}_i^{\,*}(\mathbf{r},\omega_1)\right\rangle\right]\mathrm{d}\omega_1. \tag{4.44}$$

We now introduce $\mathcal{E}_{jk}(\mathbf{r},\mathbf{r}',\tau) = \left\langle E_j(\mathbf{r},t)E_k^{\,*}(\mathbf{r}',t+\tau)\right\rangle$ as the *electric field coherence tensor* [3, 4] expressed as

$$\mathcal{E}_{jk}(\mathbf{r},\mathbf{r}',\tau) = \int_{-\infty}^{\infty}\tilde{\mathcal{E}}_{jk}(\mathbf{r},\mathbf{r}',\omega)e^{-i\omega\tau}\mathrm{d}\omega, \tag{4.45}$$

$\tilde{\mathcal{E}}_{jk}(\mathbf{r},\mathbf{r}',\omega)$ being the electric field *cross-spectral density tensor* [III.4] defined as

$$\tilde{\mathcal{E}}_{jk}(\mathbf{r},\mathbf{r}',\omega) = \mathop{\mathrm{Lim}}_{\mathrm{T}\to\infty}\frac{1}{2T}\left\langle\tilde{E}_j^*(\mathbf{r},\omega)\tilde{E}_k(\mathbf{r}',\omega)\right\rangle. \tag{4.46}$$

On introducing Eqs. (4.38) and (4.44) into Eq. (4.32), and taking Eqs. (4.33), (4.45) and (4.46) into acount, one finally obtains for the averaged force acting on a dipolar particle [44], the following expression in terms of the analytic signal associated to the random field

$$\langle F_i(\mathbf{r},t)\rangle = 4\pi\mathrm{Re}\int_{-\infty}^{\infty}\mathop{\mathrm{Lim}}_{\mathrm{T}\to\infty}\frac{1}{2T}\left\langle\tilde{p}_j(\mathbf{r},\omega)\partial_i\tilde{E}_j^{\,*}(\mathbf{r},\omega)\right\rangle\mathrm{d}\omega$$

$$= 4\pi\mathrm{Re}\int_{-\infty}^{\infty}\alpha_e\partial_i^{(*)}\mathop{Lim}_{\mathrm{T}\to\infty}\frac{1}{2T}\left\langle\tilde{E}_j(\mathbf{r},\omega)\tilde{E}_j^{\,*}(\mathbf{r},\omega)\right\rangle\mathrm{d}\omega$$

$$= 4\pi\mathrm{Re}\int_{-\infty}^{\infty}\alpha_e\partial_i^{(*)}\mathrm{Tr}\tilde{\mathcal{E}}_{jk}(\mathbf{r},\mathbf{r},\omega)\mathrm{d}\omega, \tag{4.47}$$

[III.4] It is well-known that the expression (4.46) is one of the "smoothing" alternatives to estimate the cross-spectral density of the random process $\mathbf{E}(\mathbf{r},t)$ considered as truncated in time beyond $|t| = T$ [1, 3, 4]. Another way is to write [20]: $\tilde{\mathcal{E}}_{jk}(\mathbf{r},\mathbf{r}',\omega) = \lim_{\Delta\omega\to 0}\int_{\omega-\Delta\omega/2}^{\omega+\Delta\omega/2}\left\langle\tilde{E}_j^*(\mathbf{r},\omega)\tilde{E}_k(\mathbf{r}',\omega')\right\rangle\mathrm{d}\omega'$.

where we have replaced ω_1 by ω. The symbol Tr denotes the trace. On the other hand, $\partial_i^{(*)}$ means that the derivative with respect to the *ith* component of $\mathbf{r}$ is made on the complex-conjugated component E_j^*.

Eq. (4.47) may also be expressed in terms of the coherence tensor as

$$
\begin{aligned}
\langle F_i(\mathbf{r},t)\rangle &= 4\pi \mathrm{Re}\left\{\left\langle p_j(\mathbf{r},t)\partial_i E_j^*(\mathbf{r},t)\right\rangle\right\} \\
&= 4\pi \mathrm{Re}\left\{\alpha_e \partial_i^{(*)}\left\langle E_j(\mathbf{r},t)E_j^*(\mathbf{r},t)\right\rangle\right\} \\
&= 4\pi \mathrm{Re}\left\{\alpha_e \partial_i^{(*)}\mathrm{Tr}\mathcal{E}_{jk}(\mathbf{r},\mathbf{r},0)\right\}.
\end{aligned}
\tag{4.48}
$$

In Eq. (4.48) we have recalled that according to (4.45) one has $\mathcal{E}_{jk}(\mathbf{r},\mathbf{r},0) = \int_{-\infty}^{\infty}\tilde{\mathcal{E}}_{jk}(\mathbf{r},\mathbf{r},\omega)\mathrm{d}\omega$. On introducing the mean force components at frequency ω: $\langle\tilde{F}_i(\mathbf{r},\omega)\rangle$ as

$$
\langle F_i(\mathbf{r},t)\rangle = 2\pi\int_{-\infty}^{\infty}\left\langle\tilde{F}_i(\mathbf{r},\omega)\right\rangle\mathrm{d}\omega,
\tag{4.49}
$$

we see that according to Eq. (4.47) we may express them as:

$$
\left\langle\tilde{F}_i(\mathbf{r},\omega)\right\rangle = 2\mathrm{Re}[\alpha_e\partial_i^{(*)}\mathrm{Tr}\tilde{\mathcal{E}}_{jk}(\mathbf{r},\mathbf{r},\omega)].
\tag{4.50}
$$

In most instances, specially when handling experimental data, one has access to $\mathcal{E}_{jk}(\mathbf{r},\mathbf{r}',\tau)$ or $\tilde{\mathcal{E}}_{jk}(\mathbf{r},\mathbf{r}',\omega)$ directly, but not to the field of which they are correlations, then adopting the ordering of functions and variables as written in Eq. (4.46) it may be more convenient to express the derivative $\partial_i^{(*)}$ in Eqs. (4.47)-(4.50) simply by that with respect to the *ith*-Cartesian component of $\mathbf{r}$ as:

$$
\partial_i^{(*)}\mathrm{Tr}\tilde{\mathcal{E}}_{jk}(\mathbf{r},\mathbf{r},\omega) = [\partial_i\mathrm{Tr}\tilde{\mathcal{E}}_{jk}(\mathbf{r},\mathbf{r}',\omega)]_{\mathbf{r}'=\mathbf{r}}.
\tag{4.51}
$$

$$
\partial_i^{(*)}\mathrm{Tr}\mathcal{E}_{jk}(\mathbf{r},\mathbf{r},\tau) = [\partial_i\mathrm{Tr}\mathcal{E}_{jk}(\mathbf{r},\mathbf{r}',\tau)]_{\mathbf{r}'=\mathbf{r}}.
\tag{4.52}
$$

Where it is understood that one takes first the derivative with respect to x_i ($i = 1, 2, 3$) of the corresponding element of the coherence tensor, afterwards making $\mathbf{r}' = \mathbf{r}$. In this connection, it shold be remarked that such expressions for non-local interactions of the field and the induced dipole have recently been addressed in microcavities [72].

Eq.(4.49) shows how the mean force vector at each frequency ω adds to build up the field force. Of course for a quasimonochromatic field just the component of the mean force at the center frequency $\bar{\omega}$ of the spectrum approximates the force.

The above calculations also lead to the conclusion that, being $\mathbf{p}$, $\dot{\mathbf{p}}$, $\mathbf{E}$ and $\mathbf{B}$ analytic signals of t, one also has that

$$
\begin{aligned}
\left\langle\dot{p}_j^{(r)}B_k^{(r)}\right\rangle &= 2\mathrm{Re}\left\langle\dot{p}_j B_k^*\right\rangle, \\
\left\langle p_j^{(r)}\partial_j E_i^{(r)}\right\rangle &= 2\mathrm{Re}\left\langle\alpha_e E_j\partial_j E_i^*\right\rangle.
\end{aligned}
\tag{4.53}
$$

Notice that introducing Eqs. (4.53) into Eq. (4.32), one obtains again (4.48).

Eq. (4.48) and its frequency counterpart (4.50) show that the mean force is linked to the coherence tensor of the field. This latter quantity fulfills the Helmholtz equation whose integral

representation leads to well known propagation laws in coherence theory, like the Zernike law and the Van Cittert-Zernike theorem, or to the dependence of the intensity on the degree of coherence of the wavefield in the primary or secondary source surface that emits it [1, 3, 4]. Hence all these phenomena have consequences for the averaged force.

4.4.1 *Conservative and non-conservative components of the averaged optical force. The case of magnetodielectric particles*

In Section 4.3.2 we have shown that the time averaged force from coherent fields may be expressed as the sum of three parts, *one conservative and two non-conservative*, (cf. also [34, 59]), namely, a *gradient, a scattering and a curl of a electric spin density*. Similarly, the force spectral components given by Eq. (4.50) lead to (for vacuum)

$$
\begin{aligned}
\langle \mathbf{F}(\mathbf{r},t) \rangle &= 2\pi \mathrm{Re}\alpha_e \int_{-\infty}^{+\infty} \mathop{\mathrm{Lim}}_{\mathrm{T}\to\infty} \frac{1}{2T} \left\langle \nabla \left| \tilde{\mathbf{E}}(\mathbf{r},\omega) \right|^2 \right\rangle \mathrm{d}\omega \\
&\quad + 4\pi \mathrm{Im}\alpha_e \mathrm{Re} \left\{ \int_{-\infty}^{+\infty} \mathop{\mathrm{Lim}}_{\mathrm{T}\to\infty} \frac{1}{2T} \left\langle k\tilde{\mathbf{E}}(\mathbf{r},\omega) \times \tilde{\mathbf{B}}^*(\mathbf{r},\omega) \right\rangle \mathrm{d}\omega \right\} \\
&\quad + 4\pi \mathrm{Im}\alpha_e \mathrm{Im} \left\{ \int_{-\infty}^{+\infty} \mathop{\mathrm{Lim}}_{\mathrm{T}\to\infty} \frac{1}{2T} \left\langle \left(\tilde{\mathbf{E}}^*(\mathbf{r},\omega) \cdot \nabla \right) \tilde{\mathbf{E}}(\mathbf{r},\omega) \right\rangle \mathrm{d}\omega \right\},
\end{aligned} \tag{4.54}
$$

where Im denotes the imaginary part. In Eq. (4.54) the physical meaning is the same as stated in Section 4.3.2, i.e., the first term represents the conservative or *gradient* force, whereas the second and third terms correspond to the non-conservative *scattering component*, or *radiation pressure*, and to the *curl* force, respectively. Likewise, one may write the same decomposition for the averaged force spectral components in $\omega-$space, [cf. Eq. (4.50)]:

$$
\begin{aligned}
\left\langle \tilde{\mathbf{F}}(\mathbf{r},\omega) \right\rangle &= \mathrm{Re}\alpha_e \nabla \left\langle \left| \tilde{\mathbf{E}}(\mathbf{r},\omega) \right|^2 \right\rangle + 2k\mathrm{Im}\alpha_e \mathrm{Re} \left\{ \left\langle \tilde{\mathbf{E}}(\mathbf{r},\omega) \times \tilde{\mathbf{B}}^*(\mathbf{r},\omega) \right\rangle \right\} \\
&\quad + 2\mathrm{Im}\alpha_e \mathrm{Im} \left\{ \left\langle \left(\tilde{\mathbf{E}}^*(\mathbf{r},\omega) \cdot \nabla \right) \tilde{\mathbf{E}}(\mathbf{r},\omega) \right\rangle \right\}.
\end{aligned} \tag{4.55}
$$

It should be remarked that if the particle is magnetodielectric, namely, if additionally it has a magnetic polarizability α_m [59], then in a similar way as for Eq. (4.55) one obtains for the averaged force on the particle due to the magnetic field $\bar{F}_i^m(\mathbf{r},t) = 2\mathrm{Re}\left\{ \alpha_m \partial_i^{(*)} \mathrm{Tr} \mathcal{B}_{jk}(\mathbf{r},\mathbf{r},0) \right\}$, $\mathcal{B}_{jk}(\mathbf{r},\mathbf{r}',\tau) = \left\langle B_j(\mathbf{r},t) B_k^*(\mathbf{r},t+\tau) \right\rangle$:

$$
\begin{aligned}
\left\langle \tilde{\mathbf{F}}^m(\mathbf{r},\omega) \right\rangle &= \mathrm{Re}\alpha_m \nabla \left\langle \left| \tilde{\mathbf{B}}(\mathbf{r},\omega) \right|^2 \right\rangle + 2k\mathrm{Im}\alpha_m \mathrm{Re} \left\{ \left\langle \tilde{\mathbf{E}}(\mathbf{r},\omega) \times \tilde{\mathbf{B}}^*(\mathbf{r},\omega) \right\rangle \right\} \\
&\quad + 2\mathrm{Im}\alpha_m \mathrm{Im} \left\{ \left\langle \left(\tilde{\mathbf{B}}^*(\mathbf{r},\omega) \cdot \nabla \right) \tilde{\mathbf{B}}(\mathbf{r},\omega) \right\rangle \right\}.
\end{aligned} \tag{4.56}
$$

And for the mean force due to the interaction between the electric and magnetic dipole induced in the particle $\left\langle F_i^{e-m}(\mathbf{r},t) \right\rangle = -(8/3)k^4 \mathrm{Re}\left\{ \alpha_e \alpha_m^* \epsilon_{ijk} \mathcal{G}_{jk}(\mathbf{r},\mathbf{r},0) \right\}$, with $\mathcal{G}_{jk}(\mathbf{r},\mathbf{r}',\tau) = \left\langle E_j(\mathbf{r},t) B_k^*(\mathbf{r},t+\tau) \right\rangle$ [59]:

$$
\begin{aligned}
\left\langle \tilde{\mathbf{F}}^{e-m} \right\rangle &= -\frac{4k^4}{3} \left\{ \mathrm{Re}(\alpha_e \alpha_m^*) \mathrm{Re} \left\langle \tilde{\mathbf{E}} \times \tilde{\mathbf{B}}^* \right\rangle - \mathrm{Im}(\alpha_e \alpha_m^*) \mathrm{Im} \left\langle \tilde{\mathbf{E}} \times \tilde{\mathbf{B}}^* \right\rangle \right\} \\
&= -\frac{4k^4}{3} \mathrm{Re}(\alpha_e \alpha_m^*) \mathrm{Re} \left\langle \tilde{\mathbf{E}} \times \tilde{\mathbf{B}}^* \right\rangle \\
&\quad + \frac{4k^3}{3} \mathrm{Im}(\alpha_e \alpha_m^*) \left[\frac{1}{2} \nabla \left\langle |\tilde{\mathbf{E}}|^2 \right\rangle - \mathrm{Re} \left\langle (\tilde{\mathbf{E}}^* \cdot \nabla) \tilde{\mathbf{E}} \right\rangle \right].
\end{aligned} \tag{4.57}
$$

For the sake of brevity, we have omitted in the notation of Eq. (4.57) the arguments $\mathbf{r}$ and ω of the analytic signal spectral vectors $\tilde{\mathbf{E}}$ and $\tilde{\mathbf{B}}$. In this chapter, we study the mean force on a particle with electric polarizability α_e only. [cf. Eq. (4.55)].

4.4.2 *Conservative and non-conservative components from the momentum densities*

Now let us address the contribution of the different momentum densities (linear, orbital and spin) of the partially coherent light. As we stated in Section 4.3, the total electric force can be written as

$$
\begin{aligned}
\langle \tilde{F}_{e,i} \rangle &= 2\mathrm{Re} \left\{ \alpha_e \partial_i^{(*)} \mathrm{Tr} \tilde{\mathcal{E}}_{jk} \left(\mathbf{r}, \mathbf{r}, \omega \right) \right\} \\
&= 2\mathrm{Re}\alpha_e \mathrm{Re} \left\{ \partial_i^{(*)} \mathrm{Tr} \tilde{\mathcal{E}}_{jk} \left(\mathbf{r}, \mathbf{r}, \omega \right) \right\} - 2\mathrm{Im}\alpha_e \mathrm{Im} \left\{ \partial_i^{(*)} \mathrm{Tr} \tilde{\mathcal{E}}_{jk} \left(\mathbf{r}, \mathbf{r}, \omega \right) \right\} \\
&= \langle \tilde{F}_{e,i}^{cons} \rangle + \langle \tilde{F}_{e,i}^{nc} \rangle .
\end{aligned}
\tag{4.58}
$$

From Eq. (4.6), we see that the non-conservative term is proportional to the orbital momentum density of light $\langle \mathbf{p}_e^{\circ} \rangle$

$$
\begin{aligned}
\langle \tilde{F}_{e,i}^{nc} \rangle &= -2\mathrm{Im}\alpha_e \mathrm{Im} \left\{ \partial_i^{(*)} \mathrm{Tr} \tilde{\mathcal{E}}_{jk} \left(\mathbf{r}, \mathbf{r}, \omega \right) \right\} \\
&= 16\pi\omega \mathrm{Im}\alpha_e \langle p_{e,i}^{\circ} \rangle .
\end{aligned}
\tag{4.59}
$$

Notice, that in equation we write $\langle \mathbf{p}_e^{\circ} \rangle$ with angular brackets $\langle \cdot \rangle$ because in this case, the orbital momentum density is understood within the framework of classical second-order coherence theory of vector electromagnetic fields, where the conservations laws are also established [49, 73]. Thus, without loss of generality, we can write $\langle \mathbf{p}_e^{\circ} \rangle = \langle \mathbf{p}_e \rangle - \langle \mathbf{p}_e^{s} \rangle$, and the total electric force leads to

$$
\langle \tilde{\mathbf{F}}_e \left(\mathbf{r}, \omega \right) \rangle = \mathrm{Re}\alpha_e \nabla \left\langle \left| \tilde{\mathbf{E}} \left(\mathbf{r}, \omega \right) \right|^2 \right\rangle + 16\pi\omega \mathrm{Im}\alpha_e \langle \mathbf{p}_e \rangle - 16\pi\omega \mathrm{Im}\alpha_e \langle \mathbf{p}_e^{s} \rangle ,
\tag{4.60}
$$

and analogously for the magnetic force, we have

$$
\langle \tilde{\mathbf{F}}_m \left(\mathbf{r}, \omega \right) \rangle = \mathrm{Re}\alpha_m \nabla \left\langle \left| \tilde{\mathbf{E}} \left(\mathbf{r}, \omega \right) \right|^2 \right\rangle + 16\pi\omega \mathrm{Im}\alpha_m \langle \mathbf{p}_m \rangle - 16\pi\omega \mathrm{Im}\alpha_e \langle \mathbf{p}_m^{s} \rangle .
\tag{4.61}
$$

These equations manifest the contribution of the momentum density of a partially coherent electromagnetic field.

4.4.3 *Transition to a scalar theory: Dependence of the averaged optical force of propagated fields on the coherence at a diffraction plane. A Young interference configuration*

Eqs. (4.55)-(4.61) manifest the dependence of the force on the statistical properties of the source. To illustrate this with a simple example, let us consider a wavefield whose electric and magnetic vectors at frequency ω are realizations of an ensemble of random functions each of which may be described by a scalar member $U(\mathbf{r}, \omega)$ of a statistical ensemble $U(\mathbf{r}, \omega) \exp(-i\omega t)$ of monochromatic fields, all of frequency ω. [20, 74]. (Of course, this space-frequency description may also

apply to a quasimonochromatic field, whose spectrum is centered at a mean frequency $\bar{\omega}$ of its spectrum).

The monochromatic electric vector realizations at frequency ω may be expressed as: $\tilde{\mathbf{E}}(\mathbf{r}, \omega) = U(\mathbf{r}, \omega)\mathbf{e}(\omega)$, (cf. Section 8.4 of [1]). This a common situation in Fourier optics [2]. The vector $\mathbf{e}(\omega)$ is real (linear polarization). On introducing $W(\mathbf{r}_1, \mathbf{r}_2, \omega) = \langle U^*(\mathbf{r}_1, \omega)U(\mathbf{r}_2, \omega)\rangle$ as the *cross-spectral density* of $U(\mathbf{r}, \omega)$ [3], writing $\partial_i^{(*)} W(\mathbf{r}, \mathbf{r}, \omega) = [\partial_i W(\mathbf{r}, \mathbf{r}', \omega)]_{\mathbf{r}'=\mathbf{r}} = \langle U(\mathbf{r}, \omega)\partial_i U^*(\mathbf{r}, \omega)\rangle$ and taking real and imaginary parts in Eq. (4.50) one obtains

$$
\begin{aligned}
\langle \tilde{F}_i(\mathbf{r}, \omega)\rangle &= 2|\mathbf{e}(\omega)|^2 \mathrm{Re}\left\{\alpha_e \langle \partial_i U^*(\mathbf{r}, \omega)U(\mathbf{r}, \omega)\rangle\right\} \\
&= 2|\mathbf{e}(\omega)|^2 [\mathrm{Re}\alpha_e \mathrm{Re}\langle U(\mathbf{r}, \omega)\partial_i U^*(\mathbf{r}, \omega)\rangle \\
&\quad -\mathrm{Im}\alpha_e \mathrm{Im}\langle U(\mathbf{r}, \omega)\partial_i U^*(\mathbf{r}, \omega)\rangle].
\end{aligned}
\tag{4.62}
$$

The first term of Eq. (4.62), is the *mean gradient force*, which is expressed as [see also the first term of Eq. (4.55)]:

$$
\begin{aligned}
\left\langle \tilde{F}_i^{grad}(\mathbf{r}, \omega)\right\rangle &= |\mathbf{e}(\omega)|^2 \mathrm{Re}\alpha_e \partial_i W(\mathbf{r}, \mathbf{r}, \omega) \\
&= |\mathbf{e}(\omega)|^2 \mathrm{Re}\alpha_e \partial_i \left\langle |U(\mathbf{r}, \omega)|^2\right\rangle.
\end{aligned}
\tag{4.63}
$$

The second term of Eq. (4.62) is proportional to the *mean energy flow spectral density* $\langle \mathcal{S}\rangle$ associated to the scalar wavefunction $U(\mathbf{r}, \omega)$ [10]:

$$
\langle \mathcal{S}_i(\mathbf{r}, \omega)\rangle = -\frac{1}{k}\mathrm{Im}\langle U(\mathbf{r}, \omega)\partial_i U^*(\mathbf{r}, \omega)\rangle.
\tag{4.64}
$$

As such, it is *the averaged scattering force*, or *mean radiation pressure*, i.e.

$$
\begin{aligned}
\left\langle \tilde{F}_i^{sc}(\mathbf{r}, \omega)\right\rangle &= -2|\mathbf{e}(\omega)|^2 \mathrm{Im}\alpha_e \mathrm{Im}\left\{\partial_i^{(*)} W(\mathbf{r}, \mathbf{r}, \omega)\right\} \\
&= -2|\mathbf{e}(\omega)|^2 \mathrm{Im}\alpha_e \mathrm{Im}\left\{[\partial_i W(\mathbf{r}, \mathbf{r}', \omega)]_{\mathbf{r}'=\mathbf{r}}\right\} \\
&= 2k|\mathbf{e}(\omega)|^2 \mathrm{Im}\alpha_e \langle \mathcal{S}_i(\mathbf{r}, \omega)\rangle.
\end{aligned}
\tag{4.65}
$$

Eq. (4.65) manifests the correspondence of $\langle \mathcal{S}\rangle$ in this scalar formulation of the radiation pressure with the mean Poynting vector $\langle \mathbf{S}\rangle = (c/8\pi\mu)\langle \mathbf{E}\times\mathbf{B}^*\rangle$ in the second term of Eq. (4.55) acording to the vector representation.

Notice that the *mean curl of electric spin density* which according to the third term of Eq. (4.55) takes on the form

$$
\left\langle \tilde{F}_i^{curl}(\mathbf{r}, \omega)\right\rangle = 2\mathrm{Im}\alpha_e \mathrm{Im}\left\{e_j^*(\omega)e_i(\omega)\partial_j W(\mathbf{r}, \mathbf{r}, \omega)\right\},
\tag{4.66}
$$

where ∂_i means the derivative in the non-conjugated function, i.e.,

$$
\partial_i W(\mathbf{r}, \mathbf{r}, \omega) = \langle U^*(\mathbf{r}, \omega)\partial_i U(\mathbf{r}, \omega)\rangle.
\tag{4.67}
$$

Taking into account Maxwell's divergence equation $\nabla\cdot\mathbf{E}(\mathbf{r}, \omega) = 0$ in Eq. (4.66), it is easy to demonstrate that $\langle \tilde{F}_i^{curl}(\mathbf{r}, \omega)\rangle$ will be zero if $\mathrm{Im}\left\{e_j^*(\omega)e_i(\omega)\right\} = 0$; which evidently holds since $\mathbf{e}(\omega)$ is real.

According to the Huygens-Fresnel principle [1, 3, 4] the fluctuating realizations at frequency ω of the field propagated from points $\mathbf{r}'$ of a surface $\mathcal{A}$ up to a point $\mathbf{r}$ are given by

$$
U(\mathbf{r}, \omega) = -\frac{ik}{2\pi}\int_{\mathcal{A}} U(\mathbf{r}', \omega)\frac{e^{ikR}}{R}\mathrm{d}^2 r'.
\tag{4.68}
$$

where $R = |\mathbf{r} - \mathbf{r}'|$ and $k = 2\pi/\lambda$, the wavelength being λ . Thus from Eq. (4.62) the averaged force on a dipolar particle in $\mathbf{r}$ will be

$$
\begin{aligned}
\langle \tilde{F}_i(\mathbf{r}, \omega) \rangle &= -2 \left(\frac{k}{2\pi} \right)^2 |\mathbf{e}(\omega)|^2 \mathrm{Re} \left\{ \alpha_e \int_{\mathcal{A}} \int_{\mathcal{A}} [ik + \frac{1}{R_1}] \frac{\mathbf{R_1}}{R_1} W(\mathbf{r}'_1, \mathbf{r}'_2, \omega) \right. \\
&\left. \times \frac{e^{-ikR_1}}{R_1} \frac{e^{ikR_2}}{R_2} \mathrm{d}^2 r'_1 \mathrm{d}^2 r'_2 \right\},
\end{aligned}
\tag{4.69}
$$

$\mathbf{R}_i = \mathbf{r} - \mathbf{r}'_i$, $R_i = |\mathbf{r} - \mathbf{r}'_i|$, $(i = 1, 2)$. As mentioned above, Eq. (4.69) exhibits the dependence of the mean force exerted by the propagated field on its coherence properties on a surface $\mathcal{A}$.

For instance, we consider the surface $\mathcal{A}$ being composed of an opaque screen with two point holes, (see Fig. 4.3), so that the random field wavefunction in $\mathcal{A}$ is: $U(\mathbf{r}', \omega) = U(\mathbf{q}_1, \omega)\delta(\mathbf{r}' - \mathbf{q}_1) + U(\mathbf{q}_2, \omega)\delta(\mathbf{r}' - \mathbf{q}_2)$. Then from Eqs. (4.68), (4.69), (4.63) and (4.65) we obtain for the conservative and non-conservative force components on a particle at a point P of position vector $\mathbf{r}$:

$$
\begin{aligned}
\langle \tilde{\mathbf{F}}^{grad}(\mathbf{r}, \omega) \rangle &= -2 \left(\frac{k}{2\pi} \right)^2 |\mathbf{e}(\omega)|^2 \mathrm{Re}\alpha_e \left\{ \langle |U(\mathbf{q}_1, \omega)|^2 \rangle \frac{\mathbf{R}_1}{R_1^4} + \langle |U(\mathbf{q}_2, \omega)|^2 \rangle \frac{\mathbf{R}_2}{R_2^4} \right. \\
&+ \frac{|W(\mathbf{q}_1, \mathbf{q}_2, \omega)|}{R_1 R_2} \left[\left(\frac{\mathbf{R}_1}{R_1^2} + \frac{\mathbf{R}_2}{R_2^2} \right) \cos\left(k(\mathbf{R}_1 - \mathbf{R}_2) + \alpha(\mathbf{q}_1, \mathbf{q}_2, \omega) \right) \right. \\
&\left. \left. + \left(\frac{\mathbf{R}_1}{R_1} - \frac{\mathbf{R}_2}{R_2} \right) k \sin\left(k(\mathbf{R}_1 - \mathbf{R}_2) + \alpha(\mathbf{q}_1, \mathbf{q}_2, \omega) \right) \right] \right\},
\end{aligned}
\tag{4.70}
$$

$$
\begin{aligned}
\langle \tilde{\mathbf{F}}^{sc}(\mathbf{r}, \omega) \rangle &= 4 \left(\frac{k}{2\pi} \right)^2 |\mathbf{e}(\omega)|^2 \mathrm{Im}\alpha_e \left\{ \langle |U(\mathbf{q}_1, \omega)|^2 \rangle k \frac{\mathbf{R}_1}{R_1^3} + \langle |U(\mathbf{q}_2, \omega)|^2 \rangle k \frac{\mathbf{R}_2}{R_2^3} \right. \\
&+ \frac{|W(\mathbf{q}_1, \mathbf{q}_2, \omega)|}{R_1 R_2} \left[\frac{\mathbf{R}_1}{R_1^2} \left(kR_1 \cos\left(k(\mathbf{R}_1 - \mathbf{R}_2) + \alpha(\mathbf{q}_1, \mathbf{q}_2, \omega) \right) \right. \right. \\
&+ \sin\left(k(\mathbf{R}_1 - \mathbf{R}_2) + \alpha(\mathbf{q}_1, \mathbf{q}_2, \omega) \right) \\
&+ \frac{\mathbf{R}_2}{R_2^2} \left(kR_2 \cos\left(k(\mathbf{R}_1 - \mathbf{R}_2) + \alpha(\mathbf{q}_1, \mathbf{q}_2, \omega) \right) \right. \\
&\left. \left. \left. - \sin\left(k(\mathbf{R}_1 - \mathbf{R}_2) + \alpha(\mathbf{q}_1, \mathbf{q}_2, \omega) \right) \right) \right] \right\}.
\end{aligned}
\tag{4.71}
$$

Denoting $\mathbf{R}_i = \mathbf{r} - \mathbf{q}_i$, $(i = 1, 2)$, and $\alpha(\mathbf{q}_1, \mathbf{q}_2, \omega)$ being the phase of $W(\mathbf{q}_1, \mathbf{q}_2, \omega)$.

In the Fresnel and Fraunhofer regions one may approximate $R_1 \simeq R_2$ in the denominators of Eq. (4.70). Also, for $kR_i \gg 1$, $(i = 1, 2)$, the *cos* terms are negligible versus the *sin* terms and the gradient force has a sinusoidal standing wave behavior, proportional to the difference: $\mathbf{R}_1 - \mathbf{R}_2$. On the other hand, the *sin* terms of (4.71) are negligible versus the *cos* terms, rendering a scattering force proportional to the intensity pattern. This will be discussed again in Section 4.5 in connection with the configuration of Thompson and Wolf experiment, which replaces the two point holes of this schematic example by real apertures. In addition, by dropping in Eqs. (4.70) and (4.71) the corresponding factor constituted by the real and imaginary part of the electric polarizability, we observe that the action on particles situated at points $R_i \gg \lambda$ by the $\mathrm{Im}\alpha_e$-normalized repulsive scattering force produced by each independent pinhole, is much larger along $\mathbf{R}_i$ than that of the corresponding $\mathrm{Re}\alpha_e$-normalized attractive gradient force.

4.5 INTERFERENCE OF TWO QUASIMONOCHROMATIC RANDOM WAVES: DEGREE OF COHERENCE AND AVERAGED OPTICAL FORCE

In this section we address the force on a dipolar particle in the configuration of the classical two-aperture arrangement by Thompson and Wolf, employed in 1957 to observe and characterize the degree of coherence of a light wave [6]. Like in the original work by these authors we shall address quasimonochromatic light whose spectrum is centered at the frequency $\bar{\omega}$. However, the procedure is identical working with each monochromatic member of the statistical ensemble of wavefunctions, were the disturbance spectrum broader.

As shown in the scheme of Fig. 4.3, the wavefield emitted by a spatially incoherent source is brought by a lens L_1 to the mask $\mathcal{A}$ in $z = 0$, containing two small circular apertures of radius a, centered at points $\mathbf{r}'_1 = (\mathbf{q}_1, 0)$ and $\mathbf{r}'_2 = (\mathbf{q}_2, 0)$, respectively. A second lens L_2 sends the field diffracted in $\mathcal{A}$ to points P of a screen $\mathcal{B}$ coinciding with its focal plane. Of course in this case the cross-spectral density is $W(\mathbf{r}, \mathbf{r}', \omega) = J(\mathbf{r}, \mathbf{r}')\delta(\omega - \bar{\omega})$. $J(\mathbf{r}, \mathbf{r}')$ being the *mutual intensity function* [1, 3] given by the equal-time correlation: $\langle U^*(\mathbf{r}, t)U(\mathbf{r}, t)\rangle$.

Then, the spectral degree of coherence of the wave in $\mathcal{A}$: $\mu(\mathbf{q}_1, \mathbf{q}_2, \bar{\omega}) = W(\mathbf{q}_1, \mathbf{q}_2, \bar{\omega})/$ $[W(\mathbf{q}_1, \mathbf{q}_1, \bar{\omega})W(\mathbf{q}_2, \mathbf{q}_2, \bar{\omega})]^{1/2}$ coincides with the degree of coherence $g(\mathbf{q}_1, \mathbf{q}_2, 0)$ [6], which in turn is simply: $J(\mathbf{q}_1, \mathbf{q}_2)$ $/[J(\mathbf{q}_1, \mathbf{q}_1)J(\mathbf{q}_2, \mathbf{q}_2)]^{1/2}$. μ or g (which, as seen, may indistinctly be used for quasimonochromatic light) are expressed by means of the Van-Cittert-Zernike theorem [1, 3] in terms of the intensity exiting the incoherent source, and they equal $2J_1(u)/u$ in $z = 0$. Where $u = 2\pi\rho h/(\bar{\lambda}\Delta)$. ρ being the radius of the source, assumed planar and circular, and Δ denoting the distance between the source and L_1 [6]. In this way, we establish the influence of the partial coherence in $\mathcal{A}$ of the light emitted by the random incoherent source, on the optical force from the diffracted field upon a dipolar particle placed in $\mathcal{B}$.

In the vector theory of diffraction, within the range of validity of the Kirchhoff approximation, the electric vector of frequency ω diffracted by an aperture centered in $\mathbf{r} = 0$ in a screen $\mathcal{A}$ is expressed in the far zone as [10, 43]

$$\tilde{\mathbf{E}}(\mathbf{r}, \omega) = \frac{ie^{ikr}}{2\pi r}\mathbf{k} \times \int_{\mathcal{A}} \mathbf{n} \times \tilde{\mathbf{E}}^{(i)}(\mathbf{r}', \omega)e^{-i\mathbf{k}\cdot\mathbf{r}'}ds', \tag{4.72}$$

where $\mathbf{k} = k\mathbf{s} = (2\pi/\lambda)\mathbf{s}$, $\mathbf{s} = \mathbf{r}/r$ is a unit vector in the direction of observation $\mathbf{r} = (x, y, z)$, $\mathbf{r}'$ denotes a coordinate in the aperture whose element of surface area is ds', and $\mathbf{n}$ is the unit outward normal to ds'. The time-dependence $e^{-i\omega t}$ is understood, and $\tilde{\mathbf{E}}^{(i)}(\mathbf{r}') = \mathbf{e}^{(i)}(\omega)\exp(ik\mathbf{n}^{(i)} \cdot \mathbf{r}')$, $(|\mathbf{n}^{(i)}| = 1, \text{Im}\mathbf{e}^{(i)} = 0)$, is the electric field incident on the mask $\mathcal{A}$.

Assuming $\mathbf{n}^{(i)} = (0, 0, 1)$, a flat opaque screen in $z = 0$ with a circular aperture of center $\mathbf{r}' = 0$ and radius a produces according to Eq. (4.72) the diffracted field [1, 2]

$$\tilde{\mathbf{E}}(\mathbf{r}, \omega) = U(\mathbf{r}, \omega)\mathbf{e}(\omega), \tag{4.73}$$

where

$$U(\mathbf{r}, \omega) = e^{ikz}e^{i\frac{k}{2z}(x^2+y^2)}\left(\frac{\pi a^2}{i\lambda z}\right)\left(2\frac{J_1(v_0)}{v_0}\right). \tag{4.74}$$
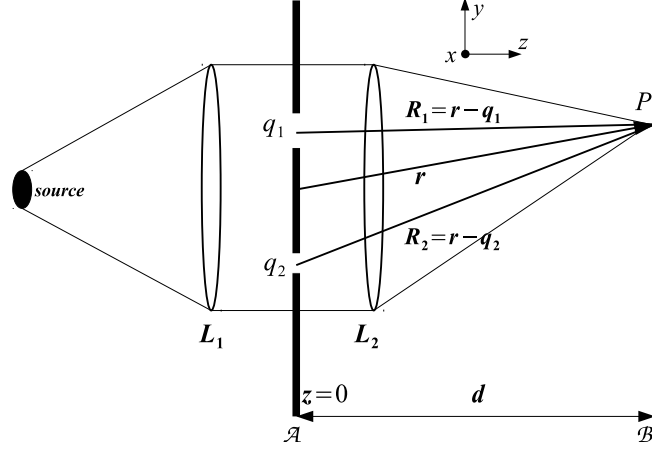
Figure 4.3: Schematics of the configuration for observing interference at points $P = (x, y, d)$ of a screen $\mathcal{B}$ by diffraction of light, propagated from an incoherent source, at two apertures in $\mathcal{A}$, centered at points $\mathbf{r}_1' = (\mathbf{q}_1, 0)$ and $\mathbf{r}_2' = (\mathbf{q}_2, 0)$, respectively. $\mathbf{q}_1 = (x_1, y_1)$, $\mathbf{q}_2 = (x_2, y_2)$. $2h = |\mathbf{q}_1 - \mathbf{q}_2|$.

In Eqs. (4.73) and (4.74) we have written $\mathbf{e}(\omega) = \mathbf{s} \times \left(\mathbf{n} \times \mathbf{e}^{(i)}(\omega) \right)$ and the v_0 the dimensionless factor $v_0 = ka\sqrt{x^2 + y^2}/z$, respectively.

Next we study the effect of the degree of coherence in $\mathcal{A}$ of the wavefield at the mean frequency $\bar{\omega}$, propagated from the quasimonochromatic fluctuating source, on the averaged optical force upon a dipolar particle in the Fraunhofer zone. Hence we shall address the consequences of the correlation between the field at the two circular apertures in $z = 0$, centered at $\mathbf{q}_1 \equiv (0, h)$ and $\mathbf{q}_2 \equiv (0, -h)$, as shown in Fig. 4.3. To this end, we evaluate the field at an arbitrary point P in the plane $\mathcal{B}$ at $z = d$ where the particle is situated, produced on diffraction in $\mathcal{A}$, (cf. Fig. 4.3) within the Kirchhoff approximation:

$$
\begin{aligned}
& U(\mathbf{r}, \bar{\omega}) \\
= \; & e^{i\bar{k}d} e^{i\frac{k}{2d}(x^2 + y^2)} \left(\frac{\pi a^2}{i\bar{\lambda}d} \right) \left(2\frac{J_1(\bar{v}_0)}{\bar{v}_0} \right) \left[U(\mathbf{q}_1, \bar{\omega}) e^{-i\frac{\bar{k}hy}{d}} + U(\mathbf{q}_2, \bar{\omega}) e^{i\frac{\bar{k}hy}{d}} \right],
\end{aligned}
$$
(4.75)

where $U(\mathbf{q}_i, \bar{\omega})$ $(i = 1, 2)$ is the complex amplitude of the random wavefield at $\mathbf{q}_1$ and $\mathbf{q}_2$ emitted by the fluctuating source. $\bar{v}_0 = \bar{k}a\sqrt{x^2 + y^2}/z$. If as in Thompson and Wolf experiment [6], one has that $\left\langle |U(\mathbf{q}_1, \bar{\omega})|^2 \right\rangle \simeq \left\langle |U(\mathbf{q}_2, \bar{\omega})|^2 \right\rangle = I_0$, the observed mean intensity at P then is known to be

$$
\begin{aligned}
& \langle I(\mathbf{r}, \bar{\omega}) \rangle \\
= \; & \left\langle \tilde{\mathbf{E}}(\mathbf{r}, \bar{\omega}) \cdot \tilde{\mathbf{E}}^*(\mathbf{r}, \bar{\omega}) \right\rangle \\
= \; & 2I_0 \left(\frac{\pi a^2 |\mathbf{e}(\bar{\omega})|}{\bar{\lambda}d} \right)^2 \left(\frac{2J_1(\bar{v}_0)}{\bar{v}_0} \right)^2 \left[1 + |\mu(\mathbf{q}_1, \mathbf{q}_2, \bar{\omega})| \cos \left(\phi(\mathbf{q}_1, \mathbf{q}_2, \bar{\omega}) + \frac{2\bar{k}hy}{d} \right) \right].
\end{aligned}
$$
(4.76)

The factor $2\bar{k}hy/d$ represents the path difference $|\mathbf{R}_1 - \mathbf{R}_2|$, (see Fig. 4.3). $\phi(\mathbf{q}_1, \mathbf{q}_2, \bar{\omega})$ is the phase of $\mu(\mathbf{q}_1, \mathbf{q}_2, \bar{\omega})$.

The interference law of Eq. (4.76) is well known [1, 6]. We shall perform calculations of the force with the same parameters as in Ref. [6], namely: $\bar{\lambda} = 579\,nm$, $2h = 6\,mm$, $a = 0.7mm$, $d = 1.5\,m$. We consider $\phi(\mathbf{q}_1, \mathbf{q}_2, \bar{\omega}) = 0$ and we will initially normalize the results to the polarizability, so that we will make $\mathrm{Re}\alpha_e = \mathrm{Im}\alpha_e = 1$; this allows us to obtain an estimation of the relative strengths of the different force components due to diffraction, independently of the polarizability.

In this far zone, the *gradient force* is governed by the expression (4.63) applied to the mean intensity (4.76). Since the apertures are aligned along the $y-$axis, the y component for $\bar{k}R_i \to \infty$ $(i = 1, 2)$ is obtained after a long but straightforward algebra

$$
\begin{aligned}
\left\langle \tilde{F}_y^{grad} \right\rangle &\approx -4\mathrm{Re}\alpha_e I_0 \left(\frac{\pi a^2 \, |\mathbf{e}(\bar{\omega})|}{\bar{\lambda}d} \right)^2 \left(2\frac{J_1(v_0)}{v_0} \right)^2 \frac{h\bar{k}}{d} \\
&\quad \times |\mu(\mathbf{q}_1, \mathbf{q}_2, \bar{\omega})| \sin\left(\phi(\mathbf{q}_1, \mathbf{q}_2, \bar{\omega}) + \frac{2\bar{k}hy}{d} \right),
\end{aligned} \tag{4.77}
$$

which agrees with the remark at the end of Section 4.4.3 concerning Eq. (4.70).

This expression is just the derivative of Eq. (4.76) with respect to y, assuming that the factor outside the brackets in (4.76) is constant, (although this is not strictly true, the terms yielded by the y-derivative of this factor become negligible, as shown in the Appendix B.1). The other two components: $\left\langle \tilde{F}_x^{grad} \right\rangle$ and $\left\langle \tilde{F}_z^{grad} \right\rangle$ are similarly obtained in the Appendix B.1. Fig. 4.5 shows the interference pattern of $\langle I \rangle$, normalized to its maximum, at the screen $\mathcal{B}$ for $|\mu(\mathbf{q}_1, \mathbf{q}_2, \bar{\omega})| = 1$, as well as the spatial distribution of the three components of the mean gradient force on a dipolar particle in $\mathcal{B}$ due to this distribution of light. To see the relative weight of each Cartesian component, we normalize it to the magnitude of the total mean force $|\langle \tilde{\mathbf{F}}^{tot} \rangle| = |\langle \tilde{\mathbf{F}}^{grad} \rangle + \langle \tilde{\mathbf{F}}^{sc} \rangle|$. We also observe an interference pattern along OY in each component of this conservative force, $\left\langle \tilde{F}_z^{grad} \right\rangle$ being much smaller than the other two. In addition, Fig. 4.4(b) exhibits an oscillatory modulation of $\left\langle \tilde{F}_x^{grad} \right\rangle$ along OX, (cf. Appendix B.1).

We remark that in the limiting case $|\mu(\mathbf{q}_1, \mathbf{q}_2, \bar{\omega})| = 0$, $\left\langle \tilde{F}_y^{grad} \right\rangle$ is just proportional to $\partial_y \left(2J_1(\bar{v}_0)/\bar{v}_0 \right)^2$ and the interference effect disappears, as it should. Since this y derivative was neglected versus the term kept in Eq. (4.77), (see also Appendix B.1), the values of $\left\langle \tilde{F}_y^{grad} \right\rangle$ then are practically zero compared to those due to a partially coherent wave. This is seen in Fig. 4.5. The intensity pattern, which acts as a potential distribution for the illuminated particle, is shifted by $\pi/2$ with respect to that of the conservative force $\left\langle \tilde{F}_y^{grad} \right\rangle$, whose oscillation amplitude progressively diminishes to zero as the value of $|\mu(\mathbf{q}_1, \mathbf{q}_2, \bar{\omega})|$ decreases. This behavior of the conservative force constitutes the basic mechanism of an optical tweezer with several equilibrium positions of the particle along the lines in the screen $\mathcal{B}$ where $\langle I \rangle$ is maximum, . Such points occur along OY at $x = 0$, [cf. Figs. 4.4(a) and 4.4(c)], and are precisely those where $\left\langle \tilde{F}_x^{grad} \right\rangle = 0$, [cf. Fig. 4.4(b)].

We next address the *scattering force* on a small particle in an arbitrary point of the screen $\mathcal{B}$, obtained on introducing Eq. (4.75) into Eq. (4.65), (see Appendix B.2). The scattering and gradient force $x-$components are of similar magnitude, but of signs opposite to each other; this is seen on comparing Fig. 4.6(a) with Fig. 4.4(b). By contrast, the y-component of $\left\langle \tilde{F}^{sc} \right\rangle$ is one
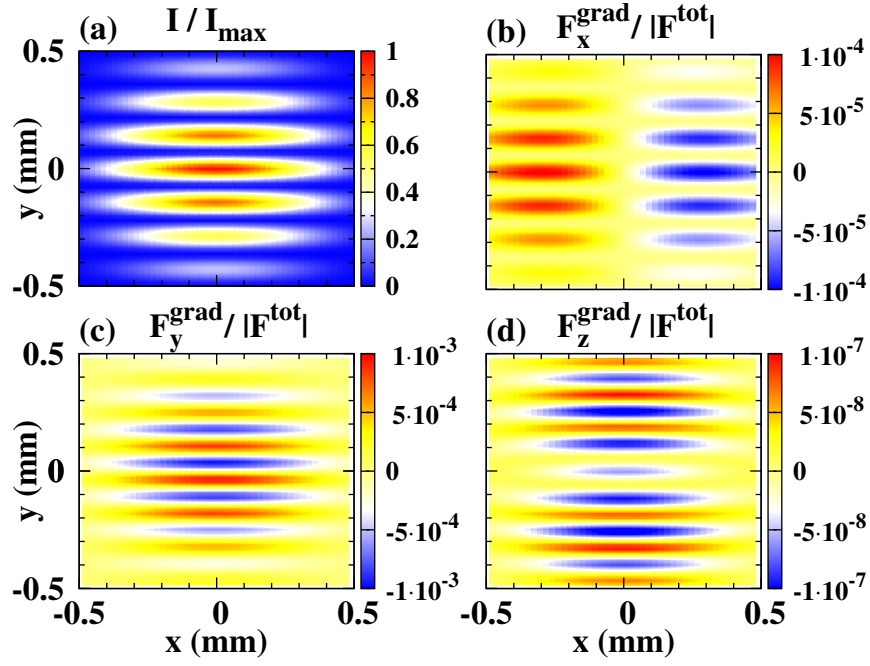
Figure 4.4: Spatial distributions in the XY plane of the mean intensity and the normalized mean gradient force components for $|\mu(\mathbf{q}_1, \mathbf{q}_2, \bar{\omega})| = 1$. (a) Normalized mean intensity $\langle I \rangle$. (b) $\left\langle \tilde{F}_x^{grad} \right\rangle$. (c) $\left\langle \tilde{F}_y^{grad} \right\rangle$. (d) $\left\langle \tilde{F}_z^{grad} \right\rangle$. All values are calculated on a dipolar particle at the screen plane $\mathcal{B}$, placed at distance $z = d = 1.5\,m$ from the aperture screen $\mathcal{A}$. The force components are normalized to $\mathrm{Re}\,\alpha_e$ and to the magnitude of the total mean force $\left| \left\langle \tilde{\mathbf{F}}^{tot} \right\rangle \right| = \left| \left\langle \tilde{\mathbf{F}}^{grad} \right\rangle + \left\langle \tilde{\mathbf{F}}^{sc} \right\rangle \right|$.
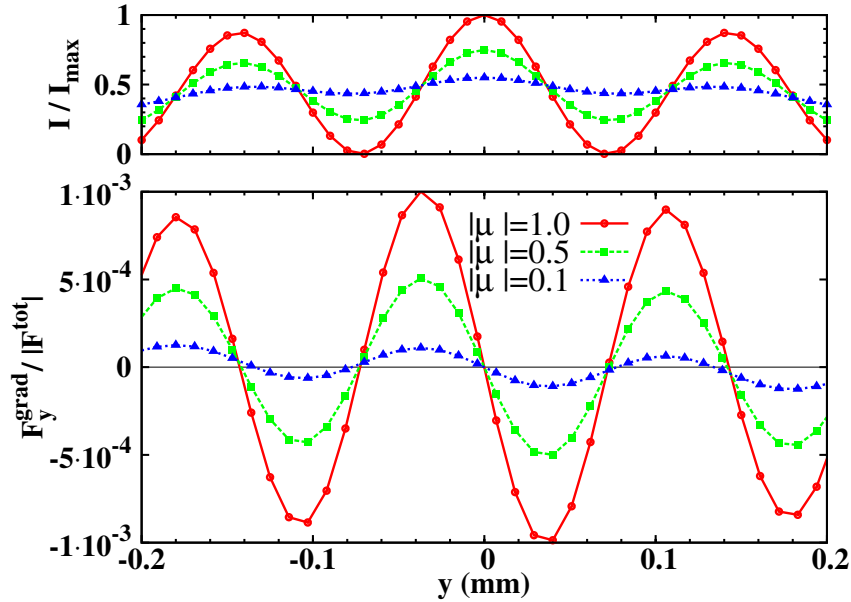
Figure 4.5: (a) Normalized mean intensity $\langle I \rangle$. (b) Normalized mean gradient force component $\left\langle \tilde{F}_y^{grad} \right\rangle$ for different values of $|\mu(\mathbf{q}_1, \mathbf{q}_2, \bar{\omega})|$.
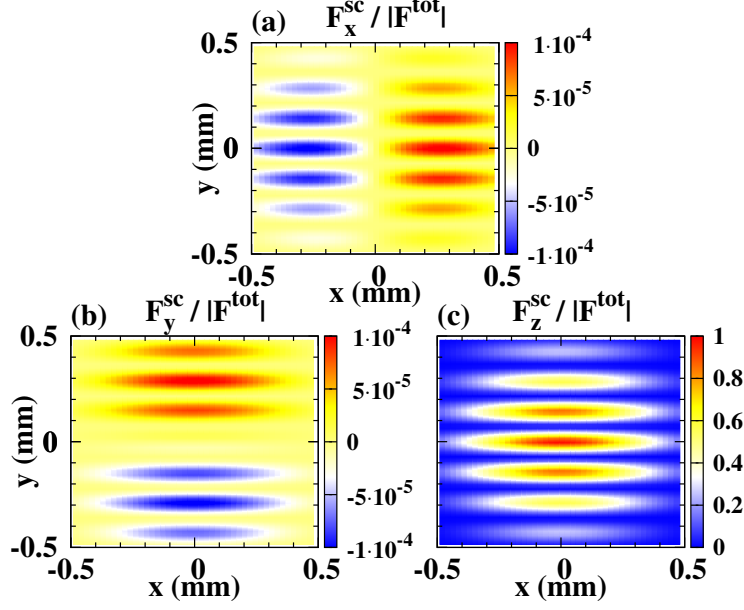
Figure 4.6: Spatial distribution in the XY plane of the normalized averaged scattering force components for $|\mu(\mathbf{q}_1, \mathbf{q}_2, \bar{\omega})| = 1$. The normalization factor is $\mathrm{Im}\alpha_e \left|\left\langle \tilde{\mathbf{F}}^{tot} \right\rangle\right|$. (a) $\left\langle F_x^{sc} \right\rangle$. (b) $\left\langle F_y^{sc} \right\rangle$. (c) $\left\langle F_z^{sc} \right\rangle$. All values are calculated on a dipolar particle in the screen plane $\mathcal{B}$, placed at distance $z = d = 1.5\,m$ from the aperture screen $\mathcal{A}$.

order of magnitude smaller than its homologous of the gradient force, suffering a sharp change of sign at $y = 0$. However, $\left\langle \tilde{F}_z^{sc} \right\rangle$ which is given by (see the Appendix B.2)

$$
\begin{aligned}
\left\langle \tilde{F}_z^{sc} \right\rangle &\approx 4\bar{k}\mathrm{Im}\alpha_e I_0 \left(\frac{\pi a^2 |\mathbf{e}(\bar{\omega})|}{\bar{\lambda}d} \right)^2 \left(2\frac{J_1(\bar{v}_0)}{\bar{v}_0} \right)^2 \\
&\quad \times \left[1 + |\mu(\mathbf{q}_1, \mathbf{q}_2, \bar{\omega})| \cos\left(\phi(\mathbf{q}_1, \mathbf{q}_2, \bar{\omega}) + \frac{2\bar{k}hy}{d} \right) \right] \\
&\approx 2\bar{k}\mathrm{Im}\alpha_e \left\langle I(\mathbf{r}, \bar{\omega}) \right\rangle,
\end{aligned}
\tag{4.78}
$$

is seven orders of magnitude larger than the corresponding conservative force $\left\langle \tilde{F}_z^{grad} \right\rangle$, [compare Fig. 4.6(c) with Fig. 4.4 (d)]. This, which is in accordance with the remark of the last paragraph of Section 4.4.3 concerning Eqs. (4.70) and (4.71) for waves from two pinholes, stems from the proportionality of $\left\langle F_z^{sc} \right\rangle$ to the Poynting vector [59] and hence to the mean scattered intensity in the far zone; [observe that the normalized $\left\langle F_z^{sc} \right\rangle$ of Fig. 4.6(c) is identical to the normalized mean intensity $\left\langle I \right\rangle$ of Fig. 4.4(a)]. As a consequence of the conservation of momentum, the particle is pushed towards $z > d$ (see Fig. 4.3). *The ratio between the maximum values of the gradient and scattering force components*, (see Eqs. (4.77), (4.78) and the Appendix B.1 and B.2), $\left\langle \tilde{F}_z^{grad} \right\rangle / \left\langle \tilde{F}_z^{sc} \right\rangle = -(y/d)\left\langle \tilde{F}_y^{grad} \right\rangle / \left\langle \tilde{F}_z^{sc} \right\rangle = \left(yh/d^2 \right)\left(|\mu|/1 + |\mu| \right)$ explains the difference between the magnitudes of these force components.

The much larger strength of the normalized scattering force may prevent the lateral manipulation of the particle in $\mathcal{B}$. If this were the case, it may be overcame with a scheme analogous to that employed in holographic optical tweezers [75].

Summing up, we observe that the Young experiment configuration shows us fundamental characteristics of the optical force components, which in this system allow a scalar formulation and thus yield no *curl* component. *The mean scattering force is proportional to the mean scattered intensity, its longitudinal z-component being several orders of magnitude larger than its x and y components.* On the other hand, *the y and z-components of the gradient force are proportional to the magnitude of the degree of coherence, thus becoming zero for incoherent light, and hence their value oscillates and decreases as $J_1(2\pi\rho h/\bar{\lambda}\Delta)/(2\pi\rho h/\bar{\lambda}\Delta)$ versus the distance h between apertures* [6].

4.5.1 *Effect of the electric polarizability on the mean optical force*

We have so far estimated the different components of the mean force by only considering the configuration of the diffracted waves; namely, by normalizing them to the particle polarizability. However, it is worth remarking that since their actual strengths, observed in an experiment, are proportional to $\text{Re}\alpha_e$ (gradient force) ant to $\text{Im}\alpha_e$ (scattering force), the relative values of these two parts of α_e should greatly influence the magnitude of these forces. Notice that although we have concluded that $\left\langle \tilde{F}_y^{grad} \right\rangle \ll \left\langle \tilde{F}_z^{sc} \right\rangle$ when they are normalized to $\text{Re}\alpha_e$ and $\text{Im}\alpha_e$, respectively, in most cases pertaining to dielectric particles one has that $\text{Re}\alpha_e \gg \text{Im}\alpha_e$, except in the presence of Mie electric and/or magnetic [59, 61] or localized plasmon [76] resonances.

For a small spherical particle of radius r_0, with relative permittivity ε_p, in the Rayleigh limit ($\bar{k}r_0 \ll 1$), we adopt the expression for the dynamic electric polarizability [59, 61]:

$$\alpha_e = \alpha_e^{(0)} \left(1 - i\frac{2}{3}\bar{k}^3\alpha_e^{(0)} \right)^{-1}, \tag{4.79}$$

$\alpha_e^{(0)}$ being the static polarizabilty

$$\alpha_e^{(0)} = r_0^3 \frac{\varepsilon_p - 1}{\varepsilon_p + 2}. \tag{4.80}$$

As an illustration, we consider a dielectric particle with $r_0 = 25\,nm$ and $\varepsilon_p = 2.25$. With these data, we observe as mentioned above that $\text{Re}\alpha_e = 4593\,nm^3 \gg \text{Im}\alpha_e = 17\,nm^3$. The illumination that reaches each aperture is assumed with a magnitude of the Poynting vector $(c/2)I_0 \left| \mathbf{e}\left(\bar{\omega}\right) \right|^2 = 10^{12}\,W/m^2$. Fig. 4.7 shows the corresponding different components of the total force, (this time of course without performing any normalization).

As seen, the patterns of Fig. 4.7(a) and Fig. 4.7(b) are equal to those of Fig. 4.4(b) and Fig. 4.4(c) respectively; this implying that the scattering force is negligible compared to the gradient force along OX and OY. However, although $\text{Re}\alpha_e \gg \text{Im}\alpha_e$, this is not enough for $\left\langle \tilde{F}_z^{grad} \right\rangle$ to exceed $\left\langle \tilde{F}_z^{sc} \right\rangle$, (remember that we obtained a difference of seven orders of magnitude between these two normalized z-components), therefore the contribution of $\left\langle \tilde{F}_z^{grad} \right\rangle$ to $\left\langle \tilde{F}_z^{tot} \right\rangle$ is negligible by four orders of magnitude. Notwithstanding, it is important for trapping purposes that the y component of the force $\left\langle \tilde{F}_y^{tot} \right\rangle$, which is of conservative nature, is of the same order of magnitude as the non-conservative z-force $\left\langle \tilde{F}_z^{tot} \right\rangle$. As the coherence diminishes, Fig. 4.5(b) gives
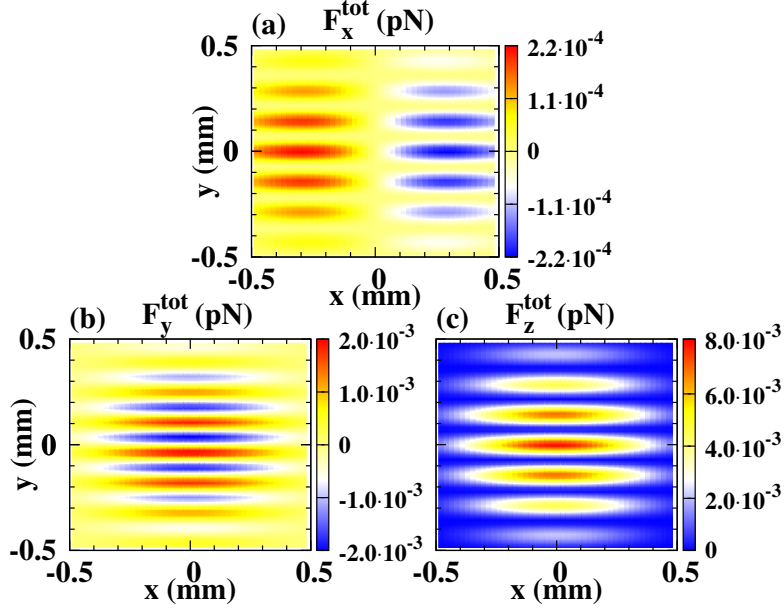
Figure 4.7: Spatial distribution, in pN, of the averaged total force Cartesian components on a dielectric particle with $r_0 = 25\,nm$ and $\varepsilon_p = 2.25$, in the screen plane $\mathcal{B}$, placed at distance $z = d = 1.5\,m$ from the aperture mask $\mathcal{A}$, $|\mu(\mathbf{q}_1, \mathbf{q}_2, \bar{\omega})| = 1$. No normalization is done. (a) $\left\langle F_x^{tot} \right\rangle$. (b) $\left\langle F_y^{tot} \right\rangle$. (c) $\left\langle F_z^{tot} \right\rangle$.

an assessment of the corresponding decrease to be expected in both $\left\langle \tilde{F}_x^{tot} \right\rangle$ and $\left\langle \tilde{F}_y^{tot} \right\rangle$ from their values in Figs. 4.7(a) and 4.7(b).

4.6 CONCLUSION

In this chapter I have established a new theory of averaged photonic forces due to random wavefields. Firstly I have demonstrated the contribution of the different momentum densities to the optical force exerted by a deterministic wavefield, giving an additional point of view of these forces.

Then, for partially coherent electromagnetic fields, I have put forward expressions for the force in terms of the cross spectral-density tensors for magnetodielectric particles. I have shown that the spatial coherence of the source will play a role in the dynamical interaction between the fields ant the particles.

The results have been illustrated, i.e., the influence of the degree of coherence of a partially coherent source, through the classical study on coherence by Thompson and Wolf [6]. Under this setup, I have calculated the force components and their dependence on the degree of coherence of the fluctuating field at the plane of the apertures. These components show a fringe pattern spatial distribution, analogous to the intensity interference pattern observed at the screen plane.

Likewise, although I have emphasized our illustration of Section 4.4 with an scalar theory, it will be of interest to study configurations in which optical forces are analyzed in terms of

the degree of polarization (cf. Chapter 3) of the fluctuating fields by making use of the full electromagnetic model of Section 4.5. This latter electromagnetic formulation will be used, for instance, in Chapter 6.

Part IV

OPTICAL FORCES FROM STATISTICALLY
HOMOGENEOUS FLUCTUATING SOURCES

5

OPTICAL FORCES FROM STATISTICALLY HOMOGENEOUS FLUCTUATING SOURCES: NEAR-FIELD EFFECTS.

5.1 MOTIVATION

ust like fields fluctuations affect an interference pattern, it has been demonstrated that these random fields influence the behavior of the interactions between fields and particles. We have studied this through a Young experiment configuration, however, we can directly analyze this phenomenon addressing a extended partially coherent source.

In Chapters 2 and 3, different quantities from statistically homogeneous sources were studied, therefore I will now discuss how the statistical properties of these sources can affect the optical forces. The formerly addressed double slit experiment contained a far-field configuration, nevertheless, we will now turn to the near-field. We will also address the effect of surface plasmon polariton excitation on the surface of the source, giving an enhancement in the magnitude of the force which will be more appreciable in the conservative components.

New analytical expressions for the forces will be obtained and I will demonstrate the crucial role of the statistical homogeneity of the source in the different components of the optical force.

5.2 INTRODUCTION

Near-field optical forces at the nanoscale convey the exchange of momentum of an evanescent optical wavefield with a micro-object. Whereas classical far-field techniques in nanomanipulation are limited by the diffraction limit $\lambda/2$, this new approach gives the possibility to place objects in the desired location with larger accuracy.

Several studies have demonstrated the possibility to trap nano-objects at near-field distances [44, 50, 51, 77], even when SPPs are excited on the source surface [78], taking advantage of the electric field enhancement.

On the other hand, as quoted in previous chapters, the subject of random fields has been extensively addressed in different contexts, ranging from macroscopic physics, (e.g. in coherence theory [3, 4], atmospheric turbulence [79, 80], wave propagation in random and dense media [81–83], speckle formation from random phase screens [5, 84], reflection from rough surfaces [85–88]), to the microscopic and nanoscopic scale, (like systems of randomly distributed nanoparticles [3, 89], quantum dots [90] and disordered photonic crystals [91], including dispersion forces between fluctuating atoms or molecules of separated objects as thermal sources and blackbodies at the nanoscale [79, 92–99]).

As we have tried to remark in Chapters 2 and 3, as one enters in the nano-scale, the correlation properties of the fields are more relevant, showing effects. Hence, it is of interest for optical manipulation to study the action of the random and partially coherent fields emanating from statistical sources. In this context this chapter will show the role of the evanescent and propagating modes.

5.3   FLUCTUATING OPTICAL FORCES

In order to perform the calculus of the near-field force, we will describe the optical force using the angular wave spectrum representation (cf. Section 1.5). Hence, let us consider a fluctuating source emitting into $z \geq 0$ from the plane $z = 0$; its volume being in the region $z < 0$ (see Fig. and 5.1). We shall assume that the radiated random field is described by an statistical ensemble which is stationary, then we may work in the space-frequency domain [3] so that its electric vector in the half-space $z > 0$ [3, 10] is (cf. Eq. (3.16)):

$$\mathbf{E}(\mathbf{r}, \omega) = \int_{-\infty}^{\infty} \mathbf{e}(k\mathbf{s}_\perp, \omega) e^{ik\mathbf{s}\cdot\mathbf{r}} \mathrm{d}^2 \mathbf{s}_\perp, \tag{5.1}$$

where the propagation vector $\mathbf{k} = k\mathbf{s}$ has been defined for homogeneous ($|\mathbf{s}_\perp|^2 \leq 1$) and evanescent ($|\mathbf{s}_\perp|^2 > 1$) modes in Eq. (2.25).

We shall describe the source as planar [3] on characterizing it by the limiting value at $z = 0$: $\mathbf{E}^{(0)}(\boldsymbol{\rho}, \omega)$, [$\mathbf{r} = (\boldsymbol{\rho}, z)$], of the random field $\mathbf{E}(\mathbf{r}, \omega)$ emitted into free space. It is known [3, 10] that

$$\mathbf{e}(k\mathbf{s}_\perp, \omega) = \left(\frac{k}{2\pi}\right)^2 \int_{\Sigma} \mathbf{E}^{(0)}(\boldsymbol{\rho}, \omega) e^{-ik\mathbf{s}_\perp\cdot\boldsymbol{\rho}} \mathrm{d}^2 \boldsymbol{\rho}. \tag{5.2}$$

Σ denoting the source domain of integration at $z = 0$ (cf. Eq. (2.5)).

For simplicity, let us assume a dipolar particle with only dynamic electric polarizability α_e placed in the source vicinity (the case of magneto-dielectric particles will be discussed in Chapter 6). At these distances, the evanescent components of the emitted electromagnetic field will be non-negligible. It should be also remarked that in writing the force as in Eq. (4.14) so far we assume that the particle dipole does not fluctuate itself. Otherwise, one should add a term similar to that of (4.14) containing both the fluctuating dipole moment and the electric field that it emits. This latter term, which I shall address in Chapter 6, has been previously considered for example in studies of Van der Waals and Casimir forces between bodies of fluctuating atoms or
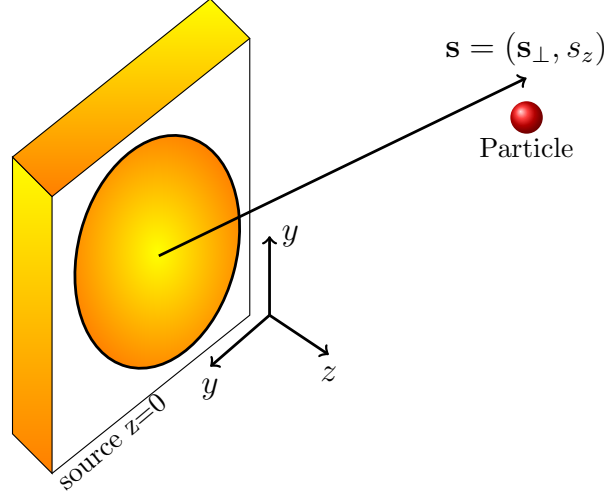
Figure 5.1: Illustrating the notation

molecules at a given temperature, whose current and polarization correlations are expressed by the fluctuation-dissipation theorem [11, 79, 92, 94–100].

Then, on using Eq. (5.1) into the conservative and non-coservative part of the electric force (cf. Eqs. (4.14) and (4.58)), one obtains

$$
\begin{aligned}
F_i^{grad}(\mathbf{r}, \omega) &= -i\frac{k}{4}\mathrm{Re}\alpha_e \iint_{-\infty}^{\infty} \mathrm{Tr}\mathcal{A}_{jk}^{(e)}\left(k\mathbf{s}_\perp, k\mathbf{s}'_\perp\omega\right) \\
&\quad \times \left(s_i^* - s_i'\right) e^{-ik(\mathbf{s}^*-\mathbf{s}')\cdot\mathbf{r}} \mathrm{d}^2\mathbf{s}_\perp \mathrm{d}^2\mathbf{s}'_\perp,
\end{aligned}
\tag{5.3}
$$

$$
\begin{aligned}
F_i^{nc}(\mathbf{r}, \omega) &= \frac{1}{2}\mathrm{Im}\alpha_e \mathrm{Im}\left\{ ik \iint_{-\infty}^{\infty} \mathrm{Tr}\mathcal{A}_{jk}^{(e)}\left(k\mathbf{s}_\perp, k\mathbf{s}'_\perp\omega\right) \right. \\
&\quad \left. \times s_i' e^{-ik(\mathbf{s}^*-\mathbf{s}')\cdot\mathbf{r}} \mathrm{d}^2\mathbf{s}_\perp \mathrm{d}^2\mathbf{s}'_\perp \right\},
\end{aligned}
\tag{5.4}
$$

$(i, j, k = 1, 2, 3)$, Tr denotes the trace of the electric angular correlation tensor $\mathcal{A}_{jk}^{(e)}\left(k\mathbf{s}_\perp, k\mathbf{s}'_\perp, \omega\right)$ $= \left\langle e_j^*(k\mathbf{s}_\perp, \omega)e_k(k\mathbf{s}'_\perp, \omega)\right\rangle$. Notice that since $\left\langle E_j^* E_j \right\rangle$ is real and non-negative, F_i^{grad} given by Eq. (5.3) which equals $\frac{1}{4}\mathrm{Re}\alpha_e\partial_i\left\langle E_j^* E_j \right\rangle$ is a real quantity. Eqs. (5.3) and (5.4) reveal that whereas the gradient force depends on a weighted sum of the difference vectors $\mathbf{s}^* - \mathbf{s}'$ and, as we shall see, it has a negative sign if $\mathrm{Re}\alpha_e$ is positive, thus pulling the particle towards the source, the non-conservative force associated to $\mathrm{Im}\alpha_e$ which is always non-negative, only depends on the weighted sum of vectors $\mathbf{s}$ and pushes the particle forward.

Notice also than in Eqs. (5.3)-(5.4), the random properties of the source are encoded into the angular correlation tensor $\mathcal{A}_{jk}^{(e)}\left(k\mathbf{s}_\perp, k\mathbf{s}'_\perp, \omega\right)$, hence, if we know this quantity, we have the optical force in terms of statistical parameters of the source.

5.3.1 *Statistically homogeneous sources. Gradient and non-conservative forces*

In Chapters 2 and 3 we studied in detail the random properties of statistically homogeneous sources, in particular, at subwalength distances. Now the goal is to extend this model to partially coherent forces. Under this assumption, the angular correlation tensor $\mathcal{A}_{jk}^{(e)}\left(k\mathbf{s}_\perp, k\mathbf{s}'_\perp, \omega\right)$ is well-defined, hence, substituting Eq. (3.17) into Eqs. (5.3)-(5.4) we obtain the optical force for the specific case of homogeneous sources, i.e.,

$$
\begin{aligned}
F_i^{grad}\left(z,\omega\right) &= F_{z,ev}^{grad}\left(z,\omega\right) \\
&= -i\frac{k^3}{4}\mathrm{Re}\alpha_e \int_{|\mathbf{s}_\perp|^2 > 1} \mathrm{Tr}\tilde{\mathcal{E}}_{jk}^{(0)}\left(k\mathbf{s}_\perp,\omega\right)\left(s_i^* - s_i\right)e^{-2k\sqrt{|\mathbf{s}_\perp|^2 - 1}z}\mathrm{d}^2\mathbf{s}_\perp, \quad (5.5)
\end{aligned}
$$

The subindex in the integral of Eq. (5.5) means that the integration only extends to the non-radiative region because the difference vector $\mathbf{s}^* - \mathbf{s}$ in Eq. (5.3) is clearly zero for propagating waves, $(|\mathbf{s}_\perp|^2 \leq 1)$. *Therefore the radiative components of the field emitted by statistically homogeneous sources do not contribute to the gradient force, which only depends on the evanescent components, $(|\mathbf{s}_\perp|^2 > 1)$, for which $\mathbf{s}^* - \mathbf{s} = (0,0,s_z^* - s_z) = (0,0,-2i\sqrt{|\mathbf{s}_\perp|^2 - 1})$. Hence this force only exists in the near field, and depends on the distance z of the particle to the source, having solely z- component normal to its surface. In addition, this force is attractive or repulsive depending on the sign of $\mathrm{Re}\alpha_e$.* Small particles with relative permittivity $\varepsilon_p > 1$ have $\mathrm{Re}\alpha_e > 0$ out of resonance and thus $F_z^{grad}\left(z,\omega\right)$ will drag them towards the source. Conversely, near a morphological resonance $\mathrm{Re}\alpha_e$ may be negative [50], thus this force being repulsive. However, further study is required in this latter case, since then the particle strongly scatterers the field emitted by the source, and therefore the analysis developed here should not be exact due to multiple scattering of the radiation between the source and the particle, (this will be done in Chapter 6). Hence we show here that the gradient force near a statistically homogeneous source is entirely of non-radiative nature and may work as a *tractor force* [68–70, 101].

Analogously, from Eq. (5.4) one also derives for the non-conservative force F_i^{nc} a dependence on z only:

$$
\begin{aligned}
&F_i^{nc}\left(z,\omega\right) \\
&= F_{i,h}^{nc}\left(z,\omega\right) + F_{i,ev}^{nc}\left(z,\omega\right) \\
&= \frac{k^3}{2}\mathrm{Im}\alpha_e\mathrm{Im}\left\{i\int_{|\mathbf{s}_\perp|^2 \leq 1}\mathrm{Tr}\tilde{\mathcal{E}}_{jk}^{(0)}\left(k\mathbf{s}_\perp,\omega\right)s_i\mathrm{d}^2\mathbf{s}_\perp\right\} \\
&+ \frac{k^3}{2}\mathrm{Im}\alpha_e\mathrm{Im}\left\{i\int_{|\mathbf{s}_\perp|^2 > 1}\mathrm{Tr}\tilde{\mathcal{E}}_{jk}^{(0)}\left(k\mathbf{s}_\perp,\omega\right)s_ie^{-2k\sqrt{|\mathbf{s}_\perp|^2 - 1}z}\mathrm{d}^2\mathbf{s}_\perp\right\}, \quad (5.6)
\end{aligned}
$$

$F_{i,h}^{nc}$ and $F_{i,ev}^{nc}$, denote propagating and evanescent wave contributions, which correspond to the first and second integral terms of Eq. (5.6), respectively. Notice that $F_{i,h}^{nc} > 0$ is constant throughout $z > 0$.

Let the source also be statistically isotropic [3] so that $\mathcal{E}_{ij}^{(0)}\left(\boldsymbol{\rho}_1, \boldsymbol{\rho}_2, \omega\right) = \mathcal{E}_{ij}^{(0)}\left(\rho, \omega\right)$, where $\rho = |\boldsymbol{\rho}_1 - \boldsymbol{\rho}_2|$. The spatial coherence function of the field in $z = 0$ is [16, 102, 103] $\mathrm{Tr}\mathcal{E}_{ij}^{(0)}\left(\rho, \omega\right)$ and

the *spectral degree of spatial coherence* $\mu^{(0)}(\rho,\omega) = \mathrm{Tr}\mathcal{E}_{ij}^{(0)}(\rho,\omega)/S^{(0)}(\omega)$, where the wavefield spectrum on the source is: $S^{(0)}(\omega) = \mathrm{Tr}\mathcal{E}_{ij}^{(0)}(0,\omega)$.

To illustrate these results, we shall consider a Gaussian spectral degree of coherence as in Eq. (2.20) (see Chapter 2), so that taking Fourier inverse one obtains

$$
\begin{aligned}
\mathrm{Tr}\tilde{\mathcal{E}}_{jk}^{(0)}(k\mathbf{s}_\perp,\omega) &= S^{(0)}(\omega)\tilde{\mu}^{(0)}(k\mathbf{s}_\perp,\omega) \\
&= \mathcal{S}(\omega)\exp\left[-\left(k\sigma\left|\mathbf{s}_\perp\right|\right)^2/2\right],
\end{aligned}
\tag{5.7}
$$

where σ is the correlation, or coherence length of the source and $S^{(0)}(\omega) = \mathcal{S}(\omega)/\left(2\pi\sigma^2\right)$ [IV.1] [I].

Hence, on introducing Eq. (5.7) for $\mathrm{Tr}\tilde{\mathcal{E}}_{jk}^{(0)}(k\mathbf{s}_\perp,\omega)$ into the force equations (5.5) and (5.6) and making use of the rotational symmetry of the source, we obtain that the transversal components of the non-conservative force are zero, viz. : $F_{x,y}^{nc}(z,\omega) = 0$ since so are the corresponding integrals of Eq. (5.6) when one performs the azimuthal angle ϕ integration. Also, since $s_z = i\sqrt{|\mathbf{s}_\perp|^2 - 1}$ for $|\mathbf{s}_\perp|^2 > 1$, the second integral in Eq. (5.6) is purely imaginary, which implies that $F_{z,ev}^{nc} = 0$. Therefore

$$
\begin{aligned}
F_i^{nc}(z,\omega) &= F_{i,h}^{nc}(z,\omega) \\
&= \frac{k^3}{2}\mathrm{Im}\alpha_e\mathrm{Im}\left\{i\int_{|\mathbf{s}_\perp|^2\leq 1}\mathrm{Tr}\tilde{\mathcal{E}}_{jk}^{(0)}(k\mathbf{s}_\perp,\omega)\,s_i\mathrm{d}^2\mathbf{s}_\perp\right\}.
\end{aligned}
\tag{5.8}
$$

Thus while $F_{z,h}^{nc}(z,\omega) > 0$ is constant throughout $z > 0$, as so is the spectrum $S^{(0)}(\omega)$ propagating into $z > 0$ [13], the evanescent waves do not contribute to the non-conservative force $F_z^{nc}(\mathbf{r},\omega)$.

In summary, *there are two force components acting on the particle: $F_{z,ev}^{grad}(z,\omega)$ and $F_{z,h}^{nc}(z,\omega)$, perfectly distinguishable from each other since the former is due to the non-radiative plane wave components of the emitted field, whereas to the latter only the radiative components contribute. As the distance from the particle to the source plane grows to values $z > \lambda$, $F_{z,ev}^{grad}(z,\omega)$ tends to zero due to its evanescent wave composition.* Nevertheless, as we shall see, the source coherence length σ plays an important role on these contributions. The integration of Eqs. (5.5) and (5.8) using the Gaussian spectral degree of coherence, quoted before: $\mu^{(0)}(\rho,\omega) = \exp\left[-\rho^2/2\sigma^2\right]$, leads to an analytical expression for the gradient and for the non-conservative force. For the latter, Eq. (5.16) yields the proportion of radiation pressure and curl components for unpolarized emission. This calculation is straightforwardly and leads to

$$
F_z^{grad}(z,\omega) = \mathrm{Re}\alpha_e\mathcal{S}(\omega)e^{-\frac{1}{2}k^2\sigma^2}\frac{1}{\sigma^2}\left[\frac{z}{\sigma^2} - \sqrt{\frac{\pi}{2}}\left(\frac{2z^2}{\sigma^3} + \frac{1}{2\sigma}\right)e^{\frac{2z^2}{\sigma^2}}\mathrm{erfc}(\sqrt{2}z/\sigma)\right],
\tag{5.9}
$$

$$
F_z^{nc}(z,\omega) = \mathrm{Im}\alpha_e\mathcal{S}(\omega)\frac{1}{2\sigma^2}\left[k - \frac{1}{\sigma}\sqrt{\frac{\pi}{2}}e^{-\frac{1}{2}k^2\sigma^2}\mathrm{erfi}(k\sigma/\sqrt{2})\right],
\tag{5.10}
$$

where $\mathrm{erfc}(x) = 1 - \mathrm{erf}(x)$, $\mathrm{erf}(x)$ being the error function: $\mathrm{erf}(x) = 2/\sqrt{\pi}\int_0^x e^{-t^2}\mathrm{d}t$, and $\mathrm{erfi}(x)$ is a positive real function defined as $\mathrm{erfi}(x) = \mathrm{erf}(ix)/i$.

[IV.1] See Chapter 2, in particular Eq. (2.26), to discuss this normalized spectrum

5.3.2 *The curl force*

The non-conservative part of the force F_i^{nc} is the sum of a *scattering force*, or *radiation pressure* [34, 104]

$$
\begin{aligned}
F_i^{nc} &= (k/2)\mathrm{Im}\alpha_e\mathrm{Re}\left\langle \mathbf{E}\times\mathbf{B}^*\right\rangle_i \\
&= (1/2)\mathrm{Im}\alpha_e\mathrm{Im}\left\{\left\langle E_j^*\partial_i E_j\right\rangle - \left\langle E_j^*\partial_j E_i\right\rangle\right\},
\end{aligned}
\tag{5.11}
$$

given by the averaged field Poynting vector, plus *the curl of a electric spin density* (cf. Section 4.3.2):

$$
\begin{aligned}
F_i^{nc,curl} &= (1/2)\mathrm{Im}\alpha_e\mathrm{Im}\left\langle \left(\mathbf{E}^*\cdot\nabla\right)\mathbf{E}\right\rangle_i \\
&= (1/2)\mathrm{Im}\alpha_e\mathrm{Im}\left\langle E_j^*\partial_j E_i\right\rangle.
\end{aligned}
\tag{5.12}
$$

If the field emitted by the source is *unpolarized*: $\mathcal{E}_{jk}^{(0)}(\rho,\omega)=\mathcal{F}^{(0)}(\rho,\omega)\delta_{jk}$, $\mathcal{F}^{(0)}(\rho,\omega)$ being a scalar spatial correlation function whose two-dimensional Fourier transform will be denoted as $\tilde{\mathcal{F}}^{(0)}(k\mathbf{s}_\perp,\omega)$. Then

$$
\mathrm{Tr}\tilde{\mathcal{E}}_{jk}^{(0)}(k\mathbf{s}_\perp,\omega)=3\tilde{\mathcal{F}}^{(0)}(k\mathbf{s}_\perp,\omega),
\tag{5.13}
$$

and the radiation pressure contribution $F_i^{nc,pr}$ to the non-conservative force is:

$$
\begin{aligned}
F_i^{nc,pr} &= \frac{k^3}{2}\mathrm{Im}\alpha_e\int_{|\mathbf{s}_\perp|\leq 1}\left[\mathrm{Tr}\tilde{\mathcal{E}}_{jk}\left(k\mathbf{s}_\perp,\omega\right)s_i - \tilde{\mathcal{E}}_{ji}\left(k\mathbf{s}_\perp,\omega\right)s_j\right]\mathrm{d}^2\mathbf{s}_\perp \\
&= \frac{k^3}{2}\mathrm{Im}\alpha_e\int_{|\mathbf{s}_\perp|\leq 1}\left[3\tilde{\mathcal{F}}^{(0)}\left(k\mathbf{s}_\perp\right)-\tilde{\mathcal{F}}^{(0)}\left(k\mathbf{s}_\perp\right)\right]s_i\mathrm{d}^2\mathbf{s}_\perp \\
&= k^3\mathrm{Im}\alpha_e\int_{|\mathbf{s}_\perp|\leq 1}\tilde{\mathcal{F}}^{(0)}\left(k\mathbf{s}_\perp\right)s_z\mathrm{d}^2\mathbf{s}_\perp = F_z^{nc,pr},
\end{aligned}
\tag{5.14}
$$

since the azimuthal angle integrations when s_i is either s_x or s_y, is zero.

In a similar manner, the curl force contribution $F_i^{nc,curl}$ to F_i^{nc} is

$$
\begin{aligned}
F_i^{nc,curl} &= \frac{k^3}{2}\mathrm{Im}\alpha_e\int_{|\mathbf{s}_\perp|\leq 1}\tilde{\mathcal{E}}_{ji}\left(k\mathbf{s}_\perp,\omega\right)s_j\mathrm{d}^2\mathbf{s}_\perp \\
&= \frac{k^3}{2}\mathrm{Im}\alpha_e\int_{|\mathbf{s}_\perp|\leq 1}\tilde{\mathcal{F}}^{(0)}\left(k\mathbf{s}_\perp\right)s_z\mathrm{d}^2\mathbf{s}_\perp = F_z^{nc,curl}.
\end{aligned}
\tag{5.15}
$$

Namely, for unpolarized radiation:

$$
F_z^{nc,pr}=2F_z^{nc,curl}=\frac{2}{3}F_z^{nc}.
\tag{5.16}
$$

5.4 EXCITATION OF SURFACE PLASMON POLARITONS. NUMERICAL RESULTS

5.4.1 *Normalized force*

Without loss of generality, we shall also address surface plasmon polaritons (SPPs), excited on the source plane $z=0$. Let this be gold for example, choosing for instance the same parameters
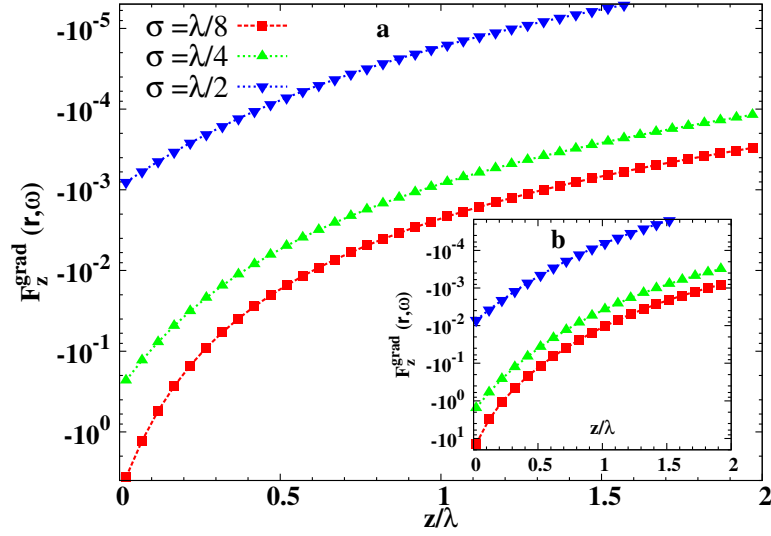
Figure 5.2: Pulling gradient optical force due to evanescent components. (a) Gradient force versus distance to the source z/λ for different values of the source coherence length σ. (b) The same force as in (a) when SPPs are excited in the source. A significant decrease of the magnitude of this force is clearly seen as σ grows about $\sigma = \lambda/2$ and beyond. The normalized value $F_z^{grad}(z,\omega)/(k^3 \mathcal{S}(\omega) \mathrm{Re}\alpha_e/(2\pi)^2)$ is represented in arbitrary units (a.u.).

as in Chapter 2, i.e., at $\lambda = 459.9 nm$ its permittivity is $\varepsilon = -2.546 + i3.37$ [105]. The SPP wave vector $k\mathbf{s}_\perp = k\mathbf{s}_\perp^{SPP}$ corresponds to a pole of the Fresnel transmission coefficient (in the assumed transmission set-up configuration), $t^p(k\mathbf{s}_\perp,\omega)$. [10, 17]. Then, for p-polarization it is easy to obtain that the former equations (5.5) and (5.6) are valid on substituting $\tilde{\mathcal{E}}_{jk}^{(0)}(k\mathbf{s}_\perp,\omega)$ by $\tilde{\mathcal{E}}^{(0)}(k\mathbf{s}_\perp,\omega)\,|t^p(k\mathbf{s}_\perp,\omega)|^2$ [I]. The expression for $\tilde{\mathcal{E}}^{(0)}(k\mathbf{s}_\perp,\omega)$ can be also given by Eq. (5.7), considering that we are in p-polarization.

Figure 5.2 shows the normalized value $F_z^{grad}(z,\omega)/(k^3 \mathcal{S}(\omega)\mathrm{Re}\alpha_e/(2\pi)^2)$ of the attractive gradient optical force due to evanescent components for two random sources: one without and one with excited SPPs (cf. Fig. 5.2(a) and Fig. 5.2(b), respectively). As predicted by Eq. (5.5), the normalized gradient force drags the particle towards the source plane; (notice that since this normalization does not include $\mathrm{Re}\alpha_e$, it does not contain an eventual negative value of this quantity). In both figures we observe its exponential increase as the distance z of the particle to the source decreases. *Nevertheless, this force is mainly governed by the coherence length σ*. For $\sigma = \lambda/8$ (red line), the magnitude of this force is maximum, but we observe that it presents an important decrease, with values between 10^{-3} and 10^{-4}, around $\sigma = \lambda/2$ (blue line) and beyond, even at subwavelength distances z; being practically zero ($F_z^{grad} \simeq 10^{-8}$) for $\sigma = \lambda$ and $z = 0$ (this latter curve is not shown).

Hence, we demonstrate that *the decrease of the source coherence length gives rise to an increase of the gradient force* and its effect is larger than that of the distance z of the particle to the source plane. Eventually, a δ-correlated source (then $\sigma \to 0$) like e.g. a thermal source, will maximize this force. In addition, we show with Fig. 5.2(b) that the excitation of SPPs in the source increases the strength of this near field force by approximately one order of magnitude.
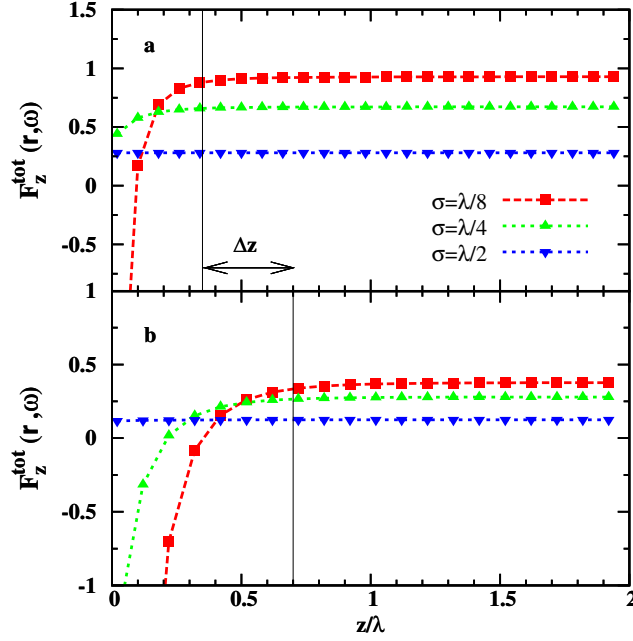
Figure 5.3: (a) Normalized total optical force, (see text), in arbitrary units (a.u.) versus distance z/λ to the source for different values of the coherence length σ. (b) The same as in (a) when SPPs are excited. In this latter case we observe an increment Δz in the value z/λ at which the magnitude of the gradient force starts to exponentially increase.

This is due to the then larger values of $\bar{\mathcal{E}}^{(0)}(k\mathbf{s}_\perp,\omega)\,|t^p(k\mathbf{s}_\perp,\omega)|^2$ stemming from the pole of $|t^p(k\mathbf{s}_\perp,\omega)|^2$ at $k\mathbf{s}_\perp^{SPP}$ (see also Fig. 2.5).

Correspondingly, Figures 5.3(a) and 5.3(b) show the normalized total force $F_z^{tot}(z,\omega) = [(2\pi)^2/k^3\mathcal{S}(\omega)]\cdot(F_z^{grad}(z,\omega)/\mathrm{Re}\alpha_e + F_z^{nc}(z,\omega)/\mathrm{Im}\alpha_e)$, in arbitrary units, without and with SPP excitation, respectively. At large distances $(z > \lambda)$, the total force is a constant of the distance z, and repulsive according to the behavior of the non-conservative component F_z^{nc}, which dominates in this region of z, regardless of the value of σ. In addition, this non-conservative force increases as σ decreases.

One might think that, due to its evanescent wave composition, the magnitude of the normalized gradient force at subwavelength distances would be higher than that of the corresponding non-conservative force, however this is not totally truth due the larger effect of the source coherence length on F_z^{grad} rather than on F_z^{nc}. In near-field $F^{tot} \simeq F^{grad}$ for $\sigma \leq \lambda/4$; but as σ increases, F^{grad} becomes negligible, being for $\sigma > \lambda/4$ $F^{tot} \simeq F^{nc}$. These effects appear in Figs. 5.3(a) and 5.3(b). Particulary, we see in Fig. 5.3(b) that if SPPs are excited, an increment Δz appears in the distance z/λ where the magnitude of the attractive gradient component is noticeable, (compare Figs. 5.3(a) and 5.3(b)). The enhancement of the near field intensity due to SPPs resonances then conveys a larger range of the gradient force.

5.5 A SOURCE SPECTRUM MODEL TO ILLUSTRATE THE OPTICAL FORCE ON A DIPOLAR PARTICLE

So far I have calculated the relative weights of the gradient and non-conservative forces without taking into account the strength of the particle induced dipole. That was done by normalizing those forces to the corresponding real and imaginary values of the particle polarizability. However, it is well known that this latter quantity largely influences the values of these forces [59, 61]; hence, its presence should be relevant in estimating the actual mechanical action of the emitted light. We shall now address this with a certain source spectrum model.

As we have done in Chapter 4 in order to provide a more realistic example, let us consider a small particle of radius r_0 with relative permittivity ε_p, in the Rayleigh limit ($kr_0 \ll 1$), is assumed. We adopt the expression for the dynamic electric polarizability which conserves energy on scattering [59] given by Eq. (4.79).

For a non-monochromatic source, the total mean force exerted by the random field on the dipolar particle is determined on ω-integration of each frequency component, i.e.

$$F_i\left(\mathbf{r}\right) = \int F_i\left(\mathbf{r}, \omega\right) \mathrm{d}\omega. \ (i = 1, 2, 3). \tag{5.17}$$

Of course, as discussed above, in our study the source contributes with the Cartesian component $F_z\left(\mathbf{r}, \omega\right)$ only.

We assume a Gaussian spectrum model [3], so that

$$\mathcal{S}(\omega) = \frac{A}{\sigma_\omega \sqrt{2\pi}} e^{-\frac{(\omega - \omega_0)^2}{2\sigma_\omega^2}}, \tag{5.18}$$

where A, σ_ω and ω_0 are positive constants. Incidentaly, it is straightforward to see that in the monochromatic case at frequency ω_0, ($\sigma_\omega \to 0$), we recover Eqs. (5.9) and (5.10) with $\mathcal{S}(\omega) = A\delta(\omega - \omega_0)$.

As an example, we perform the integral (5.17) for a small dielectric particle of radius $r_0 = 25nm$ with a constant value of $\varepsilon_p = 2.25$ in the range of studied frequencies (cf. Section 4.5.1)[IV.2]. In the case of SPP excitation, an Au source surface is considered like in Section 5.4.1, with a frequency variation of its permittivity approximated by [106, 107]

$$\varepsilon(\omega) = \varepsilon_\infty - \frac{\omega_d^2}{\omega^2 + i\gamma\omega}$$
$$+ \sum_{p=1}^{2} A_p \Omega_p \left(\frac{e^{i\phi_p}}{\Omega_p - \omega - i\Gamma_p} + \frac{e^{-i\phi_p}}{\Omega_p + \omega + i\Gamma_p}\right), \tag{5.19}$$

where the values of the parameters in (5.19) are considered the same as in Ref. [107].

An optical power of 300 mW impinging the particle is assumed at the central wavelength $\lambda_0 = 2\pi c/\omega_0 =$579 nm. The spectral width is taken as: $\sigma_\omega = 0.01 \ \omega_0$. The constant A is then adjusted to these values.

IV.2 This polarizability was used in Subsection 4.5.1 and will be also used in others chapters because it constitutes a test particle without resonant properties.
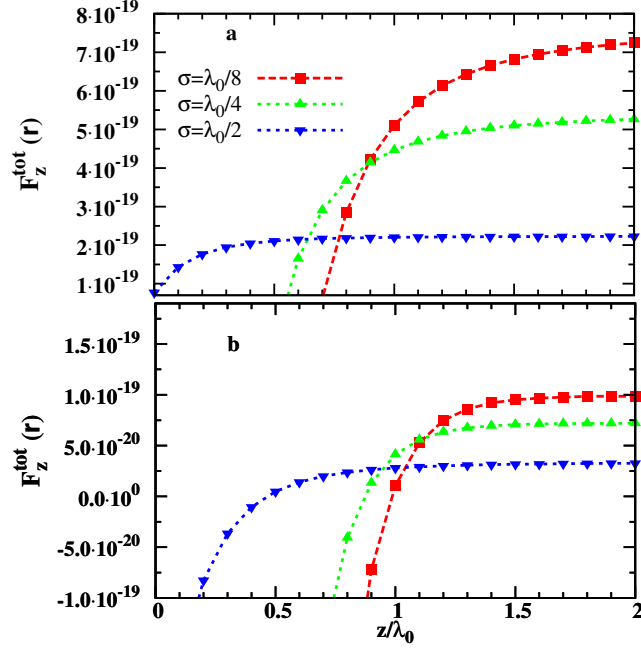
Figure 5.4: Total optical force in Newtons versus distance z/λ_0, obtained by integration over a Gaussian spectrum of the source. Results for different values of the coherence length σ_0 are shown. (a) Surface plasmons polaritons (SPP) are absent. (b) SPPs are excited in the metallic surface of the source.

The total force calculated on introducing Eqs. (5.9) and (5.10) into Eq. (5.17), (that is to say, this time without introducing any normalization), is shown in Figs. 5.4(a) and 5.4(b), without and with excitation of surface plasmon polariton resonances on the source surface, respectively.

As predicted in Section 5.4, the total force is governed in the near field by its gradient component for $\sigma \leq \lambda/4$, its magnitude increasing as the coherence length σ decreases. In addition, its exponential growth as the particle approaches the source is remarkable. Particularly, at $z/\lambda = 0.5$ and for $\sigma = \lambda/8$, the magnitude of the gradient force when SPPs are excited is practically double $(3 \times 10^{-16}$ N) than when they are absent.

For $z/\lambda > 1$ the total force is due to its non-conservative part, however, the distance at which this force begins to dominate is larger than as shown by Fig. 5.3 for the normalized force. This is due to the fact that now we have introduced in the calculations $\mathrm{Re}\alpha_e$ which is much larger than $\mathrm{Im}\alpha$.

On the other hand, Fig. 5.4 manifests a behavior of both the gradient and scattering plus curl forces similar to that of their non-integrated normalized counterparts, shown in Fig. 5.3, both without and with SPP excitation. However, the action of the gradient force reaches larger distances from the source than its normalized counterpart as Fig. 5.4 shows on comparison with Fig. 4.4, at least within the scale of values shown here.

5.6 CONCLUSIONS

In this chapter I have reported a study on photonic forces exerted on dipolar particles by discussing near field effects due to fluctuating sources. I have discussed the behavior of gradient and non-conservative forces at the nanoscale, concerning optical manipulation in such physics cases as those ranging from emission by partially correlated *primary* sources, i.e. beyond delta-correlated thermal sources and blackbodies, fluctuations in nanoantennas, to *secondary* sources resulting from light propagation through the turbulent atmosphere [79], speckle patterns from a large variety of statistical structures, also including scatterers, random rough surfaces, phase screens and optical diffusers [108–110]. Multiple scattering effects between the source and the particle have not been considered here. These latter are addressed in the next chapter, where resonant scattering from magnetodielectric spheres is studied.

We have seen that in the large variety of stationary statistically homogeneous and isotropic sources, only the evanescent components contribute to the gradient (conservative) forces, while the non-conservative part that contains radiation pressure and curl forces is due solely to emitted propagating components. Hence the subwavelength information is encoded in the gradient forces. Same numerical examples were given for statistically isotropic unpolarized emitted wavefields, showing the important effect that the source coherence length has on these forces, specially on the gradient component.

Also, due to the higher concentration of energy in the near field when there is excitation of surface waves in the source, this largely enhances the magnitude of the gradient part of these forces while it slightly diminishes the strength of their non-conservative part.

6

INTERACTION OF ELECTROMAGNETIC LIGHT WITH A MAGNETO-DIELECTRIC PARTICLE: OPTICAL GENERATION OF VACUUM PHOTONIC FORCES

6.1 MOTIVATION

In the previous chapter we studied the consequences of the interaction between a stochastic field produced by a homogeneous source and a dielectric particle without resonance effects. I commented briefly the similarity between this type of interactions and thermal (deveolped by Liftshitz) and/or that of vacuum fluctuations (studied by Van der Waals, Casimir and others).

In this chapter I will go beyond. I will remark that the optical source here addressed gives us an excellent opportunity to compare the behavior of magnetodielectric particles in an optical set-up, analogous to that of thermal interactions. I will make emphasis in the fact that the use of Rayleigh particles, i.e., particles of radius r_0 which fulfill $kmr_0 \ll 1$ (with $m = n_p/n_h$ being the relative refractive index and n_p, n_h the refractive index of the particle and the medium respectively), is not a good choice because the retardation effects cannot be neglected. Or what is the same, the polarizability cannot be approximated by its static polarizability given by the Claussius-Mossotti equation

$$\alpha_0 = r_0^3 \frac{\varepsilon_p - 1}{\varepsilon_p + 2}.$$

Therefore, we will analyze the forces in a similar way to Chapter 5, nevertheless, in this work, the Mie resonances will play a role as important as the fluctuating field, showing the richness of these interactions. In this thesis I have done emphasis on the fact that the equations of the force are valid, not only for a small particle, but also for particles where the first two resonances of the Mie coefficients are predominating. An example of this behavior is the case of semiconductor spheres. Recently these particles have demonstrated some extraordinary scattering properties (see references [60, 61, 111–114]).
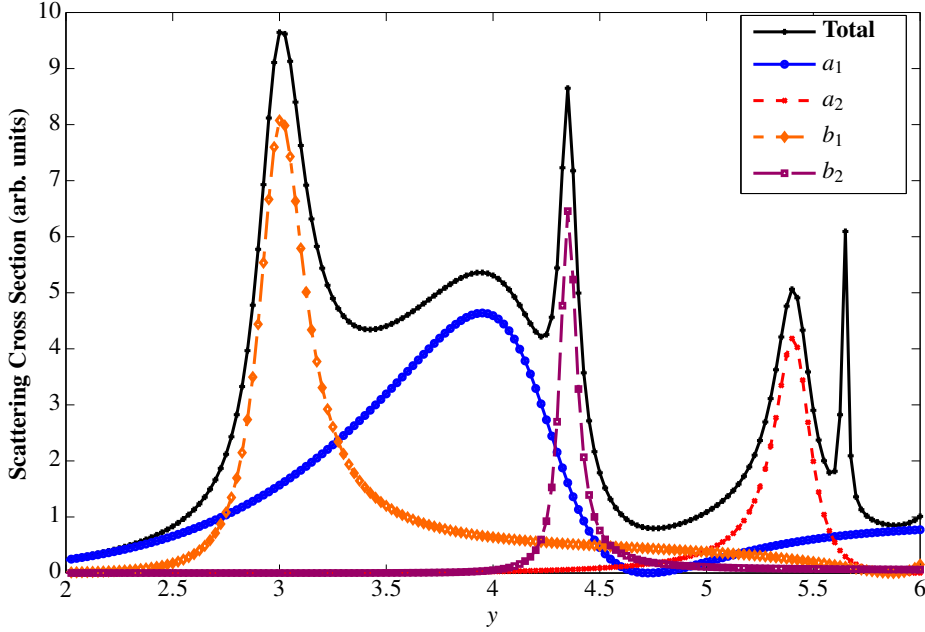
Figure 6.1: Scattering cross section for a silicon particle due to different Mie coefficients. Notice that the factor kr_0 is constant for each resonance. Adapted from [60]

Fig. 6.1 shows the scattering cross section of a silicon particle (refractive index $n_p \simeq \sqrt{12}$) immersed in vacuum for different values of the size parameter $y = n_p kr_0$, being $k = 2\pi/\lambda$ and r_0 the radius of the considered particle [60]. We have plotted the total cross section (due to all Mie coefficients (see Ref. [115])) and the cross sections due to the two first electric ($a_{1,2}$) and magnetic ($b_{1,2}$) coefficients. We can see how up to the value of $y \simeq 4.2$ the cross section is due to a_1 (electric dipole) and b_1 (magnetic dipole). It is worth remarking that this property is universal in the sense that it does not depend on the radius of the particle but on its size parameter, i.e., the dipolar resonances will always appear at $y \simeq 3$ and $y \simeq 4$. Once we have fixed the value of y for a given refractive index, the product kr_0 will give us the possibility to play with the size of the particle or with the wavelength (we can select one, the other then being imposed).

On the other hand, once we have calculated the Mie coefficients, we can obtain the response of the particle to these stochastic fields, i.e., the polarizability. I will try to make clear that the imaginary part of the polarizability is not negligible (even it can be larger than the real part), thus, the force will be given by the two previously addressed components: one conservative ($\nabla \times \mathbf{F}^{cons} = 0$) and one non-conservative force ($\nabla \times \mathbf{F}^{nc} \neq 0$).

I also discuss in detail the asymptotic behavior of these forces in order to see the role of its conservative and non-conservative components at short ($z \ll \lambda$) and large ($z \gg \lambda$) distances. I will demonstrate that for an arbitrary spectrum $\mathcal{S}(\omega)$, we recover the $-1/z^4$ behavior of the usual thermal (Liftshitz) force, showing that this power law is valid for any homogeneous source, being Planck's spectrum a particular case. In addition, we will address a new asymptotic power law $-1/z^2$ due to the interference of the electric and magnetic dipoles.

Random radiation forces are a widely studied topic within the framework of *thermal and/or vacuum fluctuations*. This idea is based on the fact that for any material in thermal equilibrium, the charges are in random thermal motion generating a random electromagnetic field.

Most of the works which appear in the bibliography have dealt with delta-correlated sources, such as those thermal and blackbodies, specially in connection with the Van der Waals (VdW) and Casimir-Polder (C-P) interactions [94, 116–130]. An important point of view of this force was given by Lifshitz who performed the first calculation of random forces by means of the fluctuation-dissipation theorem for the currents [100]:

$$\left\langle j_i\left(\mathbf{r}, \omega\right) j_j\left(\mathbf{r}', \omega'\right)\right\rangle = 2\pi\hbar\omega^2 \coth\left(\frac{\hbar\omega}{2k_B T}\right) \mathrm{Im}\varepsilon\left(\mathbf{r}, \omega\right) \delta_{ij}\delta\left(\mathbf{r} - \mathbf{r}'\right)\delta\left(\omega - \omega'\right),\qquad (6.1)$$

being $\hbar$ the normalized Planck's constant, k_B the Boltzmann's constant and T the absolute temperature. This equation reveals the important feature that the random force is not arbitrary, i.e., its correlation function is given in term of the losses of the system.

Due to the fact that this thesis develops a theory of optical forces from partially coherent light, we do not restrict ourselves to the use of delta-correlated sources. We have the possibility to create optical analogous of Van der Waals and Casimir interactions controlling and designing them through the spectrum and spatial coherence of the source. Hence, we consider a statistically homogeneous and isotropic source [3, III] emitting at visible and near-infrared (NIR) frequencies. Notice that, at thermal wavelengths, the interaction from the primary source and the induced dipoles is interpreted as a Liftshitz force [100], which in the limit of zero temperature T becomes that from vacuum fluctuations, i.e. those derived by either VdW and C-P [92], depending on the distance, and also on the use or not, of a quasistatic formulation.

Nevertheless, the optical frequencies ω addressed in the present study, are such that $\hbar\omega/k_B T \gg 1$ at $T = 300K$. If we recall Eq. (6.1) and the fact that [131]

$$\frac{\hbar\omega}{2}\coth\left(\frac{\hbar\omega}{2k_B T}\right) = \hbar\omega\left[\frac{1}{2} + \frac{1}{e^{\frac{\hbar\omega}{k_B T}} - 1}\right],\qquad (6.2)$$

the previous expression leads to the vacuum fluctuations given by the zero point energy, i.e. $\approx \hbar\omega/2$. Hence, if we consider the emitting optical source spectrum as just given by a Planck distribution, the forces in the visible and NIR ranges due to the particle induced fluctuating dipoles, will be the optical analogous to those from the vacuum fluctuations in the thermal spectrum, namely C-P and VdW. Nonetheless, we can choose by all means a random source with a different statistics or optical spectrum. Thus our optical system constitutes an excellent means to create, test and monitoring photonic analogous of such thermal forces as well as of those out of thermodynamic equilibrium [118, 119].

On the other hand, this chapter deals with particles which present electric and magnetic response due to a random electromagnetic field. Magnetodielectric particles made of non magnetic material of high permittiviy such as semiconductors in the optical regions, have showed

exotic properties as scatterers and nanoantennas, as a consequence of the coupling between their electric and magnetic dipoles induced by the illuminating light field [60, 61, 111, 132–138], in addition they are excellent laboratory systems to test and tailoring the effects of such interactions [60, 111, 139].

Due to the magnetic response of the nanoparticle, more forces come into play in addition to those from the excitation of the electric dipole of a conventional dielectric particle, and they keep the above mentioned analogy with those of VdW, C-P and out of equilibrium interactions. Such additional forces come from the excitation of a magnetic dipole in the nanoparticle; thus allowing a larger number of degrees of freedom of relevance for the control of the mechanical interaction and hence for object ensembling and manipulation. We will study in detail the contribution to the force of these induced dipoles (we will refer to them as secondary sources) versus the terms coming from the primary partially coherent source.

It should be stressed that since the total force conveys adding the contribution of waves emitted by the random source at all frequencies of its spectrum, the most interesting cases in the NIR and optical frequencies are those in which these fluctuating sources are quasi-monochromatic, ($\Delta\omega \ll \omega_0$, $\Delta\omega$ denoting the bandwidth) [3]. Then the behavior of the nanoparticle polarizability as the central frequency ω_0 varies, leads to a rich and most interesting landscape of optical forces. This is in contrast with what happens when the source emits with a broad spectrum such as that given by Planck's law, a particular case of which are e.g. those thermal widely considered in connection with C-P and VdW forces. In this latter case such effects of the radiation force if there existed a particle, or object, with such a rich response to the electric and/or magnetic vector of the emission in that range of frequencies, would be washed out.

In addition, it must be remarked that out from the Rayleigh and quasistatic approximations widely used so far for the study of thermal forces on atoms and particles, the obtention of the radiation force by frequency integration over a wide emission spectrum such as that given by Planck's law, looses its significance because all Mie resonance lines of the nanoparticle would then be swamped by this wavelength superposition. In fact the same happens also with the dispersion resonances, present as the poles of the particle permittivity $\varepsilon_p(\omega)$, as well as with those of the static plasmon: $\varepsilon_p = -2$.

Hence, I discuss the mechanical interaction of a small particle, generally being magnetodielectric, with the random fields from a fluctuating optical source whose general spectrum and bandwidth may be controlled at will: e.g. whether quasi-monochromatic, or with a broader bandwidth, in particular one may deal with one given by a Planck-like distribution, and whose coherence length is also monitored. The nanoparticle has a rich spectral response to both the fluctuating electric and magnetic vectors and thus, much beyond previous studies on C-P and VdW thermal effects, a wealth of forces landscapes may be observed by controlling the constitutive and emissive parameters of the particle and the source, respectively. This analysis also manifests the limitations of previous studies, and the way to remedy them, concerning the asymptotic spatial dependence of radiation forces.

Figure 6.2: Scheme of setup and system geometry

6.3 FORCES ON A MAGNETODIELECTRIC NANOPARTICLE FROM A PARTIALLY COHERENT RANDOM ELECTROMAGNETIC FIELD

The geometry considered in this chapter consists of two regions, (cf. Fig. 6.2). The one in $z < 0$ is occupied by the random source with its polarization currents and it will be denoted as 1; whereas the one in $z > 0$, standing as 2, is free space and contains the nanoparticle. The fluctuating source considered here may be any random emitting medium; for instance, for laboratory experiments it can be e.g. a random refractive index, or a random rough surface dielectric slab illuminated by either quasi-monochromatic radiation, (like a laser), or by any other source such as a lamp of any chosen spectral lineshape and bandwidth. Then, since this system is ergodic, on moving, e.g. rotating, the slab, ensemble averages, equivalent to time averages, are performed in such a way that the coherence length of the field emitted (i.e. transmitted) by this slab is defined by the correlation length of the random medium inhomogeneities, (see e.g. [5, 10]).

6.3.1 *Forces from the primary source*

The Cartesian components of the ensemble averaged force exerted by a random field on a magnetodielectric dipolar nanoparticle is the sum of an electric, magnetic and electric-magnetic dipole

interference parts [59, III, IV] which are expressed in terms of the first electric and magnetic
Mie coefficients a_1 and b_1, or corresponding polarizabilities α_e and α_m, as [59, 141] [IV.3].

$$
\begin{aligned}
\langle F_i\left(\mathbf{r}\right)\rangle &= \langle F_i^e\left(\mathbf{r}\right)\rangle + \langle F_i^m\left(\mathbf{r}\right)\rangle + \langle F_i^{em}\left(\mathbf{r}\right)\rangle \\
&= \frac{\varepsilon_0\varepsilon_2}{2}\mathrm{Re}\left\{\langle\alpha_e E_j\left(\mathbf{r}\right)\partial_i E_j^*\left(\mathbf{r}\right)\rangle\right\} \\
&+ \frac{\mu_0\mu_2}{2}\mathrm{Re}\left\{\langle\alpha_m H_j\left(\mathbf{r}\right)\partial_i H_j^*\left(\mathbf{r}\right)\rangle\right\} \\
&- \varepsilon_0\varepsilon_2\frac{Zk_0^4}{12\pi}\mathrm{Re}\left\{\left(\alpha_e^*\alpha_m\right)\langle\mathbf{E}^*\times\mathbf{H}\rangle_i\right\},
\end{aligned}
\tag{6.3}
$$

where the angular brackets denote ensemble average, $i, j = 1, 2, 3$, $\varepsilon_l = \varepsilon_l' + i\varepsilon_l''$ and $\mu_l = \mu_l' + i\mu_l''$ $(l = 1, 2)$ are the permittivity and susceptibility of the medium embedding the particle,
respectively, in our case being vacuum; and $Z = \sqrt{\mu_0\mu_2/\varepsilon_0\varepsilon_2}$. *This means that the small particle
is considered as dipolar. However, it is large enough to require a Mie formulation with the first
electric and magnetic partial waves fully describing its scattering.* The electric and magnetic
polarizabilities of the particle, α_e and α_m, are then expressed as

$$
\alpha_e = i\frac{6\pi}{k_0^3}a_1,
\tag{6.4}
$$

$$
\alpha_m = i\frac{6\pi}{k_0^3}b_1,
\tag{6.5}
$$

where the n-Mie coefficients a_n and b_n are [60, 115]

$$
a_n = \frac{1}{2}\left(1 - e^{-2i\alpha_n}\right) = i\sin\alpha_n e^{i\alpha_n},
\tag{6.6}
$$

$$
b_n = \frac{1}{2}\left(1 - e^{-2i\beta_n}\right) = i\sin\beta_n e^{-i\beta_n},
\tag{6.7}
$$

and

$$
\tan\alpha_n = \frac{m^2 j_n\left(y\right)\left[xj_n\left(x\right)\right]' - j_n\left(x\right)\left[yj_n\left(y\right)\right]'}{m^2 j_n\left(y\right)\left[xy_n\left(x\right)\right]' - y_n\left(x\right)\left[yj_n\left(y\right)\right]'},
\tag{6.8}
$$

$$
\tan\beta_n = \frac{j_n\left(y\right)\left[xj_n\left(x\right)\right]' - j_n\left(x\right)\left[yj_n\left(y\right)\right]'}{j_n\left(y\right)\left[xy_n\left(x\right)\right]' - y_n\left(x\right)\left[yj_n\left(y\right)\right]'}.
\tag{6.9}
$$

In these expressions $m = n_p/n_h$ is the relative refraction index, where n_p refers to the particle
and n_h to the host medium (in this chapter $n_h = n_2$), $x = ka$, $y = mka$ and $k = n_h 2\pi/\lambda$. The
functions j_n and y_n are the spherical Bessel and Neumann functions respectively.

In Eq. (6.3) $E_i(\mathbf{r})$ is the total electric vector at frequency ω at any point of the half-space
$z > 0$; hence at the position of the particle, i.e. at $\mathbf{r} = \mathbf{r}_0$, it will be

$$
E_i\left(\mathbf{r}_0, \omega\right) = E_i^{inc}\left(\mathbf{r}_0, \omega\right) + E_i^p\left(\mathbf{r}_0, \omega\right) + E_i^m\left(\mathbf{r}_0, \omega\right).
\tag{6.10}
$$

The associated magnetic field $\mathbf{H}$ can be directly obtained from Maxwell's equations [43]. Whereas
in Eq. (6.10) the first term represents the electric field emitted from the primary source consti-
tuted by the random slab and *incident* on the nanoparticle, the last two terms are the electric

---

IV.3 Both the Gaussian and SI units are used in this thesis. Generally Gaussian units are used, however, for biblio-
graphic (or computational (cf. Chapter 8)) reasons in this chapter we use SI. Due to this fact we address explicitly
the expression of the force because the interference force differs from the previously addressed in Chapter 4 in a
factor $1/4\pi\varepsilon_0$. Notice also that the expressions for the dipoles in terms of the incident fields differ from a factor
ε_0 and μ_0^{-1} for the electric and magnetic dipoles respectively

fields emitted by the particle induced dipoles: $p_i = \varepsilon_0 \alpha_e E_i^{inc}$ and $m_i = \alpha_m H_i^{inc}$, respectively, after multiple reflections at the plane $z = 0$ [142].

The electric field incident on the particle is defined through the Green's function G_{ij}^{EP} which includes the transmission Fresnel coefficients $t_{s,p}$ from $z < 0$ into $z > 0$. G_{ij}^{EP} may be written as a superposition of plane waves. Thus, in terms of the polarization currents one has

$$E_i^{inc}(\mathbf{r}_0) = \mu_0 \omega^2 \int_V G_{ij}^{EP}(\mathbf{r}_0, \mathbf{r}', \omega) P_j(\mathbf{r}', \omega)\, \mathrm{d}^3 r'. \tag{6.11}$$

V denotes the volume occupied by the source. A more detailed description about these Green's functions can be found in e.g. [131, 143] and in Appendix C.

We define the *cross-spectral density tensor* of the source polarization $P_i(\mathbf{r})$ as $W_{ij}^{(P)}(\mathbf{r}_1, \mathbf{r}_2, \omega)$ $= \langle P_i^*(\mathbf{r}_1, \omega) P_j(\mathbf{r}_2, \omega) \rangle$. We shall address the wide variety of *statistically homogeneous and isotropic* sources [3] for which

$$W_{ij}^{(P)}(\mathbf{r}_1, \mathbf{r}_2, \omega) = S^{(P)}(\omega) \mu_{ij}^{(P)}(|\mathbf{r}_1 - \mathbf{r}_2|, \omega). \tag{6.12}$$

$S^{(P)}(\omega)$ denotes the power spectrum of the source and $\mu_{ij}^{(P)}(|\mathbf{r}_1 - \mathbf{r}_2|, \omega)$ is the spectral degree of coherence [3]. We assume a Gaussian degree of coherence, therefore the correlation function reads $W_{ij}^{(P)}(\mathbf{r}_1, \mathbf{r}_2, \omega) = \mathcal{S}^{(P)}(\omega) \exp(-(|\mathbf{r}_1 - \mathbf{r}_2|)^2/2\sigma^2)\delta_{ij}/(2\pi)^{3/2}\sigma^3$, σ being the coherence length of the source and $S^{(P)}(\omega) = \mathcal{S}^{(P)}(\omega)/(2\pi)^{3/2}\sigma^3$ representing the normalized spectrum. Notice also that this Gaussian function is not exactly the same as in Chapter 2, here we use a 3D Gaussian function.

On inserting Eq. (6.11) into (6.3) and taking the statistical homogeneity and isotropy of the source into account, one obtains the total force on the nanoparticle due to the random field inciding on it after emission. Only the force along the z-axis is different from zero, namely, the mechanical action of the source on the particle is rotationally symmetric as a consequence of its the statistical isotropy. The *conservative (gradient)* part of the electric force [59, III] $\langle F_i^{e,cons} \rangle$, associated to this incident field E_j^{inc}, $\langle F_i^{e,cons} \rangle = \varepsilon_0 \mathrm{Re}\alpha_e \partial_i \langle E_j^{inc,*}(\mathbf{r}) E_j^{inc}(\mathbf{r}) \rangle/4$ is, (cf. Appendix C):

$$
\begin{aligned}
\langle F_z^{e,cons} \rangle &= -\frac{k_0^4 \pi}{8\varepsilon_0} \mathrm{Re}\alpha_e \mathcal{S}^{(P)}(\omega) \int_{K=k_0}^{K=+\infty} \frac{\sqrt{K^2 - k_0^2}}{|\gamma_1|^2} e^{-\frac{(K\sigma)^2}{2}} \\
&\quad \times \left[|t_{12}^s|^2 + \frac{|t_{12}^p|^2}{|n_1|^2 |n_2|^2 k_0^4} \left(|\gamma_2|^2 + K^2 \right) \left(|\gamma_1|^2 + K^2 \right) \right] \\
&\quad \times e^{-2z_0 \mathrm{Im}\gamma_2} \frac{1}{\mathrm{Im}\gamma_1} e^{-\frac{1}{2}\sigma^2 \mathrm{Re}\gamma_1^2} K \mathrm{d}K,
\end{aligned} \tag{6.13}
$$

where $\mathbf{K} = (K_x, K_y)$, $\hat{\mathbf{s}} = \hat{\mathbf{K}} \times \hat{\mathbf{z}}$, $\hat{\mathbf{p}}_i^{\pm} = -\left[\gamma_i \hat{\mathbf{K}} \mp K\hat{\mathbf{z}} \right]/(n_i k_0)$ and $\gamma_i = \sqrt{\varepsilon_i \mu_i k_0^2 - K^2}$, $(i = 1, 2)$. n_1 (n_2) is the refractive index of the medium placed at $z < 0$ $(z > 0)$ and the caret denotes a unit vector. It is worth stressing that the integration range in the above equation contribution is solely due to the evanescent modes, (see also Eq. (C.19) of Appendix C).

At this point it should be remarked that the main result of [119] is only an approximation to Eq. (6.13) for the electric force in the limit $K \to k_0$ for a Rayleigh particle considered in

the quasistatic limit, i.e. that with $\alpha_e = a^3(\epsilon_p - 1)/(\epsilon_p + 2)$, which does not conserve energy on interaction with the random field [59]. By contrast, Eq. (6.13) accounts for all energy conserving and retarded effects that are required for any general study, including those that otherwise could not be tackled when a larger nanoparticle, like a magnetodielectric one, is addressed.

On the other hand, the *non-conservative* part of the electric force [59, III] $\left\langle F_i^{e,nc} \right\rangle = \varepsilon_0 \mathrm{Im}\alpha_e$ $\mathrm{Im}\langle E_j^{inc,*}(\mathbf{r}) \partial_i E_j^{inc}(\mathbf{r})\rangle/2$, is determined in a similar way, (see Eq. (C.23)):

$$
\begin{aligned}
\left\langle F_z^{e,nc} \right\rangle &= \frac{k_0^4 \pi}{8\varepsilon_0} \mathrm{Im}\alpha_e \mathcal{S}^{(P)}(\omega) \int_{K=0}^{K=k_0} \frac{\sqrt{k_0^2 - K^2}}{|\gamma_1|^2} e^{-\frac{(K\sigma)^2}{2}} \\
&\quad \times \left[|t_{12}^s|^2 + \frac{|t_{12}^p|^2}{|n_1|^2 |n_2|^2 k_0^4} \left(|\gamma_1|^2 + K^2 \right) \left(|\gamma_2|^2 + K^2 \right) \right] \\
&\quad \times \frac{1}{\mathrm{Im}\gamma_1} e^{-\frac{1}{2}\sigma^2 \mathrm{Re}\gamma_1^2} K \mathrm{d}K,
\end{aligned}
\tag{6.14}
$$

where it is seen that only the homogeneous (propagating) plane wave components contribute and yield a constant non-zero value for any $\mathbf{r}$.

The magnetic and the interference forces, [cf. second and third terms of Eq. (6.3)], are calculated analogously. See also Sections C.2 and C.3 of Appendix C for a detailed deduction.

6.3.2 *Forces from the secondary sources constituted by the induced fluctuating dipoles of the nanoparticle*

As previously stated, the last two terms in Eq. (6.10) are the fields emitted by the induced dipoles in the particle, and hence connect the constitutive properties of the source and particle through the Fresnel reflection coefficients $r^{s,p}$ at $z = 0$ and the polarizabilities, being described in this case by G_{ij}^{Ep} and G_{ij}^{Hm}. Thus, the electric field can be calculated like in Eq. (6.11) using G_{ij}^{Ep} and $p_i \delta(\mathbf{r}' - \mathbf{r}_0)$ instead of G_{ij}^{EP} and $P_j(\mathbf{r}')$, i.e.,

$$
\begin{aligned}
E_i^p(\mathbf{r}) &= \mu_0 \omega^2 \int_V G_{ij}^{Ep}(\mathbf{r}, \mathbf{r}', \omega) p_j(\mathbf{r}', \omega) \delta(\mathbf{r}' - \mathbf{r}_0) \mathrm{d}^3 \mathbf{r}', \\
&= \mu_0 \omega^2 G_{ij}^{Ep}(\mathbf{r}, \mathbf{r}_0, \omega) p_j(\mathbf{r}_0, \omega),
\end{aligned}
\tag{6.15}
$$

and analogously the electric field emitted by the induced magnetic dipole reads

$$
E_i^m(\mathbf{r}) = \frac{Z_0 i\omega}{c} G_{ij}^{Hm\leftrightarrow}(\mathbf{r}, \mathbf{r}_0, \omega) m_j(\omega),
\tag{6.16}
$$

where the superscript $\leftrightarrow$ means that the electric field generated by the magnetic dipole has the same Green's function as the magnetic field radiated by the electric dipole with the interchange $r^s \leftrightarrow r^p$. Both $G_{ij}^{E(p,m)}$ and $G_{ij}^{H(p,m)}$ exponentially decay with the distance z in the evanescent wave region ($K > k_0$) and are oscillatory in the radiative one ($K \leq k_0$). They are obtained as indicated in Section C.4.

Note that r^p and t^p support SPPs. The calculations are done on considering that there is mutual incoherence between the nanoparticle electric and magnetic induced dipoles, i.e., $\langle p_i^* m_j \rangle = 0$
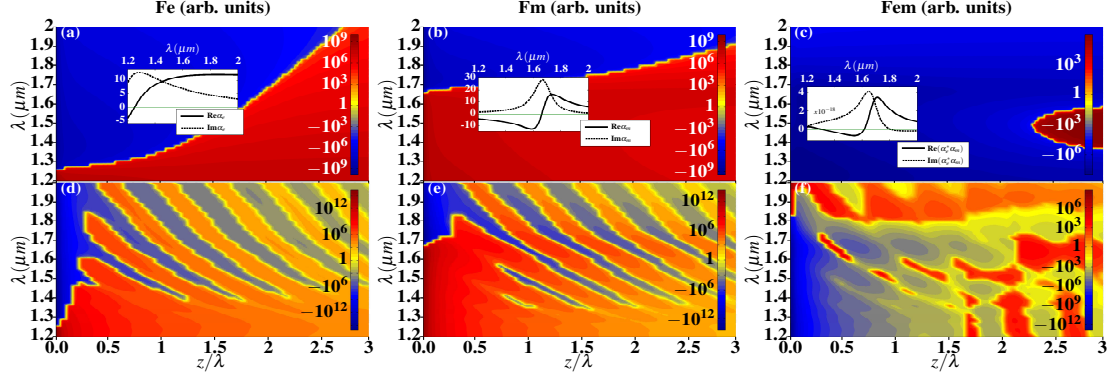
Figure 6.3: From left to right: Normalized electric $\langle F^e \rangle$, magnetic $\langle F^m \rangle$ and interference force $\langle F^{em} \rangle$ from a δ-correlated source. The first horizontal row shows the part of the force due to the field from the fluctuating primary source whose exit plane is at $z = 0$, [first term in Eq. (6.10)]. The insets exhibit the polarizabilities normalized to a^3 vs. λ: electric, magnetic and electric-magnetic product, respectively, which also depict the behavior of the corresponding force from each plane wave component [59], and hence α_e, α_m and $\alpha_e^* \alpha_m$ are factors in $\langle F^e \rangle$, $\langle F^m \rangle$ and $\langle F^{em} \rangle$, respectively. The second horizontal row represents the force from the secondary source constituted by the particle induced dipoles, [second and third terms in Eq. (6.10)]. In each figure, the warm and cold color regions, separated by a yellow line of minimum force strength, correspond to the zones where the force is positive and negative, respectively. The normalization of these forces is done on dividing their value by the power spectrum $\mathcal{S}^{(P)}(\omega)$ of the source

[79]. In the following, $\langle F_1 \rangle$ and $\langle F_2 \rangle$ will denote the total forces [cf. Eq. (6.3)] due to the above mentioned contributions of the primary fluctuating source in $z < 0$ and of the secondary source constituted by the particle induced dipoles, respectively.

6.4 EXAMPLE: THE SEMICONDUCTOR SPHERE IN THE NEAR INFRARED AND VISIBLE

We illustrate the above with a generally magnetodielectric dipolar nanoparticle constituted by a semiconductor sphere; its anomalous scattering properties have recently received a great deal of attention, both theoretically and experimentally [61, 112–114, 132, 139]. In particular, for each plane wave component of the field incident on the particle, its scattered intensity in the backscattering direction is zero [first *Kerker condition* (K1)] when $\mathrm{Re}\alpha_e = \mathrm{Re}\alpha_m$. Also, for each of these incident plane wave components, the forwardly scattered intensity becomes close to a non-zero minimum [second *Kerker condition* (K2)] when $\mathrm{Re}\alpha_e = -\mathrm{Re}\alpha_m$. There being no gains in the particle, in both cases: $\mathrm{Im}\alpha_e = \mathrm{Im}\alpha_m$ [61].

After performing all the integrations of the form of Eq. (6.11) for the primary source and for the induced electric and magnetic dipoles that constitute the above mentioned secondary source, a long but straightforward task some of whose details are shown in the Appendix C, one sees that $\langle E_i^{m*}(\mathbf{r}_0)E_i^m(\mathbf{r}_0)\rangle = \langle H_i^{p*}(\mathbf{r}_0)H_i^p(\mathbf{r}_0)\rangle = 0$. This is relevant in connection with the Kerker conditions.

6.4.1 *Results for a Silicon sphere. Forces from the primary source*

Let the sphere be made of Si with radius $a = 230nm$, the incident light being in the NIR range of $1.2\mu m - 2\mu m$. At these wavelengths the total cross section of the nanoparticle is fully determined by the electric and magnetic Mie coefficients a_1 and b_1 (see Fig. 6.2 and Ref. [60]), respectively. This justifies the use of Eq. (6.3) for the optical force.

In the configuration here addressed, (cf. Fig. 6.2), the surface at $z = 0$ is assumed to be metallic supporting SPPs for p-polarization. We consider an Au interface as in Chapter 5, hence supporting SPPs in the spectral range under consideration. It is worth remarking, however, that the presence of SPPs on $z = 0$ is considered here because it enhances by one order the magnitude the strength scale of the different force components, but it does not produce any qualitative change in their relative behaviors [cf. Chapter 5]. Results are shown in the NIR; nonetheless is worth stressing that the scaling property of these high permittivity particles leads to identical results ranging from visible to microwave regions just by appropriately changing the size and permittivity of the particle . (cf. Fig. 2 of [60] and also [112, 114, 137]

Fig. 6.3 shows the force terms, in a logarithmic scale, due to the fluctuating primary source and to the induced electric and magnetic random dipoles in the particle. This representation aims to clarifying its extremely sharp changes of sign. Unless stated otherwise, in order to see the relative weight of each force component, all results of this section are normalized to the power spectrum $\mathcal{S}^{(P)}(\omega)$ of the source. The first horizontal row shows the force $\langle F_1 \rangle$ due to the field impinging the sphere from the primary statistical source at $z = 0$. The second horizontal row represents the force $\langle F_2 \rangle$ from the secondary source constituted by the particle induced fluctuating electric and magnetic dipoles. The source coherence length σ is first assumed to be zero. The insets depicts the polarizability contributions for the range of wavelengths under which it exhibits a resonant behavior, this helps to understand the color plots.

In Figs. 6.3 (a) and 6.3 (b) we see a yellow line separating the gradient and scattering forces. For a statistically homogeneous source, the gradient force [proportional to $\text{Re}\alpha_e \langle E_i^* E_i \rangle$] is governed uniquely by the evanescent modes and is negative for a particle with $\text{Re}\alpha_e > 0$, [cf. IV and Eq. (6.13)]; hence it exponentially decays with the distance z to the source. On the other hand, the scattering force (proportional to $\text{Im}\alpha_e\text{Im}\langle E_j^* \partial_i E_j \rangle$) is positive, i.e. pushing, and constant for any $\mathbf{r}_0$. As the wavelength grows, $\text{Re}\alpha_e > \text{Im}\alpha_e$, [see the inset in Fig. 6.3 (a)]. This behavior and that corresponding to α_m shown in the inset of Fig. 6.3 (b) results, as consequence of the integrations in Eqs. (6.13) and (6.14), in an extraordinary phenomenon: the contribution of the evanescent waves to the gradient force, Eq. (6.13), is noticeable even at distances $z/\lambda > 1$. *Hence, pretty far away from the surface, the gradient force is dominant at shorter frequencies, a fact that applies to any source which behaves as quasi-monochromatic [1] in this range of selected wavelengths.* This is a remarkable new feature of the forces introduced by the resonant nature of these particles that we put forward for the first time.

Fig. 6.3 (c) represents the force component $\langle F_1^{em} \rangle$ due to interference between the nanoparticle induced electric and magnetic dipoles. In the near field this is attractive for any wavelength, even

at distances larger than λ, where the force is proportional to $-\text{Re}(\alpha_e^* \alpha_m) S_i$, $[\mathbf{S} = \text{Re}(\mathbf{E}^* \times \mathbf{H})/2$ denotes the Poynting vector, which is independent of the distance z as one can see from Eq. (C.36)]. Such a negative force is known as a *pulling* force, and its interest has increased in the last years [68, 69, 101]. In this respect, Fig. 6.3 (c) shows the relevant role of the magnetodielectric behavior of these particles, although in this latter specific case when the two other force components: electric and magnetic, are added this pulling effect becomes small. We state, however, that although not shown here for brevity, *the sum of three components $\langle F^e \rangle$, $\langle F^m \rangle$ and $\langle F^{em} \rangle$ yields a tractor force up to the distance $z \simeq 3\lambda$ in the range $\lambda \simeq 1.7 - 2\mu m$*. This is a new feature stemming from the magnetodielectric character of this particle.

Concerning the force $\langle F_2 \rangle$ from the particle induced dipoles, we see in the second horizontal row of Fig. 6.3 that its amplitude exponentially decays with the distance z to the primary source exit plane $z = 0$, and its sign depends on that of the particle polarizability; nevertheless, the oscillatory behavior of the Green's function due to propagating plane wave components manifests in this force. We also observe that it is six orders of magnitude larger than its counterpart $\langle F_1 \rangle$ from the primary fluctuating source, at least at subwavelength distances z. We shall later discuss this fact.

To get a deeper understanding, Fig. 6.4 represents $\langle F_1 \rangle$ for some selected wavelengths and for two different source coherence lengths: $\sigma = 0$ and $\sigma = \lambda/4$. The huge sharp changes in the sign of the force at a given distance z/λ are clearly seen. For an statistically homogeneous source, the electric and magnetic cross-spectral density tensors fulfill [32]

$$\varepsilon_0 \left\langle E_i^*(\mathbf{r}_1, \omega) E_j(\mathbf{r}_2, \omega) \right\rangle = \mu_0 \left\langle H_i^*(\mathbf{r}_1, \omega) H_j(\mathbf{r}_2, \omega) \right\rangle, \tag{6.17}$$

hence, in the near field one has $\langle F_1^e \rangle = \langle F_1^m \rangle$ and $\langle F_1^e \rangle = -\langle F_1^m \rangle$ when the first and the second Kerker condition hold, respectively. However, in the far zone $\langle F_1^e \rangle = \langle F_1^m \rangle$ for any value of $\mathbf{r}_0$ at Kerker conditions. For the Si nanoparticle addressed, the Kerker conditions are fulfilled at $\lambda_1 \simeq 1.825\mu m$ and $\lambda_2 \simeq 1.53\mu m$, (cf. Figs. 6.3 (a) and 6.3 (b) and [61]).

Fig. 6.5 depicts the range of wavelengths where the magnetic dipole predominates over the electric one. In the near-field, where the electric (magnetic) force is solely due to the evanescent modes, the weight of such force is due to the response of the nanoparticle through its proportionality to the real part of the electric (magnetic) polarizability. Fig. 6.5 (a) exhibits a peak near $\lambda \simeq 1.25\mu m$ where the magnetic polarizability is more than one order of magnitude larger than its electric counterpart; thus, the magnetic force will also surpass the electric one by one order of magnitude. We can also distinguish in this figure two zones close to $\lambda \simeq 1.6\mu m$ and $\lambda \simeq 1.76\mu m$ where $\langle F_1^m \rangle > \langle F_1^e \rangle$. On the other hand, the behavior of the force at larger distances, will be ruled by the imaginary part of the polarizability. Fig. 6.5 (b) shows the zone, where the magnetic dipole predominates, and thus *the magnetic force is five times larger than the electric one. These effects, due to the magnetic response of the dielectric particle to the light field, constitutes another main result of this chapter.*
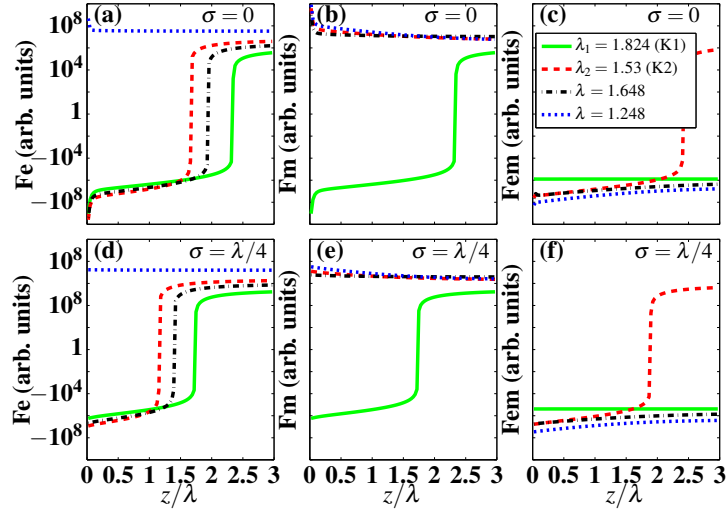
Figure 6.4: Normalized $\langle F_1^e \rangle$, $\langle F_1^m \rangle$ and $\langle F_1^{em} \rangle$ versus the distance from the plane of the source (in wavelength units) for some values of the wavelength (in μm). The two Kerker conditions occur at λ_1, (K1), and λ_2, (K2), respectively.
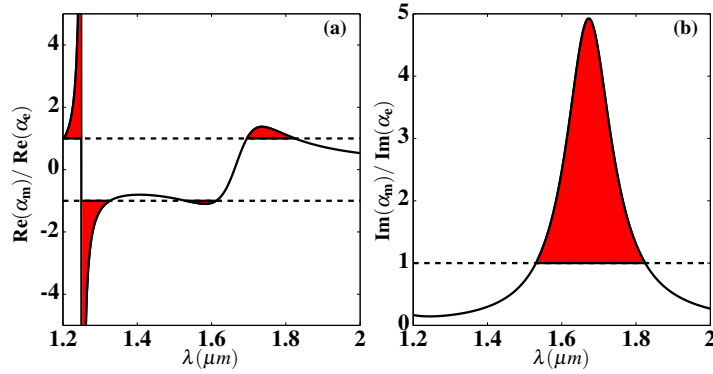

Figure 6.5: (a) $\mathrm{Re}\alpha_m / \mathrm{Re}\alpha_e$. (b) $\mathrm{Im}\alpha_m / \mathrm{Im}\alpha_e$. The colored areas denote the zones where the magnetic dipole predominates.

6.4.2 *Influence of the coherence length and forces from the induced dipoles*

I now address the influence of the coherence length of the source. This establishes the differences between the mechanical action of our partially coherent optical sources and most previously studied that are δ-correlated. In particular at thermal wavelengths this would predict differences between Liftshitz, C-P and VdW forces from thermal sources and blackbodies, both in and out of thermodynamic equilibrium, and those generated from bodies whose currents are partially correlated.

In our study, the transversal part of the spectral degree of coherence (cf. Section 6.3.1) $\exp[-(K\sigma)^2/2]$, governs the coherence tensors and the mean forces from the random field emitted by the primary source, (see Appendix C), acting as a low-pass filter in **K**-space, [see Eqs. (6.13) and (6.14)], being maximum for $\sigma = 0$, i.e. when the source is white noise. Because of this
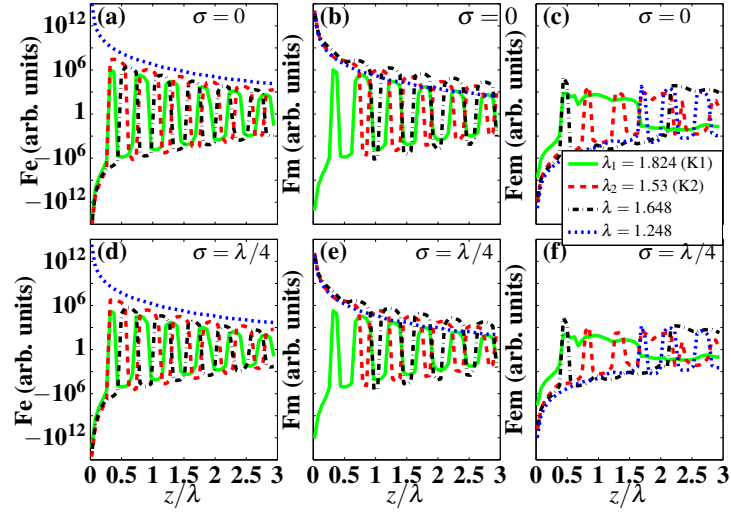
Figure 6.6: Normalized $\langle F_2^e \rangle$, $\langle F_2^m \rangle$ and $\langle F_2^{em} \rangle$ versus distance z (in units of wavelength) from the exit plane $z = 0$ of the source for different values of the wavelength (in μm). The two Kerker conditions are fulfilled at λ_1, (K1), and λ_2, (K2), respectively.

fact, the evanescent modes present two such filters: the first is due to their own nature, while the second stems from the spatial coherence of the source. The shape of Figs. 6.4 (d)-6.4 (f) is similar to that of Figs. 6.4 (a)- 6.4 (c), shifted by a distance $\Delta z \simeq 0.5\lambda$, therefore for $\sigma > \lambda$ the force is solely due to the non-conservative (scattering) contribution and to the interference component $\langle F_1^{em} \rangle$, which becomes constant and positive or negative depending on the wavelength. It is worth pointing out that the price paid on increasing the coherence length is expensive, because at the same time there is a reduction of the force strength by various orders of magnitude [cf. e.g. the forces shown in Figs. 6.4 (a) and 6.4 (d) at $z < \lambda$].

We now turn our study to analyze its influence on the force $\langle F_2 \rangle$ generated by the secondary source, namely by the particle induced dipoles. Fig. 6.6 represents $\langle F_2 \rangle$ for the same wavelengths as in Fig. 6.4. The magnitude of this force $\langle F_2 \rangle$ in the near-field $z < \lambda$ is much larger than that of $\langle F_1 \rangle$ in Fig. 6.4, thus the effect of the mechanical action $\langle F_2 \rangle$ of the field emitted by the particle induced dipoles substantially dominates over that $\langle F_1 \rangle$ of the field that is due solely to the primary fluctuating source. Nevertheless, as the distance z grows, all the fastly oscillating components, electric, magnetic and that of interference of this force $\langle F_2 \rangle$ rapidly tend to zero, and hence is the force $\langle F_1 \rangle$ from the primary source the one that dominates.

I remark that, as follows from the calculation of $E^{p,m}$ and $H^{p,m}$, the cross spectral density tensors of the electric and magnetic dipoles are not equal to each other; therefore although at first sight it could seem that under Kerker conditions $\langle F_2^e \rangle$ and $\langle F_2^m \rangle$ would fulfill relationships similar to those of $\langle F_1^e \rangle$ and $\langle F_1^m \rangle$, in fact they do not. This is seen in Fig. 6.6.

The role of the coherence length in this case is exactly the same as in Fig. 6.3; the magnitude of the force decreases as σ grows. Future work should find a minimum value of σ for which this optical analogous to the C-P force predominates over the contributions discussed here.

In order to provide an estimation of the actual magnitude of these forces, now instead of studying their relative values by using a normalization to $\mathcal{S}^{(P)}(\omega)$ as before, *we evaluate them in terms of the optical power I_0 of the source*. To this end, we consider a Gaussian quasi-monochromatic spectrum [3] centered at frequency ω_0 and spectral width $\sigma_\omega = 0.01\,\omega_0$: $\mathcal{S}^{(P)}(\omega) = (\varepsilon_0/ck_0^3)$ $(I_0/\sqrt{2\pi}\sigma_\omega)\exp[-(\omega-\omega_0)^2/2\sigma_\omega^2]$, where I_0 is the optical power in W/m^2. Let this power be: $I_0 = 1mW/\mu m^2$.

The resulting force exerted by the random field on the particle is determined by ω-integration of all frequency components in the support of $\mathcal{S}^{(P)}(\omega)$, i.e. $F_z(\mathbf{r}) = \int F_z(\mathbf{r},\omega)\,\mathrm{d}\omega$. (cf. Eqs. (6.13) and (6.14) for $F_z(\mathbf{r},\omega)$. Notice that in the integrand we have now explicitly written the ω-dependence of the force at each frequency ω).

First I calculate the forces $\langle F_1 \rangle$ due to the primary source assuming it to be δ-correlated. As seen in Fig. 6.4, the maximum magnitude of the force, (independently of whether its origin is from the electric, magnetic, or electric-magnetic interference dipoles), occurs at subwalength distances z where the evanescent modes are more relevant. For instance, for $\lambda_0 = 1.6\mu m$, $(\lambda_0 = 2\pi c/\omega_0)$, the particle being at $z < \lambda_0/2$, the magnitude (in absolute value) of the electric force $\langle F_1^e \rangle$ is in the interval: $[1 \times 10^{-14},\ 1 \times 10^{-13}Newton]$; and as the distance z of the particle to the source increases, this electric force tends to a constant value, (governed by the propagating modes), in this interval. Obviously, the sign of the force will be frequency-dependent through the polarizability of the particle.

Analogously, and as a consequence of Eq. (6.17), the behavior of the magnitude of the magnetic force $\langle F_1^m \rangle$ is similar to that of $\langle F_1^e \rangle$. At the same distance z, the interference force $\langle F_1^{em} \rangle$ is slightly different to these former. Indeed, as one sees on comparing Figs. 6.4 (b) and 6.4 (c), $\langle F_1^{em} \rangle$ is two orders of magnitude smaller than either the electric or magnetic forces.

Subsequently, this calculation is performed for the forces $\langle F_2 \rangle$ induced by the secondary source, (i.e. from the induced dipoles in the particle). The same parameters as before are assumed for the primary source. As pointed out above in this section, at subwalength distances z, these forces are much larger than those $\langle F_1 \rangle$ from the primary source. At a distance $z \simeq \lambda_0/10$, the electric force $\langle F_2^e \rangle$, is of the order of $10^{-12}N$, a value which is certainly larger than the aforementioned one for $\langle F_1^e \rangle$. On the other hand, at a distance $z \simeq \lambda_0/4$, $\langle F_1^e \rangle$ starts to compete with $\langle F_2^e \rangle$; the latter becoming negligible at distances comparable to the wavelength λ_0 of the emitted field. Similar effects are found for the other two components $\langle F_2^m \rangle$ and $\langle F_2^{em} \rangle$.

All these forces diminish when the coherence length σ of the primary source increases. For instance, when $\sigma = \lambda/4$, they all become about three to four orders of magnitude smaller than those previously obtained for a δ-correlated source.

6.5 ASYMPTOTIC LAWS IN THE NEAR-FIELD

6.5.1 *Fields from the primary source*

In this section I discuss the asymptotic behavior of the forces due to the field emerged from the primary source when we are at extreme near-field distances, ($z \ll \lambda$), and for different correlation lengths σ. This analysis in the optical range makes a contact with previous studies of C-P, VdW and out of equilibrium forces corresponding to broad spectra like those from thermal or blackbody sources, and shows their analogies as well as the limitations of applying to particles previous studies on atoms.

In this connection, I stress the different sign of these forces in the region $z \ll \lambda$, either attractive or repulsive, shown in Figs. 6.4 and 6.6, depending on the sign of the particle polarizability according to the emission wavelength.

Multiple studies have led to a rather large landscape of C-P forces depending on both the nature of the fluctuations and the electromagnetic properties of the sources [144]. We address the interaction from the polarization currents of the primary source, (the magnetic currents are negligible), and the nanoparticle, generally considered as magnetodielectric.

At distances $z \ll \lambda$ the main contribution to the integral Eq. (6.13) comes from large values of K, i.e., $K \gg k_0$. Notice that in this case, the total electric force is solely due to the conservative force $F_z^{e,cons}$ and consequently only the evanescent modes contribute.

We shall now consider two regimes in the quaistatic approximation $K \gg k_0$ [31]: the first is when $\sigma \to 0$. This is the most studied one because it can be extrapolated to a thermal source whose fluctuations come from Rytov's theory [79]. Thus, in this case Eq. (6.13) leads to (see Section C.1.2)

$$F_z^{e,cons} \simeq -\frac{3\pi}{4\varepsilon_0 z^4}\mathrm{Re}\alpha_e \frac{\mathcal{S}^{(P)}(\omega)}{|\varepsilon_1 + 1|^2}, \qquad (z \ll \lambda, \ \sigma \to 0). \tag{6.18}$$

As we can see, the force decays as $1/z^4$ and its sign depends on the sign of the polarizability of the nanoparticle, which can be positive (negative) leading to a negative (positive) force respectively. This is analogous to the well-known quasistatic dependence of the VdW force when $\mathcal{S}^{(P)}(\omega)$ is the wide Planck's spectrum.

The second regime will be when $z \ll \lambda$ and $\sigma > z$, in this case the electric force is given by

$$F_z^{e,cons} \simeq -\frac{4\pi}{\varepsilon_0 \sigma^4}\mathrm{Re}\alpha_e \frac{\mathcal{S}^{(P)}(\omega)}{|\varepsilon_1 + 1|^2}, \ \ (z \ll \lambda, \ \ \sigma > z). \tag{6.19}$$

Now the source with a non-zero coherence length σ gives rise to a force which does not depend on the distance z, i.e., *for an arbitrary value of σ, the force is constant with distance* and the role of z that appeared in Eq. (6.18) is now played by σ. Notice also that when $\sigma \gg \lambda > z$ the resulting force is negligible.

At this point I wish to point out that the conservative forces obtained in Eqs. (6.18) and (6.19) are compatible with recent results on spatial correlations of speckle patterns at extremely close distances form disordered media interfaces, (cf. Sec. IV of [31]).

The conservative force $F_z^{m,cons}$ on the magnetic dipole, induced in the particle by the field emitted from the fluctuating primary source, is similarly calculated. As stated before, these electric and magnetic forces hold:

$$F_z^{m,cons} = \frac{\mathrm{Re}\alpha_m}{\mathrm{Re}\alpha_e} F_z^{e,cons} \qquad (6.20)$$

Next I calculate the term F_i^{em} of the force due to the interference between the induced electric and magnetic dipoles in the particle. At these distances, this force is solely due the evanescent modes of the angular spectrum as in the case of electric and magnetic force. We have

$$F_i^{em}(\mathbf{r}) \simeq -\frac{k_0^5}{24\varepsilon_0 z^2}\mathrm{Im}(\alpha_e^*\alpha_m)\frac{\mathcal{S}^{(P)}(\omega)}{|\varepsilon_1+1|^2},$$
$$(z \ll \lambda \ , \ \sigma \to 0), \qquad (6.21)$$

$$F_i^{em}(\mathbf{r}) \simeq -\frac{k_0^5\pi}{6\varepsilon_0\sigma^2}\mathrm{Im}(\alpha_e^*\alpha_m)\frac{\mathcal{S}^{(P)}(\omega)}{|\varepsilon_1+1|^2},$$
$$(z \ll \lambda \ , \ \sigma > z), \qquad (6.22)$$

In contrast with the corresponding Eqs. (6.18) and (6.19), the interference force decays with the distance as $1/z^2$, or with the coherence length as $1/\sigma^2$.

I now turn out to study the opposite asymptotic case, i.e. that of larger distances $z > \lambda$; this excludes any quasistatic approximation. At such large z/λ, one may expect almost no contribution of evanescent plane wave components and thus, if like in [119] one approximated $K \to k_0$ in the integration of Eq. (6.13), one would obtain, in analogy with the calculation leading to Eqs. (6.18) and (6.19), an asymptotic power law for the conservative force, either electric [119], magnetic, or electric-magnetic interference, which depending on the value of σ, would decay as $\propto -1/z^3$ or $\propto -1/\sigma^3$.

However, in the range $z > \lambda$, the non-conservative component of the force Eq. (6.14) is no longer negligible, hence contrary to what might initially be thought, the conservative component is not enough to describe the total force on the particle at such distances. This completely changes the variation with z of the resulting force which, as a consequence of adding the conservative and non-conservative components, is no longer of the form $\propto -1/z^3$ or $\propto -1/\sigma^3$. Notice that the existence of the non-conservative force in this regime of z/λ is a consequence of the fact that, as mentioned before, the particle polarizabilities cannot be described by their quasistatic expressions.

To clarify this point, Fig. 6.7 shows the different components of the force in two axes. At these distances z, the exact expression Eq. (6.13) of $F_z^{e,cons}$ leads to the asymptotic power law $\propto -1/z^3$ [119]. Nevertheless, on taking also into account $F_z^{e,nc}$, [cf. Eq. (6.14)], the total electric force $F_z^e = F_z^{e,cons} + F_z^{e,nc}$ does no longer follow the power law $-1/z^3$ but practically
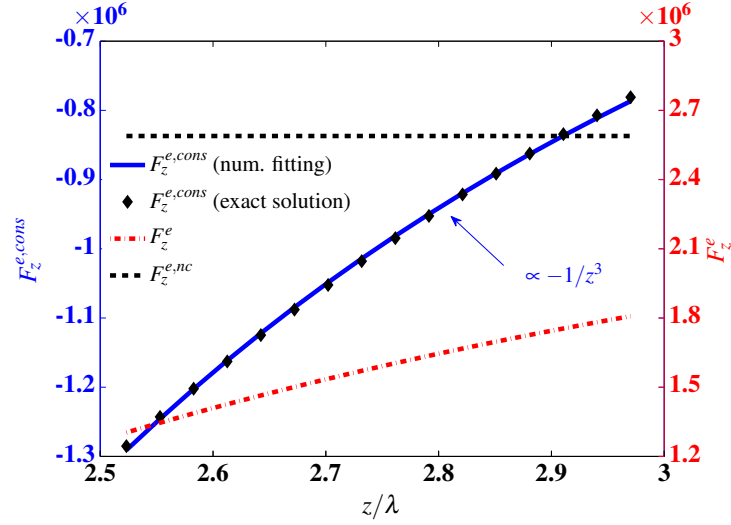
Figure 6.7: Components of the electric force at $\lambda = 1.63\mu m$. The diamonds and the blue-solid line (left axis) represent the exact solution and the numerical fitting $-1/z^3$, respectively, for the conservative component [cf. Eq. (6.13)]. The dashed lines (right axis) depict the non-conservative force (black dashed line) (cf. Eq. (6.14) , and the total force $F_z^e = F_z^{e,cons} + F_z^{e,nc}$, (red dash-dot line). Notice how this latter sum makes the asymptotic behavior $-1/z^3$ of $F_z^{e,cons}$ to disappear, becoming almost linear with z in the resulting total force F_z^e.

varies proportional as $\simeq 1.33z$ and becomes repulsive. *This result points out the inadequacy of extrapolating previous quasistatic studies made for atoms to the analysis of the mechanical action on particles from both optical and thermal radiation.* [118, 119].

6.5.2 *Fields from the nanoparticle induced dipoles*

I now proceed with the interaction from the fluctuating induced dipoles. The electric force will now be proportional to $\text{Re}\left\langle \alpha_e E_j^p(\mathbf{r}) \partial_i E_j^{p*}(\mathbf{r}) \right\rangle$, (with an analogous expression for the magnetic and electric-magnetic interference forces). Now,

$$
\begin{aligned}
\left\langle E_j^{p*} \partial_i E_j^p \right\rangle &= \mu_0^2 \omega^4 \left\langle G_{jk}^{p*}(\mathbf{r},\mathbf{r}') \partial_i G_{jl}^p(\mathbf{r},\mathbf{r}') \right\rangle \left\langle p_k^*(\mathbf{r}') p_l(\mathbf{r}') \right\rangle \\
&= k_0^4 |\alpha_e|^2 \left\langle G_{jk}^{p*}(\mathbf{r},\mathbf{r}') \partial_i G_{jl}^p(\mathbf{r},\mathbf{r}') \right\rangle I_{kl}(\mathbf{r}',\mathbf{r}_1),
\end{aligned}
\tag{6.23}
$$

where $I_{kl}(\mathbf{r}',\mathbf{r}_1) = \left\langle E_k^{inc*}(\mathbf{r}',\mathbf{r}_1) E_l^{inc}(\mathbf{r}',\mathbf{r}_1) \right\rangle$, $\mathbf{r}, \mathbf{r}'$ denote points of the half-space $z > 0$, where the dipole particle is placed, while $\mathbf{r}_1$ stands for a point of $z < 0$, (cf. Fig. 6.2). Note that Eq. (6.23) differs from that employed for calculating the vacuum fluctuations and the C-P force because in Eq. (6.23) the particle induced dipoles are expressed in terms of the incident field and not by the usual fluctuation-dissipation theorem [79]. Now to calculate the asymptotic behavior of the force, we have to approximate two Green's function, one for the field which is transmitted from the primary source and another for the field which is reflected at $z = 0$. As for the Green's

function G^{EP}, we make the same approximations as in the previous section. On the other hand, for the Green's function G^{Ep}, one can approximate the reflection Fresnel coefficients by [145]

$$r_s \simeq \frac{k_0^2 \, (\varepsilon_1 - 1)}{4K^2}, \qquad\qquad r_p \simeq \frac{\varepsilon_1 - 1}{\varepsilon_1 + 1}. \qquad (6.24)$$

Taking these considerations into account, we address the first asymptotic laws for this type of configuration. Thus, for the electric force we get in the quasistatic approximation

$$
\begin{aligned}
F_z^{e,cons}\,(\mathbf{r}) \quad \simeq \quad &-\frac{|\alpha_e|^2}{128\varepsilon_0 z^{10}}\mathrm{Re}\alpha_e \mathcal{S}^{(P)}(\omega)\frac{|\varepsilon_1 - 1|^2}{|\varepsilon_1 + 1|^4}, \\
&(z \ll \lambda \quad, \quad \sigma \to 0), \qquad (6.25)
\end{aligned}
$$

$$
\begin{aligned}
F_z^{e,cons}\,(\mathbf{r}) \quad \simeq \quad &-\frac{\sqrt{2\pi}\,|\alpha_e|^2}{64\varepsilon_0 z^7 \sigma^3}\mathrm{Re}\alpha_e \mathcal{S}^{(P)}(\omega)\frac{|\varepsilon_1 - 1|^2}{|\varepsilon_1 + 1|^4}, \\
&(z \ll \lambda \quad, \quad \sigma > z). \qquad (6.26)
\end{aligned}
$$

Thus showing dependence on the distance either as $1/z^{10}$ or $1/z^7$. Therefore, there is a difference of three orders of magnitude between the incoherent ($\sigma \to 0$) and the partially coherent $\sigma > 0$ limits. This difference is given by I_{kl} which contains the coherence length σ of the source. At these small distances, the nonconservative components of the forces are zero.

In a similar way, we derive the expression for the force from the particle induced magnetic dipole. In this case we get

$$
\begin{aligned}
F_z^{m,cons}\,(\mathbf{r}) \quad \simeq \quad &-\frac{k_0^4 \, |\alpha_m|^2}{128\varepsilon_0 z^6}\mathrm{Re}\alpha_m \mathcal{S}^{(P)}(\omega)\frac{|\varepsilon_1 - 1|^4}{|\varepsilon_1 + 1|^4}, \\
&(z \ll \lambda \,, \, \sigma \to 0), \qquad (6.27)
\end{aligned}
$$

$$
\begin{aligned}
F_z^{m,cons}\,(\mathbf{r}) \quad \simeq \quad &-\frac{\sqrt{2\pi}k_0^4 \, |\alpha_m|^2}{256\varepsilon_0 z^3 \sigma^3}\mathrm{Re}\alpha_m \mathcal{S}^{(P)}(\omega)\frac{|\varepsilon_1 - 1|^4}{|\varepsilon_1 + 1|^4}, \\
&(z \ll \lambda \,, \, \sigma > z). \qquad (6.28)
\end{aligned}
$$

Eq. (6.27) does not show the same decay with z as Eq. (6.25) exhibits for the electric force, this shows that the induced magnetic dipole does not interact with the source plane at $z = 0$ in the half-space $z > 0$ in the same way as the particle induced electric dipole.

The expressions for the electric-magnetic interference force are a bit more complicated to analytically derive, however, making a numerical fitting we see that it decays as $-1/z^8$ or $-1/(z^5\sigma^3)$ in the incoherent and partially coherent cases, respectively.

The asymptotic expression for this secondary source force components is not meaningful at larger distances. As remarked in Section 6.4.1, the forces from the particle induced dipole fields decay much faster than those from the primary source fields, thus, the nonconservative component will predominate, being constant with distance z as shown in Section 6.4.1. It should also be noticed that in order to recover the retarded typical power law $1/z^5$ associated to C-P forces from vacuum fluctuations [92], no primary source fluctuating fields should be present. As mentioned in the introduction, $\hbar\omega/kT \gg 1$ at the frequencies considered, and hence if the source obeyed a Planck law the resulting spectral distribution would be the optical analogous to that of the vacuum fluctuations with energy $\hbar\omega/2$ [121], therefore a short of switch-off of the emitted field would be necessary to detect such vacuum fluctuation optical analogous force.

6.6 CONCLUSIONS

In this chapter I have analyzed in detail the new effects and asymptotic power laws of photonic forces on a resonant magnetodielectric nanoparticle due to the random electromagnetic field emitted by a partially coherent statistically homogeneous source. Due to the universality of the resonances peaks in the scattering cross-section of these particles, we have selected those frequencies in the NIR in order to make an optical force analogous to vacuum fluctuations studies

I have shown the different contributions to the force due to the Mie resonances of these magnetodielectric particles. Namely, we have addressed the electric, magnetic and interference force in the near of a partially coherent source. Firstly, at near-field distances, we have demonstrated that by a properly selection of the emission wavelength, the optical force can be attractive even far from the emission plane. This attraction is due to the evanescent modes of the angular wave spectrum. Secondly, at far-field distances, the force is constant, due to the homogeneous modes. In addition, at *Kerker conditions*, the electric and magnetic forces can be canceled between them predominating the force due to the interference of the induced dipoles.

I have emphasized that quasimonochromatic primary sources are the best candidates to observing the above mentioned rich variety of wavelength dependent forces. We have remarked that a frequency superposition to determine these forces, as usually done with thermal interactions, does not change their spatial dependence, however, it washes out their respective wavelength behavior. Conversely, we have shown configurations where one may choose the frequency, or the spectral position and bandwidth of illumination, to tailor a predominance of either the induced dipole fluctuations, (the optical analogous and generalizations of the C-P or VdW forces); or those from the primary fluctuating source emitted field, in analogy with those thermal forces out of equilibrium.

Additionally, this chapter manifests the problems of using a quasistatic formulation of optical forces. As we have emphasized, for these particles one has to use a rigorous Mie theory (far away from any quasistatic approximation). In this way, we have addressed new asymptotic power laws in the extreme near-field, namely, for the electric and magnetic forces we have shown a spatial dependence of the form $-1/z^3$ or $-1/\sigma^3$, according to whether the source coherence length σ is null or not. At these distances, the interference force shows a $-1/z^2$ or $-1/\sigma^2$ behavior.

On the other hand, for the induced dipoles (the secondary source) a new dependence on the distance to the source is found for the fields from the nanoparticle induced dipoles. This is shown to be $-1/z^{10}$ or $-1/z^7$, depending again on whether the source coherence length σ is zero or not.

Part V

OPTICAL FORCES FROM GAUSSIAN SCHELL-MODEL
SOURCES

7

OPTICAL SYSTEMS WHICH PRODUCE THE SAME OPTICAL FORCE AS A FULLY COHERENT BEAM

7.1 MOTIVATION

p to this point, all I have been talking about optical forces has been due to sources whose spectrum was homogeneous throughout their exit plane, however, there is a different kind of random source of interest, specially in the generation of partially coherent beams [3]. This pertains to sources whose spectrum depends on the position, at least in a some selected range, thus from now on we will consider this model. This concept will be introduced in the same way as the homogeneous sources in Chapter 2.

The sources whose spectral degree of coherence depends on two positions only through their difference are denoted Schell sources. The study about optical forces from Gaussian-Schell Model Sources (GSMS) was briefly started in reference [56], however, many details need to be analyzed carefully.

In the context of GSMS, E. Collet and E. Wolf discovered in 1978 that these sources can generate the same radial intensity as a fully coherent laser, or as a different GSMS. This result was named *equivalende theorem*(ET). Since we are working in the field of stochastic sources, it is natural the use of GSMS to try to demonstrate if an equivalent theorem can be derived for optical forces (and the most important concept of optical tweezers).

Firstly, I will demonstrate an equivalence theorem can also be derived for optical forces in the far-field regime, nevertheless, we will go beyond. For practical applications, the optical tweezer is the usual way to trap particles. Usually, this trapping is due to the gradient force of light, in a divergent Gaussian beam, the conservation of momentum will push the particle towards the direction of propagation. Thus, I will demonstrate that the ET in far-field is only a particular case, for free-space propagation, of a result that applies to any ABCD optical system.

7.2 INTRODUCTION

In previous chapters I have mentioned the importance of nanomanipulation, however, I have not shown an optical trap in itself, i.e., a position where the sum of the forces on the particle are zero. Usually the experimental techniques use $\mathrm{TEM_{00}}$ laser Gaussian beams in order to get a configuration of optical tweezer; nevertheless, this point does not consider the fluctuation of the fields (apart of a few works [56, 58]). Then, we will deal with optical traps generated by statistically fluctuating optical sources.

Within this framework, it is worth remarking as said above, that about thirty years ago important equivalence properties were demonstrated [146–148] between laser beams and those in the far zone of the wide variety of Gaussian-Schell model fluctuating sources (GSMS) [3, 149]. Although not realized so far, when such equivalences are generalized to ABCD optical systems, they become very relevant for optical manipulation, and showing it constitutes the main message of this chapter.

Specifically, the equivalence theorem (ET) was established [146, 147] according to which a fully coherent laser is not necessary to produce a highly directional intensity distribution, but a partially coherent source of the variety of GSMSs, fulfill this property in its far zone.

In this chapter I demonstrate that *a fluctuating GSMS produces the same optical force as a laser beam, not only in the far zone, but at any output plane of a general ABCD system and, in particular, in an optical trapping configuration.* In addition, this may be done with a much lower peak intensity. We fairly think that this opens a new door in the area of optical manipulation because, as we will show, it is not necessary to have a rather intense spatially coherent beam in order to create a potential well with an equilibrium position. On the contrary, *lower values of the peak intensity will produce the same optical force.*

7.3 ON THE CONCEPT OF STATISTICALLY FLUCTUATING SCHELL-MODEL SOURCES

Now I will introduce the concept of Gaussian Schell model sources. This important definition was introduced by Schell in 1961 in his Doctoral dissertation [150, Section 7.5]:

"The most important assumption of the following is that the fields are stationary in space and time. This means that the correlation between the signal at two points depend only on the difference in times of observation and the difference in positions, and not upon the times are positions themselves. While in an optical system the statistics may be a function of position in the image or object plane, a measurement of the correlation between the signals arriving at two points in an antenna is unlikely to change from one part of the antenna to another"
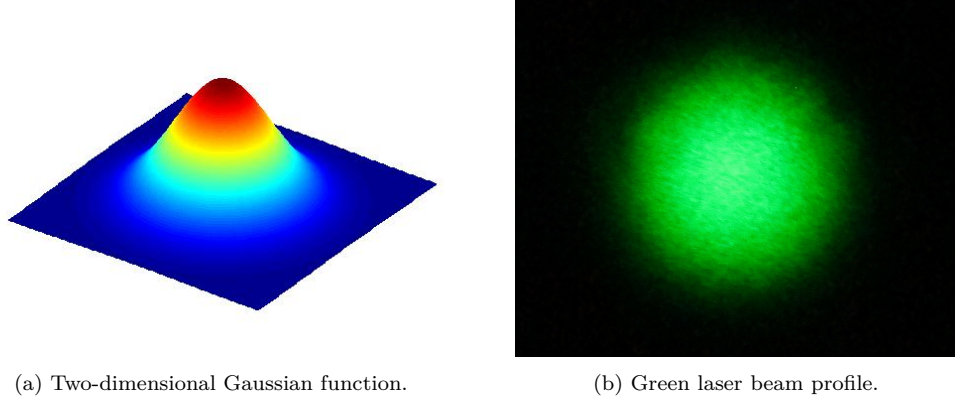
(a) Two-dimensional Gaussian function.

(b) Green laser beam profile.

Figure 7.1

In $\omega-$space, this means that the cross spectral density at the plane of the source $z = 0$ is given by

$$W^{(0)}\left(\boldsymbol{\rho}_1, \boldsymbol{\rho}_2, \omega\right) = \sqrt{S^{(0)}\left(\boldsymbol{\rho}_1, \omega\right)}\sqrt{S^{(0)}\left(\boldsymbol{\rho}_2, \omega\right)}\mu^{(0)}\left(\boldsymbol{\rho}_2 - \boldsymbol{\rho}_1, \omega\right). \tag{7.1}$$

This condition for the correlations at the source is denoted as *Schell-model sources*. Notice that for $\boldsymbol{\rho}_1 = \boldsymbol{\rho}_2 = \boldsymbol{\rho}$, the cross spectral density is $W^{(0)}\left(\boldsymbol{\rho}, \boldsymbol{\rho}, \omega\right) = S^{(0)}\left(\boldsymbol{\rho}, \omega\right)$, and the spectrum of the source is not *homogeneous* at the whole plane $z = 0$, it will depend on the position through the two-dimensional vector $\boldsymbol{\rho}$.

It was later introduced the concept of *Gaussian-Schell model sources*. For these sources, the spectral density $S^{(0)}\left(\boldsymbol{\rho}, \omega\right)$ and the spectral degree of coherence $\mu^{(0)}\left(\boldsymbol{\rho}_1, \boldsymbol{\rho}_2, \omega\right)$ of the source are both Gaussian. This situation is very common in optics, for instance, a fully coherent Gaussian beam is a type of beam whose electric field at a transverse plane is a Gaussian function (see 7.1(a) and (b)). Some lasers such as Hermite-Gaussian beams have the fundamental mode (also denoted TEM$_{00}$) with this Gaussian profile.

7.4 OPTICAL FORCES AND EQUIVALENCE THEOREM IN THE FAR-FIELD

Once we have introduced the concept of GSMSs, we are able to obtain the optical force due to this fluctuation sources. Eqs. (5.3)-(5.4) express the force in terms of the angular wave spectrum, then, we only need to calculate the term $\mathcal{A}_{jk}^{(e)}\left(k\mathbf{s}_\perp, k\mathbf{s}'_\perp\omega\right)$.

For a planar GSMS, its cross spectral density tensor $W_{ij}^{(0)}\left(\boldsymbol{\rho}_1, \boldsymbol{\rho}_2, \omega\right) = \left\langle E_i^*\left(\boldsymbol{\rho}_1\right) E_j\left(\boldsymbol{\rho}_2\right)\right\rangle$ at the plane $z = 0$ of the source is given by Eq. (7.1) [3], however, for the case of electromagnetic fields it reads

$$W_{ij}^{(0)}\left(\boldsymbol{\rho}_1, \boldsymbol{\rho}_2, \omega\right) = \sqrt{S_i^{(0)}\left(\boldsymbol{\rho}_1, \omega\right)}\sqrt{S_j^{(0)}\left(\boldsymbol{\rho}_2, \omega\right)}\mu_{ij}^{(0)}\left(\boldsymbol{\rho}_2 - \boldsymbol{\rho}_1, \omega\right). \tag{7.2}$$

In particular, for GSMS, these quantities are Gaussian, i.e.,

$$S_i\left(\boldsymbol{\rho},\omega\right) = A_i\exp[-\rho^2/(2\sigma_{s,i}^2(\omega))], \tag{7.3}$$

$$\mu_{ij}\left(\boldsymbol{\rho}_2 - \boldsymbol{\rho}_1,\omega\right) = B_{ij}\exp[-|\boldsymbol{\rho}_2 - \boldsymbol{\rho}_1|^2/(2\sigma_{g,ij}^2(\omega))]. \tag{7.4}$$

The widths $\sigma(\omega)_{s,i}$ and $\sigma(\omega)_{g,ij}$ are usually known as the spot size and the correlation or spatial coherence length of the source, respectively. Whereas in Chapters 2, 3, 5 and 6 the transverse coherence length was denoted simply by σ, from now on this parameter will be denoted as σ_g in order to avoid confusions[V.1]. Notice that these parameters cannot be chosen arbitrarily, but they have to fulfill a set of conditions [149]. In this chapter, for simplicity, we restrict ourselves to completely polarized fields, i.e., the degree of polarization is equal to 1 [20], or equivalently, the electric field only fluctuates in one direction (for example in the $x-$direction). At fixed frequency and in order to simplify the notation, in what follows we shall write $\sigma_{i,s}$ and $\sigma_{ij,g}$ without the ω dependence nor the Cartesian subindex, understanding that we are dealing with the $x-$component of the electric field (the consequences of this last assumption will be discussed in Chapter 8)

Now I turn to calculate the optical forces. In order to make a direct illustration of the ET previously derived in [146, 147], we first consider the zone far from the source. Then we shall address the general ABCD system and the optical tweezer configuration. To this end, we need the trace of the angular correlation tensor [3]:

$$\mathrm{Tr}\mathcal{A}_{ij}(k\mathbf{s}_{\perp,1}, k\mathbf{s}_{\perp,2})$$
$$\simeq \mathcal{A}_{xx}(k\mathbf{s}_{\perp,1}, k\mathbf{s}_{\perp,2}) = \frac{Ak^4}{(4\pi)^2(a^2 - b^2)}e^{-(\alpha k^2\mathbf{s}_{\perp,1}^2 + \alpha k^2\mathbf{s}_{\perp,2}^2 - 2k^2\beta\mathbf{s}_{\perp,1}\mathbf{s}_{\perp,2})}, \tag{7.5}$$

where $a = 1/(4\sigma_s^2) + 1/(2\sigma_g^2)$, $b = 1/(2\sigma_g^2)$, $\alpha = a/4(a^2 - b^2)$ and $\beta = b/4(a^2 - b^2)$. One of the most important characteristics of these GSMS sources is that the behavior of the emitted field can be beam-like. To ensure this in the far-zone, the following necessary and sufficient conditions have to be fulfilled: [3]

$$1/(2\sigma_s)^2 + 1/\sigma_g^2 \ll 2\pi^2/\lambda^2. \tag{7.6}$$

Next, in order to obtain the force in SI units, we redefine the parameter A as $A/(\varepsilon_0 c)$, where A is the peak intensity of the source in W/m^2. Substituting Eq. (7.5) into Eqs. (5.3)-(5.4), approximating $s_z \simeq 1 - 1/2s_\perp^2$, and after a long tedious but straightforward calculation, one derives the different components of the force. Then, performing the $\mathbf{s}_\perp$ and $\mathbf{s}_\perp'$ integrations, the conservative components finally are

$$F_{x,y}^{cons} = -\mathrm{Re}\alpha_e\frac{A}{c}\frac{1}{4\sigma_s^2\Delta(z)^4}e^{-\frac{\rho^2}{2(\sigma_s\Delta(z))^2}}(x,y) \tag{7.7}$$

and

$$F_z^{cons} = \mathrm{Re}\alpha_e\frac{Az}{4k^2\sigma_s^4\delta^2\Delta(z)^6 c}\left(\rho^2 - 2\sigma_s^2\Delta(z)^2\right)e^{-\frac{\rho^2}{2(\sigma_s\Delta(z))^2}}. \tag{7.8}$$

On the other hand the non-conservative forces read

$$F_{x,y}^{nc} = \mathrm{Im}\alpha_e\frac{A}{c}\frac{z}{2k\sigma_s^2\delta^2\Delta(z)^4}e^{-\frac{\rho^2}{2(\sigma_s\Delta(z))^2}}(x,y) \tag{7.9}$$

V.1 In fact, as we commented in Section 2.3 we have been considering that $\sigma_s \gg \sigma_g$
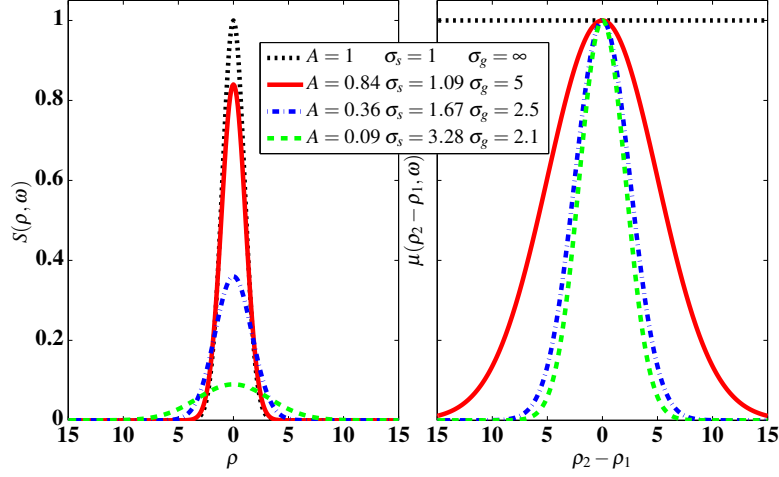
Figure 7.2: Spectral density (left) and spectral degree of coherence (right) at $z = 0$ for different source parameters which generate the same radiant intensity in the far-zone.

and

$$F_z^{nc} = \mathrm{Im}\alpha_e \frac{A}{2k^7\sigma_s^4\delta^4\Delta(z)^6 c}\left[\frac{1}{2}k^8\sigma_s^4\delta^4\Delta(z)^4 - \alpha k^6\sigma_s^2\delta^2\Delta(z)^2 \right.$$
$$\left. + \left(\frac{k^4}{2^4}\delta^4 - \frac{k^2}{4}z^2\right)k^2\rho^2\right]e^{-\frac{\rho^2}{2(\sigma_s\Delta(z))^2}}, \tag{7.10}$$

where $1/\delta^2 = 1/(2\sigma_s)^2 + 1/\sigma_g^2$ and $\Delta(z) = [1 + (z/k\sigma_s\delta)^2]^{1/2}$. Eqs. (7.7)-(7.10) express the force exerted on a dipolar particle in the far zone by the field emitted from a GSMS in any state of coherence. The ET [147, 148] establishes that any GSMS will generate in the far zone the same radiant intensity $J(\theta) = r^2\mathrm{Tr}W_{ij}(\mathbf{r},\mathbf{r},\omega)$, $(\theta = \rho/z)$, as a laser whose spectral density at the plane $z = 0$ is $S_l(\boldsymbol{\rho},\omega) = A_l\exp[-\rho^2/(2\sigma_l)]$, if the following conditions are fulfilled:

$$\frac{1}{\sigma_g^2} + \frac{1}{(2\sigma_s)^2} = \frac{1}{(2\sigma_l)^2}, \quad A = \left(\frac{\sigma_l}{\sigma_s}\right)^2 A_l. \tag{7.11}$$

Fig. 7.2 shows the spectral density and the spectral degree of coherence for the same parameters as in Ref. [147]. Any of these source configurations produce exactly the same radiant intensity.

When the field is beam-like, $kz \to \infty$ and the following approximation is made in $\Delta(z)$ (cf. Eq. (7.10) and below): $\Delta(z) \simeq z/(k\sigma_s\delta)$ [146]. On the other hand, and in order to perform the force calculations, we consider the same dipolar latex-like particle as in Chapter 4, i.e., $\mathrm{Re}\alpha_e = 4593\mathrm{nm}^3 \gg \mathrm{Im}\alpha_e = 17\mathrm{nm}^3$. We have chosen this particle because we are focused on the statistically properties of the source instead of the scattering properties, nevertheless, *it should be stressed that much larger particles would lead to similar results providing that they may be considered as dipolar* (see Chapter 6 and [59, 61]) .

Next we calculate the optical forces in this regime. Fig. 7.3 shows the different contributions (conservative and non-conservative) for the same parameters as in Fig. 7.2. As seen on comparing Figs. 7.2 and 7.3, a source with e.g. a small coherence length $\sigma_g = 2.1$ and peak intensity as low as $A = 0.09$ provides the same far zone force as a fully coherent one with a much larger power $A = 1$ providing the spot size at the partially coherent source $\sigma_s = 3.28$ is larger than the one
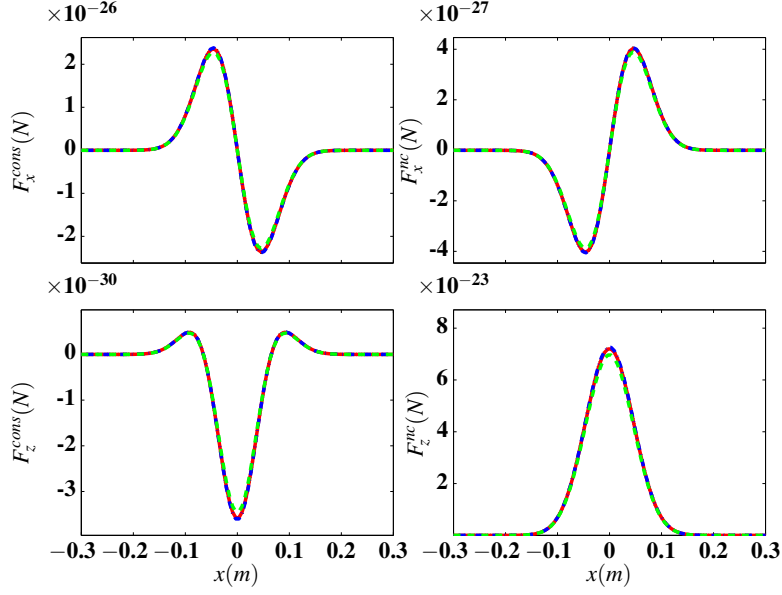
Figure 7.3: (Conservative (first column) and non-conservative (second column) forces in the far zone for the same source parameters as in Fig. 7.2, with A in $mW/\mu m^2$ and σ_g and σ_s in mm.

$\sigma_s = 1$ of the fully coherent source. We see that all force plots coincide with each other, i.e. one does not need a globally spatially coherent source, like a laser beam, as the only light source to create a given force distribution. Any partially coherent Gaussian-Schell model source with appropriate spot size and coherence length also does it. This constitutes one of the main results of this chapter. As we shall now see, the same applies to the potential well of an optical trap.

It should be noticed that given the trade-off between σ_g and σ_s contained in the parameter $4a$, [cf. below Eq.(7.5)], there are infinite GSMS that yield the same radiant intensity [3], providing they all lead to the same $4a$ or σ_l. Thus, the same conclusion may be derived for the optical force induced by their emitted wavefield. On the other hand, it worth remarking that a peak intensity A and width σ_s in the spectral density yields an integrated value of this latter magnitude in the source plane: $A\sigma_S^2/2\pi$, which by the Parseval theorem , of Fourier transforms is kept in the far-zone. Therefore, a decrease of A while controlling σ_s, may also lead to lower values of the total power while maintaining the essential characteristics of the force distribution.

7.5 OPTICAL FORCES AND EQUIVALENCE THEOREM FOR OPTICAL TWEEZERS

At this point, it is natural to ask whether the GSMS fields would trap a particle like a laser beam does. In biophysical experiments, where there is sample damage produced by high values of the peak intensity of the incident beam, this issue acquires vital importance, *the equivalence of low peak intensity partially coherent fluctuating beams and a high power laser beam, (or in general between different GSMS wavefields)*, in regards to the depth and width of the potential well that forms the photonic trap, constitutes a new principle for optical nanomanipulation. On
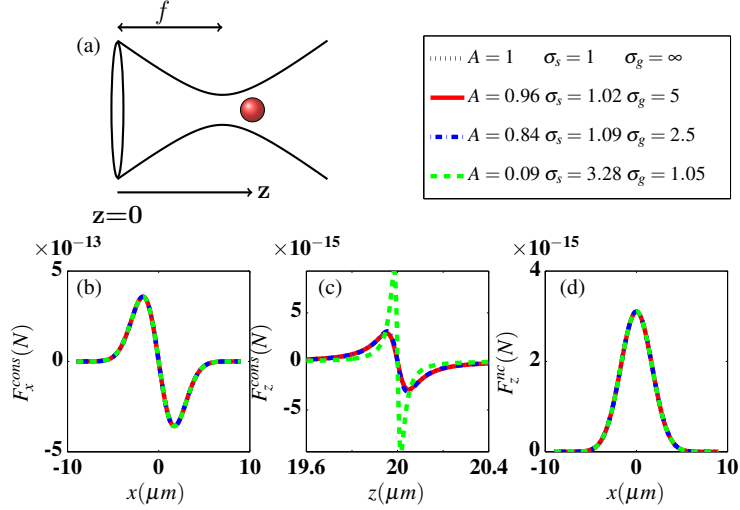
Figure 7.4: (a) Scheme of the optical tweezer focusing for the equivalence theorem. (b) F_x^{cons}, (c) F_z^{cons}, (d) F_z^{nc}. The focus distance is $z = f = 2cm$, and the units of the parameters are A in $W/\mu m^2$ and σ_g and σ_s in mm.

adequately selecting the source parameters, one can minimize the optical peak intensity (see the lowest row parameters of Fig. 7.2). As a matter of fact, this peak power can be reduced over one order of magnitude without varying the effectiveness of the force. This is observed in the far zone (cf. Fig. 7.3) and, as shown next, equally occurs in the focusing configuration of an optical tweezer.

Therefore, although the far zone addressed up till now does not constitute an optical trap in itself, (in fact, the condition $1 \ll (z/k\sigma_s\delta)^2$ above employed for $\Delta(z)$ is contrary to that corresponding to a high numerical aperture (NA): $(z/k\sigma_s\delta)^2 \ll 1$ required for an optical tweezer [42]), we now put forward an analogous ET for the focusing geometry of an optical trap. This is based on a *a more general equivalence theorem that we establish for any ABCD system*.

For the wavefield from a GSMS, propagating in an ABCD system in air, the width of the output intensity w_2 is written in terms of the input width w_1 of the source [151] as

$$w_2^2 = w_1^2 \left[\left(A + \frac{B}{R_1} \right)^2 + \left(\frac{\lambda}{\pi w_1 w_c} \right)^2 B^2 \right]. \tag{7.12}$$

R_1 being the curvature radius at the input plane and $1/w_c^2 = 1/w_1^2 + 1/\sigma_g^2$.

On the other hand, for the laser beam, $(w_c \to w_l)$, one has

$$w_{2,l}^2 = w_{1,l}^2 \left[\left(A + \frac{B}{R_1} \right)^2 + \left(\frac{\lambda}{\pi w_{1,l}^2} \right)^2 B^2 \right], \tag{7.13}$$

where the subscript l refers to the laser. Analogously, the output intensities of the GSMS, I_2, and of the laser, $I_{2,l}$, fulfill:

$$I_2 = I_1 \left(\frac{w_1}{w_2} \right)^2, \quad I_{2,l} = I_{1,l} \left(\frac{w_{1,l}}{w_{2,l}} \right)^2. \tag{7.14}$$

109

I_1, and $I_{1,l}$ being the input intensities at $\boldsymbol{\rho} = 0$ corresponding to the GSMS and the laser, respectively.

For the optical tweezer configuration the potential well is created on focusing the emitted light through a thin lens of high NA, [see Fig. 7.4(a)]. Also, $A = -(z - f)/f$, $B = z$, $C = -1/f$ and $D = 1$. Assuming that the GSMS is placed at $z = 0$, then w_1 becomes σ_s, $w_{1,l} = \sigma_l$ and $R_1 \to \infty$. Therefore the conditions: $w_2 = w_{2,l}$ and $I_2 = I_{2,l}$ at the focus: $z = f$, lead to

$$\frac{1}{\sigma_l^2} = \frac{1}{\sigma_s^2} + \frac{1}{\sigma_g^2}, \ A = \left(\frac{\sigma_l}{\sigma_s}\right)^2 A_l. \tag{7.15}$$

Now the parameter $\Delta(z)$ acquires the form: $\Delta(z) = \left[\left(\frac{f-z}{f}\right)^2 + \left(\frac{\lambda z}{\pi \sigma_s w_c}\right)^2\right]$, and $1/w_c^2 = 1/\sigma_s^2 + 1/\sigma_g^2$.

Figs. 7.4(b)-(d) show the forces on the particle at $z = f = 2cm$ [56]. Due to we have imposed that the conditions are fulfilled for $z = f$ in Fig. 7.4(c) the forces are equal at this position. Notices also that in Fig. 7.4(c) is the most incoherent case (dashed line) the case which give us a larger value of F_z^{cons} This confirms that one gets the same force as a laser in the focus for different values of σ_g, σ_s and amplitude A. Again the latter allowing to be reduced over one order of magnitude with respect to that of the laser beam.

7.6 CONCLUSIONS

In summary, I have introduced the concept of GSMS and the effects of using these type of forces for optical manipulation. In particular, this chapter demonstrates the importance of the selection of the parameters which define a GSMS. We have shown that either in the far zone or in the focus of an optical tweezer configuration, a GSMS can produce a photonic force equal to that exerted by a fully coherent Gaussian laser beam.

I remark the fact that even decreasing the peak of the intensity at the source plane in almost two-orders of magnitude, we get exactly the same optical force.

8

COHERENT-MODE REPRESENTATION OF OPTICAL FORCES: OPTICAL BINDING OF PHOTONIC MOLECULES.

8.1 MOTIVATION

hroughout all the previous chapters I have always tried to do all calculations in an analytical way, so that one can see and understand the results just by looking at the equations. This is very nice, but the reality is that it is very difficult to know how are the electromagnetic fields in complex structures. In this case, the calculus of the electromagnetic fields is a hard task, which has to be performed trough computational codes. Notice that if we want to calculate (for instance), the optical force at subwalength distances, we have to use Eqs. (5.3) and (5.4), i.e., we have to resolve 4-integrals whose solutions, in general, will be very complicate to obtain.

Nowadays, the propagation of electromagnetic fields through different situations are usually resolved through numerical methods. Therefore, the challenge will be to try to implement the concept of partially coherent light by a code I choose employing finite elements. This type of programs are conceived to resolve Maxwell's equations under different circumstances, however, they do not include the concept of random wave-field (as far as I know), indeed, they work with deterministic fields inside a calculation window, and we have to control the boundary conditions in this window.

Our main problem is how to include in the the code that the field to propagate and interact with the desired particle is random. Notice that so far, in all previous chapters, we have not shown an image of any stochastic field spatial distribution. This is because in analytic calculations we do not know how the spatial structure of this field is, what we know are statistical momenta, like correlation functions, power spectra, or mean values at a given source. Thus, in order to resolve this problem, we implement the coherent mode representation (CMR) of the covariance that amounts to the Mercer decomposition into eigenfunctions of a stochastic process [152].

This procedure to write the cross-spetral density function has been addressed before (see references of this chapter), but its application to optical forces is a new tool. The method is based on the possibility to write the cross spectral density as a superposition of coherent states. These coherent states are well defined for a one-dimensional Gaussian Schell model source, which is the case of interest for us.

Once I have developed this numerical method, I will put it into practice for a study of the optical binding between particles.

8.2 INTRODUCTION

Chapter 6 studied the interaction between a half-space and a resonant Mie particle excited from a statistically homogeneous source. Then, in Chapter 7 I considered a new approach, the case of Gaussian Schell Model Sources (GSMSs) in optical systems where the evanescent modes did not play any role. This chapter goes beyond: I will analyze in detail the behavior of random wavefields in the near-field of a GSMS, namely, the interaction with semiconductor particles.

Firstly, I will deal with one of the main ideas of this thesis: at near-field distances, the fluctuations of the electromagnetic fields along the propagation direction are not negligible. In particular, I will study the contribution of the different Cartesian components of the trace of the angular correlation tensor to the force, demonstrating that I have to use a full electromagnetic theory in order to calculate the optical forces.

Secondly, I will present a new theory of optical forces based on the coherent mode representation (CMR) of a partially coherent source. This representation is based on the works of E. Wolf (see Refs. [153, 154]) and establishes that the cross spectral density of a system of any state of coherence may be expressed as the sum of contributions from spatially completely coherent elementary sources, and so are its consequences for the electromagnetic force.

I shall use this CMR of optical forces not only on single particles, but also for studying radiation-induced forces between objects, usually referred to as *optical binding* [51, 155]. In this connection, recent work deals with interaction between two dipoles in presence of random wavefields [156]. Specifically, I shall address the forces due to one-dimensional GSMS, acting between two high refractive index dielectric cylinders. I will exploit the morphology dependent resonances (MDR) of these objects to form different types of bonds between them. It will also be shown how the spatial coherence of the source affects the attraction or repulsion of these bodies. Prior to this, and in order to play with the MDRs of the cylinders, I will study the scattering properties of non-absorbing cylinders. As mentioned in Chapter 6, these systems have provoked much interest because they show magnetic properties in dielectric structures [60, 137, 157, 158].

In this section I deal with the ensemble-averaged force experienced by a small non-resonant particle. Chapter 5 (specifically Section 5.3) showed that this force is fully determined if we know the trace of the angular cross-correlation tensor, i.e., $\mathcal{A}_{jk}^{(e)}(k\mathbf{s}_{\perp}, k\mathbf{s}'_{\perp}\omega)$.

Now we address the case of a planar GSMS. This is characterized by a cross-spectral density tensor $W_{ij}^{(0)}(\boldsymbol{\rho}_1, \boldsymbol{\rho}_2, \omega) = \langle E_i^*(\boldsymbol{\rho}_1) E_j(\boldsymbol{\rho}_2)\rangle$ at the plane $z = 0$ given by Eq. (7.2), where the spectral density and the spectral degree of coherence of the source are both Gaussian (cf. Eq. (7.4)). Again, the parameters $\sigma_{s,i}$ and $\sigma_{g,ij}$ are the *spot size* and the *correlation - or spatial coherence - length*, respectively.

In this section, for simplicity, the electric field will be assumed to fluctuate in the X-direction, so that the factor B in Eq. (7.4) is $B = 1$. It is worth remarking that fluctuations along OZ, i.e. in the direction of propagation, are negligible in the far-field (this approach was done in Chapter 7); nevertheless as we shall show, in the near-field they can be relevant and even larger that the rest of fluctuations. In what follows we denote the parameters $\sigma_{i,s}$ and $\sigma_{ij,g}$ without the Cartesian subindex, understanding that they refer to the X-component of the electric vector.

8.3.1 *Near Field Forces*

Let us address the optical forces of fields from GSMSs on a small sphere, at distances from the source shorter than the wavelength. Whereas at larger distances, the trace of the angular correlation tensor can be approximated as $\text{Tr}\mathcal{A}_{ij} \simeq \mathcal{A}_{xx}$ (cf. Eq. (7.5)), in the near-field, where the resolution of the system is beyond the diffraction limit: $\lambda/2$, the fluctuations on the $Z-$direction are as important as the rest of them [11]. It is well-known that this conveys a non-straightforward 3D generalization in the definition of the degree of polarization $P(\mathbf{r}, \omega)$ [25, 26, 159, II].

Therefore, and in order to quantify the importance of these fluctuations we shall write the third component of the angular component of the electromagnetic field $e_z(ks_x, \omega)$ (cf. Eq. (5.2)) in terms of s_x, i.e., $e_z(k\mathbf{s}_{\perp}, \omega) = -e_x(k\mathbf{s}_{\perp}, \omega)s_x/s_z$, with the help of the divergence law: $\mathbf{e}(k\mathbf{s}_{\perp}) \cdot \mathbf{s} = 0$ (see Section 1.5). Hence, $\text{Tr}\mathcal{A}_{ij} = \mathcal{A}_{xx} + \mathcal{A}_{zz}$. The forces are calculated from Eqs. (5.3)-(5.4) on writing $(s_x, s_y) = s(\cos\theta, \sin\theta)$. The component $\mathcal{A}_{xx}$ is addressed in Eq. (7.5) and the term $\mathcal{A}_{zz}$ is calculated from $\langle e_z^*(k\mathbf{s}_{\perp}, \omega)e_z(k\mathbf{s}_{\perp}\prime, \omega)\rangle$, i.e.,

$$\langle e_z^*(k\mathbf{s}_{\perp}, \omega)e_z(k\mathbf{s}_{\perp}\prime, \omega)\rangle = \frac{\langle e_x^*(k\mathbf{s}_{\perp}, \omega)e_x(k\mathbf{s}'_{\perp}, \omega)\rangle \mathbf{s}_{\perp}^* \mathbf{s}'_{\perp}}{s_z^* s'_z} = \frac{\mathcal{A}_{xx}(k\mathbf{s}_{\perp}, k\mathbf{s}'_{\perp}, \omega)\mathbf{s}_{\perp}^* \mathbf{s}'_{\perp}}{s_z^* s'_z}. \quad (8.1)$$

The azimuthal integrals are performed analytically, whereas the radial one is numerically done for $\sigma_g \gg \sigma_s$, this corresponds to a globally spatially coherent source. In this limit, the four integrals of the calculation can be expressed as a product of two integrals. We shall consider the same small spherical particle as in Chapter 4, i.e., the polarizability is calculated from Eq. (4.79) with a radius $r_0 = 25$nm and $\varepsilon_p = 2.25$.
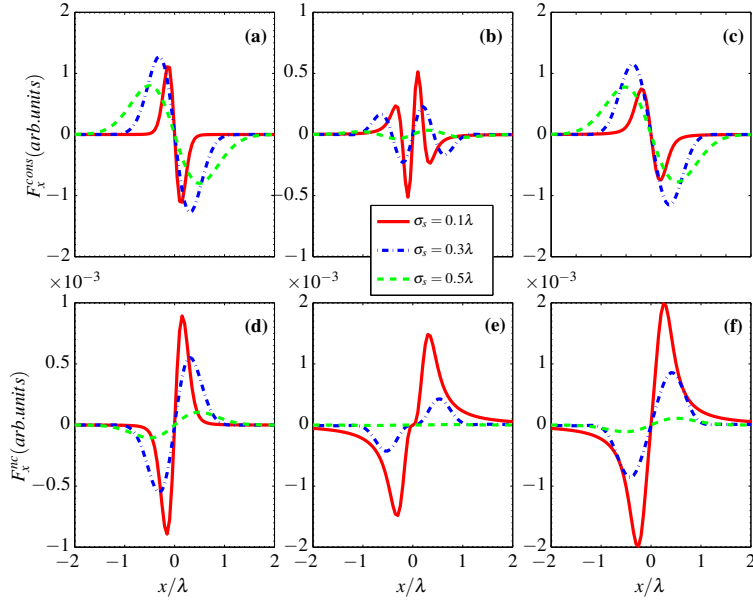
Figure 8.1: Mean forces. Conservative component F_x^{cons}, (first row), and non-conservative component F_x^{nc}, (second row), of F_x due to the contribution of e_x, (first column), and of e_z, (second column), versus the lateral displacement x of the sphere, (in wavelength units), for different spot sizes σ_s. The third column displays the sum of the first and second columns. The distance of the particle to the source is $z = 0.1\lambda$ and the radius and the permittivity of the particle are $r_0 = 25$nm and $\varepsilon_p = 2.25$ respectively.

Fig. 8.1 shows the conservative force, (first row), and the non-conservative force, (second row), in the $X-$direction at a distance $z = 0.1\lambda$ from the source. The contributions of the angular amplitudes e_x, (first column), and e_z, (second column), are separated. The third column is the sum of both forces. We see that all contributions of the components of $\mathbf{e}\,(k\mathbf{s}_\perp, \omega)$ to F_x^{cons} are of the same order, [compare the magnitude in Figs. 8.1(a) and 8.1(b) or 8.1(d) and 8.1(e)]; thus the fluctuating e_z-s in the propagation direction are not negligible like in the far-field, namely, $\mathrm{Tr}\mathcal{A}_{ij} \not\simeq \mathcal{A}_{xx}$. Fig. 8.2 shows the same as Fig. 8.1 but for the forces along the $Z-$axis. In this case we have the same effect as in the previous figure, although F_z^{nc} is larger for the contribution of the $x-$fluctuations, [compare the magnitudes in Figs. 8.2 (d)-(e)]. By adding the conservative and non-conservative components of the force, i.e. Fig. 8.1(c) and Fig. 8.1(f), [and analogously for Fig. 8.2], we see that the total force is only contributed by the gradient force, i.e., $F_x \simeq F_x^{cons}$ and $F_z \simeq F_z^{cons}$. This fact is due to the distance to the source being subwavelength.

These results also show that, in general, as σ_s increases, the magnitude of the forces decreases, contrary to far-field results of previous studies as well as to other configurations where the evanescent components do not play any role [56, 58, VI]. Notice that for $\sigma_s = 0.1\lambda$ the beam condition: $1/(2\sigma_s)^2 + 1/\sigma_g^2 \ll 2\pi^2/\lambda^2$ (cf. [3]) is not fulfilled, and it is precisely this value σ_s that for which we obtain the largest magnitude of the force. Thus *the maximum force produced by a GSMS in the near-field corresponds to a minimum force in the far-field.*
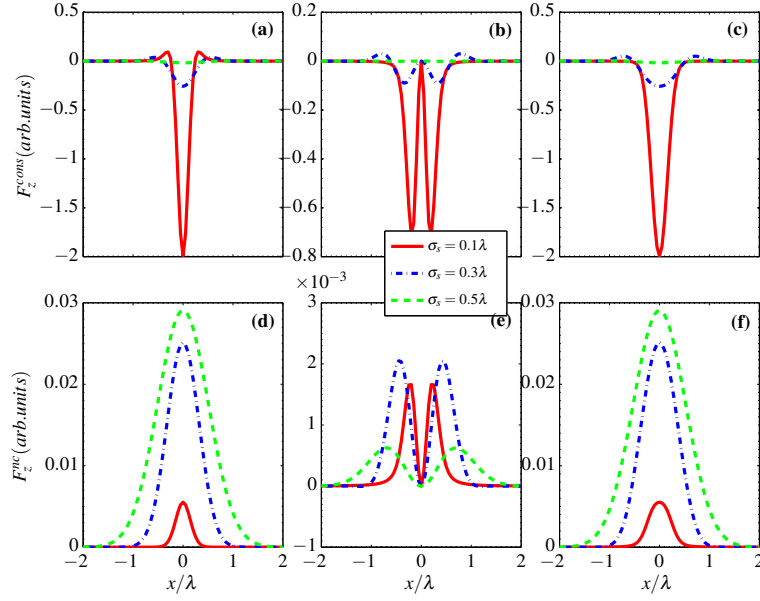
Figure 8.2: The same as in Fig. 8.1 for F_z

It should be pointed out that force calculations from an arbitrary partially coherent source are difficult without approximations, and are much more lengthy than those considered next. Electromagnetic fields in complex structures are usually computed by finite element methods (FEM) or by finite difference time domain procedures (FDTD). In Section 8.4 and Section 8.5 we develop a robust method in order to evaluate the cross spectral density tensor $W_{ij}(\mathbf{r}_1, \mathbf{r}_2, \omega)$, the degree of polarization $P(\mathbf{r}, \omega)$, and the optical forces $F(\mathbf{r}, \omega)$ in whatever set of particles. A test of this theoretical construction is shown in Appendix D, which confirms the results of Fig. 8.1 and Fig. 8.2.

8.4 COHERENT MODE REPRESENTATION

The coherent mode representation (CMR) establishes that the coherence tensor of a stationary optical field of any state of coherence may be represented as a superposition of coherent modes [154, 162], i.e.,

$$
\begin{aligned}
W_{ij}(\mathbf{r}_1, \mathbf{r}_2, \omega) &= \langle E_i^*(\mathbf{r}_1, \omega) E_j(\mathbf{r}_2, \omega) \rangle \\
&= \sum_{q=0}^{N} \lambda_q(\omega) \phi_{i,q}^*(\mathbf{r}_1, \omega) \phi_{j,q}(\mathbf{r}_2, \omega),
\end{aligned}
\tag{8.2}
$$

where $\lambda_q(\omega)$ are the eigenvalues, N is an arbitrary natural number and $\phi_{q,i}$ denote the eigenfunctions which fulfill the equation [154]:

$$
\int_D \phi_{i,q}(\mathbf{r}_1, \omega) W_{ij}(\mathbf{r}_1, \mathbf{r}_2, \omega) \, \mathrm{d}^3\mathbf{r}_1 = \lambda_q(\omega) \phi_{i,q}(\mathbf{r}_2, \omega).
\tag{8.3}
$$

115

Let us consider an statistical ensemble of electromagnetic fields $\{\mathbf{E}(\mathbf{r}, \omega)\}$ where each realization can be expressed as a sum of individual eigenfunctions:

$$E_i(\mathbf{r}, \omega) = \sum_q a_q(\omega) \phi_{i,q}(\mathbf{r}, \omega), \tag{8.4}$$

a_q being a random coefficient. Substituting Eq. (8.4) into Eq. (8.2) we see that

$$
\begin{aligned}
\langle a_q^*(\omega) a_{q'}(\omega) \rangle &= \lambda_q(\omega) \delta_{qq'}, \\
a_q(\omega) &= \lambda_q^{1/2}(\omega) e^{i\alpha_q},
\end{aligned} \tag{8.5}
$$

where α_q is a real random variable uniformly distributed in the interval $0 \leq \alpha_q < 2\pi$.

8.4.1 *Coherent Mode representation of Optical forces*

We can now write the ensemble-averaged force as a sum of coherent modes by using its expression from the momentum conservation law in terms of the Maxwell stress tensor (MST) [43, 44, 163]:

$$
\begin{aligned}
\langle \mathbf{F}(\mathbf{r}, \omega) \rangle &= \sum_q \iint_\Sigma \frac{\varepsilon}{2} \mathrm{Re}\left\{ \langle (\mathbf{E}_q \cdot \mathbf{n}) \mathbf{E}_q^* \rangle \right\} - \frac{\varepsilon}{4} \langle \mathbf{E}_q^* \cdot \mathbf{E}_q \rangle \mathbf{n} \\
&\quad + \frac{\mu}{2} \mathrm{Re}\left\{ \langle (\mathbf{H}_q \cdot \mathbf{n}) \mathbf{H}_q^* \rangle \right\} - \frac{\mu}{4} \langle \mathbf{H}_q^* \cdot \mathbf{H}_q \rangle \mathbf{n} \, ds.
\end{aligned} \tag{8.6}
$$

Σ is a surface enclosing the object experiencing the force. $\mathbf{n}$ represents the outward unit normal. In our 2D calculations Σ will be a closed line. $\mathbf{E}_q$, $\mathbf{H}_q$ and $\mathbf{E}^*_q$, $\mathbf{H}^*_q$ are the q-modes and their complex conjugates. For brevity we have omitted the space and frequency dependence of the fields. ε and μ are the permittivity and permeability of the surrounding medium embedding the particles, which in this work will be assumed to be vacuum. The sum of the partial forces from each propagated eigenmode renders the resulting force exerted on the particles by the total fields $\mathbf{E}$ and $\mathbf{H}$. Notice that Eq. (8.6) applies to any configuration, regardless of whether the source is spatially coherent ($N = 0$) or partially coherent ($N > 0$).

For dipolar particles the averaged total force can now be expressed in terms of the coherent q-modes:

$$
\begin{aligned}
\langle F_i(\mathbf{r}, \omega) \rangle &= \frac{1}{2} \sum_{q=0}^N \mathrm{Re}\left\{ \alpha_e E_{j,q} \partial_i E_{j,q}^* \right\} \\
&= \frac{1}{2} \sum_{q=0}^N \lambda_q \mathrm{Re}\left\{ \alpha_e \phi_{j,q} \partial_i \phi_{j,q}^* \right\}.
\end{aligned} \tag{8.7}
$$

8.5 CHARACTERIZATION OF THE FIELD EMITTED BY THE GSMS

Using the CMR, we shall follow the procedure put forward in [164] to characterize the fluctuating field from a GSMS. Then the problem is 2D so that plane of work will be XY. y is the direction

of propagation and the field fluctuates along $0Z$ (see Fig. 8.10). The GSMS plane is $y = 0$, thus the cross-spectral density function will be:

$$W_{zz}^{(0)}(x_1, x_2, \omega) = Ae^{-\frac{x_1^2 + x_2^2}{4\sigma_s^2}} e^{-\frac{(x_1 - x_2)^2}{2\sigma_g^2}}. \tag{8.8}$$

For this case, the eigenfunctions and the eigenvalues have been determined previously [3, 165]:

$$\phi_q(x, \omega) = \left(\frac{2c}{\pi}\right)^{1/4} \frac{1}{(2^q q!)^{1/2}} H_q\left(x\sqrt{2c}\right) e^{-cx^2}, \tag{8.9}$$

$$\lambda_q(\omega) = \left(\frac{\pi}{a + b + c}\right)^{1/2} \left(\frac{b}{a + b + c}\right)^q, \tag{8.10}$$

where $H_q(x)$ is the Hermite polynomial of order q, and

$$a = \frac{1}{4\sigma_s^2}, \quad b = \frac{1}{2\sigma_g}, \quad c = \left(a^2 + 2ab\right)^{1/2}. \tag{8.11}$$

The angular amplitude $\Phi(ks_x)$ of the eigenfunction $\phi_q(x, \omega)$, is calculated by inverse Fourier transform of Eq. (8.9), (see [164]):

$$
\begin{aligned}
\Phi(ks_x) &= \frac{1}{2\pi} \int_{-\infty}^{\infty} \phi(x, \omega) e^{-iks_x x} \mathrm{d}x \\
&= \frac{(-i)^q}{2\pi} \left(\frac{2\pi}{c}\right)^{1/4} \frac{1}{(2^q q!)^{1/2}} e^{-\frac{k^2 s_x^2}{4c}} H_q\left(\frac{ks_x}{\sqrt{2c}}\right).
\end{aligned}
\tag{8.12}
$$

8.6 EFFICIENCY FACTORS AND POLARIZABILITY OF AN INFINITELY CYLINDER

From now on, I will work with two-dimensional structures. Then, let us first address, in an analogous way to references [60, 115, 166], the efficiency factors and the polarizability of an isolated infinitely long dielectric cylinder for s and p-polarization. This formulation will be valid in the rest of this chapter in order to localize the resonant positions.
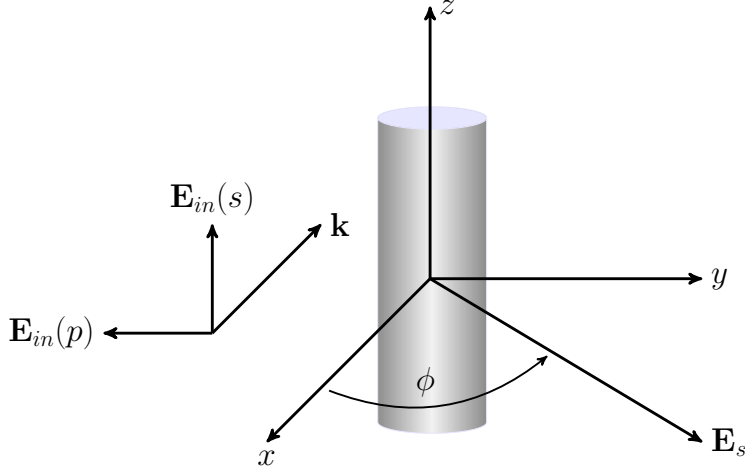
8.6.1 *S-polarization (TE)*

Since we work with two-dimensional structures such as cylinders, we will make an study of the scattered electromagnetic field. To this end, let us consider an incident electric field impinging in a long dielectric cylinder being the electric field parallel to the cylinder axis

$$\mathbf{E}_{in}(\mathbf{r}) = E_0 \hat{\mathbf{e}}_z e^{i\mathbf{kr}}. \tag{8.13}$$

Under this plane wave illumination, from a rigorous scattering Mie theory, the scattered electric field is (see Eq. (8.34) of [115])

$$\mathbf{E}_s \sim E_0 e^{i3\pi/4} \sqrt{\frac{2}{\pi kr}} e^{ikr} \left(b_0 + 2\sum_{n=1}^{\infty} b_n \cos(n(\pi - \phi))\right) \hat{\mathbf{e}}_z \tag{8.14}$$

Figure 8.3: Cylinder illuminated under s or p-polarization.

where the angle ϕ is defined in Fig. (8.3) and in this case, the Mie coefficient b_n [V.2] is defined as [115]

$$b_n = \frac{J_n\left(y\right) J_n'\left(x\right) - m J_n'\left(y\right) J_n\left(x\right)}{J_n\left(y\right) H_n'\left(x\right) - m J_n'\left(y\right) H_n'\left(x\right)}, \tag{8.15}$$

being $m = n_p/n_h$, $y = mx$, $x = kr_0$ and $k = n_h 2\pi/\lambda$. $n_p = \sqrt{\varepsilon}$ and n_h refer to the refractive index of the particle (cylinder) and the host medium respectively and r_0 is the radius of the cylinder. J_n and H_n are the Bessel and Hankel functions of the first kind respectively, and the prime denotes the derivative.

Now let us write the scattered field using the Green's formalism. If we assume that our cylinder has a polarization and magnetization densities $\mathbf{P}\left(\mathbf{r},\omega\right)$ and $\mathbf{M}\left(\mathbf{r},\omega\right)$ respectively, and the scattered field is due to these induced densities, we have

$$\mathbf{E}_s = \mu_0 \omega^2 \int_C \overset{\leftrightarrow}{G}^{EP}\left(\boldsymbol{\rho}, \boldsymbol{\rho}', \omega\right) \mathbf{P}\left(\boldsymbol{\rho}', \omega\right) \mathrm{d}^2 r' - \int_C \overset{\leftrightarrow}{G}^{EM}\left(\boldsymbol{\rho}, \boldsymbol{\rho}', \omega\right) \mathbf{M}\left(\boldsymbol{\rho}', \omega\right) \mathrm{d}^2 r', \tag{8.16}$$

where C is the circular cylinder cross section and $\boldsymbol{\rho}$, $\boldsymbol{\rho}'$ are two-dimensional vectors which denote the observation point and the source point, respectively. For a single electric p and magnetic m moment (per unit length), the previous equation reduces to:

$$\mathbf{E}_s = \mu_0 \omega^2 \overset{\leftrightarrow}{G}^{EP}\left(\boldsymbol{\rho}, \boldsymbol{\rho}_0, \omega\right) \mathbf{p}\left(\boldsymbol{\rho}_0, \omega\right) - \overset{\leftrightarrow}{G}^{EM}\left(\boldsymbol{\rho}, \boldsymbol{\rho}_0, \omega\right) \mathbf{m}\left(\boldsymbol{\rho}_0, \omega\right). \tag{8.17}$$

In our case, $\overset{\leftrightarrow}{G}^{EP}\left(\boldsymbol{\rho}, \boldsymbol{\rho}_0, \omega\right)$ and $\overset{\leftrightarrow}{G}^{EM}\left(\boldsymbol{\rho}, \boldsymbol{\rho}_0, \omega\right)$ are the well-known dyadic Green's functions in vacuum [10, 43]:

$$\overset{\leftrightarrow}{G_0}^{EP}\left(\boldsymbol{\rho}, \boldsymbol{\rho}_0, \omega\right) = \left(\overset{\leftrightarrow}{I} + \frac{1}{k^2}\nabla\nabla\right) G_0\left(\boldsymbol{\rho}, \boldsymbol{\rho}_0, \omega\right), \tag{8.18}$$

$$\overset{\leftrightarrow}{G_0}^{EM}\left(\boldsymbol{\rho}, \boldsymbol{\rho}_0, \omega\right) = \nabla G_0\left(\boldsymbol{\rho}, \boldsymbol{\rho}_0, \omega\right) \times \overset{\leftrightarrow}{I}, \tag{8.19}$$

being $G_0\left(\boldsymbol{\rho}, \boldsymbol{\rho}_0, \omega\right)$ the scalar Green's function

$$G_0\left(\boldsymbol{\rho}, \boldsymbol{\rho}_0, \omega\right) = \frac{i}{4} H_0\left(kr\right), \tag{8.20}$$

V.2 This Mie coefficient is not the same as in Eq. 6.7

with $r = |\boldsymbol{\rho} - \boldsymbol{\rho}_0|$. For simplicity, let us consider the electric dipole (the magnetic one is similar). For arbitrary polarization, the dyadic product $\overset{\leftrightarrow}{G}^{EP}(\boldsymbol{\rho}, \boldsymbol{\rho}_0, \omega) \, \mathbf{p}(\boldsymbol{\rho}_0, \omega)$ is

$$\overset{\leftrightarrow}{G}_0^{EP}(\boldsymbol{\rho}, \boldsymbol{\rho}_0, \omega) \, \mathbf{p} = \frac{i}{4} H_0(kr)(\hat{\boldsymbol{\rho}} \times \mathbf{p}) \times \hat{\boldsymbol{\rho}} + \frac{i}{kR} H_1(kr)(2\hat{\boldsymbol{\rho}}(\hat{\boldsymbol{\rho}} \cdot \mathbf{p}) - \mathbf{p}), \tag{8.21}$$

and for s-polarization ($\mathbf{p} = p\hat{\mathbf{e}}_z$)

$$\overset{\leftrightarrow}{G}_0^{EP}(\boldsymbol{\rho}, \boldsymbol{\rho}_0, \omega) \, \mathbf{p}_z = \frac{i}{4} H_0(kr) \, p\hat{\mathbf{e}}_z. \tag{8.22}$$

Substituting this last equation in the first term of Eq. (8.17), the scattered field due to a single electric dipole is

$$\mathbf{E}_s = \frac{ik^2}{4\varepsilon_0} H_0(kr) \, p\hat{\mathbf{e}}_z. \tag{8.23}$$

On the other hand, at infinity, the Hankel function can be approximated to [115]

$$H_n(kr) \sim \sqrt{\frac{2}{\pi kr}} e^{ikr} (-i)^n e^{-i\pi/4}, \tag{8.24}$$

thus, from Eqs. (8.23)-(8.24), if we write the induced electric dipole $\mathbf{p} = \varepsilon_0 \alpha_{zz}^e \mathbf{E}_{in}$, α_{zz}^e representing the electric polarizability along the z-axis, and comparing with the first order ($n = 0$) of Eq. (8.14) this leads to

$$\alpha_{zz}^e = \frac{4i}{k^2} b_0. \tag{8.25}$$

In analogous way for the second term of Eq. (8.17), the magnetic polarizability along the y-axis ($\mathbf{m} = \alpha_{yy}^m \mathbf{H}_{in}$) reads

$$\alpha_{yy}^m = \frac{4i}{k^2} b_1. \tag{8.26}$$

Eqs. (8.25)-(8.26) express the polarizability in terms of the two-first Mie coefficients b_0 and b_1. These expressions are analogous to those defined in Eq. (6.5) of SubSection (6.3.1) for the spherical particles in the sense that they are fully characterized by the Mie coefficients (in this case by b_0 and b_1). Notice that under this formulation, we go beyond the well-known Rayleigh limit of small particles: $k_0 m r_0 \ll 1$.

Now we turn to the efficiency factors (or cross sections) for the cylinder. This quantity represents the energy extinguished from the incident wave in the form of absorption and/or angular distribution of scattered intensity. Namely, for s-polarization, the scattering, extinction and absorption efficiency factors are [115]:

$$Q_{sca} = \frac{2}{x}\left[|b_0|^2 + 2\sum_{n=1}^{\infty}|b_n|^2\right], \tag{8.27}$$

$$Q_{ext} = \frac{2}{x}\text{Re}\left\{b_0 + 2\sum_{n=1}^{\infty}b_n\right\}, \tag{8.28}$$

$$Q_{abs} = Q_{ext} - Q_{sca}. \tag{8.29}$$

Note that these equations are dimensionless. Instead of efficiency factors, one can also work with the scattering cross sections. If we define G as the geometrical cross section, the scattering cross sections are:

$$\sigma_{sca} = Q_{sca}G, \tag{8.30}$$

$$\sigma_{sca} = Q_{ext}G, \tag{8.31}$$
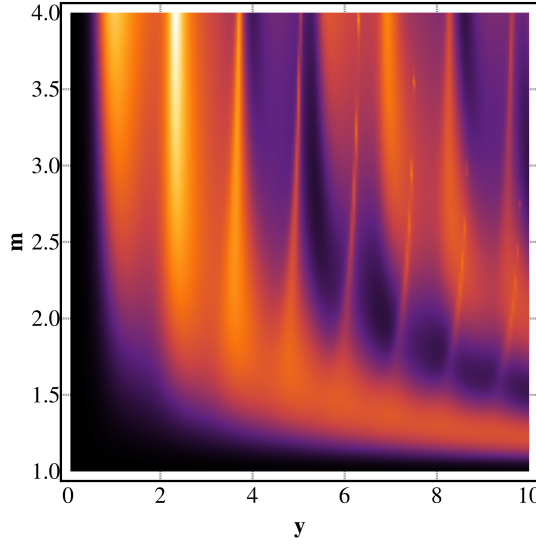
$$\sigma_{sca} = Q_{abs}G. \tag{8.32}$$

Figure 8.4: Efficiency factor Q_{sca} of an absorptionless cylinder for s-polarization

From Eqs. (8.25) and (8.26), we can write the $Q-$factors in terms of the polarizabilities

$$Q_{sca} = \frac{k^4}{8x} \left[|\alpha_{zz}^e|^2 + 2 |\alpha_{yy}^m|^2 \right], \tag{8.33}$$

$$Q_{ext} = \frac{k^2}{2x} \text{Im} \left\{ \alpha_{zz}^e + 2\alpha_{yy}^m \right\}, \tag{8.34}$$

and in absence of absorption (m real, thus $Q_{ext} = Q_{abs}$) the $Q-$factors fulfill

$$\text{Im}\alpha_{zz}^e = \frac{k^2}{4} |\alpha_{zz}^e|^2, \tag{8.35}$$

$$\text{Im}\alpha_{yy}^m = \frac{k^2}{4} |\alpha_{yy}^m|^2. \tag{8.36}$$

Let us now address the case of a non-absorbing cylinder. Fig. (8.4) shows the efficiency factor Q_{sca} (see Eq. (8.27)) as function of the relative refractive index m and the size factor $y = mkr_0$. From this figure, we clearly identify the different Mie resonances at different values of y.

As we discussed in Section (6.2) for a sphere, we have now a very similar situation for the cylinder. Fig. (8.4) shows a universal scaling-law for the efficiencies, once the value of the refractive index m is fixed, we can play with the $x = kr_0$ factor to be in the range of wavelengths of interest since for different values of the efficiency the resonance peaks constantly remain at the same y positions. Fig. (8.5) shows the efficiency factor Q_{sca} and the contributions of the three first Mie orders for the cylinder of radius $r_0 = 300\,nm$ and relative refractive index $m = 3.2$. For $\lambda \geq 2\,\mu m$, the behavior of the particle is magnetodielectric, and we only need the two first Mie-coefficients to calculate the total Q_{sca} (or scattering cross section), this plot justifies the use of the usual expression for the electric force for not so small particles, in fact, the factor $x = kr_0$ is ~ 1.

Fig. (8.6) shows the real and imaginary part of α_{zz}^e and α_{yy}^m for the previous parameters.
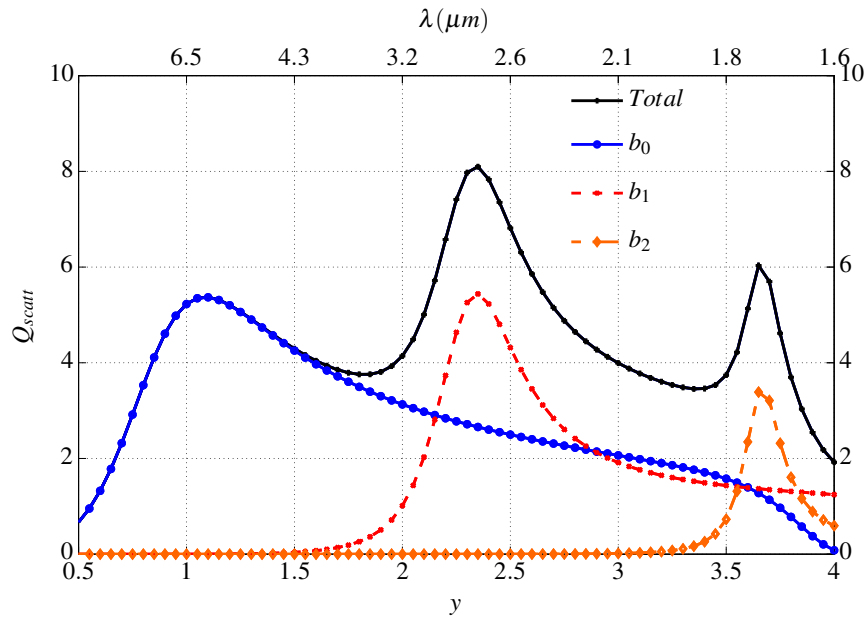
Figure 8.5: Q_{sca} computed from Eq. (8.27) and contributions of the three first Mie coefficients in the range of wavelength selected for a cylinder $r_0 = 300$nm and $m = 3.2$. Compare these resonances with the peaks of Fig. (8.11). S-polarization
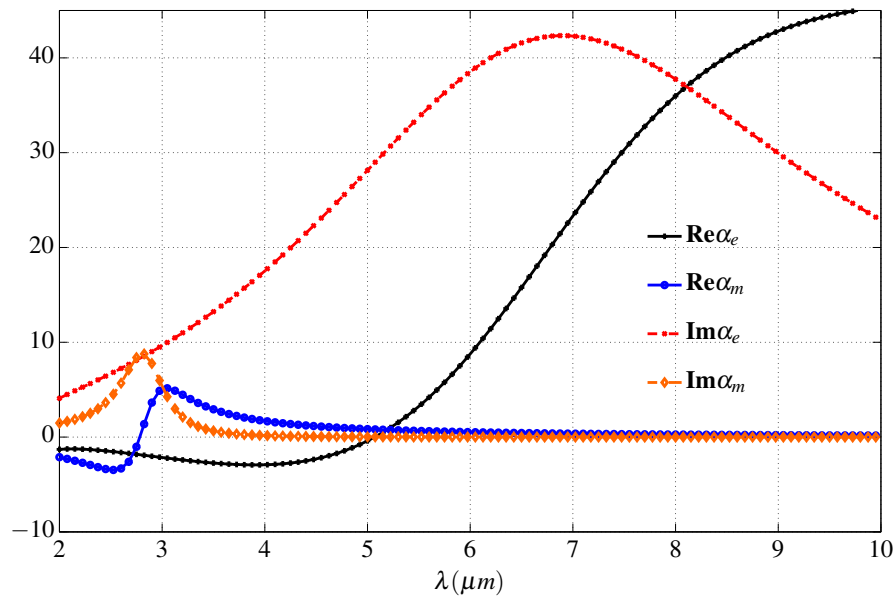

Figure 8.6: Electric and Magnetic polarizabilities given by Eqs. (8.25) and (8.26) normalized to r_0^2. S-polarization

8.6.2 *P-polarization (TM)*

Let us nos write the same quantities as in the previous subsection for p-polarization. In this case our incident electric field is perpendicular to the cylinder axis, or what is the same, the magnetic field is parallel to the this axis (see Fig. (8.3)):

$$\mathbf{E}_{in}\left(\mathbf{r}\right) = E_0 \hat{\mathbf{e}}_y e^{i\mathbf{k}\mathbf{r}}. \tag{8.37}$$

As for s-polarization, we can determinate the electric and magnetic polarizabilities in terms of the two first Mie coefficients, i.e.

$$\alpha_{yy}^e = \frac{4i}{k^2} a_1, \tag{8.38}$$

$$\alpha_{zz}^m = \frac{4i}{k^2} a_0, \tag{8.39}$$

where the a_n Mie coefficients are

$$a_n = \frac{m J_n'\left(x\right) J_n\left(y\right) - J_n\left(x\right) J_n'\left(y\right)}{m J_n\left(y\right) H_n'\left(x\right) - J_n'\left(y\right) H_n'\left(x\right)}. \tag{8.40}$$

Notice that in Eqs. (8.38)-(8.39) the electric polarizability is given by the $n = 1$ Mie coefficient instead of the zero order as in s-polarization. In addition, because we are in p-polarization, the electric polarizability is directed along the y-axis. Apart from this, the rest of the quantities are exactly the same making the next exchange: $b_n \to a_n$, thus, the efficienty factors are

$$Q_{sca} = \frac{2}{x}\left[|a_0|^2 + 2\sum_{n=1}^{\infty} |a_n|^2\right], \tag{8.41}$$

$$Q_{ext} = \frac{2}{x}\text{Re}\left\{a_0 + 2\sum_{n=1}^{\infty} a_n\right\}, \tag{8.42}$$

$$Q_{abs} = Q_{ext} - Q_{sca}. \tag{8.43}$$

Figs. (8.7), (8.8) and (8.9) shows Q_{sca} (for an arbitrary refractive index and for the previous cylinder) and the electric and magnetic polarizability respectively. All these figures are similar to Figs. (2) and (3) of [60] and Fig. (1) of [61]. This is due to the symmetry of the cylinder. Under p-polarization, the electric field *sees* the same geometrical cross section G as for a sphere.

It is worth remarking the magnetodielectric character of the cylinder, again, we need only the two first Mie coefficients to determinate Q_{sca}, being negligible the rest of the contributions. Notice also the relative position and strength of the electric resonance with respect to the magnetic one, in Figs. (8.5) and (8.8). In this case, the imaginary part of the polarizability is the twice that the electric one.
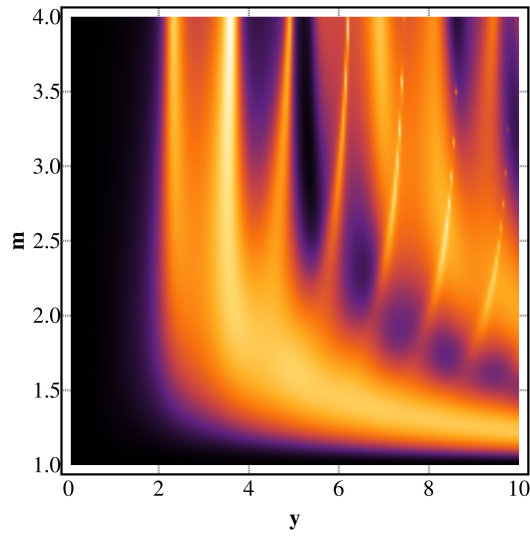
Figure 8.7: Efficiency factor Q_{sca} of a lossless cylinder for p-polarization
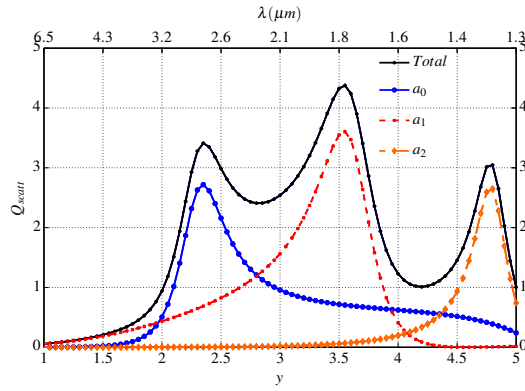

Figure 8.8: Q_{sca} computed from Eq. (8.41) and contributions of three first Mie coefficients in the range of wavelength selected for a cylinder $r_0 = 300$nm and $m = 3.2$. P-polarization

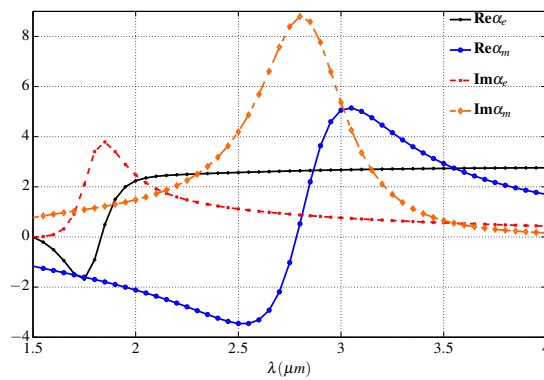Figure 8.9: Electric and Magnetic polarizabilities given by Eqs. (8.38) and (8.39) normalized to r_0^2. P-polarization

8.7 NUMERICAL SETUP

Once we know the scattering properties, we turn to the numerical setup. Let us consider a pair of particles illuminated by the GSMS wavefield whose mechanical action produces optical binding effects with characteristics of a photonic molecule. [167–169]. 2D numerical calculations are done by means of a FEM (RF module of COMSOL 4.3a, http://www.comsol.com) and MATLAB. Aside from some depolarization effects, the main features of the physical process: light scattering, resonance excitation and binding, are analogous to those in 3D [166, 170, 171].

Without loss of generality, a Si cylinder with $\varepsilon = 10.24$ and radius $r_0 = 0.3\mu m$ [168] has been considered, due to its rich Mie resonance spectra in both the visible and near IR [172] (cf. Section 8.6). This will allow us to analyze the effects of spatial coherence on these resonances and their consequences for the induced optical forces on this pair, (see Section 8.5).
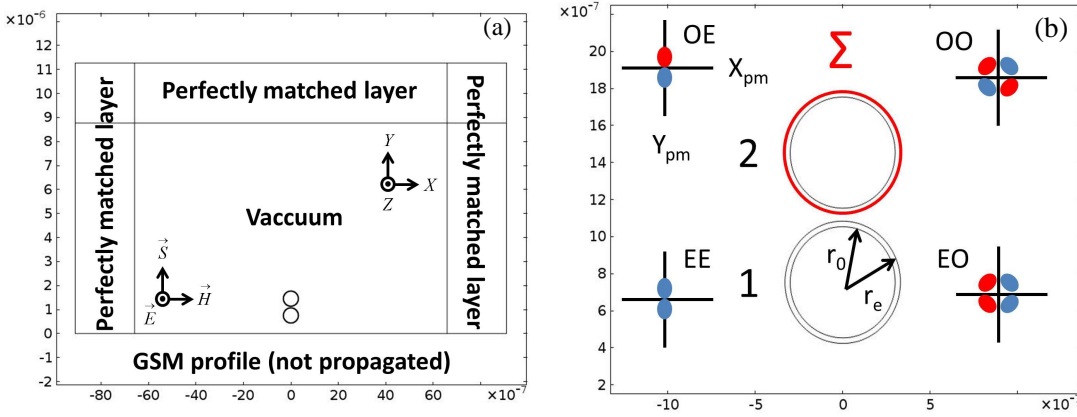
Figure 8.10: (a) Illustration of the geometry for resonant wavelength identification of both the single particle and the pair; as well as for the computation of the optical forces. An incident s-polarized field with a GSMS profile, (amplitude $A = 1W/m^2$, width of its intensity $\sigma_s = 0.05 \times 1500nm$, degree of coherence $\sigma_g = 100\sigma_s, 2\sigma_s, 0.5\sigma_s$), impinges the Si cylinders of radius r_0 with excitation of their WGMs: TE_{mn}. (a) In order to simulate infinite space, three absorbent, or perfectly matched, layers (PML) are located at the upper and lateral boundaries of the calculation window; the lower boundary containing the incident wave profile of the GSMS. (b) Detail of the geometrical cross sections of the particles conforming the "photonic" molecule, where the light intensity $|\langle \mathbf{S}(\mathbf{r}) \rangle|$ is averaged to the surface of the cilinder of radius r_0, and the circumference Σ of radius r_e surrounding each particle is employed to calculate the electromagnetic forces (per axial unit length), [cf. Eq. (13)], (see also [173]). Particles 1 and 2 stand for the lower/right, directly illuminated by the beam, and the upper/left ones, respectively.

Following the scheme shown in Fig. 8.10(a), an incident wavefield with electric vector E_z perpendicular to the XY-plane, is launched upwards, propagating along OY. The choice of s-polarization (TE), in contrast with p-polarization (TM), excites whispering-gallery modes (WGMs): TE_{mn}, (where m and n indicate the angular and radial orders, respectively), which extend to the near field region surrounding the cylinders. This facilitates the electromagnetic interaction between these particles. The light directly illuminates the right or lower particle, depending on whether the orientation of the molecular set is horizontal or oblique/vertical. Cor-

respondingly, either the left or the upper cylinder is mostly excited by the resonance of its partner. This technique is performed so that the molecular states associated to anti-symmetric field patterns with respect to the transversal axis of the molecule, [see insets OE and OO in Fig. 8.10(b)] are not destroyed, especially when the molecule is inclined with respect to the propagation direction of the beam. Notice that if both particles were simultaneously illuminated by the beam, only those WGMs related to symmetric field patterns with respect to the molecule axis would be excited, [see insets EE and EO in Fig. 8.10(b)].

The separation between the particles is $d_0 = 100nm$, which makes subwavelength the molecule dimensions, (compare the set size, $1.3\mu m$, to the range of wavelngths under study: $1.6\mu m -$ $8.0\mu m$). The center of the lower particle is $\approx 0.75\mu m$. We follow the nomenclature of [167, 169] for the molecular states, the classification being based on the $\mathbf{E}(\mathbf{r})$ field symmetry with respect to the main directions defined by the molecule geometry, i.e. its longitudinal (Y_{pm}) and transversal (X_{pm}) axes, [see Fig. 8.10(b)]. As an example, we will examine the upper-left inset of Fig. 8.10(b). In this case, the upper lobe is opposite to the lower one, thus it is said that E is even, (E), with respect to OX; however, E is odd. (O), with respect to $0Y$. Therefore the photonic state is even-odd (EO). If they mismatch one another, it would be $X_{pm}Y_{pm}/OO$, [cf. the upper-right inset in Fig. 8.10(b)]. These would be similar to a double bound in the molecule. In the case in which only one lobe of each particle interacts with the other (simple bound), the states will be $X_{pm}Y_{pm}/EE$ and $X_{pm}Y_{pm}/OE$, respectively.

In all cases the E_z profile at frequency ω is that of a GSMS, described in Section 8.5. The field has an intensity $1W/m^2$ and $\sigma_s = 0.05 \times 1500nm$. The spatial coherence of the near field is gradually established as the ratio between the coherence length and the width of the beam $\sigma_g/\sigma_s = 100, 2, 0.5$ diminishes. The GSMS is placed in the lower boundary of the simulation window and is implemented as a discrete sum of modes q, [see Eq. (8.9)]. As explained in Section 8.5, the lower the ratio of σ_g/σ_s, the higher the value of q, (cf. Fig. 5.17 of [3]). An iterative process is followed in order to simulate the propagation of each of these q-modes through the calculation window. Subsequently, they are summed up to get the propagated total fields $\mathbf{E}(\mathbf{r})$ and $\mathbf{H}(\mathbf{r})$.

The next results show the time-averaged energy flow $\langle \mathbf{S}(x, y) \rangle$, that shows light concentration in the probe cylinders. Because of their dielectric nature, we average $|\langle \mathbf{S}(x, y) \rangle|$ in a circle which coincides with the geometrical cross section of the probe cylinder of radius r_0, [see Fig. 8.10(b)]. This stems from the fact that, if the particle is dielectric, the intensity of the light beam that couples to the particle WGM, is concentrated inside the cylinders, (see [174]), not outside them, (the latter occurs for plasmonic cilinders [175]). In all cases, these intensities are normalized to the maximum intensity of the incident Gaussian beam: $|\langle \mathbf{S}_{max} \rangle| = 1W/m^2$.

The averaged force on the probe cylinders is calculated by employing the MST, Eq. (8.6). The line of integration Σ surrounds each particle as seen in Fig. 8.10(b). In our 2D geometry, Σ is the circumference of radius r_e, (see Fig. 8.10(b)). $\varepsilon = \mu = 1$. Because of this 2D geometry, our results are expressed as force per axial length unit, in N/m.

The COMSOL calculation with complex values of $\mathbf{E}(\mathbf{r})$ and $\mathbf{H}(\mathbf{r})$ as well as of the real physical fields: $\mathbf{E}^{\mathbf{R}}(\mathbf{r}, t) = \text{Re}[\mathbf{E}(\mathbf{r}) \exp(-i\omega t)]$ and $\mathbf{H}^{\mathbf{R}}(\mathbf{r}, t) = \text{Re}[\mathbf{H}(\mathbf{r}) \exp(-i\omega t)]$, is not straightforward. The details of the procedure have been given in [173]. The meshing used in the simulation has a maximum and a minimum element of $\lambda_{ref}/8$ and $2.7nm$, respectively. The reference wavelength being $\lambda_{ref} = 1620nm$. The maximum element growth rate, resolution of curvature, and resolution of narrow regions are 1.3, 0.3, and 1, respectively.

8.8 A BI-PARTICLE PHOTONIC MOLECULE ILLUMINATED BY A GAUSSIAN SCHELL MODEL SOURCE. EFFECTS OF PARTIAL COHERENCE IN THE "MOLECULAR" STATES

8.8.1 *Localization of resonances of a single particle. Bi-particle set: Production of "molecular" states*

In order to identify the resonant states of a photonic molecule, the spectral location of the resonances of the single particle is required. For the sake of accuracy needed in the calculations, and in order to deal with not too complex bonds between the particles, our study limits the search of resonances in each individual particle to those of low angular order. This suffices to illustrate the analysis in this work.
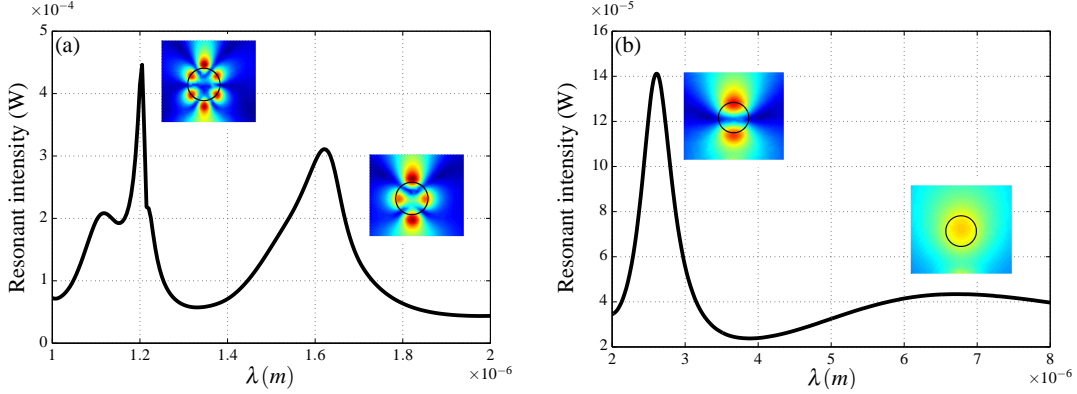

Figure 8.11: Spatially coherent illumination. (a) Spectral variation of the mean of the ensemble-averaged Poynting vector norm $|\langle \mathbf{S}(\mathbf{r}) \rangle|$, (i.e. the light intensity), in a single cylinder illuminated by a totally coherent GSMS beam. The two magnetic multipole peaks are swhown. (b) The same quantity in a range of higher λ in which the Mie coefficients contributing to the scattering cross section are b_0, (electric dipole, $\lambda = 6 - 7nm$), and b_1, (magnetic dipole, $\lambda = 2.7nm$); hence the particle being magneto-dielectric. The insets in (a) and (b) show the spatial distribution of $|\langle \mathbf{S}(\mathbf{r}) \rangle|$ for WGMs: TE_{31}/WGE_{21} and TE_{11}/TE_{01}, respectively.

Hence, the chosen wavelength is the near infrared, (NIR), in which two multipolar peaks of field intensity localized in the cylinder, associated to its morphology dependent resonances (MDR) are found, [see Fig. 8.11(a)]. As the insets show, these are the WGMs TE_{31} ($\lambda \approx 1205nm$) and a TE_{21} ($\lambda \approx 1620nm$). At larger λ, as shown in Fig. 8.11(b) the MDRs TE_{11} ($\lambda \approx 2610nm$) and
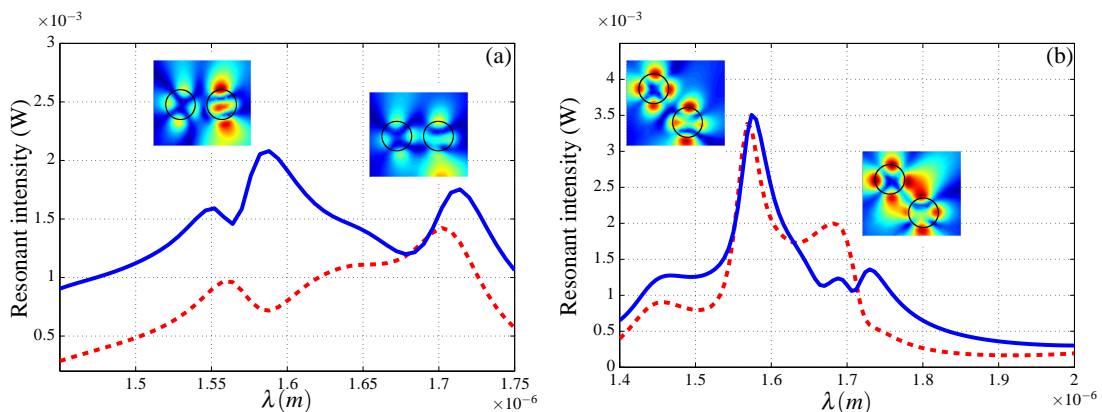
Figure 8.12: Spatially coherent illumination. (a) $|\langle \mathbf{S}(\mathbf{r})\rangle|$ localized in each particle of a "bi-atomic" photonic molecule vs. λ, illuminated as in Fig. 8.11(a). This leads to the splitting of the TE_{21} mode of a single particle, which produces a blue-shifted, (anti-symmetric), and a red-shifted, (symmetric), molecular state, respectively. (b) The same quantity showing the other possibility of splitting associated to the same MDR. The blue solid and red dashed lines in (a) stand for the right, (i.e. the one directly illuminated), and the left particle, respectively. The same code is used in (b), now for the lower, (directly illuminated), and the upper particle, respectively. The insets show the intensity maps of the "molecular" states, again related to each intensity peak concentrated by both particles.

TE_{01} ($\lambda \approx 6710nm$) are excited, (cf. the insets of this figure). The TE_{11} is interesting because, as shown in [157, 158, 172], the cylinder scattering cross section is dominated by the Mie coefficients b_0 and b_1 [166], associated to the electric and magnetic dipolar moments, $\mathbf{p}$ and $\mathbf{m}$, respectively, of the cylinder; therefore this particle behaves as magnetodielectric in this spectral range. In addition, if we compare Fig. 8.6 and Fig. 8.11(b) we see how the theory developed in Section 8.6 agrees with the numerical simulation.

The concentration of intensity $|\langle \mathbf{S}(\mathbf{r})\rangle|$ inside each particle conforming the photonic molecule is shown in Figs. 8.12(a) and 8.12(b). A comparison between the blue solid and the red dashed lines in Fig. 8.12(a) shows that the intensity $|\langle \mathbf{S}(\mathbf{r})\rangle|$ in the right particle is generally higher than that in the left one, [the same happens for the lower and the upper cylinders in 8.12(b)]. This happens because the particle directly illuminated by the beam concentrates more intensity $|\langle \mathbf{S}(\mathbf{r})\rangle|$.

The calculation is focused on the different non-degenerate collective states that can produce the TE_{21} mode excited in both cylinders. Due to the disposition of the lobes of the resonance, ("even", E, or "odd", O in the field $\mathbf{E}$ spatial distribution), for each particle with respect to the symmetry axes defined by the ensemble, which are longitudinal and transversal with respect to the molecule axis (hereafter denoted as Y_{pm} and X_{pm}, respectively), such a resonance excited in this configuration can generate four "molecular" states [167–169, 176]. The collective states Y_{pm}/E can be obtained by illuminating the ensemble either in the direction parallel or transversal to the molecule axis.

The reason to select the configuration in which the Y_{pm} axis appears inclined by an angle $\pi/2$ while the direction of the beam is parallel to the Y axis of the calculation window, is
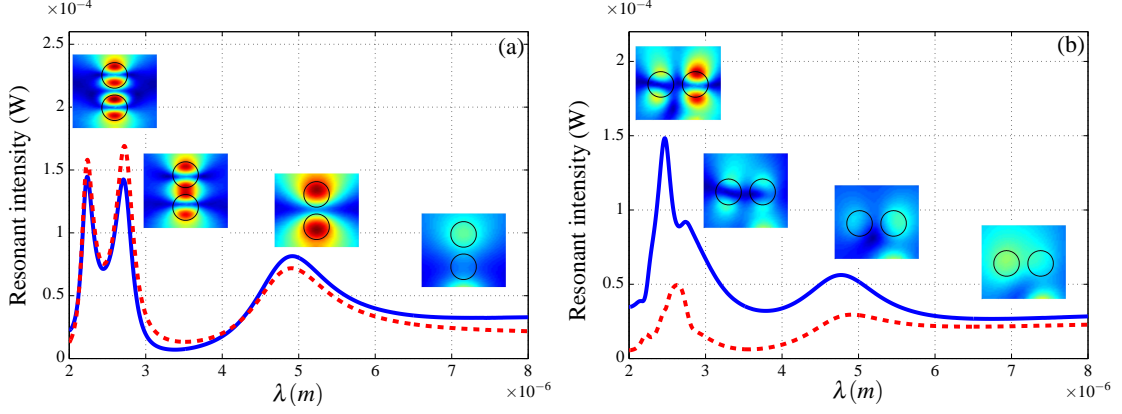
Figure 8.13: (a) The same as in Fig. 8.12(a) in the spectral range in which the single particle is magneto-dielectric, [cf. Fig. 8.11(b)]. The first two peaks from the left are associated to the WGM: TE_{11}, while the third one is related to the TE_{01} mode. (b) The same as in Fig. 8.13(a) showing the other possibility of splitting for the same MDRs. The interpretation of the so formed "molecular" states is similar to that of Fig. 8.12(a) and Fig. 8.12(b).

explained in Subsection 8.8.2. Figure 8.12(a) shows this geometrical configuration, which renders the molecular states Y_{pm}/E as consequence of the splitting of the resonance TE_{21} of the single particle into two new MDRs, associated to the disposition of the lobes with respect to the X_{pm} axis, i.e. $X_{pm}Y_{pm}/OE$ and $X_{pm}Y_{pm}/EE$, at $\lambda = 1597nm$ and $\lambda = 1665nm$, respectively (see the insets) [168].

On the other hand, in order to reproduce the collective states Y_{pm}/O, the Y_{pm} axis must be inclined by an angle of $\pi/4$ with respect to the propagation direction of the beam because of the number of intensity lobes for the resonance TE_{21} in the single particle. This is seen in Fig. 8.12(b), where the molecular states Y_{pm}/O arise as a new splitting of the resonance TE_{21} of the single particle, i.e. $X_{pm}Y_{pm}/OO$ and $X_{pm}Y_{pm}/EO$, at $\lambda = 1582nm$ and $\lambda = 1693nm$, respectively, (see the detail in this figure).

All the non-degenerate states of this photonic molecule associated to the MDR TE_{21} in each particle are shown by these two orientations of the ensemble. Both orientations present two collective resonances, the X_{pm}/O and X_{pm}/E being blue- and red- shifted, (i.e. more and less energetic, respectively). This can be explained by the insets of this figure: the X_{pm}/O states concentrate relatively much more light intensity inside the cylinders than the X_{pm}/E ones. Each set of orientation also reminds the formation either of a simple, [Fig. 8.12(a)], or a double, [Fig. 8.12(b)], bond between the particles [168].

By increasing the wavelength λ of illumination on this particle pair around the same range as in Fig. 8.11(b), the behavior of the collective resonances appears to be similar to that of Fig. 8.12(a) and Fig. 8.12(b) regarding the connection between their symmetry, (X_{pm}/O and X_{pm}/E lobes in **E**), and energy, (blue- and red-shifted peaks). These states being in this case originated by the TE_{11} and TE_{01} resonances excited in the single particle. Aiming to reproduce its Y_{pm}/E and Y_{pm}/O states, the Y_{pm} axis is constrained to be either parallel, [see Fig. 8.13(a)], or perpendicular, [see Fig. 8.13(b)], to the direction of the light beam, respectively. The suppression,
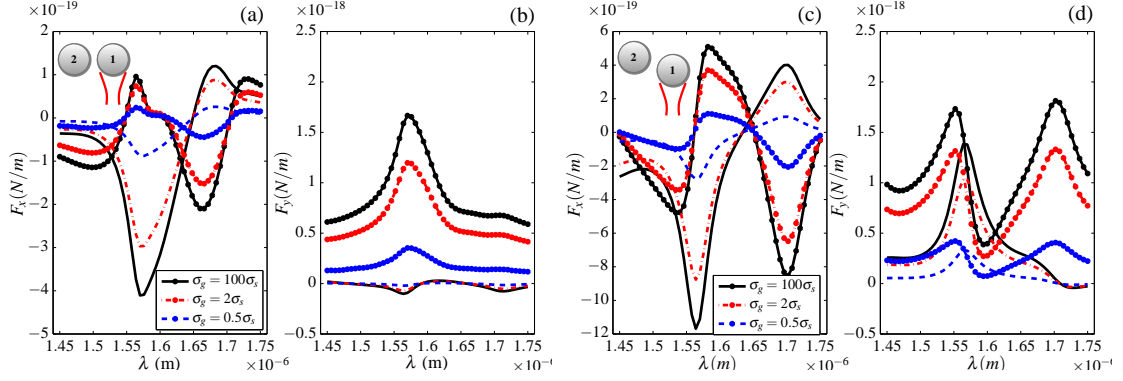
Figure 8.14: (a) Horizontal and (b)vertical components of the time-averaged electromagnetic forces per axial unit length on each cylinder of the particle pair for the orientation shown in Fig. 8.12(a). (c)-(d) The same quantities for the molecule oriented according to Fig. 8.12(b). The lines with and without points correspond to the force on the particle 1 and 2, respectively. The colors are associated to an illuminating GSMS beam with different coherence length-to-spot size ratios: σ_g/σ_s: $\sigma_g = 100\sigma_s$ (black), $\sigma_g = 2\sigma_s$ (red), and $\sigma_g = 0.5\sigma_s$ (blue).

in both orientations, of the less energetic molecular state associated to the TE_{01} WGM of the single particle, i.e.the $X_{pm}Y_{pm}/EE$, is due to the fact that the illuminating wavelength λ is much longer than the dimensions of the molecule, this latter now being almost invisible.

8.8.2 *Effects of partially coherent illumination on the electromagnetic forces between the particles. Bonding and anti-bonding "molecular" states*

Next, I consider the cylinder pair illuminated by a GSMS with different coherence lengths σ_g. This allows us to understand its effect of the electromagnetic forces acting on its collective states. As previously remarked, for this s-polarization the fields associated to these states, although localized inside the particles, reach high intensity values in the area immediately outside them. Taking into account the calculation from the CMR of MST, Eq. (8.6), maximum forces are thus expected to appear when these states are excited. Two of the MDRs of the single particle: TE_{21} and TE_{11}, are selected to study the electromagnetic forces acting in the optical binding between the two cylinders which conform the photonic molecule. As discussed in Section 8.8.1, each of these resonances splits into two collective states whose symmetry and energy are related to each other. The TE_{21} mode is chosen due to its possibility to generate states in the particle pair which remind those of a simple [Fig. 8.12(a)] and a double [Fig. 8.12(b)] bond in an atomic molecule. The TE_{11} mode causes the particles to behave as magneto-dielectric, giving rise to an interaction not only between its electric dipoles, but also between its induced magnetic ones.

Figures 8.14(a)-(b) and 8.14(c)-(d) show the electromagnetic force between the two particles in the case of the collective states corresponding to the two first peaks of intensity $|\langle \mathbf{S}(\mathbf{r}) \rangle|$ in Fig. 8.12(a) and Fig. 8.12(b), respectively. They correspond to the splitting of the magnetic quadrupole b_2 of the single particle of Fig. 8.11(a). The reason to choose the orientation shown

in Fig. 8.14(a) for the molecule is now clear since the total force on the particles has two contributions: the gradient force between the particles and that of scattering related to the radiation pressure of the incident beam along OX and OY. On the other hand, the orientation used in Figs. 8.14(c)-(d) causes those two force components to mix with each other along OY, notwithstanding remaining possible to study the interaction between both particles by means of the force X-component.

Under completely coherent illumination, peaks of repulsive and attractive force between the two particles appear at $\lambda \approx 1597nm$ and $\lambda \approx 1665nm$, (cf. in Fig. 8.14(a) black lines with and without points for the X-component of the forces on particles 1 and 2, respectively]. The same happens in Fig. 8.14(c) at $\lambda \approx 1582nm$ and $\lambda \approx 1693nm$. These results allow to identify the blue-shifted $X_{pm}Y_{pm}/OE$ and the red-shifted $X_{pm}Y_{pm}/EE$ in Fig. 8.12(a) collective states ($X_{pm}Y_{pm}/OO$ and $X_{pm}Y_{pm}/EO$ in Fig. 8.12(b)) as anti-bonding and bonding ones, respectively [50, 167–169, 176].

The forces in the vertical direction are higher for particle 1 (which is directly illuminated) in both orientations. In Fig. 8.14(a) this component, associated to the scattering force from the beam, is lower for the bonding molecular state at $\lambda \approx 1665nm$ than that for the antibonding one (at $\lambda \approx 1597nm$), since the former renders higher values of field intensity immediately outside the particles. For the orientation of Fig. 8.14(c), both collective states, the repulsive and the attractive one, at $\lambda \approx 1582nm$ and $\lambda \approx 1693nm$, suffer comparable Y-components of the total force because now in this direction the gradient force between the particles must also be taken into account.

When we decrease the coherence length of the source, (see red and blue lines standing for $\sigma_g = 2\sigma_s$ and $\sigma_g = 0.5\sigma_s$, respectively), both components of the force invariably diminish. Although the dimension of the molecule and its position with respect to the source, which is in the lower boundary of the calculation window), are subwavelength, these results are opposite to those of Fig. 5.2 in Chapter 5, the interaction between the GSMS beam and the particles now being more complex due to the addition of the effect from the MDRs. In fact, the intensity pattern of the interference process which renders the particle resonance decreases, i.e. the field lobes corresponding to the formation of the resonance in each particle loose contrast. This leads, taking into account the force calculation, to a decrement in the field intensity values reached outside the particles and hence in their optical attraction or repulsion.

Finally, the optical forces on the molecular states associated to the first two peaks of Fig. 8.13(a) and Fig. 8.13(b), [associated to the magnetic dipole of Fig. 8.11(b)], are shown in Figs. 8.15(a)-(b) and 8.15(c)-(d), respectively. The vertical orientation of the pair, although now mixing both contributions to the total force, (i.e. gradient component between the particles and scattering one due to radiation pressure of the light beam), renders its Y-component being the only significant one, and behaves just as expected at $\lambda \approx 2230nm$ and $\lambda \approx 2680nm$. Namely, repulsive and attractive forces arise acting on the blue-shifted, $X_{pm}Y_{pm}/OE$, and the red-shifted, $X_{pm}Y_{pm}/EE$, collective states, respectively [see Fig. 8.15(a)]. The force X-component remains null because of the orientation of the pair. On the other hand, the horizontal orientation, [see
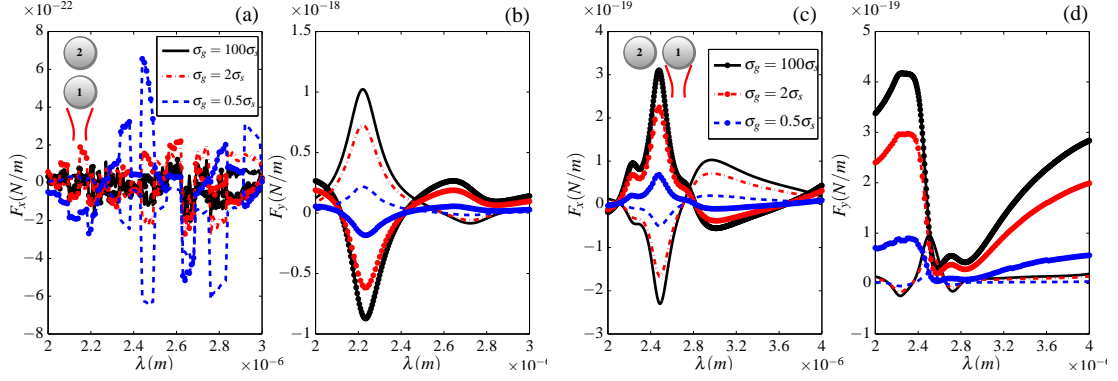
Figure 8.15: (a)-(b) The same quantities as in Fig. 8.14(a)-(b) with the molecule oriented as in Fig. 8.13(a). (c)-(d) The same as in Fig. 8.15(a)-(b), the molecule now being oriented as in Fig. 8.13(b). The code of lines and colors is identical to that of Fig. 8.14

Fig. 8.15(c)], deserves the same discussion on both components of the total force as that concerning Fig. 8.14(a)-(b): repulsive and attractive forces between the particles now emerge at $\lambda \approx 2480nm$ and $\lambda \approx 2985nm$, which correspond to the blue-shifted, $X_{pm}Y_{pm}/OO$, and the red-shifted, $X_{pm}Y_{pm}/EO$, molecular states. As in the previous case, the loss of coherence in the light beam causes the decrement in the magnitude of both force components.

8.9 CONCLUSIONS

In this chapter I have presented several results. Firstly I have demonstrated how at near-field distances from the source one needs a full electromagnetic theory in order to obtain the total photonic force, i.e., the fluctuations of the field along the propagation direction can be as important as the rest of them.

Secondly I have presented a new theory of photonic forces illuminated by partially coherent fields, specifically for a Gaussian-Schell model source. We have demonstrated how the optical force can be calculated by means of the MST, being this quantity decomposed into the sum of N-coherent states. This representation is based on the coherent mode representation [154]. I have illustrated the results with computer simulations of optical binding of Mie dipolar dielectric cylinders with magnetodielectric behavior. This behavior has been studied in detail showing the rich landscape of resonant states for s- or p-polarization associated to the different Mie coefficients.

Finally I have extended the analysis to the dynamical interaction of two dielectric cylinders forming a photonic molecule. I have shown explicitly the effects of the spatial coherence in these resonant configurations, which are linked to the symmetric and anti-symmetric molecular resonances, associated to bonding and anti-bonding states, respectively. The role of the interplay between the electric and magnetic induced dipoles when such Mie resonances are induced, has been demonstrated to be important. Now the threshold of evanescent wave contribution to the

scattered field is critical. Namely, in addition to being at subwavelength distances from the source plane, the particles need to be practically in contact with each other for a substantial contribution of the inhomogeneous modes. As a consequence, as few evanescent modes are present, a decrease of the coherence length σ_g conveys lower bonding and antibonding forces.

Part VI

APPENDIX

A

NEAR-FIELD SPECTRA FROM PARTIALLY COHERENT THERMAL SOURCES

In Chapter 2 we demonstrated the effects of the correlation length σ of the source on the cross-spectral density at near-field. In this appendix we address the effects of the spatial coherence on the spectral density $W(\mathbf{r}, \mathbf{r}, \omega) = S(\mathbf{r}, \omega)$. This effect was observed by Roychowdhury and Wolf in [13]. In that reference they demonstrated, using a simple model of statistically homogeneous source as we have considered in Eq. (2.18), that the spectrum observed differs from those whose correlations at the source are $\delta-$correlated. That paper appears pointing out the insufficiency of the conclusions reached in [12].

In this appendix, following the steps employed in [12, 177] and using a modified version of the fluctuation-dissipation theorem in order to take different correlation lengths into account, we will confirm the conclusions established in [13].

Let us consider the electric field $\mathbf{E}(\mathbf{r}, \omega)$ in the half-space $z > 0$ generated by the thermal currents $\mathbf{j}(\mathbf{r}, \omega)$ placed at $z < 0$. Using the Green's formalism, $\mathbf{E}(\mathbf{r}, \omega)$ can be written [11, 143]

$$E_i(\mathbf{r}, \omega) = i\mu_0\omega \int_V G_{ij}(\mathbf{r}, \mathbf{r}', \omega) j_j(\mathbf{r}', \omega) \, \mathrm{d}^3\mathbf{r}', \quad (i, j = x, y, z), \qquad (A.1)$$

where $G_{ij}(\mathbf{r}, \mathbf{r}', \omega)$ is the dyadic Green's function which relates the properties of the source with the emitted field thought the transmission Fresnel coefficients [1]. We will no enter in detail about G_{ij} because it will be addressed in Section C.1 of this thesis.

In this example, the role of the cross-spectral density at the source ($W^{(0)}(\mathbf{r}_1, \mathbf{r}_2, \omega)$) will be played by the correlation between the different Cartesian component of $\mathbf{j}(\mathbf{r}, \omega)$. These correlations are given by the well-known fluctuation-dissipation theorem [79]

$$\langle j_i(\mathbf{r}_1, \omega) j_j(\mathbf{r}_2, \omega') \rangle = \frac{\omega\Theta(\omega, T)}{4\pi^2}\varepsilon_0 \mathrm{Im}\varepsilon(\omega) \delta_{ij}\delta(\mathbf{r}_1 - \mathbf{r}_2) \delta(\omega - \omega'), \qquad (A.2)$$

where $\varepsilon(\omega)$ is the permittivity of the half-space where the currents are contained. $\Theta(\omega, T)$ is the thermal energy $\Theta(\omega, T) = \hbar\omega/[\exp(\hbar\omega/k_B T) - 1]$, being $\hbar$ the normalized Planck's constant, k_B the Boltzmann's constant and T the temperature. In Eq. (A.2) the factor $\delta(\omega - \omega')$ is a consequence of the Wiener-Khintchine theorem (see Section 1.2). The function $\delta(\mathbf{r}_1 - \mathbf{r}_2)$ express
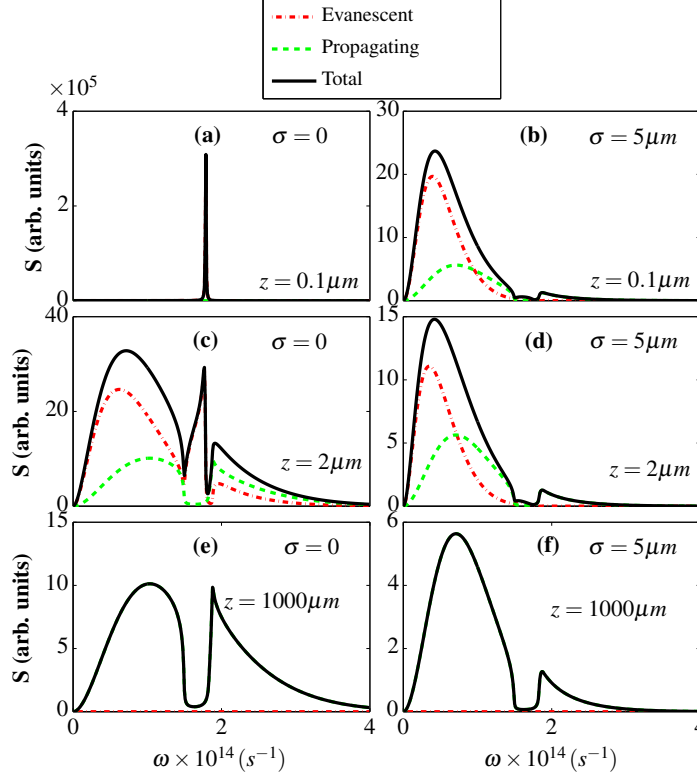
Figure A.1: $\mathrm{Tr}W_{ij}(\mathbf{r},\mathbf{r},\omega)$ for two values of the coherence length, $\sigma = 0$ (left column) and $\sigma = 5\mu m$ (right column) and for different distances from the plane of the source $z = 0$. The red dashed-dot line represent the contribution of the evanescent modes and the green dashed line that of the propagating modes. The black solid line is the the sum of both contributions.

that the sources are uncorrelated ($\sigma \to 0$), however, we will introduce in Eq. (A.2) a Gaussian function in order to consider different values of σ, i.e.

$$\left\langle j_i(\mathbf{r}_1,\omega)\, j_j(\mathbf{r}_2,\omega')\right\rangle = \frac{\omega\Theta(\omega,T)}{4\pi^2}\varepsilon_0 \mathrm{Im}\varepsilon(\omega)\, \frac{e^{-\frac{|\mathbf{r}_1-\mathbf{r}_2|^2}{2\sigma^2}}\delta_{ij}}{(2\pi)^{3/2}\sigma^3}\delta(\omega-\omega'). \tag{A.3}$$

Notice that for $\sigma \to 0$ we recover the original fluctuation-dissipation theorem. As we are dealing with an electromagnetic field instead of a scalar one, the cross-spectral density function will be a tensor

$$W_{ij}(\mathbf{r}_1,\mathbf{r}_2,\omega) = \left\langle E_i^*(\mathbf{r}_1,\omega)\, E_j(\mathbf{r}_2,\omega)\right\rangle, \quad (i,j = x,y,z), \tag{A.4}$$

in order to take into account the three Cartesian components of the electric field $\mathbf{E}(\mathbf{r},\omega)$. Hence, the power spectrum of the field will be calculated as the trace of the cross-spectral density tensor $W_{ij}(\mathbf{r}_1,\mathbf{r}_2,\omega)$:

$$S(\mathbf{r},\omega) = \mathrm{Tr}W_{ij}(\mathbf{r},\mathbf{r},\omega). \tag{A.5}$$

Substituting Eq. (A.1) into Eq. (A.4), taking the trace, and using the modified fluctuation-dissipation theorem Eq. (A.3) we can calculate the power spectrum at distances of the order of

the wavelength λ. The calculation can be found in Appendix C (cf. Eq. (C.17)). To make the calculus we have considered the same values of $\varepsilon(\omega)$ and T as in Ref. [12]; i.e.

$$\varepsilon(\omega) = \varepsilon_\infty \frac{\omega_L^2 - \omega^2 - i\gamma\omega}{\omega_T^2 - \omega^2 - i\gamma\omega}, \tag{A.6}$$

with $\varepsilon_\infty = 6.7$, $\omega_L = 182.7 \times 10^{12} s^{-1}$, $\omega_T = 149.5 \times 10^{12} s^{-1}$ and $\gamma = 0.9 \times 10^{12} s^{-1}$; and a temperature $T = 300K$.

Fig. A.1 shows our main results of this Appendix, which are in agreement with those of [12]. The left column, where we have considered that the coherence length is zero ($\sigma = 0$), we get the same results as in [12]. Now we will see how as we increase the distance from the plane of the source, the spectrum changes drastically. In Fig. A.1(a), the spectrum is almost monochromatic, where the position of the peak is due to the dielectric function ε considered (SiC which supports SPPs in the range of thermal emission, see Ref. [12]), however, as we increase the distance from the source z, the spectrum becomes broader. The latter effect is due to the loss of evanescent modes. In Fig. A.1(a), the black solid line coincides with the red dashed-dot line, which represent the evanescent modes, we could say that the propagating components of the angular wave spectrum are negligible. Nevertheless, in Fig. A.1(c) we can see how the evanescent modes start to decrease, being zero in Fig. A.1(e).

In the right column we have considered a value of $\sigma = 5\mu m$. Comparing Figs. A.1(a) and (b), we can see something similar to Fig. 2.4. In this case, a larger value of the σ give us a spectrum that is more similar to Fig. A.1(c) than Fig. A.1(a). As we increase σ, we loss the evanescent modes, which are responsible for the monochromatic spectrum at subwavelength distances.

In summary and according to Ref. [13], the effects on the near-field spectra are not only due to the evanescent modes, the spatial coherence of the source is as important as the contribution of these modes. Interestingly, and consistent with the results of Reference Chapter 2, it is again the completely uncorrelated source which yields the most interesting results.

B

ANALYTICAL EXPRESSION FOR THE FORCE IN THE THOMPSON AND WOLF CONFIGURATION

In this appendix we address the complete expressions for the different component of the optical force within the framework developed in Chapter 4

B.1 ANALYTICAL EXPRESSIONS OF THE GRADIENT FORCE

The following equations express the gradient force in term of the spectral degree of coherence $|\mu\left(\mathbf{q}_1, \mathbf{q}_2, \bar{\omega}\right)|$

- *Calculation of $\tilde{F}_x^{grad}$*

$$
\left\langle \tilde{F}_x^{grad} \right\rangle
$$
$$
= -4\mathrm{Re}\alpha_e I_0 \left(\frac{a\bar{k}}{z\bar{v}_0} \right)^2 \left(\frac{\pi a^2 \left|\mathbf{e}\left(\bar{\omega}\right)\right|^2}{\bar{\lambda} z} \right)^2 x \left[\left(2\frac{J_1\left(\bar{v}_0\right)}{\bar{v}_0} \right)^2 + 2\frac{J_1\left(\bar{v}_0\right)}{\bar{v}_0} \right.
$$
$$
\times \left[J_0\left(\bar{v}_0\right) - J_2\left(\bar{v}_0\right) \right] \left[1 + \left|\mu\left(\mathbf{q}_1, \mathbf{q}_2, \bar{\omega}\right)\right| \cos\left(\phi\left(\mathbf{q}_1, \mathbf{q}_2, \bar{\omega}\right) + \frac{2\bar{k}hy}{z} \right) \right].
$$

(B.1)

$\bar{v}_0 = \bar{k}a\sqrt{x^2 + y^2}/z$. Observe that in this equation, none of the two terms may be neglected.

- *Calculation of $\tilde{F}_y^{grad}$*

$$
\left\langle \tilde{F}_y^{grad} \right\rangle
$$

$$
\begin{aligned}
= \quad & 4\mathrm{Re}\alpha_e I_0 \left(\frac{a\bar{k}}{z\bar{v}_0} \right)^2 \left(\frac{\pi a^2 \left| \mathbf{e}\left(\bar{\omega}\right) \right|^2}{\bar{\lambda}z} \right)^2 y \left[\left(2\frac{J_1\left(\bar{v}_0\right)}{\bar{v}_0} \right)^2 + 2\frac{J_1\left(\bar{v}_0\right)}{\bar{v}_0} \right. \\
& \times \left[J_0\left(\bar{v}_0\right) - J_2\left(\bar{v}_0\right) \right] \left] \left[1 + \left| \mu\left(\mathbf{q}_1, \mathbf{q}_2, \bar{\omega}\right) \right| \cos\left(\phi\left(\mathbf{q}_1, \mathbf{q}_2, \bar{\omega}\right) + \frac{2\bar{k}hy}{z} \right) \right] \right. \\
& -4\mathrm{Re}\alpha_e I_0 \left(\frac{\pi a^2 \left| \mathbf{e}\left(\bar{\omega}\right) \right|^2}{\bar{\lambda}z} \right)^2 \frac{h\bar{k}}{z} \left(2\frac{J_1\left(\bar{v}_0\right)}{\bar{v}_0} \right)^2 \\
& \times \left| \mu\left(\mathbf{q}_1, \mathbf{q}_2, \bar{\omega}\right) \right| \sin\left(\phi\left(\mathbf{q}_1, \mathbf{q}_2, \bar{\omega}\right) + \frac{2\bar{k}hy}{z} \right) \\
= \quad & \left\langle \tilde{F}_x^{grad} \right\rangle \frac{y}{x} - 4\mathrm{Re}\alpha_e I_0 \left(\frac{\pi a^2 \left| \mathbf{e}\left(\bar{\omega}\right) \right|^2}{\bar{\lambda}z} \right)^2 \frac{h\bar{k}}{z} \left(2\frac{J_1\left(\bar{v}_0\right)}{\bar{v}_0} \right)^2 \\
& \times \left| \mu\left(\mathbf{q}_1, \mathbf{q}_2, \bar{\omega}\right) \right| \sin\left(\phi\left(\mathbf{q}_1, \mathbf{q}_2, \bar{\omega}\right) + \frac{2\bar{k}hy}{z} \right). \tag{B.2}
\end{aligned}
$$

Hence

$$
\begin{aligned}
\left\langle \tilde{F}_y^{grad} \right\rangle \approx \quad & -4\mathrm{Re}\alpha_e I_0 \left(\frac{\pi a^2 \left| \mathbf{e}\left(\bar{\omega}\right) \right|^2}{\bar{\lambda}z} \right)^2 \frac{h\bar{k}}{z} \left(2\frac{J_1\left(\bar{v}_0\right)}{\bar{v}_0} \right)^2 \\
& \times \left| \mu\left(\mathbf{q}_1, \mathbf{q}_2, \bar{\omega}\right) \right| \sin\left(\phi\left(\mathbf{q}_1, \mathbf{q}_2, \bar{\omega}\right) + \frac{2\bar{k}hy}{z} \right). \tag{B.3}
\end{aligned}
$$

- *Calculation of $\tilde{F}_z^{grad}$*

$$
\left\langle \tilde{F}_z^{grad} \right\rangle
$$

$$
\begin{aligned}
= \quad & -4\mathrm{Re}\alpha_e I_0 \left(\frac{\pi a^2 \left| \mathbf{e}\left(\bar{\omega}\right) \right|^2}{\bar{\lambda}z} \right)^2 \frac{1}{z} \left(2\frac{J_1\left(\bar{v}_0\right)}{\bar{v}_0} \right)^2 \left[J_0\left(\bar{v}_0\right) - J_2\left(\bar{v}_0\right) \right] \\
& \times \left[1 + \left| \mu\left(\mathbf{q}_1, \mathbf{q}_2, \bar{\omega}\right) \right| \cos\left(\phi\left(\mathbf{q}_1, \mathbf{q}_2, \bar{\omega}\right) + \frac{2\bar{k}hy}{z} \right) \right] \\
& +4\mathrm{Re}\alpha_e I_0 \left(\frac{\pi a^2 \left| \mathbf{e}\left(\bar{\omega}\right) \right|^2}{\bar{\lambda}z} \right)^2 \frac{h\bar{k}y}{z^2} \left(2\frac{J_1\left(\bar{v}_0\right)}{\bar{v}_0} \right)^2 \\
& \times \left| \mu\left(\mathbf{q}_1, \mathbf{q}_2, \bar{\omega}\right) \right| \sin\left(\phi\left(\mathbf{q}_1, \mathbf{q}_2, \bar{\omega}\right) + \frac{2\bar{k}hy}{z} \right). \tag{B.4}
\end{aligned}
$$

Therefore

$$
\begin{aligned}
\left\langle \tilde{F}_z^{grad} \right\rangle \approx \quad & 4\mathrm{Re}\alpha_e I_0 \left(\frac{\pi a^2 \left| \mathbf{e}\left(\bar{\omega}\right) \right|^2}{\bar{\lambda}z} \right)^2 \frac{h\bar{k}y}{z^2} \left(2\frac{J_1\left(\bar{v}_0\right)}{\bar{v}_0} \right)^2 \\
& \times \left| \mu\left(\mathbf{q}_1, \mathbf{q}_2, \bar{\omega}\right) \right| \sin\left(\phi\left(\mathbf{q}_1, \mathbf{q}_2, \bar{\omega}\right) + \frac{2\bar{k}hy}{z} \right) \\
= \quad & -\frac{y}{z} \left\langle \tilde{F}_y^{grad} \right\rangle. \tag{B.5}
\end{aligned}
$$

The following equations express the scattering force in term of the spectral degree of coherence $|\mu\left(\mathbf{q}_1, \mathbf{q}_2, \bar{\omega}\right)|$

- *Calculation of $\tilde{F}_x^{sc}$*

$$
\begin{aligned}
\left\langle \tilde{F}_x^{sc} \right\rangle &= 4\mathrm{Im}\alpha_e I_0 \left(\frac{\pi a^2 \left|\mathbf{e}\left(\bar{\omega}\right)\right|^2}{\bar{\lambda}z}\right)^2 \frac{\bar{k}x}{z}\left(2\frac{J_1\left(\bar{v}_0\right)}{\bar{v}_0}\right)^2 \\
&\quad \times \left[1 + \left|\mu\left(\mathbf{q}_1, \mathbf{q}_2, \bar{\omega}\right)\right|\cos\left(\phi\left(\mathbf{q}_1, \mathbf{q}_2, \bar{\omega}\right) + \frac{2\bar{k}hy}{z}\right)\right].
\end{aligned} \tag{B.6}
$$

- *Calculation of $\tilde{F}_y^{sc}$*

$$
\begin{aligned}
\left\langle \tilde{F}_x^{sc} \right\rangle &= 4\mathrm{Im}\alpha_e I_0 \left(\frac{\pi a^2 \left|\mathbf{e}\left(\bar{\omega}\right)\right|^2}{\bar{\lambda}z}\right)^2 \frac{\bar{k}y}{z}\left(2\frac{J_1\left(\bar{v}_0\right)}{\bar{v}_0}\right)^2 \\
&\quad \times \left[1 + \left|\mu\left(\mathbf{q}_1, \mathbf{q}_2, \bar{\omega}\right)\right|\cos\left(\phi\left(\mathbf{q}_1, \mathbf{q}_2, \bar{\omega}\right) + \frac{2\bar{k}hy}{z}\right)\right].
\end{aligned} \tag{B.7}
$$

- *Calculation of $\tilde{F}_z^{sc}$*

$$
\begin{aligned}
\left\langle \tilde{F}_z^{sc} \right\rangle &= 4\bar{k}\mathrm{Im}\alpha_e I_0 \left(\frac{\pi a^2 \left|\mathbf{e}\left(\bar{\omega}\right)\right|^2}{\bar{\lambda}z}\right)^2 \left(2z^2 - x^2 - y^2\right)\left(2\frac{J_1\left(\bar{v}_0\right)}{\bar{v}_0}\right)^2 \\
&\quad \times \left[1 + \left|\mu\left(\mathbf{q}_1, \mathbf{q}_2, \bar{\omega}\right)\right|\cos\left(\phi\left(\mathbf{q}_1, \mathbf{q}_2, \bar{\omega}\right) + \frac{2\bar{k}hy}{z}\right)\right] \\
&\simeq 4\bar{k}\mathrm{Im}\alpha_e I_0 \left(\frac{\pi a^2 \left|\mathbf{e}\left(\bar{\omega}\right)\right|^2}{\bar{\lambda}z}\right)^2 \left(2\frac{J_1\left(\bar{v}_0\right)}{\bar{v}_0}\right)^2 \\
&\quad \times \left[1 + \left|\mu\left(\mathbf{q}_1, \mathbf{q}_2, \bar{\omega}\right)\right|\cos\left(\phi\left(\mathbf{q}_1, \mathbf{q}_2, \bar{\omega}\right) + \frac{2\bar{k}hy}{z}\right)\right] \\
&= 2\bar{k}\mathrm{Im}\alpha_e \left\langle I\left(\mathbf{r}, \bar{\omega}\right)\right\rangle.
\end{aligned} \tag{B.8}
$$

C

ANALYTICAL DERIVATION OF EXPRESSIONS FOR THE ELECTRIC, MAGNETIC AND INTERFERENCE FORCES OF CHAPTER 6

OPTICAL FORCES DUE TO THE PRIMARY SOURCE

In this part of the Appendix we address the main expressions which appear in Chapter 6 for the electromagnetic field which emerges into $z > 0$ the half-space.

C.1 ELECTRIC FORCE

The Green's function which relates the properties of the source placed at $z < 0$ and the free-propagation in $z > 0$ is expressed on using Weyl's expansion in terms of an angular spectrum of plane waves is [10, 131, 143]

$$G_{ij}^{EP}\left(\mathbf{r}, \mathbf{r}', \omega\right) = \frac{i}{2} \int_{-\infty}^{\infty} \frac{\mathrm{d}^2\mathbf{K}}{\left(2\pi\right)^2} G_{ij}^{EP}\left(\mathbf{K}\right) e^{i\mathbf{K}(\mathbf{R}-\mathbf{R}')} e^{i\gamma_2 z - i\gamma_1 z'}, \tag{C.1}$$

where the position vector is defined as $\mathbf{r} = (\mathbf{R}, z)$. In this equation, the angular Green's function is

$$G_{ij}^{EP}\left(\mathbf{K}\right) = \frac{1}{\gamma_1}\left(\hat{s}_i t_{12}^s \hat{s}_j + \hat{p}_{2i}^+ t_{12}^p \hat{p}_{1j}^+\right), \tag{C.2}$$

with $\gamma_i = \sqrt{\varepsilon_i \mu_i k_0^2 - K^2}$ if $\varepsilon_i \mu_i k_0^2 \geq K^2$, (homogeneous waves), and $\gamma_i = i\sqrt{K^2 - \varepsilon_i \mu_i k_0^2}$ if $\varepsilon_i \mu_i k_0^2 < K^2$, (evanescent waves); $(i = 1, 2)$. The vectors $\hat{s}$ and $\hat{p}$ are defined in the main text of Chapter 6. The superindices s and p denote the Fresnel transmission coefficient t_{12} from region 1 to region 2 through $z = 0$ under s and p-polarization, respectively, i.e. [1, 131]

$$t_{12}^s = \frac{2\gamma_1}{\gamma_1 + \gamma_2}, \qquad t_{12}^p = \frac{2n_1 n_2 \gamma_1}{\varepsilon_2 \gamma_1 + \varepsilon_1 \gamma_2}. \tag{C.3}$$

Notice that this notation is completely analogous to that of Chapter 2 using the wavevector $\mathbf{k} = (\mathbf{K}, \gamma_i)$ instead of the unitary wavevector $\mathbf{s} = (\mathbf{s}_\perp, s_z)$.

C.1.1 *Conservative electric force*

In this subsection I will calculate the gradient force. Using Eq. (6.11) of the main text, the auto-correlation function leads to

$$\left\langle E_j^{inc*}\left(\mathbf{r}\right) E_j^{inc}\left(\mathbf{r}\right)\right\rangle = \mu_0^2 \omega^4 \int_{V_{1,2}} G_{jk}^{EP*}\left(\mathbf{r},\mathbf{r}'_1\right) G_{jl}^{EP}\left(\mathbf{r},\mathbf{r}'_2\right) W_{kl}^{(P)}\left(\mathbf{r}'_1,\mathbf{r}'_2,\omega\right) d^3\mathbf{r}'_1 d^3\mathbf{r}'_2, \quad \text{(C.4)}$$

where $W_{kl}^{(P)}\left(\mathbf{r}'_1,\mathbf{r}'_2,\omega\right)$ is the cross-correlation function of the polarization currents. Substituting Eqs. (C.1) and (C.2) into Eq. (C.4) we obtain the auto-correlation function in terms of the angular Green's function

$$\begin{aligned}
\left\langle E_j^{inc*}\left(\mathbf{r}\right) E_j^{inc}\left(\mathbf{r}\right)\right\rangle &= \frac{\mu_0^2 \omega^4}{4} \int_{V_{1,2}} \int_{-\infty}^{\infty} \frac{d^2\mathbf{K}_1}{(2\pi)^2} \frac{d^2\mathbf{K}_2}{(2\pi)^2} G_{jk}^{EP*}\left(\mathbf{K}_1\right) G_{jl}^{EP}\left(\mathbf{K}_2\right) \\
&\times e^{-i\mathbf{K}_1\left(\mathbf{R}-\mathbf{R}'_1\right)} e^{i\mathbf{K}_2\left(\mathbf{R}-\mathbf{R}'_2\right)} e^{-\left(i\gamma_{2,1}^* z - i\gamma_{1,1}^* z'_1\right)} e^{i\gamma_{2,2} z - i\gamma_{1,2} z'_2} \\
&\times W_{kl}^{(P)}\left(\mathbf{r}'_1,\mathbf{r}'_2,\omega\right) d^3\mathbf{r}'_1 d^3\mathbf{r}'_2,
\end{aligned} \quad \text{(C.5)}$$

where $\gamma_{i,j}^2 = \varepsilon_i \mu_i k_0^2 - K_j^2$ and $(i,j) = 1,2$. Now we have to perform ten-integrals (six over the real space and four over the $\mathbf{K}$-space). To this end, we assume that $W_{kl}^{(P)}\left(\mathbf{r}'_1,\mathbf{r}'_2,\omega\right)$ has the following dependence

$$W_{kl}^{(P)}\left(\mathbf{r}'_1,\mathbf{r}'_2,\omega\right) = \mathcal{S}^{(P)}\left(\omega\right) \frac{e^{-\frac{|\mathbf{R}'_1-\mathbf{R}'_2|^2}{2\sigma^2}} e^{-\frac{|z'_1-z'_2|^2}{2\sigma^2}} \delta_{kl}}{(2\pi)^{3/2}\sigma^3} \quad \text{(C.6)}$$

Substituting Eq. (C.6) into Eq. (C.5) we obtain

$$\begin{aligned}
\left\langle E_j^{inc*}\left(\mathbf{r}\right) E_j^{inc}\left(\mathbf{r}\right)\right\rangle &= \frac{\mu_0^2 \omega^4}{4} \int_{V_{1,2}} \int_{-\infty}^{\infty} \frac{d^2\mathbf{K}_1}{(2\pi)^2} \frac{d^2\mathbf{K}_2}{(2\pi)^2} G_{jk}^{EP*}\left(\mathbf{K}_1\right) G_{jl}^{EP}\left(\mathbf{K}_2\right) \\
&\times e^{-i\mathbf{K}_1\left(\mathbf{R}-\mathbf{R}'_1\right)} e^{i\mathbf{K}_2\left(\mathbf{R}-\mathbf{R}'_2\right)} e^{-\left(i\gamma_{2,1}^* z - i\gamma_{1,1}^* z'_1\right)} e^{i\gamma_{2,2} z - i\gamma_{1,2} z'_2} \\
&\times \mathcal{S}^{(P)}\left(\omega\right) \frac{e^{-\frac{|\mathbf{R}'_1-\mathbf{R}'_2|^2}{2\sigma^2}} e^{-\frac{|z'_1-z'_2|^2}{2\sigma^2}} \delta_{kl}}{(2\pi)^{3/2}\sigma^3} d^2\mathbf{R}'_1 d^2\mathbf{R}'_2 dz'_1 dz'_2.
\end{aligned} \quad \text{(C.7)}$$

Our goal is to simplify this expression step by step in order to extract a physical meaning. Hence, we make the following change of variables: $\mathbf{R}'_1 = \mathbf{R}'' + \mathbf{R}'/2$, $\mathbf{R}'_2 = \mathbf{R}'' - \mathbf{R}'/2$.

$$\begin{aligned}
\left\langle E_j^{inc*}\left(\mathbf{r}\right) E_j^{inc}\left(\mathbf{r}\right)\right\rangle &= \frac{\mu_0^2 \omega^4}{4} \int_{V_{1,2}} \int_{-\infty}^{\infty} \frac{d^2\mathbf{K}_1}{(2\pi)^2} \frac{d^2\mathbf{K}_2}{(2\pi)^2} G_{jk}^{EP*}\left(\mathbf{K}_1\right) G_{jl}^{EP}\left(\mathbf{K}_2\right) \\
&\times e^{i(\mathbf{K}_2-\mathbf{K}_1)\mathbf{R}} e^{i\left(\frac{\mathbf{K}_2+\mathbf{K}_1}{2}\right)\mathbf{R}'} e^{-i(\mathbf{K}_2-\mathbf{K}_1)\mathbf{R}''} e^{-\left(i\gamma_{2,1}^* z - i\gamma_{1,1}^* z'_1\right)} e^{i\gamma_{2,2} z - i\gamma_{1,2} z'_2} \\
&\times \mathcal{S}^{(P)}\left(\omega\right) \frac{e^{-\frac{|\mathbf{R}'|^2}{2\sigma^2}} e^{-\frac{|z'_1-z'_2|^2}{2\sigma^2}} \delta_{kl}}{(2\pi)^{3/2}\sigma^3} d^2\mathbf{R}' d^2\mathbf{R}'' dz'_1 dz'_2.
\end{aligned} \quad \text{(C.8)}$$

Looking in detail this last expression we can see that the $\mathbf{R}''$-integration gives a two-dimensional delta function $\delta^{(2)}\left(\mathbf{K}_1-\mathbf{K}_2\right)$

$$\begin{aligned}
\left\langle E_j^{inc*}\left(\mathbf{r}\right) E_j^{inc}\left(\mathbf{r}\right)\right\rangle &= \frac{\mu_0^2 \omega^4}{4}(2\pi)^2 \int_{\mathbf{R}',z'_1,z'_2} \int_{-\infty}^{\infty} \frac{d^2\mathbf{K}_1}{(2\pi)^2} \frac{d^2\mathbf{K}_2}{(2\pi)^2} G_{jk}^{EP*}\left(\mathbf{K}_1\right) G_{jl}^{EP}\left(\mathbf{K}_2\right) \\
&\times e^{i(\mathbf{K}_2-\mathbf{K}_1)\mathbf{R}} e^{i\left(\frac{\mathbf{K}_2+\mathbf{K}_1}{2}\right)\mathbf{R}'} \delta\left(\mathbf{K}_2-\mathbf{K}_1\right) e^{-\left(i\gamma_{2,1}^* z - i\gamma_{1,1}^* z'_1\right)} e^{i\gamma_{2,2} z - i\gamma_{1,2} z'_2} \\
&\times \mathcal{S}^{(P)}\left(\omega\right) \frac{e^{-\frac{|\mathbf{R}'|^2}{2\sigma^2}} e^{-\frac{|z'_1-z'_2|^2}{2\sigma^2}} \delta_{kl}}{(2\pi)^{3/2}\sigma^3} d^2\mathbf{R}' dz'_1 dz'_2.
\end{aligned} \quad \text{(C.9)}$$

Now we perform the two-dimensional integral in $\mathbf{R}'$, in this case we have the Fourier transform of a Gaussian function, i.e.,

$$\frac{1}{(2\pi)^2} \int_{\mathbf{R}'} e^{i\left(\frac{\mathbf{K}_2 + \mathbf{K}_1}{2}\right)\mathbf{R}'} e^{-\frac{|\mathbf{R}'|^2}{2\sigma^2}} \mathrm{d}^2\mathbf{R}' = 2\pi\sigma^2 e^{-\frac{(\mathbf{K}_2 + \mathbf{K}_1)^2\sigma^2}{8}}, \tag{C.10}$$

then substituting in our main expression this leads to

$$\begin{aligned}
\left\langle E_j^{inc*}(\mathbf{r}) E_j^{inc}(\mathbf{r}) \right\rangle &= \frac{\mu_0^2\omega^4}{4}(2\pi)^4 2\pi\sigma^2 \int_{z_1', z_2'} \int_{-\infty}^{\infty} \frac{\mathrm{d}^2\mathbf{K}_1}{(2\pi)^2} \frac{\mathrm{d}^2\mathbf{K}_2}{(2\pi)^2} G_{jk}^{EP*}(\mathbf{K}_1) G_{jl}^{EP}(\mathbf{K}_2) \\
&\times\ e^{i(\mathbf{K}_2 - \mathbf{K}_1)\mathbf{R}} e^{-\frac{(\mathbf{K}_2 + \mathbf{K}_1)^2\sigma^2}{8}} \delta(\mathbf{K}_2 - \mathbf{K}_1) e^{-\left(i\gamma_{2,1}^* z - i\gamma_{1,1}^* z_1'\right)} e^{i\gamma_{2,2} z - i\gamma_{1,2} z_2'} \\
&\times\ \mathcal{S}^{(P)}(\omega) \frac{e^{-\frac{|z_1' - z_2'|^2}{2\sigma^2}} \delta_{kl}}{(2\pi)^{3/2}\sigma^3} \mathrm{d}z_1' \mathrm{d}z_2'.
\end{aligned} \tag{C.11}$$

The integral in $\mathbf{K}_1$ (or $\mathbf{K}_2$) is straightforward, thus eliminating the Kronecker function our complex integrals are reduced to

$$\begin{aligned}
\left\langle E_j^{inc*}(\mathbf{r}) E_j^{inc}(\mathbf{r}) \right\rangle &= \frac{\mu_0^2\omega^4}{4} 2\pi\sigma^2 \int_{z_1', z_2'} \int_{-\infty}^{\infty} \mathrm{d}^2\mathbf{K} \left| G_{jk}^{EP*}(\mathbf{K}) \right|^2 \\
&\times\ e^{-\frac{(\mathbf{K}\sigma)^2}{2}} e^{i(\gamma_2 - \gamma_2^*)z} e^{\left(i\gamma_1^* z_1'\right)} e^{-i\gamma_1 z_2'} \\
&\times\ \mathcal{S}^{(P)}(\omega) \frac{e^{-\frac{|z_1' - z_2'|^2}{2\sigma^2}}}{(2\pi)^{3/2}\sigma^3} \mathrm{d}z' \mathrm{d}z''.
\end{aligned} \tag{C.12}$$

Now we make a similar change of variables for the z-coordinate: $z_1' = z'' + z'/2$ and $z_2' = z'' - z'/2$, which gives

$$\begin{aligned}
\left\langle E_j^{inc*}(\mathbf{r}) E_j^{inc}(\mathbf{r}) \right\rangle &= \frac{\mu_0^2\omega^4}{4} 2\pi\sigma^2 \int_{z', z''} \int \mathrm{d}^2\mathbf{K} \left| G_{jk}^{EP*}(\mathbf{K}) \right|^2 \\
&\times\ e^{-\frac{(\mathbf{K}\sigma)^2}{2}} e^{-2\mathrm{Im}\gamma_2 z} e^{i\mathrm{Re}\gamma_1 z'} e^{2\mathrm{Im}\gamma_1 z''} \mathcal{S}^{(P)}(\omega) \frac{e^{-\frac{|z'|^2}{2\sigma^2}}}{(2\pi)^{3/2}\sigma^3} \mathrm{d}z' \mathrm{d}z''.
\end{aligned} \tag{C.13}$$

Notice that after making the change of variable, and due the fact that the volume of the source is at $z < 0$, we can perform the following integrals:

$$\int_{-\infty}^{0} e^{2z''\mathrm{Im}\gamma_1} \mathrm{d}z'' = \frac{1}{2\mathrm{Im}\gamma_1}, \tag{C.14}$$

$$\int_{-\infty}^{\infty} e^{i\mathrm{Re}\gamma_1 z'} e^{-\frac{z'^2}{2\sigma^2}} \mathrm{d}z' = e^{-\frac{1}{2}(\sigma\mathrm{Re}\gamma_1)^2} \sqrt{2\pi}\sigma. \tag{C.15}$$

Thus, substituting Eqs. (C.14)-(C.15) into Eq. (C.13) we have

$$\left\langle E_j^{inc*}(\mathbf{r}) E_j^{inc}(\mathbf{r}) \right\rangle = \frac{\mu_0^2\omega^4}{4} \mathcal{S}^{(P)}(\omega) \int_{-\infty}^{\infty} \frac{1}{2\mathrm{Im}\gamma_1} \left| G_{jk}^{EP}(\mathbf{K}) \right|^2 e^{-\frac{(\mathbf{K}\sigma)^2}{2}} e^{-2\mathrm{Im}\gamma_2 z} e^{-\frac{1}{2}\sigma^2 \mathrm{Re}\gamma_1^2} \mathrm{d}^2\mathbf{K} \tag{C.16}$$

Now, using cylindrical coordinates $(K_x, K_y) = K(\cos\theta, \sin\theta)$ our complex expression is simplified to :

$$\left\langle E_j^{inc*}(\mathbf{r}) E_j^{inc}(\mathbf{r}) \right\rangle = \frac{k_0^4\pi}{4\varepsilon_0^2} \mathcal{S}^{(P)}(\omega) \int_{-\infty}^{\infty} \frac{1}{\mathrm{Im}\gamma_1} \left| G_{jk}^{EP}(K) \right|^2 e^{-\frac{(K\sigma)^2}{2}} e^{-2\mathrm{Im}\gamma_2 z} e^{-\frac{1}{2}\sigma^2 \mathrm{Re}\gamma_1^2} K \mathrm{d}K \tag{C.17}$$

This equation will be very useful in order to calculate the electric force from the induced dipoles and to verify the results of Chapter 2 (cf. Appendix A). We see that Eq. (C.17) only depends on the position trough the z-component of the space, hence, if we calculate the gradient electric force we obtain that $F_{x,y} = 0$. Notice also that the range of integration of this quantity is $[-\infty, \infty]$. If we take the expression of the angular Green's function into account we have

$$\left| G_{jk}^{EP} \left(\mathbf{K} \right) \right|^2 = \frac{1}{|\gamma_1|^2} \left[|t_{12}^s|^2 \, |\hat{\mathbf{s}}|^2 \, |\hat{\mathbf{s}}|^2 + |t_{12}^p|^2 \, |\hat{\mathbf{p}}_1^+|^2 \, |\hat{\mathbf{p}}_2^+|^2 \right], \tag{C.18}$$

and the third component of the gradient force is

$$\begin{aligned}
\langle F_z^{e,cons} \rangle &= -\frac{k_0^4 \pi}{8\varepsilon_0} \mathrm{Re}\alpha_e \mathcal{S}^{(P)}(\omega) \int_{K=k_0}^{K=+\infty} \frac{\sqrt{K^2 - k_0^2}}{|\gamma_1|^2} e^{-\frac{(K\sigma)^2}{2}} \\
&\times \left[|t_{12}^s|^2 + \frac{|t_{12}^p|^2}{|n_1|^2 |n_2|^2 k_0^4} \left(|\gamma_2|^2 + K^2 \right) \left(|\gamma_1|^2 + K^2 \right) \right] \\
&\times e^{-2z\mathrm{Im}\gamma_2} \frac{1}{\mathrm{Im}\gamma_1} e^{-\frac{1}{2}\sigma^2 \mathrm{Re}\gamma_1^2} K\mathrm{d}K
\end{aligned} \tag{C.19}$$

In this nice expression, the integral is performed over the evanescent modes. This is because the partial derivative ∂_z of Eq. (C.17) is proportional to $\mathrm{Im}\gamma_2$, and this expression is different from zero for these modes only. The last integral has to be done numerically.

C.1.2 *Asymptotic expression in extreme near-field*

Now we will calculate the force in the near-field. Firstly let us explicitly introduce the Fresnel coefficients into Eq. (C.19), this leads to

$$\begin{aligned}
\langle F_z^{e,cons} \rangle &= -\frac{k_0^4 \pi}{2\varepsilon_0} \mathrm{Re}\alpha_e \mathcal{S}^{(P)}(\omega) \int_{K=k_0}^{K=+\infty} \sqrt{K^2 - k_0^2} e^{-\frac{(K\sigma)^2}{2}} \\
&\times \left[\frac{1}{|\gamma_1 + \gamma_2|^2} + \frac{1}{|\varepsilon_2\gamma_1 + \varepsilon_1\gamma_2|^2 k_0^4} \left(|\gamma_2|^2 + K^2 \right) \left(|\gamma_1|^2 + K^2 \right) \right] \\
&\times e^{-2z\mathrm{Im}\gamma_2} \frac{1}{\mathrm{Im}\gamma_1} e^{-\frac{1}{2}\sigma^2 \mathrm{Re}\gamma_1^2} K\mathrm{d}K.
\end{aligned} \tag{C.20}$$

Because we are very near of the source ($z \ll \lambda$), the main contribution in Eq. (C.19) is given by values of $K \gg k_0$. Under this assumption $\gamma_1 \approx \gamma_2 = iK$, giving

$$\langle F_z^{e,cons} \rangle = -\frac{k_0^4 \pi}{2\varepsilon_0} \mathrm{Re}\alpha_e \mathcal{S}^{(P)}(\omega) \int_{K=k_0}^{K=+\infty} e^{-\frac{(K\sigma)^2}{2}} \left[\frac{1}{4K^2} + \frac{4K^2}{|\varepsilon_2 + \varepsilon_1|^2 k_0^4} \right] e^{-2zK} K\mathrm{d}K. \tag{C.21}$$

In this expression, the term $1/K^2$ is negligible giving an integral which can be performed analytically:

$$\langle F_z^{e,cons} \rangle = -\frac{2\pi}{|\varepsilon_2 + \varepsilon_1|^2 \varepsilon_0} \mathrm{Re}\alpha_e \mathcal{S}^{(P)}(\omega) \int_{K=k_0}^{K=+\infty} e^{-\frac{(K\sigma)^2}{2}} e^{-2zK} K^3 \mathrm{d}K. \tag{C.22}$$

This integral will give an asymptotic behavior $1/z^4$ or $1/\sigma^4$ depending on whether the correlation length is null or not (cf. Eqs. (6.18)-(6.19)).

c.1.3 *Non-conservative electric force*

As we have seen in many parts of this thesis, the non-conservative force is proportional to $\mathrm{Im}\left\{E_j^* \partial_i E_j\right\}$. If we calculate the term $E_j^* \partial_i E_j$ we will obtain:

$$
\begin{aligned}
\left\langle E_j^{inc*}\left(\mathbf{r}\right) \partial_i E_j^{inc}\left(\mathbf{r}\right)\right\rangle &= \frac{\mu_0^2 \omega^4}{4} \int_{V_{1,2}} \int_{-\infty}^{\infty} \frac{\mathrm{d}^2 \mathbf{K}_1}{(2\pi)^2} \frac{\mathrm{d}^2 \mathbf{K}_2}{(2\pi)^2} G_{jk}^{EP*}\left(\mathbf{K}_1\right) G_{jl}^{EP}\left(\mathbf{K}_2\right) i\left(\mathbf{K}_2, \gamma_{2,2}\right) \\
&\times\ e^{-i\mathbf{K}_1\left(\mathbf{R}-\mathbf{R}_1'\right)} e^{i\mathbf{K}_2\left(\mathbf{R}-\mathbf{R}_2'\right)} e^{-\left(i\gamma_{2,1}^* z - i\gamma_{1,1}^* z_1'\right)} e^{i\gamma_{2,2} z - i\gamma_{1,2} z_2'} \\
&\times\ W_{kl}^{(P)}\left(\mathbf{r}_1', \mathbf{r}_2', \omega\right) \mathrm{d}^3 \mathbf{r}_1' \mathrm{d}^3 \mathbf{r}_2',
\end{aligned}
\tag{C.23}
$$

where this last expression is exactly the same as Eq. (C.5) with an important exception which will be discussed in brief.

Due to the similarity between this equation and the theoretical development of the previous section we will no enter in detail about how to obtain the non-conservative force, nevertheless, the important key is in the first line of this equation. In this line we have the term $i\left(\mathbf{K}, \gamma_2\right)$, if we assume that the integration over the lateral components of the force is zero (this can be easily proved), we have that the third component of the force is proportional to $i\gamma_2$, where this quantity will be imaginary if and only if $\varepsilon_i \mu_i k_0^2 \geq K^2$, i.e., for propagating modes. Due to this fact, the range of integration of Eq. (6.14) of the main text is extended over the homogeneous part of the angular wave spectrum, and the factor $\exp\left(-2z_0 \mathrm{Im}\gamma_2\right)$ is equal to 1, then the non-conservative force does not depend on the position.

c.2 MAGNETIC FORCE

For a statistically homogeneous source, the electric and magnetic energy are equal (see reference [32]), hence

$$
\begin{aligned}
F_i^m\left(\mathbf{r}\right) &= \frac{\mu_0 \mu_2}{2} \mathrm{Re}\left\{\left\langle \alpha_m H_j^*\left(\mathbf{r}\right) \partial_i H_j\left(\mathbf{r}\right)\right\rangle\right\} \\
&= \frac{\varepsilon_0 \mu_2}{4} \mathrm{Re}\left\{\alpha_m\right\} \partial_i \left\langle E_j^*\left(\mathbf{r}\right) E_j\left(\mathbf{r}\right)\right\rangle \\
&+ \frac{\varepsilon_0 \mu_2}{2} \mathrm{Re}\left\{\alpha_m\right\} \mathrm{Im}\left\{\left\langle E_j^*\left(\mathbf{r}\right) \partial_i E_j\left(\mathbf{r}\right)\right\rangle\right\}
\end{aligned}
\tag{C.24}
$$

The conservative (second line) and the non-conservative (third line) magnetic forces have been calculated in the previous section.

C.3 INTERFERENCE FORCE

The force due to the interference of the electric and magnetic dipoles is proportional to $\langle \mathbf{E}^* \times \mathbf{H} \rangle_i$ $= \epsilon_{ijk} \left\langle E_j^* H_k \right\rangle$. The electric and magnetic incident fields are

$$E_j^{inc}(\mathbf{r}) = \mu_0 \omega^2 \int_V G_{jl}^{EP}(\mathbf{r}, \mathbf{r}', \omega) P_l(\mathbf{r}', \omega) d^3\mathbf{r}' \tag{C.25}$$

$$H_k^{inc}(\mathbf{r}) = -i\omega \int_V G_{km}^{HP}(\mathbf{r}, \mathbf{r}', \omega) P_m(\mathbf{r}', \omega) d^3\mathbf{r}' \tag{C.26}$$

The first equation is the same of Section (C.1) with the electric Green's function $G_{jl}^{EP}(\mathbf{r}, \mathbf{r}', \omega)$, however, the magnetic Green's function $G_{km}^{HP}(\mathbf{r}, \mathbf{r}', \omega)$ is

$$G_{km}^{HP}(\mathbf{r}, \mathbf{r}', \omega) = \frac{k_0 n_2}{2} \int \frac{d^2\mathbf{K}}{(2\pi)^2} G_{km}^H(\mathbf{K}) e^{i\mathbf{K}(\mathbf{R}-\mathbf{R}')} e^{i\gamma_2 z - i\gamma_1 z'}, \tag{C.27}$$

with

$$G_{km}^H(\mathbf{K}) = \frac{1}{\gamma_1} \left(\hat{p}_{2k}^+ t_{21}^s \hat{s}_m - \hat{s}_k t_{21}^p \hat{p}_{1m}^+ \right). \tag{C.28}$$

If we calculate the quantity $\langle \mathbf{E}^* \times \mathbf{H} \rangle_i$ we have

$$\epsilon_{ijk} \left\langle E_j^{inc*} H_k^{inc} \right\rangle = -i\mu_0 \omega^3 \epsilon_{ijk} \int_{V_1, V_2} G_{jl}^{EP*}(\mathbf{r}, \mathbf{r}_1') G_{km}^{HP}(\mathbf{r}, \mathbf{r}_2') W_{kl}^{(P)}(\mathbf{r}_1', \mathbf{r}_2', \omega) \, d^3\mathbf{r}_1' d^3\mathbf{r}_2'. \tag{C.29}$$

This equation is analogous to Eq. (C.4), hence, the methodology is very similar, (the spatial dependence of the Green's functions is the same), however, the difference will be given by the product of the electric and magnetic angular Green's functions which is:

$$\begin{aligned} \varepsilon_{ijk} G_{jl}^{EP*}(\mathbf{K}) G_{kl}^{HP}(\mathbf{K}) &= \frac{1}{|\gamma_1|^2} \left[\left(\hat{s}_i t_{12}^{s*} \hat{s}_j + \hat{p}_{2i}^{+*} t_{12}^{p*} \hat{p}_{1j}^{*+} \right) \left(\hat{p}_{2k}^+ t_{21}^s \hat{s}_m - \hat{s}_k t_{21}^p \hat{p}_{1m}^+ \right) \right] \\ &= -\frac{1}{n_2 k_0} \left(\gamma_2 |\hat{s}_l|^2 |t_{12}^s|^2 + \gamma_2^* |t_{12}^p|^2 |\hat{p}_{1l}^+|^2 \right) \end{aligned} \tag{C.30}$$

Hence, we have an expression analogous to Eq. (C.17) (again, only the third component $i = 3 = z$ will be different from zero) where the range of integration in K will be $[-\infty, \infty]$. However, at the end, we have to extract the real and the imaginary parts. If we look at Eq (C.30), this expression will be purely imaginary for evanescent modes

$$\varepsilon_{3jk} \mathrm{Im} G_{jl}^{EP}(\mathbf{K})^* G_{kl}^H(\mathbf{K}) = -\frac{\sqrt{K^2 - k_0^2}}{n_2 k_0} \left(|\hat{s}_l|^2 |t_{12}^s|^2 - |t_{12}^p|^2 |\hat{p}_{1l}^+|^2 \right), \tag{C.31}$$

and purely real for propagating waves

$$\varepsilon_{3jk} \mathrm{Re} G_{jl}^{EP}(\mathbf{K})^* G_{kl}^H(\mathbf{K}) = -\frac{\sqrt{k_0^2 - K^2}}{n_2 k_0} \left(|\hat{s}_l|^2 |t_{12}^s|^2 + |t_{12}^p|^2 |\hat{p}_{1l}^+|^2 \right). \tag{C.32}$$

Taking these last two expressions into account, and the part of the interference force which has the imaginary part of the product of the polarizabilities, i.e.,

$$F_i^{em,imag}(\mathbf{r}) = \varepsilon_0 \varepsilon_2 \frac{Z k_0^4}{12\pi} \mathrm{Im}\{\alpha_e^* \alpha_m\} \mathrm{Im}\left\{ \langle \mathbf{E}^*(\mathbf{r}) \times \mathbf{H}(\mathbf{r}) \rangle_i \right\}, \tag{C.33}$$

we obtain that the third component is

$$
\begin{aligned}
F_z^{em,imag}\left(\mathbf{r}\right) &= \frac{k_0^7}{48\varepsilon_0}\operatorname{Im}\left\{\alpha_e^*\alpha_m\right\}S^{(P)}\left(\omega\right)\int_{K=k_0}^{K=\infty}\frac{\sqrt{K^2-k_0^2}}{\left|\gamma_1\right|^2}e^{-\frac{(\mathbf{K}\sigma)^2}{2}} \\
&\times \left[\left|t_{12}^s\right|^2-\left|t_{12}^p\right|^2\frac{1}{\left|n_1\right|^2k_0^2}\left(\left|\gamma_1\right|^2+K^2\right)\right]\frac{1}{\operatorname{Im}\gamma_1}e^{-2z\operatorname{Im}\gamma_2}e^{-\frac{1}{2}\sigma^2\operatorname{Re}\gamma_1^2}K\mathrm{d}K.
\end{aligned}
\tag{C.34}
$$

Notice that this equation is similar to that of the conservative forces in the sense that the integration has to be performed only for non-propagating modes and it has an evanescent behavior with the distance. Contrary to this, the part of the interference force which has the real part of the product of the polarizabilities, i.e.,

$$
F_i^{em,real}\left(\mathbf{r}\right) = -\varepsilon_0\varepsilon_2\frac{Zk_0^4}{12\pi}\operatorname{Im}\left\{\alpha_e^*\alpha_m\right\}\operatorname{Im}\left\{\left\langle\mathbf{E}^*\left(\mathbf{r}\right)\times\mathbf{H}\left(\mathbf{r}\right)\right\rangle_i\right\},
\tag{C.35}
$$

is given by

$$
\begin{aligned}
F_z^{em,real}\left(\mathbf{r}\right) &= -\frac{k_0^7}{48\varepsilon_0}\operatorname{Re}\left\{\alpha_e^*\alpha_m\right\}S^{(P)}\left(\omega\right)\int_{K=0}^{K=k_0}\frac{\sqrt{k_0^2-K^2}}{\left|\gamma_1\right|^2}e^{-\frac{(\mathbf{K}\sigma)^2}{2}} \\
&\times \left[\left|t_{12}^s\right|^2+\left|t_{12}^p\right|^2\frac{1}{\left|n_1\right|^2k_0^2}\left(\left|\gamma_1\right|^2+K^2\right)\right]\frac{1}{\operatorname{Im}\gamma_1}e^{-\frac{1}{2}\sigma^2\operatorname{Re}\gamma_1^2}K\mathrm{d}K
\end{aligned}
\tag{C.36}
$$

This expression plays the role of a non-conservative force in the sense that only the propagating modes are relevant. It is worth remarking that this force does not depend on the position and will be negative (positive) when $\operatorname{Re}\left\{\alpha_e^*\alpha_m\right\}$ is positive (negative), pulling the particle towards the plane of the source.

OPTICAL FORCES DUE TO THE INDUCED DIPOLES

C.4 ELECTRIC FORCE

In this case, the electric field will be due to the electric and magnetic induced dipoles, i.e, $E_i^p(\mathbf{r})$, $E_i^m(\mathbf{r})$. Now the source (the dipoles) will be placed in front of the primary source, hence it will exist an interaction between them in the $z > 0$ half-space. This interaction will be encoded in the Green's function of the system. The expressions for the electromagnetic field generated by the electric dipole will be

$$
\begin{align}
E_i^p(\mathbf{r}) &= \mu_0\mu_1\omega^2 G_{ij}^{Ep}(\mathbf{r},\mathbf{r}',\omega)\, p_j(\omega), \tag{C.37}\\
H_i^p(\mathbf{r}) &= -i\omega G_{ij}^{Hp}(\mathbf{r},\mathbf{r}',\omega)\, p_j(\omega), \tag{C.38}
\end{align}
$$

and for the magnetic dipole [43, 121],

$$
\begin{align}
E_i^m(\mathbf{r}) &= \frac{Z_0 i\omega}{c} G_{ij}^{Hp\leftrightarrow}(\mathbf{r},\mathbf{r}',\omega)\, m_j(\omega), \tag{C.39}\\
H_i^m(\mathbf{r}) &= \frac{\mu_0\mu_1\omega^2}{Z_0 c} G_{ij}^{Ep\leftrightarrow}(\mathbf{r},\mathbf{r}',\omega)\, m_j(\omega), \tag{C.40}
\end{align}
$$

where the symbol $\leftrightarrow$ refers to we are using the same Green's function with the reflection Fresnel coefficients interchanged, i.e.,

$$
\begin{align}
G_{ij}^{Ep}(\mathbf{r},\mathbf{r}',\omega) &= \frac{i}{2}\int\frac{d^2\mathbf{K}}{(2\pi)^2}\frac{1}{\gamma_2}G_{ij}^{Ep}(\mathbf{K})\,e^{i\mathbf{K}(\mathbf{R}-\mathbf{R}')}e^{i\gamma_2(z+z')}, \tag{C.41a}\\
G_{ij}^{Hp}(\mathbf{r},\mathbf{r}',\omega) &= \frac{k_0 n_2}{2}\int\frac{d^2\mathbf{K}}{(2\pi)^2}\frac{1}{\gamma_2}G_{ij}^{Hp}(\mathbf{K})\,e^{i\mathbf{K}(\mathbf{R}-\mathbf{R}')}e^{i\gamma_2(z+z')}, \tag{C.41b}\\
G_{ij}^{Ep\leftrightarrow}(\mathbf{r},\mathbf{r}',\omega) &= \frac{i}{2}\int\frac{d^2\mathbf{K}}{(2\pi)^2}\frac{1}{\gamma_2}G_{ij}^{Ep\leftrightarrow}(\mathbf{K})\,e^{i\mathbf{K}(\mathbf{R}-\mathbf{R}')}e^{i\gamma_2(z+z')}, \tag{C.41c}\\
G_{ij}^{Hp\leftrightarrow}(\mathbf{r},\mathbf{r}',\omega) &= \frac{k_0 n_2}{2}\int\frac{d^2\mathbf{K}}{(2\pi)^2}\frac{1}{\gamma_2}G_{ij}^{Hp\leftrightarrow}(\mathbf{K})\,e^{i\mathbf{K}(\mathbf{R}-\mathbf{R}')}e^{i\gamma_2(z+z')}. \tag{C.41d}
\end{align}
$$

The angular Green's function are

$$
\begin{align}
G_{ij}^{Ep}(\mathbf{K}) &= \hat{s}_i r_{21}^s \hat{s}_j + \hat{p}_{1i}^+ r_{21}^p \hat{p}_{1j}^-, \tag{C.42a}\\
G_{ij}^{Hp}(\mathbf{K}) &= \hat{p}_{1i}^+ r_{21}^s \hat{s}_j - \hat{s}_i r_{21}^p \hat{p}_{1j}^-, \tag{C.42b}\\
G_{ij}^{Ep\leftrightarrow}(\mathbf{K}) &= \hat{s}_i r_{21}^p \hat{s}_j + \hat{p}_{2i}^+ r_{21}^s \hat{p}_{2j}^-, \tag{C.42c}\\
G_{ij}^{Hp\leftrightarrow}(\mathbf{K}) &= \hat{p}_{2i}^+ r_{21}^p \hat{s}_j - \hat{s}_i r_{21}^s \hat{p}_{2j}^-, \tag{C.42d}
\end{align}
$$

being r_{21}^s, r_{21}^p the reflection Fresnel coefficients

$$
r_{21}^s = \frac{\gamma_2 - \gamma_1}{\gamma_2 + \gamma_1}, \quad r_{21}^p = \frac{\varepsilon_1\gamma_2 - \varepsilon_2\gamma_1}{\varepsilon_1\gamma_2 + \varepsilon_2\gamma_1}. \tag{C.43}
$$

C.4.1 *Conservative electric force*

For the electric force we need the auto-correlation function $\left\langle E_j^* \left(\mathbf{r} \right) E_j \left(\mathbf{r} \right) \right\rangle$ of the fields from the electric and magnetic dipoles. In this case, we have assumed that the cross-correlation between the electric and magnetic dipole is zero, i.e., $\left\langle p_k^* \left(\mathbf{r}_1', \omega \right) m_l \left(\mathbf{r}_1', \omega \right) \right\rangle = 0$ (see [79]), hence

$$
\left\langle E_j^{p*} \left(\mathbf{r} \right) E_j^p \left(\mathbf{r} \right) \right\rangle = \mu_0^2 \mu_2^2 \omega^4 G_{jk}^{E*} \left(\mathbf{r}, \mathbf{r}', \omega \right) G_{jl}^{E} \left(\mathbf{r}, \mathbf{r}', \omega \right) \left\langle p_k^* \left(\mathbf{r}_1', \omega \right) p_l \left(\mathbf{r}_1', \omega \right) \right\rangle, \tag{C.44}
$$

$$
\left\langle E_j^{m*} \left(\mathbf{r} \right) E_j^m \left(\mathbf{r} \right) \right\rangle = \left(\frac{Z\omega}{c} \right)^2 G_{jk}^{H\leftrightarrow*} \left(\mathbf{r}, \mathbf{r}', \omega \right) G_{jl}^{H\leftrightarrow} \left(\mathbf{r}, \mathbf{r}', \omega \right) \left\langle m_k^* \left(\mathbf{r}_1', \omega \right) m_l \left(\mathbf{r}_1', \omega \right) \right\rangle, \tag{C.45}
$$

where the induced dipoles can be written in terms of the incident fields

$$
p_k \left(\mathbf{r}, \omega \right) = \varepsilon_0 \varepsilon_2 \alpha_e \left(\omega \right) E_k^{inc} \left(\mathbf{r}, \mathbf{r}_1', \omega \right), \tag{C.46}
$$

$$
m_k \left(\mathbf{r}, \omega \right) = \alpha_m \left(\omega \right) H_k^{inc} \left(\mathbf{r}, \mathbf{r}_1', \omega \right), \tag{C.47}
$$

leading to

$$
\begin{aligned}
\left\langle E_j^{p*} \left(\mathbf{r} \right) E_j^p \left(\mathbf{r} \right) \right\rangle &= \mu_0^2 \mu_2^2 \omega^4 G_{jk}^{Ep*} \left(\mathbf{r}, \mathbf{r}', \omega \right) G_{jl}^{Ep} \left(\mathbf{r}, \mathbf{r}', \omega \right) \left\langle p_k^* \left(\mathbf{r}_2', \omega \right) p_l \left(\mathbf{r}_2', \omega \right) \right\rangle \\
&= |\varepsilon_2|^2 |\alpha_e|^2 k_0^4 G_{jk}^{Ep*} \left(\mathbf{r}, \mathbf{r}', \omega \right) G_{jl}^{Ep} \left(\mathbf{r}, \mathbf{r}', \omega \right) \left\langle E_k^{inc*} E_l^{inc} \right\rangle,
\end{aligned} \tag{C.48}
$$

and analogously for $\left\langle E_j^{m*} \left(\mathbf{r} \right) E_j^m \left(\mathbf{r} \right) \right\rangle$. As we can see from this last equation, the term $\left\langle E_k^{inc*} E_l^{inc} \right\rangle$ has been calculated previously and the product of the Green's functions is

$$
G_{jk}^{Ep*} \left(\mathbf{r}, \mathbf{r}', \omega \right) G_{jl}^{Ep} \left(\mathbf{r}, \mathbf{r}', \omega \right) = \left| \frac{i}{2} \int \frac{KdK}{\left(2\pi \right)} \frac{1}{\gamma_2} \left(r_{121}^s + \frac{r_{21}^p}{\left(n_2 k_0 \right)^2} \left(\gamma_2^2 - K^2 \right) \right) e^{i\gamma_2 \left(z + z' \right)} \right|^2, \tag{C.49}
$$

hence we can calculate the conservative gradient force because we have the expression for $\left\langle E_j^{p*} \left(\mathbf{r} \right) E_j^p \left(\mathbf{r} \right) \right\rangle$. It is worth saying that for the electric force due to the magnetic dipole, and because we want the force at the position of the dipole, the integration of the product of the functions $G_{jk}^{Hp\leftrightarrow*} \left(\mathbf{r}, \mathbf{r}', \omega \right) G_{jl}^{Hp\leftrightarrow} \left(\mathbf{r}, \mathbf{r}', \omega \right)$ is zero, then, the electric force due to the induced magnetic dipole is also zero. Similar to this will occur for the magnetic force due to the electric dipole.

The rest of the procedure is analogous to Section C.1, leading to the product of two single integrals in K, one for $G_{jk}^{Ep*} \left(\mathbf{r}, \mathbf{r}', \omega \right) G_{jl}^{Ep} \left(\mathbf{r}, \mathbf{r}', \omega \right)$ and one for $\left\langle E_k^{inc*} \left(\mathbf{r}_2, \mathbf{r}_1', \omega \right) E_l^{inc} \left(\mathbf{r}_2, \mathbf{r}_1', \omega \right) \right\rangle$ which are solved numerically.

C.4.2 *Non-conservative electric force*

The calculus of the force will be similar to the previous one, however, we have to calculate the product $G_{jk}^{EP*}\left(\mathbf{r},\mathbf{r}',\omega\right)\partial_i G_{jk}^{EP}\left(\mathbf{r},\mathbf{r}',\omega\right)$, i.e,

$$
\begin{aligned}
G_{jk}^{E*}\left(\mathbf{r},\mathbf{r}',\omega\right)\partial_i G_{jk}^{E}\left(\mathbf{r},\mathbf{r}',\omega\right) &= \frac{-i}{2}\int\frac{d^2\mathbf{K}}{(2\pi)^2}\frac{1}{\gamma_2^*}G_{ij}^{E*}\left(\mathbf{K}\right)e^{-i\mathbf{K}(\mathbf{R}-\mathbf{R}')}e^{-i\gamma_2^*(z+z')} \\
&\times \frac{-1}{2}\int\frac{d^2\mathbf{K}}{(2\pi)^2}\frac{1}{\gamma_2}G_{ij}^{E}\left(\mathbf{K}\right)\left(\mathbf{K},\gamma_2\right)e^{i\mathbf{K}(\mathbf{R}-\mathbf{R}')}e^{i\gamma_2(z+z')}.
\end{aligned}
$$

(C.50)

The induced electric dipole (again, the contribution of the magnetic dipole will be zero) will be given by the term $\left\langle E_k^{inc*}\left(\mathbf{r}_2,\mathbf{r}_1',\omega\right)E_l^{inc}\left(\mathbf{r}_2,\mathbf{r}_1',\omega\right)\right\rangle$.

C.5 MAGNETIC AND INTERFERENCE FORCES

For obviously reasons, from the above sections it is not necessary to give details of the calculation of these equations.

D

NEAR-FIELD PHOTONIC FORCES FROM GAUSSIAN-SCHELL MODEL SOURCES

This appendix deals with numerical calculations from COMSOL software. Here I will try to understand the role of the spot size, coherence length and evanescent modes of a one-dimensional GSMS. The fundamentals of the simulations are explained in detail in Chapter 8.

I illustrate force calculations based on the coherent mode representation (CMR) of Section 8.5 (cf. Chapter 8). We address a cylinder of radius $\lambda/100$, made of Silica glass ($\varepsilon_p = 2.1$), illuminated by a GSMS placed at $y = 0$, (cf. Eq. (8.8)). The distance between the source and the center of the particle is $\lambda/10$. The number of modes is determined by the ratio σ_g/σ_s, the first mode ($q = 0$) corresponding to the globally spatial coherent case studied in Section 8.3.1. The scheme of the simulation window in which the beam propagates and is scattered by the particle, as well as the method to calculate the optical forces, is similar to that previously explained in Section 8.10, now for a single particle.

Fig. D.1 displays the calculated force Cartesian components. Here one cannot separate the conservative and non-conservative components of the force since in Eq. (8.6) the MST flow yields the total force. Each row of Fig. D.1 represents the ensemble-averaged forces $\langle F_x \rangle$ and $\langle F_y \rangle$ for different values of σ_s and σ_g, (see the legend of the figure). The first column, [Figs. D.1(a), (d)], contains $\langle F_x \rangle$ and $\langle F_y \rangle$ for the same parameters of Figs. 8.1 and 8.2, (by inverting the color - line code). We see that for a fully coherent source, as we decrease the value of the spot size σ_s, the magnitude of the force increases. We also observe how $\langle F_y \rangle$ is negative, (i.e. the particle is pulled to the plane of the source), for $\sigma_s < 0.3\lambda$; this is due to the contribution of the evanescent waves. In the main text of Chapter 8 this fact is discussed.

The second column, [(Figs. D.1 (b), (e)], represents the force due to a partially coherent GSMS. We have fixed the spot size to $\sigma_s = 0.3\lambda$. Contrary to what one could expect, it is the most incoherent emitted field that which produces the maximum force. In the last column, although we can see a similar behavior, we also observe that for $\sigma_g > 0.5\lambda$ the force is positive, i.e., the particle is pushed by the source towards $y > 0$.

In order to explain these results, in Fig. D.2 we show the exponential function $\exp[-k^2 s_x^2/(4c^2)]$ of the angular spectrum, [cf. Eq. (8.12)], for different values of σ_g and σ_s; this helps us to
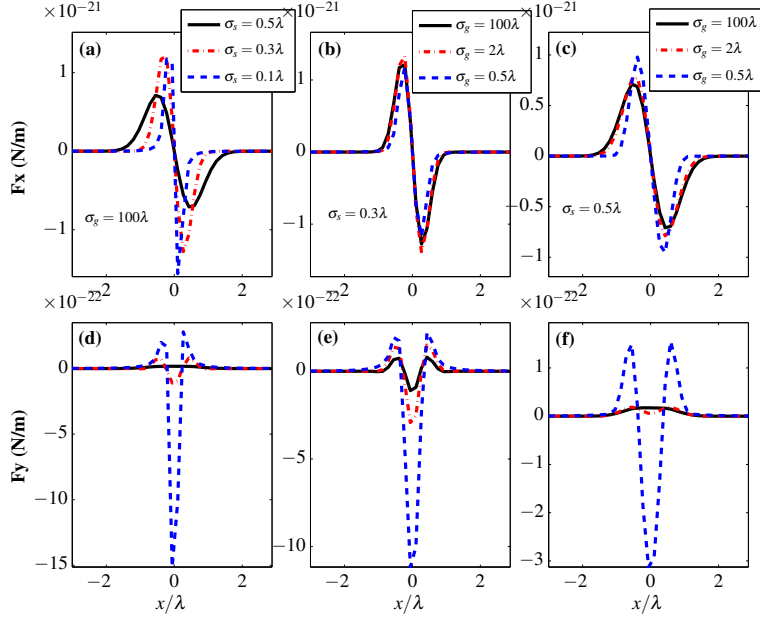
Figure D.1: Ensemble-averaged forces F_x, (first row), and F_y, (second row), from a partially coherent GSMS. The first column from the left pertains to the fully coherent source, $(\sigma_g = 100\lambda \gg \sigma_s)$, which would correspond to the case of Section 8.3. For the center and right columns $\sigma_s = 0.3\lambda$ and 0.5λ, respectively

.
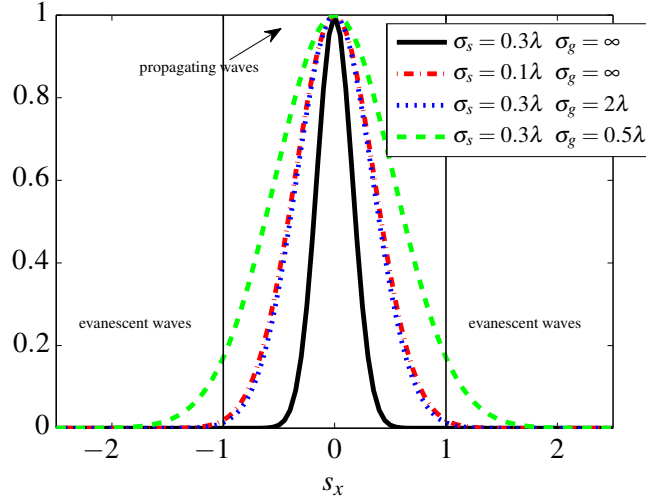
Figure D.2: The function $\exp(-k^2 s_x^2/(4c^2))$ versus the transversal component s_x for different values of the spot size σ_g and coherence length σ_s. For $s_x > 1$ the evanescent waves are not negligible.

understand the behavior of the previous figure. The black and the blue point lines represent the width of the Gaussian function for two cases represented in the force in Figs. D.1(a) and (d). One sees that for a fully coherent source, the Gaussian is broader for a lower value of the spot size, thus taking more evanescent modes of the angular spectrum. The red point-dashed line and the green-dashed lines represent two cases of Figs. D.1(b) and (e). Now, for a partially

coherent source, fixing the value of the spot size, the evanescent modes are more important as the coherence length of the source decreases. All this agrees with the results of Fig. D.1 and Fig. 5.2 of Chapter 5.

BIBLIOGRAPHY

[1] M. Born and E. Wolf, *Principles of optics: electromagnetic theory of propagation, interference and diffraction of light* (Cambridge U. Press, Cambridge, UK, 1999). (Cited on pages 3, 45, 48, 49, 50, 52, 54, 56, 58, 60, 90, 135, and 143.)

[2] J. W. Goodman, *Introduction to Fourier optics* (McGraw-Hill, New York, 1996). (Cited on pages 3, 12, 18, 21, 56, and 58.)

[3] L. Mandel and E. Wolf, *Optical Coherence and Quantum Optics* (Cambridge U. Press, Cambridge, UK, 1995). (Cited on pages 3, 7, 11, 16, 18, 22, 26, 28, 29, 31, 32, 36, 44, 45, 49, 50, 52, 54, 56, 58, 70, 72, 77, 83, 84, 87, 94, 103, 104, 105, 106, 108, 114, 117, and 125.)

[4] J. Peřina, *Coherence of light* (Springer-Verlag, Berlin, 1985). (Cited on pages 50, 52, 54, 56, and 70.)

[5] J. W. Goodman, *Statistical Optics* (John Wiley & Sons, Inc., New York, 1985), 1st ed. (Cited on pages 3, 7, 44, 70, and 85.)

[6] B. J. Thompson and E. Wolf, "Two-beam interference with partially coherent light," J. Opt. Soc. Am. **47**, 895 (1957).
doi: 10.1364/JOSA.47.000895. (Cited on pages 10, 45, 58, 59, 60, 63, and 64.)

[7] P. van Cittert, "Die wahrscheinliche schwingungsverteilung in einer von einer lichtquelle direkt oder mittels einer linse beleuchteten ebene," Physica **1**, 201 – 210 (1934).
doi: 10.1016/S0031-8914(34)90026-4. (Cited on page 12.)

[8] F. Zernike, "The concept of degree of coherence and its application to optical problems," Physica **5**, 785 – 795 (1938).
doi: 10.1016/S0031-8914(38)80203-2. (Cited on page 12.)

[9] W. H. Knox, M. Alonso, and E. Wolf, "Spatial coherence from ducks," Physics Today **63**, 11–11 (2010).
doi: 10.1063/1.3366225. (Cited on page 14.)

[10] M. Nieto-Vesperinas, *Scattering and Diffraction in Physical Optics* (World Science, Singapur, 2006). (Cited on pages 16, 17, 18, 27, 36, 48, 56, 58, 70, 75, 85, 118, and 143.)

[11] R. Carminati and J.-J. Greffet, "Near-field effects in spatial coherence of thermal sources," Phys. Rev. Lett. **82**, 1660–1663 (1999).
doi: 10.1103/PhysRevLett.82.1660. (Cited on pages 22, 36, 40, 71, 113, and 135.)

[12] A. V. Shchegrov, K. Joulain, R. Carminati, and J.-J. Greffet, "Near-field spectral effects due to electromagnetic surface excitations," Phys. Rev. Lett. **85**, 1548–1551 (2000).
doi: 10.1103/PhysRevLett.85.1548. (Cited on pages 135 and 137.)

[13] H. Roychowdhury and E. Wolf, "Effects of spatial coherence on near-field spectra," Opt. Lett. **28**, 170–172 (2003).
doi: 10.1364/OL.28.000170. (Cited on pages 22, 73, 135, and 137.)

[14] A. Apostol and A. Dogariu, "Spatial correlations in the near field of random media," Phys. Rev. Lett. **91**, 093901 (2003).
doi: 10.1103/PhysRevLett.91.093901. (Cited on page 22.)

[15] E. Wolf and W. H. Carter, "Angular distribution of radiant intensity from sources of different degrees of spatial coherence," Optics Communications **13**, 205 – 209 (1975).
doi: 10.1016/0030-4018(75)90081-4. (Cited on page 23.)

[16] W. H. Carter and E. Wolf, "Coherence properties of lambertian and non-lambertian sources," J. Opt. Soc. Am. **65**, 1067–1071 (1975).
doi: 10.1364/JOSA.65.001067. (Cited on pages 23, 36, and 72.)

[17] H. Raether, *Surface plasmons* (Springer-Verlag Berlin, 1988). (Cited on pages 24, 27, 28, and 75.)

[18] C. Kittel, *Introduction to Solid State Physics* (Wiley, 2004). (Cited on page 24.)

[19] E. Wolf and W. Carter, "Fields generated by homogeneous and by quasi-homogeneous planar secondary sources," Optics Communications **50**, 131 – 136 (1984).
doi: http://dx.doi.org/10.1016/0030-4018(84)90332-8. (Cited on pages 26 and 27.)

[20] E. Wolf, *Introduction to the Theory of Coherence and Polarization of Light* (Cambridge U. Press, New York, 2007). (Cited on pages 27, 28, 29, 44, 52, 55, and 106.)

[21] J. T. Foley and E. Wolf, "Frequency shifts of spectral lines generated by scattering from space-time fluctuations," Phys. Rev. A **40**, 588–598 (1989).
doi: 10.1103/PhysRevA.40.588. (Cited on page 27.)

[22] A. Luis, "Degree of polarization for three-dimensional fields as a distance between correlation matrices," Optics Communications **253**, 10 – 14 (2005).
doi: http://dx.doi.org/10.1016/j.optcom.2005.04.046. (Cited on page 31.)

[23] M. R. Dennis, "A three-dimensional degree of polarization based on rayleigh scattering," Journal of the Optical Society of America A **24** (2007).
doi: 10.1364/JOSAA.24.002065. (Cited on page 31.)

[24] R. J. Glauber, "The Quantum Theory of Optical Coherence," Phys. Rev. **130**, 2529–2539 (1963).
doi: 10.1103/PhysRev.130.2529. (Cited on page 31.)

[25] T. Setälä, A. Shevchenko, M. Kaivola, and A. T. Friberg, "Degree of polarization for optical near fields," Phys. Rev. E **66**, 016615 (2002).
doi: 10.1103/PhysRevE.66.016615. (Cited on pages 32, 35, 36, and 113.)

[26] J. Ellis, A. Dogariu, S. Ponomarenko, and E. Wolf, "Degree of polarization of statistically stationary electromagnetic fields," Optics Communications **248**, 333–337 (2005).
doi: 10.1016/j.optcom.2004.12.050. (Cited on pages 32, 35, 36, and 113.)

[27] T. Setälä, J. Tervo, and A. T. Friberg, "Complete electromagnetic coherence in the space-frequency domain," Opt. Lett. **29**, 328–330 (2004).
doi: 10.1364/OL.29.000328.

[28] E. Wolf, "Comment on "Complete electromagnetic coherence in the space-frequencydomain"," Opt. Lett. **29**, 1712–1712 (2004).
doi: 10.1364/OL.29.001712. (Cited on page 36.)

[29] T. Setälä, J. Tervo, and A. T. Friberg, "Reply to comment on "Complete electromagnetic coherence in thespace-frequency domain"," Opt. Lett. **29**, 1713–1714 (2004).
doi: 10.1364/OL.29.001713. (Cited on pages 32 and 36.)

[30] J. M. Auñón and M. Nieto-Vesperinas, "Near-field spatial correlations from partially coherent homogeneous planar sources: effects on surface wave excitation," Opt. Lett. **36**, 3410–3412 (2011).
doi: 10.1364/OL.36.003410. (Cited on pages 36, 37, 38, 73, and 75.)

[31] R. Carminati, "Subwavelength spatial correlations in near-field speckle patterns," Phys. Rev. A **81**, 053804 (2010).
doi: 10.1103/PhysRevA.81.053804. (Cited on pages 36, 95, and 96.)

[32] T. Jouttenus, T. Setälä, M. Kaivola, and A. T. Friberg, "Connection between electric and magnetic coherence in free electromagnetic fields," Phys. Rev. E **72**, 046611 (2005).
doi: 10.1103/PhysRevE.72.046611. (Cited on pages 37, 91, and 147.)

[33] T. Setälä, M. Kaivola, and A. T. Friberg, "Degree of Polarization in Near Fields of Thermal Sources: Effects of Surface Waves," Phys. Rev. Lett. **88**, 123902 (2002).
doi: 10.1103/PhysRevLett.88.123902. (Cited on pages 37 and 40.)

[34] S. Albaladejo, M. I. Marqués, M. Laroche, and J. J. Sáenz, "Scattering forces from the curl of the spin angular momentum of a light field," Phys. Rev. Lett. **102**, 113602 (2009).
doi: 10.1103/PhysRevLett.102.113602. (Cited on pages 43, 44, 48, 54, and 74.)

[35] M. V. Berry, "Optical currents," Journal of Optics A: Pure and Applied Optics **11**, 094001 (2009).
doi: 10.1088/1464-4258/11/9/094001. (Cited on page 46.)

[36] K. Y. Bliokh and F. Nori, "Transverse spin of a surface polariton," Phys. Rev. A **85**, 061801 (2012).
doi: 10.1103/PhysRevA.85.061801. (Cited on page 46.)

[37] M. I. Marqués and J. J. Saénz, "Scattering forces and electromagnetic momentum density in crossed circularly polarized standing waves," Opt. Lett. **37**, 2787–2789 (2012).
doi: 10.1364/OL.37.002787.

[38] A. Y. Bekshaev, O. V. Angelsky, S. G. Hanson, and C. Y. Zenkova, "Scattering of inhomogeneous circularly polarized optical field and mechanical manifestation of the internal energy flows," Phys. Rev. A **86**, 023847 (2012).
doi: 10.1103/PhysRevA.86.023847. (Cited on page 47.)

[39] A. Canaguier-Durand, A. Cuche, C. Genet, and T. W. Ebbesen, "Force and torque on an electric dipole by spinning light fields," Phys. Rev. A **88**, 033831 (2013).
doi: 10.1103/PhysRevA.88.033831.

[40] A. Y. Bekshaev, "Subwavelength particles in an inhomogeneous light field: optical forces associated with the spin and orbital energy flows," Journal of Optics **15**, 044004 (2013).
doi: 10.1088/2040-8978/15/4/044004. (Cited on pages 43 and 47.)

[41] A. Ashkin, "Acceleration and trapping of particles by radiation pressure," Phys. Rev. Lett. **24**, 156–159 (1970).
doi: 10.1103/PhysRevLett.24.156. (Cited on page 44.)

[42] A. Ashkin, J. M. Dziedzic, J. E. Bjorkholm, and S. Chu, "Observation of a single-beam gradient force optical trap for dielectric particles," Opt. Lett. **11**, 288–290 (1986).
doi: 10.1364/OL.11.000288. (Cited on pages 44 and 109.)

[43] J. D. Jackson, *Classical Electrodynamics* (Wiley, New York, New York, 1998). (Cited on pages 44, 45, 58, 86, 116, 118, and 150.)

[44] P. C. Chaumet and M. Nieto-Vesperinas, "Time-averaged total force on a dipolar sphere in an electromagnetic field," Opt. Lett. **25**, 1065–1067 (2000).
doi: 10.1364/OL.25.001065. (Cited on pages 44, 47, 52, 69, and 116.)

[45] M. Mansuripur, "Radiation pressure and the linear momentum of the electromagnetic field," Opt. Express **12**, 5375–5401 (2004).
doi: 10.1364/OPEX.12.005375.

[46] M. Mansuripur, "Radiation pressure and the linear momentum of the electromagnetic field in magnetic media," Opt. Express **15**, 13502–13518 (2007).
doi: 10.1364/OE.15.013502.

[47] B. Kemp, T. Grzegorczyk, and J. Kong, "Ab initio study of the radiation pressure on dielectric and magnetic media," Opt. Express **13**, 9280–9291 (2005).
doi: 10.1364/OPEX.13.009280. (Cited on page 44.)

[48] S. M. Kim and G. Gbur, "Momentum conservation in partially coherent wave fields," Phys. Rev. A **79**, 033844 (2009).
doi: 10.1103/PhysRevA.79.033844. (Cited on page 44.)

[49] W. Wang and M. Takeda, "Linear and angular coherence momenta in the classical second-order coherence theory of vector electromagnetic fields," Opt. Lett. **31**, 2520–2522 (2006).
doi: 10.1364/OL.31.002520. (Cited on pages 44 and 55.)

[50] M. Nieto-Vesperinas, P. C. Chaumet, and A. Rahmani, "Near-field photonic forces," Phil. Trans. R. Soc. Lond. A **362**, 719–737 (2004).
doi: 10.1098/rsta.2003.1343. (Cited on pages 44, 69, 72, and 130.)

[51] K. Dholakia and P. Zemánek, "*Colloquium* : Gripped by light: Optical binding," Rev. Mod. Phys. **82**, 1767–1791 (2010).
doi: 10.1103/RevModPhys.82.1767. (Cited on pages 69 and 112.)

[52] A. S. Zelenina, R. Quidant, and M. Nieto-Vesperinas, "Enhanced optical forces between coupled resonant metal nanoparticles," Opt. Lett. **32**, 1156–1158 (2007).
doi: 10.1364/OL.32.001156.

[53] M. Righini, A. S. Zelenina, C. Girard, and R. QUidant, "Parallel and selective trapping in a patterned plasmonic landscape," Nature Physics **3**, 477–480 (2007).
doi: 10.1038/nphys624.

[54] P. C. Chaumet and M. Nieto-Vesperinas, "Electromagnetic force on a metallic particle in the presence of a dielectric surface," Phys. Rev. B **62**, 11185–11191 (2000).
doi: 10.1103/PhysRevB.62.11185. (Cited on page 44.)

[55] J. M. Auñón and M. Nieto-Vesperinas, "Optical forces on small particles from partially coherent light," J. Opt. Soc. Am. A **29**, 1389–1398 (2012).
doi: 10.1364/JOSAA.29.001389. (Cited on pages 44, 83, 86, 87, and 88.)

[56] L.-G. Wang, C.-L. Zhao, L.-Q. Wang, X.-H. Lu, and S.-Y. Zhu, "Effect of spatial coherence on radiation forces acting on a rayleigh dielectric sphere," Opt. Lett. **32**, 1393–1395 (2007).
doi: 10.1364/OL.32.001393. (Cited on pages 44, 103, 104, 110, and 114.)

[57] C. Zhao, Y. Cai, X. Lu, and H. T. Eyyuboğlu, "Radiation force of coherent and partially coherent flat-topped beams on a rayleigh particle," Opt. Express **17**, 1753–1765 (2009).
doi: 10.1364/OE.17.001753.

[58] C. Zhao, Y. Cai, and O. Korotkova, "Radiation force of scalar and electromagnetic twisted gaussian schell-model beams," Opt. Express **17**, 21472–21487 (2009).
doi: 10.1364/OE.17.021472. (Cited on pages 44, 104, and 114.)

[59] M. Nieto-Vesperinas, J. J. Sáenz, R. Gómez-Medina, and L. Chantada, "Optical forces on small magnetodielectric particles," Opt. Express **18**, 11428–11443 (2010).
doi: 10.1364/OE.18.011428. (Cited on pages 45, 47, 48, 54, 62, 63, 77, 86, 87, 88, 89, and 107.)

[60] A. García-Etxarri, R. Gómez-Medina, L. S. Froufe-Pérez, C. López, L. Chantada, F. Scheffold, J. Aizpurua, M. Nieto-Vesperinas, and J. J. Sáenz, "Strong magnetic response of submicron silicon particles in the infrared," Opt. Express **19**, 4815–4826 (2011).
doi: 10.1364/OE.19.004815. (Cited on pages 81, 82, 84, 86, 90, 112, 117, and 122.)

[61] M. Nieto-Vesperinas, R. Gomez-Medina, and J. J. Saenz, "Angle-suppressed scattering and optical forces on submicrometer dielectric particles," J. Opt. Soc. Am. A **28**, 54–60 (2011).
doi: 10.1364/JOSAA.28.000054. (Cited on pages 45, 63, 77, 81, 84, 89, 91, 107, and 122.)

[62] L. Allen, M. W. Beijersbergen, R. J. C. Spreeuw, and J. P. Woerdman, "Orbital angular momentum of light and the transformation of laguerre-gaussian laser modes," Phys. Rev. A **45**, 8185–8189 (1992).
doi: 10.1103/PhysRevA.45.8185. (Cited on page 45.)

[63] R. A. Beth, "Mechanical detection and measurement of the angular momentum of light," Phys. Rev. **50**, 115–125 (1936).
doi: 10.1103/PhysRev.50.115. (Cited on page 45.)

[64] F. Belinfante, "On the current and the density of the electric charge, the energy, the linear momentum and the angular momentum of arbitrary fields," Physica **7**, 449 – 474 (1940).
doi: 10.1016/S0031-8914(40)90091-X. (Cited on page 45.)

[65] P. C. Chaumet and A. Rahmani, "Electromagnetic force and torque onmagnetic and negative-index scatterers," Opt. Express **17**, 2224–2234 (2009).
doi: 10.1364/OE.17.002224. (Cited on page 47.)

[66] J. R. Arias-González and M. Nieto-Vesperinas, "Optical forces on small particles: attractive and repulsive nature and plasmon-resonance conditions," J. Opt. Soc. Am. A **20**, 1201–1209 (2003). doi: 10.1364/JOSAA.20.001201. (Cited on page 47.)

[67] K. Y. Bliokh, A. Y. Bekshaev, and F. Nori, "Dual electromagnetism: helicity, spin, momentum and angular momentum," New Journal of Physics **15**, 033026 (2013). doi: 10.1088/1367-2630/15/3/033026. (Cited on page 48.)

[68] S. Sukhov and A. Dogariu, "Negative nonconservative forces: optical 'tractor beams' for arbitrary objects," Phys. Rev. Lett. **107**, 203602 (2011). doi: 10.1103/PhysRevLett.107.203602. (Cited on pages 48, 72, and 91.)

[69] A. Novitsky, C. W. Qiu, and H. Wang, "Single Gradientless Light Beam Drags Particles as Tractor Beams," Phys. Rev. Lett. **107**, 203601 (2011). doi: 10.1103/PhysRevLett.107.203601. (Cited on page 91.)

[70] J. J. Sáenz, "Optical forces: Laser tractor beams," Nature Photon. **5**, 514–515 (2011). doi: 10.1038/nphoton.2011.201. (Cited on page 72.)

[71] A. Novitsky, C.-W. Qiu, and A. Lavrinenko, "Material-independent and size-independent tractor beams for dipole objects," Phys. Rev. Lett. **109**, 023902 (2012). doi: 10.1103/PhysRevLett.109.023902. (Cited on page 48.)

[72] J. T. Rubin and L. Deych, "On optical forces in spherical whispering gallery mode resonators," Opt. Express **19**, 22337–22349 (2011). doi: 10.1364/OE.19.022337. (Cited on page 53.)

[73] W. Wang and M. Takeda, "Separation of spin and orbital angular coherence momenta in the second-order coherence theory of vector electromagnetic fields," Opt. Lett. **32**, 2656–2658 (2007). doi: 10.1364/OL.32.002656. (Cited on page 55.)

[74] E. Wolf, "New theory of partial coherence in the space-frequency domain. part i: spectra and cross spectra of steady-state sources," J. Opt. Soc. Am. **72**, 343–351 (1982). doi: 10.1364/JOSA.72.000343. (Cited on page 55.)

[75] J. E. Curtis, B. A. Koss, and D. G. Grier, "Dynamic holographic optical tweezers," Optics Communications **207**, 169 – 175 (2002). doi: 10.1016/S0030-4018(02)01524-9. (Cited on page 62.)

[76] J. R. Arias-González and M. Nieto-Vesperinas, "Optical forces on small particles: attractive and repulsive nature and plasmon-resonance conditions," J. Opt. Soc. Am. A **20**, 1201–1209 (2003). doi: 10.1364/JOSAA.20.001201. (Cited on page 63.)

[77] L. Novotny, R. X. Bian, and X. S. Xie, "Theory of nanometric optical tweezers," Phys. Rev. Lett. **79**, 645–648 (1997). doi: 10.1103/PhysRevLett.79.645. (Cited on page 69.)

[78] M. L. Juan, M. Righini, and R. Quidant, "Plasmon nano-optical tweezers," Nature Photon. **5**, 349–356 (2011). doi: 10.1038/nphoton.2011.56. (Cited on page 69.)

[79] S. M. Rytov, Y. A. Kravtsov, and V. I. Tatarskii, *Principles of statistical radiophysics. Part 3: elements of Random Fields* (Springer-Verlag, Berlin, 1989). (Cited on pages 70, 71, 79, 89, 95, 97, 135, and 151.)

[80] J. W. Strohben, *Laser beam propagation in the atmosphere* (Topics in Applied Physics, Vol. 25, Springer-Verlag, Berlin., 1978). (Cited on page 70.)

[81] L. A. Chernov, *Wave propagation in a random medium* (Dover, New York., 1967). (Cited on page 70.)

[82] A. Ishimaru, *Wave propagation and scattering in random media* (Academic Press, New York, 1997).

[83] M. Nieto-Vesperinas and J. C. Dainty, *Scattering in Volumes and Surfaces* (North Holland, Amsterdam., 1990). (Cited on page 70.)

[84] J. C. Dainty, *Laser speckle and related phenomena* (Topics in Applied Physics, Vol. 9, Springer-Verlag, Berlin., 1984). (Cited on page 70.)

[85] J. A. Ogilvy, *Theory of Wave Scattering From Random Rough Surfaces* (Taylor and Francis., 1991). (Cited on page 70.)

[86] N. Garcia, V. Celli, and M. Nieto-Vesperinas, "Exact multiple scattering of waves from random rough surfaces," Optics Communications **30**, 279 – 281 (1979).
doi: 10.1016/0030-4018(79)90353-5.

[87] N. García and M. Nieto-Vesperinas, "Near-field optics inverse-scattering reconstruction of reflective surfaces," Opt. Lett. **18**, 2090–2092 (1993).
doi: 10.1364/OL.18.002090.

[88] N. García and M. Nieto-Vesperinas, "Direct solution to the inverse scattering problem for surfaces from near-field intensities without phase retrieval," Opt. Lett. **20**, 949–951 (1995).
doi: 10.1364/OL.20.000949. (Cited on page 70.)

[89] G. S. Agarwal, "Quantum electrodynamics in the presence of dielectrics and conductors. i. electromagnetic-field response functions and black-body fluctuations in finite geometries," Phys. Rev. A **11**, 230–242 (1975).
doi: 10.1103/PhysRevA.11.230. (Cited on page 70.)

[90] A. L. Efros and M. Rosen, "Random telegraph signal in the photoluminescence intensity of a single quantum dot," Phys. Rev. Lett. **78**, 1110–1113 (1997).
doi: 10.1103/PhysRevLett.78.1110. (Cited on page 70.)

[91] R. Ferrini, D. Leuenberger, R. Houdré, H. Benisty, M. Kamp, and A. Forchel, "Disorder-induced losses in planar photonic crystals," Opt. Lett. **31**, 1426–1428 (2006).
doi: 10.1364/OL.31.001426. (Cited on page 70.)

[92] H. B. G. Casimir and D. Polder, "The influence of retardation on the london-van der waals forces," Phys. Rev. **73**, 360–372 (1948).
doi: 10.1103/PhysRev.73.360. (Cited on pages 70, 71, 83, and 98.)

[93] H. Failache, S. Saltiel, M. Fichet, D. Bloch, and M. Ducloy, "Resonant van der waals repulsion between excited cs atoms and sapphire surface," Phys. Rev. Lett. **83**, 5467–5470 (1999).
doi: 10.1103/PhysRevLett.83.5467.

[94] S. Y. Buhmann and S. Scheel, "Thermal casimir versus casimir-polder forces: Equilibrium and nonequilibrium forces," Phys. Rev. Lett. **100**, 253201 (2008). doi: 10.1103/PhysRevLett.100.253201. (Cited on pages 71 and 83.)

[95] S. Scheel and S. Y. Buhmann, "Casimir-polder forces on moving atoms," Phys. Rev. A **80**, 042902 (2009). doi: 10.1103/PhysRevA.80.042902.

[96] J. A. Crosse, S. A. Ellingsen, K. Clements, S. Y. Buhmann, and S. Scheel, "Thermal casimir-polder shifts in rydberg atoms near metallic surfaces," Phys. Rev. A **82**, 010901 (2010). doi: 10.1103/PhysRevA.82.010901.

[97] S. Y. Buhmann, S. Scheel, and J. Babington, "Universal scaling laws for dispersion interactions," Phys. Rev. Lett. **104**, 070404 (2010). doi: 10.1103/PhysRevLett.104.070404.

[98] S. A. Ellingsen, S. Y. Buhmann, and S. Scheel, "Temperature-independent casimir-polder forces despite large thermal photon numbers," Phys. Rev. Lett. **104**, 223003 (2010). doi: 10.1103/PhysRevLett.104.223003.

[99] S. A. Ellingsen, S. Y. Buhmann, and S. Scheel, "Casimir-polder energy-level shifts of an out-of-equilibrium particle near a microsphere," Phys. Rev. A **85**, 022503 (2012). doi: 10.1103/PhysRevA.85.022503. (Cited on page 70.)

[100] E. Lifshitz, "The theory of molecular attractive forces between solids," Sov. Phys. JETP **2**, 73–83 (1956). (Cited on pages 71 and 83.)

[101] J. Chen, J. Ng, Z. Lin, and C. T. Chan, "Optical pulling force," Nature Photon. **5**, 531–534 (2011). doi: 10.1038/nphoton.2011.153. (Cited on pages 72 and 91.)

[102] G. Gbur, D. James, and E. Wolf, "Energy conservation law for randomly fluctuating electromagnetic fields," Phys. Rev. E **59**, 4594–4599 (1999). doi: 10.1103/PhysRevE.59.4594. (Cited on page 72.)

[103] T. Setälä, K. Blomstedt, M. Kaivola, and A. T. Friberg, "Universality of electromagnetic-field correlations within homogeneous and isotropic sources," Phys. Rev. E **67**, 026613 (2003). doi: 10.1103/PhysRevE.67.026613. (Cited on page 72.)

[104] V. Wong and M. A. Ratner, "Gradient and nongradient contributions to plasmon-enhanced optical forces on silver nanoparticles," Phys. Rev. B **73**, 075416 (2006). doi: 10.1103/PhysRevB.73.075416. (Cited on page 74.)

[105] E. D. Palik and G. Ghosh, *Handbook of Optical Constants of Solids*, vol. 3 (Academic press, 1998). (Cited on page 75.)

[106] C. David, M. Richter, A. Knorr, I. M. Weidinger, and P. Hildebrandt, "Image dipoles approach to the local field enhancement in nanostructured ag–au hybrid devices," The Journal of Chemical Physics **132**, 024712 (2010). doi: 10.1063/1.3291438. (Cited on page 77.)

[107] A. Vial and T. Laroche, "Comparison of gold and silver dispersion laws suitable for fdtd simulations," Applied Physics B **93**, 139–143 (2008).
doi: 10.1007/s00340-008-3202-4. (Cited on page 77.)

[108] A. García-Martín, T. J. A., Sáenz., and M. Nieto-Vesperinas, "Transition from diffusive to localized regimes in surface corrugated optical waveguides," Applied Physics Letters **71**, 1912–1914 (1997).
doi: 10.1063/1.119978. (Cited on page 79.)

[109] J. Riley, H. Dehghani, M. Schweiger, S. Arridge, J. Ripoll, and M. Nieto-Vesperinas, "3d optical tomography in the presence of void regions," Opt. Express **7**, 462–467 (2000).
doi: 10.1364/OE.7.000462.

[110] J. Ripoll, V. Ntziachristos, J. P. Culver, D. N. Pattanayak, A. G. Yodh, and M. Nieto-Vesperinas, "Recovery of optical parameters in multiple-layered diffusive media: theory and experiments," J. Opt. Soc. Am. A **18**, 821–830 (2001).
doi: 10.1364/JOSAA.18.000821. (Cited on page 79.)

[111] A. B. Evlyukhin, C. Reinhardt, A. Seidel, B. S. Luk'yanchuk, and B. N. Chichkov, "Optical response features of si-nanoparticle arrays," Phys. Rev. B **82**, 045404 (2010).
doi: 10.1103/PhysRevB.82.045404. (Cited on pages 81 and 84.)

[112] J. Geffrin, B. García-Cámara, R. Gómez-Medina, P. Albella, L. Froufe-Pérez, C. Eyraud, A. Litman, R. Vaillon, F. González, M. Nieto-Vesperinas, J. Sáenz, and F. Moreno, "Magnetic and electric coherence in forward- and back-scattered electromagnetic waves by a single dielectric subwavelength sphere," Nature Communications **3**, 1171– (2012).
doi: 10.1038/ncomms2167. (Cited on pages 89 and 90.)

[113] S. Person, M. Jain, Z. Lapin, J. J. Sáenz, G. Wicks, and L. Novotny, "Demonstration of zero optical backscattering from single nanoparticles," Nano Letters **13**, 1806–1809 (2013).
doi: 10.1021/nl4005018.

[114] Y. H. Fu, A. I. Kuznetsov, A. E. Miroshnichenko, Y. F. Yu, and B. Luk'yanchuk, "Directional visible light scattering by silicon nanoparticles," Nature Communications **4**, 1527 (2013).
doi: 10.1038/ncomms2538. (Cited on pages 81, 89, and 90.)

[115] C. F. Bohren and D. R. Huffman, *Absorption and scattering of light by small particles* (Wiley, 1983).
(Cited on pages 82, 86, 117, 118, and 119.)

[116] T. H. Boyer, "Quantum electromagnetic zero-point energy of a conducting spherical shell and the casimir model for a charged particle," Phys. Rev. **174**, 1764–1776 (1968).
doi: 10.1103/PhysRev.174.1764. (Cited on page 83.)

[117] T. H. Boyer, "Van der waals forces and zero-point energy for dielectric and permeable materials," Phys. Rev. A **9**, 2078–2084 (1974).
doi: 10.1103/PhysRevA.9.2078.

[118] C. Henkel, K. Joulain, J.-P. Mulet, and J.-J. Greffet, "Radiation forces on small particles in thermal near fields," Journal of Optics A: Pure and Applied Optics **4**, S109 (2002).
doi: 10.1088/1464-4258/4/5/356. (Cited on pages 83 and 97.)

[119] M. Antezza, L. P. Pitaevskii, and S. Stringari, "New asymptotic behavior of the surface-atom force out of thermal equilibrium," Phys. Rev. Lett. **95**, 113202 (2005).
doi: 10.1103/PhysRevLett.95.113202. (Cited on pages 83, 87, 96, and 97.)

[120] A. W. Rodriguez, D. Woolf, A. P. McCauley, F. Capasso, J. D. Joannopoulos, and S. G. Johnson, "Achieving a strongly temperature-dependent Casimir effect," Physical Review Letters **105**, 060401 (2010).
doi: 10.1103/PhysRevLett.105.060401.

[121] D. Dalvit, P. Milonni, D. Roberts, and F. da Rosa, *Casimir Physics*, Lecture Notes in Physics (Springer, 2011). (Cited on pages 98 and 150.)

[122] A. W. Rodriguez, D. Woolf, P.-C. Hui, E. Iwase, A. P. McCauley, F. Capasso, M. Loncar, and S. G. Johnson, "Designing evanescent optical interactions to control the expression of casimir forces in optomechanical structures," Applied Physics Letters **98**, 194105 (2011).
doi: 10.1063/1.3589119.

[123] K. Pan, A. P. McCauley, A. W. Rodriguez, M. T. H. Reid, J. K. White, and S. G. Johnson, "Calculation of nonzero-temperature casimir forces in the time domain," Phys. Rev. A **83**, 040503 (2011).
doi: 10.1103/PhysRevA.83.040503.

[124] J. Kohoutek, D. Dey, A. Bonakdar, R. Gelfand, A. Sklar, O. G. Memis, and H. Mohseni, "Optomechanical force mapping of deep subwavelength plasmonic modes," Nano Letters **11**, 3378–3382 (2011).
doi: 10.1021/nl201780y.

[125] K. Wang, E. Schonbrun, P. Steinvurzel, and K. B. Crozier, "Trapping and rotating nanoparticles using a plasmonic nano-tweezer with an integrated heat sink," Nature Communications **2**, 469– (2011).
doi: 10.1038/ncomms1480.

[126] M. T. H. Reid, J. White, and S. G. Johnson, "Computation of Casimir interactions between arbitrary three-dimensional objects with arbitrary material properties," Physical Review A **84**, 010503(R) (2011).
doi: 10.1103/PhysRevA.84.010503.

[127] A. W. Rodriguez, D. Woolf, P.-C. Hui, E. Iwase, A. P. McCauley, F. Capasso, M. Lončar, and S. G. Johnson, "Designing evanescent optical interactions to control the expression of Casimir forces in optomechanical structures," Applied Physics Letters **98**, 194105 (2011).
doi: 10.1063/1.3589119.

[128] J. Varela, A. W. Rodriguez, A. P. McCauley, and S. G. Johnson, "Casimir micro-sphere diclusters and three-body effects in fluids," Physical Review A **83**, 042516 (2011).
doi: doi:10.1103/PhysRevA.83.042516.

[129] A. W. Rodriguez, F. Capasso, and S. G. Johnson, "The Casimir effect in microstructured geometries," Nature Photonics **5**, 211–221 (2011). Invited review.
doi: 10.1038/nphoton.2011.39.

[130] J. Zou, Z. Marcet, A. W. Rodriguez, M. T. H. Reid, A. P. McCauley, I. I. Kravchenko, T. Lu, Y. Bao, S. G. Johnson, and H. B. Chan, "Casimir forces on a silicon micromechanical chip," Nature Communications **4**, 1845 (2013).
doi: 10.1038/ncomms2842. (Cited on page 83.)

[131] K. Joulain, J.-P. Mulet, F. Marquier, R. Carminati, and J.-J. Greffet, "Surface electromagnetic waves thermally excited: Radiative heat transfer, coherence properties and Casimir forces revisited in the near field," Surface Science Reports **57**, 59–112 (2005).
doi: 10.1016/j.surfrep.2004.12.002. (Cited on pages 83, 87, and 143.)

[132] W. Liu, A. E. Miroshnichenko, D. N. Neshev, and Y. S. Kivshar, "Broadband unidirectional scattering by magneto-electric core-shell nanoparticles," ACS Nano **6**, 5489–5497 (2012).
doi: 10.1021/nn301398a. (Cited on pages 84 and 89.)

[133] J. A. Schuller, E. S. Barnard, W. Cai, Y. C. Jun, J. S. White, and M. L. Brongersma, "Plasmonics for extreme light concentration and manipulation," Nature materials **9**, 193–204 (2010).
doi: 10.1038/nmat2630.

[134] B. Rolly, B. Stout, and N. Bonod, "Boosting the directivity of optical antennas with magnetic and electric dipolar resonant particles," Opt. Express **20**, 20376–20386 (2012).
doi: 10.1364/OE.20.020376.

[135] J. A. Schuller, R. Zia, T. Taubner, and M. L. Brongersma, "Dielectric metamaterials based on electric and magnetic resonances of silicon carbide particles," Phys. Rev. Lett. **99**, 107401 (2007).
doi: 10.1103/PhysRevLett.99.107401.

[136] M. Kerker, D.-S. Wang, and C. L. Giles, "Electromagnetic scattering by magnetic spheres," J. Opt. Soc. Am. **73**, 765–767 (1983).
doi: 10.1364/JOSA.73.000765.

[137] A. I. Kuznetsov, A. E. Miroshnichenko, Y. H. Fu, J. Zhang, and B. Luk'yanchuk, "Magnetic light," Scientific Reports **2** (2012).
doi: 10.1038/srep00492. (Cited on pages 90 and 112.)

[138] A. B. Evlyukhin, S. M. Novikov, U. Zywietz, R. L. Eriksen, C. Reinhardt, S. I. Bozhevolnyi, and B. N. Chichkov, "Demonstration of magnetic dipole resonances of dielectric nanospheres in the visible region," Nano Letters **12**, 3749–3755 (2012).
doi: 10.1021/nl301594s. (Cited on page 84.)

[139] X. Fan, Z. Shen, and B. Luk'yanchuk, "Huge light scattering from active anisotropic spherical particles," Opt. Express **18**, 24868–24880 (2010).
doi: 10.1364/OE.18.024868. (Cited on pages 84 and 89.)

[140] J. M. Auñón and M. Nieto-Vesperinas, "Photonic forces in the near field of statistically homogeneous fluctuating sources," Phys. Rev. A **85**, 053828 (2012).
doi: 10.1103/PhysRevA.85.053828. (Cited on pages 86 and 90.)

[141] R. Gómez-Medina, B. García-Cámara, I. Suárez-Lacalle, L. Froufe-Pérez, F. González, F. Moreno, M. Nieto-Vesperinas, and J. Sáenz, "Electric and magnetic optical response of dielectric nanospheres: Optical forces and scattering anisotropy," Photonics and Nanostructures - Fundamentals and Applications **10**, 345 – 352 (2012).
doi: http://dx.doi.org/10.1016/j.photonics.2012.05.009. (Cited on page 86.)

[142] J. M. Wylie and J. E. Sipe, "Quantum electrodynamics near an interface," Phys. Rev. A **30**, 1185–1193 (1984).
doi: 10.1103/PhysRevA.30.1185. (Cited on page 87.)

[143] J. E. Sipe, "New Green-function formalism for surface optics," J. Opt. Soc. Am. B **4**, 481–489 (1987).
doi: 10.1364/JOSAB.4.000481. (Cited on pages 87, 135, and 143.)

[144] S. Y. Buhmann and D.-G. Welsch, "Dispersion forces in macroscopic quantum electrodynamics," Progress in Quantum Electronics **31**, 51 – 130 (2007).
doi: 10.1016/j.pquantelec.2007.03.001. (Cited on page 95.)

[145] C. Henkel, S. Pötting, and M. Wilkens, "Loss and heating of particles in small and noisy traps," Applied Physics B **69**, 379–387 (1999).
doi: 10.1007/s003400050823. (Cited on page 98.)

[146] E. Collett and E. Wolf, "Is complete spatial coherence necessary for the generation of highly directional light beams?" Opt. Lett. **2**, 27–29 (1978).
doi: 10.1364/OL.2.000027. (Cited on pages 104, 106, and 107.)

[147] E. Wolf and E. Collett, "Partially coherent sources which produce the same far-field intensity distribution as a laser," Optics Communications **25**, 293 – 296 (1978).
doi: 10.1016/0030-4018(78)90131-1. (Cited on pages 104, 106, and 107.)

[148] P. D. Santis, F. Gori, G. Guattari, and C. Palma, "An example of a collett-wolf source," Optics Communications **29**, 256 – 260 (1979).
doi: 10.1016/0030-4018(79)90094-4. (Cited on pages 104 and 107.)

[149] H. Roychowdhury and O. Korotkova, "Realizability conditions for electromagnetic gaussian schell-model sources," Optics Communications **249**, 379 – 385 (2005).
doi: 10.1016/j.optcom.2005.01.054. (Cited on pages 104 and 106.)

[150] A. Schell, *The Multiple Plate Antenna* (Doctoral Dissertation. Massachusetts Institute of Technology, 1961). (Cited on page 104.)

[151] A. T. Friberg and J. Turunen, "Imaging of gaussian schell-model sources," J. Opt. Soc. Am. A **5**, 713–720 (1988).
doi: 10.1364/JOSAA.5.000713. (Cited on page 109.)

[152] W. Davenport and W. Root, *An introduction to the theory of random signals and noise*, Lincoln Laboratory publications (McGraw-Hill, 1958). (Cited on page 111.)

[153] A. Starikov and E. Wolf, "Coherent-mode representation of gaussian schell-model sources and of their radiation fields," J. Opt. Soc. Am. **72**, 923–928 (1982).
doi: 10.1364/JOSA.72.000923. (Cited on page 112.)

[154] E. Wolf, "New theory of partial coherence in the space-frequency domain. part i: spectra and cross spectra of steady-state sources," J. Opt. Soc. Am. **72**, 343–351 (1982).
doi: 10.1364/JOSA.72.000343. (Cited on pages 112, 115, and 131.)

[155] P. C. Chaumet and M. Nieto-Vesperinas, "Optical binding of particles with or without the presence of a flat dielectric surface," Phys. Rev. B **64**, 035422 (2001). doi: 10.1103/PhysRevB.64.035422. (Cited on page 112.)

[156] S. Sukhov, K. M. Douglass, and A. Dogariu, "Dipole–dipole interaction in random electromagnetic fields," Opt. Lett. **38**, 2385–2387 (2013). doi: 10.1364/OL.38.002385. (Cited on page 112.)

[157] L. Peng, L. Ran, H. Chen, H. Zhang, J. A. Kong, and T. M. Grzegorczyk, "Experimental observation of left-handed behavior in an array of standard dielectric resonators," Phys. Rev. Lett. **98**, 157403 (2007). doi: 10.1103/PhysRevLett.98.157403. (Cited on pages 112 and 127.)

[158] K. Vynck, D. Felbacq, E. Centeno, A. I. Căbuz, D. Cassagne, and B. Guizal, "All-dielectric rod-type metamaterials at optical frequencies," Phys. Rev. Lett. **102**, 133901 (2009). doi: 10.1103/PhysRevLett.102.133901. (Cited on pages 112 and 127.)

[159] J. Ellis and A. Dogariu, "On the degree of polarization of random electromagnetic fields," Optics Communications **253**, 257 – 265 (2005). doi: http://dx.doi.org/10.1016/j.optcom.2005.05.020. (Cited on page 113.)

[160] J. M. Auñón and M. Nieto-Vesperinas, "On two definitions of the three-dimensional degree of polarization in the near field of statistically homogeneous partially coherent sources," Opt. Lett. **38**, 58–60 (2013). doi: 10.1364/OL.38.000058. (Cited on page 113.)

[161] J. M. Auñón and M. Nieto-Vesperinas, "Partially coherent fluctuating sources that produce the same optical force as a laser beam," Opt. Lett. **38**, 2869–2872 (2013). doi: 10.1364/OL.38.002869. (Cited on page 114.)

[162] J. Tervo, T. Setälä, and A. T. Friberg, "Theory of partially coherent electromagnetic fields in the space–frequency domain," J. Opt. Soc. Am. A **21**, 2205–2215 (2004). doi: 10.1364/JOSAA.21.002205. (Cited on page 115.)

[163] X. Cui, D. Erni, and C. Hafner, "Optical forces on metallic nanoparticles induced by a photonic nanojet," Opt. Express **16**, 13560–13568 (2008). doi: 10.1364/OE.16.013560. (Cited on page 116.)

[164] J. Lindberg, T. Setälä, M. Kaivola, and A. T. Friberg, "Spatial coherence effects in light scattering from metallic nanocylinders," J. Opt. Soc. Am. A **23**, 1349–1358 (2006). doi: 10.1364/JOSAA.23.001349. (Cited on pages 116 and 117.)

[165] F. Gori, "Collett-wolf sources and multimode lasers," Optics Communications **34**, 301 – 305 (1980). doi: http://dx.doi.org/10.1016/0030-4018(80)90382-X. (Cited on page 117.)

[166] H. C. Hulst and H. van de Hulst, *Light scattering by small particles* (Dover Pubns, 1981). (Cited on pages 117, 124, and 127.)

[167] S. V. Boriskina, "Theoretical prediction of a dramatic q-factor enhancement and degeneracy removal of whispering gallery modes in symmetrical photonic molecules," Opt. Lett. **31**, 338–340 (2006). doi: 10.1364/OL.31.000338. (Cited on pages 124, 125, 127, and 130.)

[168] S. V. Boriskina, T. M. Benson, and P. Sewell, "Photonic molecules made of matched and mismatched microcavities: new functionalities of microlasers and optoelectronic components," in "Proc. SPIE," , vol. 6452 (2007), vol. 6452, p. 64520X. (Cited on pages 124 and 128.)

[169] S. Boriskina, "Photonic molecules and spectral engineering," in "Photonic Microresonator Research and Applications," , vol. 156 of *Springer Series in Optical Sciences*, I. Chremmos, O. Schwelb, and N. Uzunoglu, eds. (Springer US, 2010), pp. 393–421. (Cited on pages 124, 125, 127, and 130.)

[170] Z. Chen, A. Taflove, and V. Backman, "Photonic nanojet enhancement of backscattering of light by nanoparticles: a potential novel visible-light ultramicroscopy technique," Opt. Express **12**, 1214–1220 (2004).
doi: 10.1364/OPEX.12.001214. (Cited on page 124.)

[171] M. K. Chin, D. Y. Chu, and S.-T. Ho, "Estimation of the spontaneous emission factor for microdisk lasers via the approximation of whispering gallery modes," Journal of Applied Physics **75**, 3302–3307 (1994).
doi: 10.1063/1.356137. (Cited on page 124.)

[172] F. Valdivia-Valero and M. Nieto-Vesperinas, "Composites of resonant dielectric rods: A test of their behavior as metamaterial refractive elements," Photonics and Nanostructures - Fundamentals and Applications **10**, 423 – 434 (2012).
doi: 10.1016/j.photonics.2012.04.012. (Cited on pages 124 and 127.)

[173] F. Valdivia-Valero and M. Nieto-Vesperinas, "Optical forces on cylinders near subwavelength slits: effects of extraordinary transmission and excitation of mie resonances," Optics Express **20**, 13368–13389 (2012).
doi: 10.1364/OE.20.013368. (Cited on pages 124 and 126.)

[174] F. J. Valdivia-Valero and M. Nieto-Vesperinas, "Resonance excitation and light concentration in sets of dielectric nanocylinders in front of a subwavelength aperture. effects on extraordinary transmission," Opt. Express **18**, 6740–6754 (2010).
doi: 10.1364/OE.18.006740. (Cited on page 125.)

[175] F. J. Valdivia-Valero and M. Nieto-Vesperinas, "Propagation of particle plasmons in sets of metallic nanocylinders at the exit of subwavelength slits," Journal of Nanophotonics **5**, 053520–053520–15 (2011).
doi: 10.1117/1.3615984. (Cited on page 125.)

[176] S. V. Boriskina, "Spectrally engineered photonic molecules as optical sensors with enhanced sensitivity: a proposal and numerical analysis," J. Opt. Soc. Am. B **23**, 1565–1573 (2006).
doi: 10.1364/JOSAB.23.001565. (Cited on pages 127 and 130.)

[177] C. Henkel, K. Joulain, R. Carminati, and J.-J. Greffet, "Spatial coherence of thermal near fields," Optics Communications **186**, 57 – 67 (2000).
doi: 10.1016/S0030-4018(00)01048-8. (Cited on page 135.)

IF YOU GOT HERE, THANKS.